

# **ASSESSMENT OF BASIC STEEL I-SECTION BEAM BRACING REQUIREMENTS BY TEST SIMULATION**

A Thesis

By

Evan P. Prado

In Partial Fulfillment  
Of the Requirements for the Degree  
Master of Science in Civil Engineering

Georgia Institute of Technology

December 2014

Copyright © Evan P. Prado 2014

# **ASSESSMENT OF BASIC STEEL I-SECTION BEAM BRACING REQUIREMENTS BY TEST SIMULATION**

Approved by:

Dr. Donald W. White, Advisor  
School of Civil and Environmental Engineering  
*Georgia Institute of Technology*

Dr. Kenneth M. Will  
School of Civil and Environmental Engineering  
*Georgia Institute of Technology*

Dr. Russell T. Gentry  
School of Architecture  
*Georgia Institute of Technology*

Date Approved: August 20, 2014

To my family, for all their love and support

## **ACKNOWLEDGEMENTS**

I wish to express my deepest gratitude to all who were of assistance to the completion of this thesis. Especially to my advisor Professor Donald W. White, who regularly went above and beyond as a mentor and who's prodigious knowledge and love for research in structural engineering is of the most admirable. He has had a significant role in my studies and research. I am deeply indebted to the tremendous amount of time and effort he has dedicated to not only the mentoring of this thesis work, but also my growth as an engineer.

I also wish to extend my deepest gratitude to the rest of my committee members Professor Kenneth M. Will and Professor Russell T. Gentry who's mentoring and guidance have been invaluable for my studies.

Special thanks are due to my friends and fellow students Lakshmi Subramanian, Cliff D. Bishop, Ajinkya Lokhande, Oguzhan Togay, and Thanh Van Nguyen for their help and support.

Finally, I wish to extend gratitude to my parents for their support and encouragement.

# TABLE OF CONTENTS

	Page
<b>ACKNOWLEDGEMENTS</b>	iii
<b>LIST OF TABLES</b>	vi
<b>LIST OF FIGURES</b>	vii
<b>SUMMARY</b>	xiii
<b><u>CHAPTER</u></b>	
<b>1 INTRODUCTION.....</b>	<b>1</b>
1.1 Problem Statement .....	1
1.2 Research Objectives .....	2
1.3 Organization .....	3
<b>2 BACKGROUND .....</b>	<b>5</b>
2.1 Shear Panel (Relative) Lateral Bracing Requirements.....	5
2.2 Extension of the Basic Relative Bracing Case to Beams .....	14
2.3 Point (Nodal) Lateral Bracing Requirements.....	17
2.4 Extension Of Basic Nodal Lateral Bracing Case To Beams.....	23
2.5 Torsional Bracing Requirements.....	25
2.6 Fundamental Definition of Terms .....	34
2.7 Bracing Stiffness Interaction.....	36
2.8 Maximum Strength Knuckle Curves and Brace Force versus Brace Stiffness Curves..	38
<b>3 FINITE ELEMENT PROCEDURES.....</b>	<b>43</b>
3.1 General Modeling Considerations.....	43
3.2 Modeling of Braces .....	47
3.3 Material Properties .....	47
3.4 Residual Stresses .....	48
3.5 Geometric Imperfections.....	50
<b>4 STUDY DESIGN .....</b>	<b>59</b>

4.1	Overview .....	59
4.2	Study Constants.....	61
4.3	Study Variables .....	62
4.3.1	Unbraced Length and Member Inelasticity.....	62
4.3.2	Number of Intermediate Brace Locations and Member Continuity Effects .....	63
4.3.3	Ratios of Combined Lateral to Torsional Bracing Stiffnesses and Bracing Lateral versus Torsional Stiffness Interaction .....	67
4.4	Naming Convention for Test Cases .....	68
4.5	Benchmark Studies.....	69
4.6	Rigidly Braced Member Strengths.....	71
<b>5</b>	<b>NODAL LATERAL BRACING REQUIREMENTS.....</b>	<b>75</b>
5.1	Category A: Nodal Lateral Bracing Results.....	75
<b>6</b>	<b>RELATIVE (SHEAR PANEL) LATERAL BRACING REQUIREMENTS .....</b>	<b>95</b>
6.1	Category B: Relative (Shear Panel) Lateral Bracing Results.....	95
<b>7</b>	<b>TORSIONAL BRACING REQUIREMENTS .....</b>	<b>115</b>
7.1	Category C: Nodal Torsional Bracing Results.....	115
<b>8</b>	<b>COMBINED BRACING REQUIREMENTS.....</b>	<b>135</b>
8.1	Category D Nodal Lateral and Torsional Combined Bracing.....	135
8.2	Category E: Combined Relative (Shear Panel) Lateral and Torsional Bracing.....	142
<b>9</b>	<b>SUMMARY AND CONCLUSIONS.....</b>	<b>147</b>
	<b>APPENDIX A .....</b>	<b>151</b>
A.1	Category Dn .....	152
A.2	Category Dp .....	164
A.3	Category En.....	171
A.4	Category Ep.....	183
A.5	Category A Representative Deflected Geometry at Member Bending Limit Load .....	190
A.6	Category B Representative Deflected Geometry at Member Bending Limit Load .....	196
A.7	Category C Representative Deflected Geometry at Member Bending Limit Load .....	202
	<b>REFERENCES.....</b>	<b>209</b>

## LIST OF TABLES

	Page
Table 4.1. Benchmark case results and comparisons.....	71
Table 4.2. Rigidly braced strengths.....	72
Table 4.3. $M_{max}$ numerical values for the governing Cases C110, C210 and C310.....	72
Table 5.1. Category A rigidly-braced strengths and base nominal bracing stiffnesses.....	75
Table 6.1. Category B rigidly-braced strengths and base nominal bracing stiffnesses.....	95
Table 7.1. Category C maximum strengths with required bracing stiffness.....	113

## LIST OF FIGURES

	Page
Fig. 2.1. Basic shear panel (relative) column bracing idealization.....	6
Fig. 2.2. Single shear panel (relative) column bracing idealization showing the shear panel racking displacement $\Delta$ .....	6
Fig. 2.3. Shear panel (relative) bracing model with shear panel replaced by a spring at the top of the column.....	7
Fig. 2.4. Nodal lateral bracing at the mid-height of a column.....	18
Fig. 2.5. Torsional bracing of an I-beam.....	25
Fig. 2.6. Relative brace between the top and bottom flanges equivalent to a torsional brace.....	32
Fig. 2.7. Example maximum strength knuckle curve.....	40
Fig. 2.8. Example brace force versus brace stiffness curve.....	42
Fig. 3.1. Representative example beam study case, case A110, a 10ft long I-section member with a single intermediate nodal lateral brace ( $n = 1$ ) at the mid-span of the top flange creating two equal unbraced lengths of $L_b = 5$ ft.....	44
Fig. 3.2. Steel stress-strain curve assumed in the structural analysis.....	49
Fig. 3.3. Lehigh residual stress pattern (Galambos and Ketter, 1959).....	50
Fig. 3.4. Beam compression flange imperfections utilized in this research.....	52
Fig. 3.5. Imperfect geometry for a beam with two intermediate brace points.....	53
Fig. 3.6. Possible selections for the imperfection in the bottom flange of a beam-column, $\Delta_{of2}$ , based on the ratio of the flange loads $P_{f1}/P_{f2}$ .....	55
Fig. 3.7 Imperfection patterns for members with $n = 1, 2$ , or $3$ .....	56
Fig. 4.1. Overview of bracing configurations considered within each test category.....	64
Fig. 4.2. Bracing graphics key.....	66
Fig. 4.3. Test design selection of lateral to torsional stiffness ratios for Categories D and E.....	67
Fig. 4.4. Comparison of maximum test simulations strengths ( $M_{max}$ ) for W21x44 members with 5, 10, and 15 ft unbraced lengths to the elastic buckling, yield and plastic moment resistances ( $M_{cr}$ , $M_y$ and $M_p$ ) as well as nominal strengths from the AISC Specification and the Eurocode 3 Standard.....	70
Fig. 4.5. Comparison of rigidly braced strengths for all categories.....	73
Fig. 5.1. Representative nodal lateral model for cases A*10 and A*20.....	76
Fig. 5.2. Case A1*0 knuckle and brace force vs. brace stiffness curves (Compression flange nodal lateral bracing, $L_b = 5$ ft).....	77
Fig. 5.3. Case A2*0 knuckle and brace force vs. brace stiffness curves (Compression flange nodal lateral bracing, $L_b = 10$ ft).....	78
Fig. 5.4. Case A3*0 knuckle and brace force vs. brace stiffness curves (Compression flange nodal lateral bracing, $L_b = 15$ ft).....	79

Fig. 5.5. Bar graph comparison of ideal full bracing stiffness values, $\beta_{iF.AISC}$ , versus full bracing stiffness values based on developing 98 % of the rigidly braced member strength, $\beta_{F98}$ , for Category A (Compression flange nodal lateral bracing) .....	81
Fig. 5.6. Line plot comparison of ideal full bracing stiffness values, $\beta_{iF.AISC}$ , versus full bracing stiffness values based on developing 98 % of the rigidly braced member strength, $\beta_{F98}$ , for Category A (Compression flange nodal lateral bracing) .....	81
Fig. 5.7. Bar graph comparison of base AISC required strength corresponding to $\beta = 2\beta_{iF.AISC}$ versus the test simulation required brace strength at the member limit load, using this brace stiffness (Category A, compression flange nodal lateral bracing) .....	83
Fig. 5.8. Case A110 $M/M_p$ vs. % brace force curves for a progression of increasing brace stiffnesses (Compression (top) flange nodal lateral bracing, $L_b = 5$ ft, $n = 1$ , $\beta_{iF.AISC} = 6.5$ kip/in) .....	88
Fig. 5.9. Case A120 $M/M_p$ vs. % brace force curves for a progression of increasing brace stiffnesses (Compression (top) flange nodal lateral bracing, $L_b = 5$ ft, $n = 2$ , $\beta_{iF.AISC} = 9.7$ kip/in) .....	89
Fig. 5.10. Case A210 $M/M_p$ vs. % brace force curves for a progression of increasing brace stiffnesses (Compression (top) flange nodal lateral bracing, $L_b = 10$ ft, $n = 1$ , $\beta_{iF.AISC} = 2.2$ kip/in) .....	90
Fig. 5.11. Case A220 $M/M_p$ vs. % brace force curves for a progression of increasing brace stiffnesses (Compression (top) flange nodal lateral bracing, $L_b = 10$ ft, $n = 2$ , $\beta_{iF.AISC} = 3.4$ kip/in) .....	91
Fig. 5.12. Case A310 $M/M_p$ vs. % brace force curves for a progression of increasing brace stiffnesses (Compression (top) flange nodal lateral bracing, $L_b = 15$ ft, $n = 1$ , $\beta_{iF.AISC} = 0.97$ kip/in) .....	92
Fig. 5.13. Case A320 $M/M_p$ vs. % brace force curves for a progression of increasing brace stiffnesses (Compression (top) flange nodal lateral bracing, $L_b = 15$ ft, $n = 2$ , $\beta_{iF.AISC} = 1.5$ kip/in) .....	93
Fig. 6.1. Representative relative bracing model for cases B*20 and B*30 .....	96
Fig. 6.2. Case B120 knuckle and brace force vs. brace stiffness curves (Compression flange shear panel (relative) lateral bracing, $L_b = 5$ ft, $n = 2$ , $\beta_{iF.AISC} = 3.2$ kip/in) .....	98
Fig. 6.3. Case B220 knuckle and brace force vs. brace stiffness curves (Compression flange shear panel (relative) lateral bracing, $L_b = 10$ ft, $n = 2$ , $\beta_{iF.AISC} = 1.1$ kip/in) .....	99
Fig. 6.4. Case B320 knuckle and brace force vs. brace stiffness curves (Compression flange shear panel (relative) lateral bracing, $L_b = 15$ ft, $n = 2$ , $\beta_{iF.AISC} = 0.48$ kip/in) .....	100

Fig. 6.5. Case B130 knuckle and brace force vs. brace stiffness curves (Compression flange shear panel (relative) lateral bracing, $L_b = 5$ ft, $n = 3$ , $\beta_{iF.AISC} = 3.2$ kip/in)	101
Fig. 6.6. Case B230 knuckle and brace force vs. brace stiffness curves (Compression flange shear panel (relative) lateral bracing, $L_b = 10$ ft, $n = 3$ , $\beta_{iF.AISC} = 1.1$ kip/in)	102
Fig. 6.7. Case B330 knuckle and brace force vs. brace stiffness curves (Compression flange shear panel (relative) lateral bracing, $L_b = 15$ ft, $n = 3$ , $\beta_{iF.AISC} = 0.48$ kip/in)	103
Fig. 6.8. Bar graph comparison of ideal full bracing stiffness values, $\beta_{iF.AISC}$ , versus full bracing stiffness values based on developing 98 % of the rigidly braced member strength, $\beta_{F98}$ , for Case B (Compression flange shear panel (relative) lateral bracing)	105
Fig. 6.9. Line plot comparison of ideal full bracing stiffness values, $\beta_{iF.AISC}$ , versus full bracing stiffness values based on developing 98 % of the rigidly braced member strength, $\beta_{F98}$ , for Case B (Compression flange shear panel (relative) lateral bracing)	106
Fig. 6.10. Bar graph comparison of base AISC required strength corresponding to $\beta = 2\beta_{iF.AISC}$ versus the test simulation required brace strength at the member limit load, using this brace stiffness (Case B, compression flange shear panel (relative) lateral bracing)	107
Fig. 6.11. Case B120 $M/M_p$ vs. % brace force curves for a progression of increasing brace stiffnesses (Compression flange shear panel (relative) bracing, $L_b = 5$ ft, $n = 2$ , $\beta_{iF.AISC} = 3.2$ kip/in)	108
Fig. 6.12. Case B220 $M/M_p$ vs. % brace force curves for a progression of increasing brace stiffnesses (Compression flange shear panel (relative) bracing, $L_b = 10$ ft, $n = 2$ , $\beta_{iF.AISC} = 1.1$ kip/in)	110
Fig. 6.13. Case B320 $M/M_p$ vs. % brace force curves for a progression of increasing brace stiffnesses (Compression flange shear panel (relative) bracing, $L_b = 15$ ft, $n = 2$ , $\beta_{iF.AISC} = 0.48$ kip/in)	111
Fig. 6.14. Case B130 $M/M_p$ vs. % brace force curves for a progression of increasing brace stiffnesses (Compression flange shear panel (relative) bracing, $L_b = 5$ ft, $n = 3$ , $\beta_{iF.AISC} = 3.2$ kip/in)	112
Fig. 6.15. Case B230 $M/M_p$ vs. % brace force curves for a progression of increasing brace stiffnesses (Compression flange shear panel (relative) bracing, $L_b = 10$ ft, $n = 3$ , $\beta_{iF.AISC} = 1.1$ kip/in)	112
Fig. 6.16. Case B330 $M/M_p$ vs. % brace force curves for a progression of increasing brace stiffnesses (Compression flange shear panel (relative) bracing, $L_b = 15$ ft, $n = 3$ , $\beta_{iF.AISC} = 0.48$ kip/in)	113
Fig. 7.1. Representative torsional bracing model for cases C*10, C*20, and C*30	114
Fig. 7.2. Case C1*0 knuckle and brace force vs. brace stiffness curves (Nodal torsional bracing, $L_b = 5$ ft)	117

Fig. 7.3. Case C2*0 knuckle and brace force vs. brace stiffness curves (Nodal torsional bracing, $L_b = 10$ ft).....	118
Fig. 7.4. Case C3*0 knuckle and brace force vs. brace stiffness curves (Nodal torsional bracing, $L_b = 15$ ft).....	119
Fig. 7.5. Bar graph comparison of ideal full bracing stiffness values, $\beta_{iF.AISC}$ , versus full bracing stiffness values based on developing 98 % of the rigidly braced member strength, $\beta_{F98}$ , for Category C (Nodal torsional bracing).....	123
Fig. 7.6. Line plot comparison of ideal full bracing stiffness values, $\beta_{iF.AISC}$ , versus full bracing stiffness values based on developing 98 % of the rigidly braced member strength, $\beta_{F98}$ , for Category C (Nodal torsional bracing).....	124
Fig. 7.7. Bar graph comparison of base AISC required strength corresponding to $\beta = 2\beta_{iF.AISC}$ versus the test simulation required brace strength at the member limit load, using this brace stiffness (Category C, nodal torsional bracing) .....	124
Fig. 7.8. Case C110 $M/M_p$ vs. % brace force curves for a progression of increasing brace stiffnesses (Nodal torsional bracing, $L_b = 5$ ft, $n = 1$ , $\beta_{iF.AISC} = 7.6$ kip/in).....	126
Fig. 7.9. Case C120 $M/M_p$ vs. % brace force curves for a progression of increasing brace stiffnesses (Nodal torsional bracing, $L_b = 5$ ft, $n = 2$ , $\beta_{iF.AISC} = 5.7$ kip/in).....	127
Fig. 7.10. Case C130 $M/M_p$ vs. % brace force curves for a progression of increasing brace stiffnesses (Nodal torsional bracing, $L_b = 5$ ft, $n = 3$ , $\beta_{iF.AISC} = 5.1$ kip/in).....	128
Fig. 7.11. Case C210 $M/M_p$ vs. % brace force curves for a progression of increasing brace stiffnesses (Nodal torsional bracing, $L_b = 10$ ft, $n = 1$ , $\beta_{iF.AISC} = 7.2$ kip/in).....	129
Fig. 7.12. Case C220 $M/M_p$ vs. % brace force curves for a progression of increasing brace stiffnesses (Nodal torsional bracing, $L_b = 10$ ft, $n = 2$ , $\beta_{iF.AISC} = 5.4$ kip/in).....	130
Fig. 7.13. Case C230 $M/M_p$ vs. % brace force curves for a progression of increasing brace stiffnesses (Nodal torsional bracing, $L_b = 10$ ft, $n = 3$ , $\beta_{iF.AISC} = 4.8$ kip/in).....	131
Fig. 7.14. Case C310 $M/M_p$ vs. % brace force curves for a progression of increasing brace stiffnesses (Nodal torsional bracing, $L_b = 15$ ft, $n = 1$ , $\beta_{iF.AISC} = 4.6$ kip/in).....	132
Fig. 7.15. Case C330 $M/M_p$ vs. % brace force curves for a progression of increasing brace stiffnesses (Nodal torsional bracing, $L_b = 15$ ft, $n = 3$ , $\beta_{iF.AISC} = 3.1$ kip/in).....	133
Fig. 8.1. Representative combined nodal lateral and torsional bracing model for cases D*10** and D*20** .....	135
Fig. 8.2 Cross-section view of combined nodal lateral and nodal torsional bracing at an intermediate brace point.....	135
Fig. 8.3. Category D nodal lateral – nodal torsional brace stiffness interactions ( $L_b = 5$ ft) .....	137
Fig. 8.4. Category D nodal lateral – nodal torsional brace stiffness interactions ( $L_b = 10$ ft)....	136
Fig. 8.5. Category D nodal lateral – nodal torsional brace stiffness interactions ( $L_b = 15$ ft) ...	139
Fig. 8.6. Representative combined relative and torsional bracing model for cases E*20** and E*30** .....	142
Fig. 8.7. Category E shear panel lateral – nodal torsional brace stiffness interactions ( $L_b = 5$ ft) .....	143

Fig. 8.8. Category E shear panel lateral – nodal torsional brace stiffness interactions ( $L_b = 10$ ft)	144
Fig. 8.9. Category E shear panel lateral – nodal torsional brace stiffness interactions ( $L_b = 15$ ft)	145
Fig. A.1. Case D110*n knuckle and brace force vs. brace stiffness curves (Combined nodal lateral and nodal torsional bracing, $L_b = 5$ ft, $n = 1$ , negative bending)	152
Fig. A.2. Case D120*n knuckle and brace force vs. brace stiffness curves (Combined nodal lateral and nodal torsional bracing, $L_b = 5$ ft, $n = 2$ , negative bending)	154
Fig. A.3. Case D210*n knuckle and brace force vs. brace stiffness curves (Combined nodal lateral and nodal torsional bracing, $L_b = 10$ ft, $n = 1$ , negative bending)	156
Fig. A.4. Case D220*n knuckle and brace force vs. brace stiffness curves (Combined nodal lateral and nodal torsional bracing, $L_b = 10$ ft, $n = 2$ , negative bending)	158
Fig. A.5. Case D310*n knuckle and brace force vs. brace stiffness curves (Combined nodal lateral and nodal torsional bracing, $L_b = 15$ ft, $n = 1$ , negative bending)	159
Fig. A.6. Case D320*n knuckle and brace force vs. brace stiffness curves (Combined nodal lateral and nodal torsional bracing, $L_b = 15$ ft, $n = 2$ , negative bending)	160
Fig. A.7. Case D110*p knuckle and brace force vs. brace stiffness curves (Combined nodal lateral and nodal torsional bracing, $L_b = 5$ ft, $n = 1$ , positive bending)	162
Fig. A.8. Case D120*p knuckle and brace force vs. brace stiffness curves (Combined nodal lateral and nodal torsional bracing, $L_b = 5$ ft, $n = 2$ , positive bending)	164
Fig. A.9. Case D210*p knuckle and brace force vs. brace stiffness curves (Combined nodal lateral and nodal torsional bracing, $L_b = 10$ ft, $n = 1$ , positive bending)	166
Fig. A.10. Case D220*p knuckle and brace force vs. brace stiffness curves (Combined nodal lateral and nodal torsional bracing, $L_b = 10$ ft, $n = 2$ , positive bending)	167
Fig. A.11. Case D310*p knuckle and brace force vs. brace stiffness curves (Combined nodal lateral and nodal torsional bracing, $L_b = 15$ ft, $n = 1$ , positive bending)	168
Fig. A.12. Case D320*p knuckle and brace force vs. brace stiffness curves (Combined nodal lateral and nodal torsional bracing, $L_b = 15$ ft, $n = 2$ , positive bending)	169
Fig. A.13. Case E120*n knuckle and brace force vs. brace stiffness curves (Combined shear panel lateral lateral and nodal torsional bracing, $L_b = 5$ ft, $n = 2$ , negative bending)	171
Fig. A.14. Case E130*n knuckle and brace force vs. brace stiffness curves (Combined shear panel lateral and nodal torsional bracing, $L_b = 5$ ft, $n = 3$ , negative bending)	173
Fig. A.15. Case E220*n knuckle and brace force vs. brace stiffness curves (Combined shear panel lateral and nodal torsional bracing, $L_b = 10$ ft, $n = 2$ , negative bending)	175
Fig. A.16. Case E230*n knuckle and brace force vs. brace stiffness curves (Combined shear panel lateral and nodal torsional bracing, $L_b = 10$ ft, $n = 3$ , negative bending)	177
Fig. A.17. Case E320*n knuckle and brace force vs. brace stiffness curves (Combined shear panel lateral and nodal torsional bracing, $L_b = 15$ ft, $n = 2$ , negative bending)	179
Fig. A.18. Case E330*n knuckle and brace force vs. brace stiffness curves (Combined shear panel lateral and nodal torsional bracing, $L_b = 15$ ft, $n = 3$ , negative bending)	181

Fig. A.19. Case E120*p knuckle and brace force vs. brace stiffness curves (Combined shear panel lateral and nodal torsional bracing, $L_b = 5$ ft, $n = 2$ , positive bending).....	183
Fig. A.20. Case E130*p knuckle and brace force vs. brace stiffness curves (Combined shear panel lateral and nodal torsional bracing, $L_b = 5$ ft, $n = 2$ , positive bending) .....	185
Fig. A.21. Case E220*p knuckle and brace force vs. brace stiffness curves (Combined shear panel lateral and nodal torsional bracing, $L_b = 10$ ft, $n = 2$ , positive bending) .....	186
Fig. A.22. Case E230*p knuckle and brace force vs. brace stiffness curves (Combined shear panel lateral and nodal torsional bracing, $L_b = 10$ ft, $n = 3$ , positive bending) .....	187
Fig. A.23. Case E320*p knuckle and brace force vs. brace stiffness curves (Combined shear panel lateral and nodal torsional bracing, $L_b = 15$ ft, $n = 2$ , positive bending) .....	188
Fig. A.24. Case E330*p knuckle and brace force vs. brace stiffness curves (Combined shear panel lateral and nodal torsional bracing, $L_b = 15$ ft, $n = 3$ , positive bending) .....	189
Fig. A.25. Case A110 deflected geometry at limit load.....	190
Fig. A.26. Case A210 deflected geometry at limit load.....	191
Fig. A.27. Case A310 deflected geometry at limit load.....	192
Fig. A.28. Case A120 deflected geometry at limit load.....	193
Fig. A.29. Case A220 deflected geometry at limit load.....	194
Fig. A.30. Case A320 deflected geometry at limit load.....	195
Fig. A.31. Case B120 deflected geometry at limit load.....	196
Fig. A.32. Case B220 deflected geometry at limit load.....	197
Fig. A.33. Case B320 deflected geometry at limit load.....	198
Fig. A.34. Case B130 deflected geometry at limit load.....	199
Fig. A.35. Case B230 deflected geometry at limit load.....	200
Fig. A.36. Case B330 deflected geometry at limit load.....	201
Fig. A.37. Case C110 deflected geometry at limit load.....	202
Fig. A.38. Case C210 deflected geometry at limit load.....	203
Fig. A.39. Case C310 deflected geometry at limit load.....	204
Fig. A.40. Case C120 deflected geometry at limit load.....	205
Fig. A.41. Case C220 deflected geometry at limit load.....	206
Fig. A.42. Case C320 deflected geometry at limit load.....	207
Fig. A.43. Case C130 deflected geometry at limit load.....	208
Fig. A.44. Case C230 deflected geometry at limit load.....	209
Fig. A.45. Case C330 deflected geometry at limit load.....	210

## SUMMARY

Appendix 6 of the ANSI/AISC 360-10 Specification provides methods for assessing the required stiffness and strength for basic bracing of columns and of beams. Substantial evidence exists showing that the Appendix 6 equations provide an accurate characterization of the stability bracing requirements, particularly when various refinements from the AISC Commentary are employed. Nevertheless, the development of these equations is based largely on elastic stability theory and various practical approximations are invoked to make the equations useful for design. Some of the important approximations relate to the handling of member inelasticity as well as the influence of member continuity across brace point locations. To the knowledge of the author, no comprehensive studies have been conducted to date to evaluate the specific nature of these approximations. Furthermore, the current Appendix 6 provisions do not recognize the benefits of combined lateral and torsional bracing. Limited prior research studies have shown substantial reduction in the demands on the individual bracing components by using them in combination.

This thesis presents a methodical and comprehensive study of basic beam bracing behavior via refined FEA test simulation. Various point (nodal) lateral, shear panel (relative) lateral, point torsional, combined point lateral and point torsional, and combined shear panel lateral and point torsional bracing cases are studied for representative beams subjected to uniform bending. Detailed comparisons to the current Appendix 6 rules are provided, where applicable, and recommendations for improvements are forwarded. Specific questions addressed in this research are:

- What is the effect of inelasticity on the bracing response and requirements?
- What is the influence of member continuity across the brace points on the bracing response and requirements?
- What are the benefits of combined torsional and lateral bracing when the lateral bracing is placed on the compression flange versus when it is placed on the tension flange

# CHAPTER 1

## INTRODUCTION

### 1.1 Problem Statement

It is well known that to be effective in enhancing member strengths, stability bracing systems must possess both sufficient strength as well as sufficient stiffness (Yura 1995 & 2001). Appendix 6 of the AISC 360-10 Specification (AISC 2010) provides equations that define the stability bracing design requirements for basic column and beam members. Substantial evidence exists showing that the Appendix 6 equations work well, particularly when the various refinements included in the Commentary are provided. However, these equations were largely derived from elastic models, and various approximations are involved in the application of the equations to inelastic buckling cases as well as to the handling of the effects of member continuity across brace locations. For instance, the Appendix 6 beam torsional bracing requirements are derived assuming an elastic I-section member restrained by discrete elastic torsional springs. Both the elastic member as well as the elastic torsional springs resist the twisting at the member torsional brace locations. To the knowledge of the author, the influence of member inelasticity on the torsional bracing stiffness and strength demands has not been addressed in any methodical and comprehensive fashion in the research to date.

In addition, targeted prior research studies have shown the benefits of the combined usage of lateral and torsional bracing in reducing the demands on the individual bracing components. However, to the author's knowledge, no comprehensive studies have been conducted to investigate both the stiffness and the strength requirements for combined bracing cases, particularly for situations where the lateral bracing is placed on the tension flange rather

than on the compression flange. This situation is common due to the existence of lateral bracing on an “outside” flange, from wall or roof panels, but where the “inside” flange of the member is subjected to flexural compression. To the author’s knowledge, only Tran (2009) has studied cases with negative bending for combined torsional and lateral bracing, with the lateral bracing on the tension flange. The current AISC Specification does not address the influence of combined torsional and lateral bracing.

This research presents a methodical and comprehensive study of basic beam bracing behavior via load-deflection studies generated by refined FEA test simulation. Various point (nodal) lateral, shear panel (relative) lateral, point torsional, combined point lateral and point torsional, and combined shear panel lateral and point torsional bracing cases are studied for representative beams subjected to uniform bending. The results of the study are compared with AISC Appendix 6 rules, including AISC Commentary refinements.

This study is part of an overall research program to investigate the stability bracing behavior of beam and beam-column members and to provide recommendations for updates to AISC Appendix 6, particularly for the bracing of beam-columns. This study provides the foundation for on-going research specifically directed at beam-column bracing behavior and bracing requirements.

## 1.2 **Research Objectives**

The objectives of this research are:

- Produce a comprehensive evaluation of the nodal lateral, relative lateral, nodal torsional, combined nodal lateral and nodal torsional, and combined relative lateral and nodal torsional bracing of beams via refined test simulation.

- Provide detailed comparisons to the current Appendix 6 rules where applicable and give recommendations for improvements.

The following specific questions are addressed in this research:

- What is the effect of inelasticity on the bracing response and requirements for beams?
- What is the influence of member continuity across the brace points on the bracing response and requirements?
- What are the benefits of combined torsional and lateral bracing? Combinations with both lateral bracing on the compression flange as well as on the tension flange are considered.

### 1.3 Organization

Chapter 2 presents the background for this study. Chapter 3 summarizes the details of the finite element procedures used for the test simulations conducted in this work. Chapter 4 explains the overall design of the current study. Chapters 5 through 8 then present various results in the order of point (nodal) lateral bracing, shear panel (relative) lateral bracing, point torsional bracing, and combined bracing. Chapter 9 provides a summary and conclusions. Appendices are provided that give detailed results from the combined bracing studies as well as various secondary developments.



## CHAPTER 2

### BACKGROUND

#### 2.1 Shear Panel (Relative) Lateral Bracing Requirements

The AISC shear panel bracing requirements for beams are based on a simple shear panel column bracing model. The base model has a pin inserted in the column at each brace location and flexible shear panels are attached to the column at each of the brace points. Each of the shear panels is assumed to have a rigid back-up system. That is, the boundary elements of the shear panels are assumed to be sufficiently stiff such that any flexing of the bracing system is negligible. Shear racking of the panels between each brace point is assumed to be the only significant deformation of the bracing system. The shear panels can either be composed of solid panels, such as panels of a roof or wall diaphragms, or they can be composed of X or single diagonal bracing members in a truss system, assuming that the chords and verticals of the truss are sufficiently stiff such that the only significant source of deformation comes from the elongation or shortening of the diagonal member(s).

Figure 2.1 shows an example idealization of this type. Each of the three unbraced lengths of this example column have a different length and are subjected to a different internal axial force. The shear panel system is shown to be supported at the base elevation of the column. However, because the back-up system for the shear panels is assumed to be rigid, the location of this support could also be at the top elevation of the column and the behavior would be the same. Given this idealization, each of the shear panels works independently within each unbraced length. As such, the basic relative bracing response can be analyzed by focusing on just a single isolated column unbraced length and the corresponding relative bracing shear panel. The shear

panel simply resists the relative lateral movement between the ends of the corresponding column unbraced length. Figure 2.2 shows this more basic model in a deformed configuration illustrating the shear racking displacement  $\Delta$ .

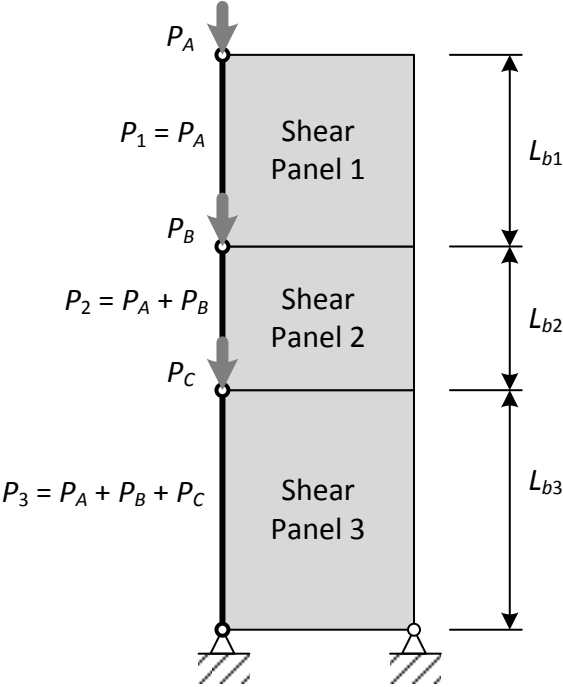


Fig. 2.1. Basic shear panel (relative) column bracing idealization

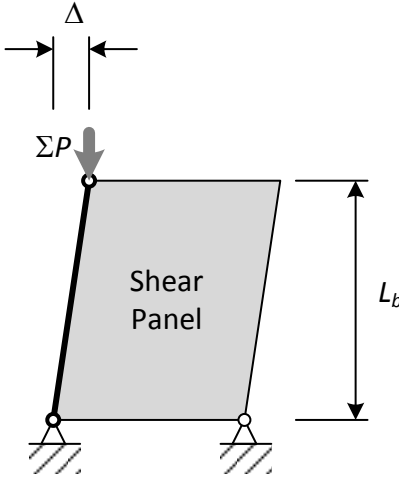


Fig. 2.2. Single shear panel (relative) column bracing idealization showing the shear panel racking displacement  $\Delta$

The summation sign on the axial load in this figure represents not only the total load applied to an individual column. It also represents the total sum of the axial loads in potential multiple columns that may be braced by an individual shear panel within a given unbraced length.

The basic model shown in Figure 2.2 is often simplified to the representation shown in Figure 2.3, where the shear panel is replaced by a spring with a stiffness of  $\beta$  located at the top of the column, representing the restraint of the relative displacements between the column ends by the shear panel.

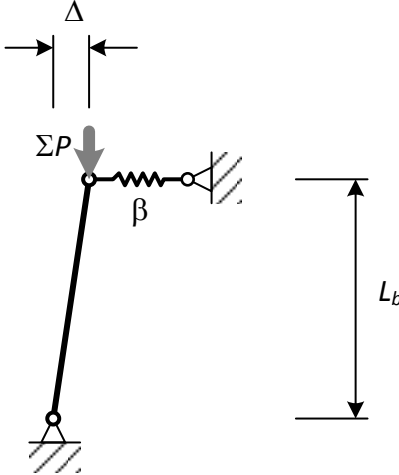


Fig. 2.3. Shear panel (relative) bracing model with shear panel replaced by a spring at the top of the column

The fundamental shear panel (relative) bracing requirements can be derived by considering equilibrium on the model shown in Figure 2.3. If one assumes that the column is ideally plumb in its initial geometry under zero load, such that the displacement  $\Delta$  is a lateral displacement due to buckling of the column and its bracing system, then moment equilibrium in Figure 2.3 requires

$$\Sigma P \Delta = (\beta \Delta) L_b \quad (2-1)$$

The displacement  $\Delta$  can be canceled from both sides of this equation, resulting in the solution for the critical buckling load of the column and its bracing system

$$\Sigma P_{cr} = \beta L_b \quad (2-2)$$

where the subscript “*cr*” is added to denote that this is the critical buckling load. Alternately, this equation can be rearranged to

$$\beta_i = \frac{\Sigma P}{L_b} \quad (2-3)$$

where the subscript “*i*” is added to denote that the bracing stiffness satisfying this relationship is the “ideal bracing stiffness.” The ideal bracing stiffness is defined as the stiffness of the bracing system that is just sufficient to develop the applied load prior to buckling of the bracing system.

Any physical column will generally have an unavoidable initial out-of-plumbness (or out-of-alignment) of the column denoted by the symbol  $\Delta_o$ . This initial displacement is assumed to exist under zero load, and with zero initial force in the bracing system. When this initial geometric imperfection is considered, the total lateral displacement in Figure 2.3 becomes  $\Delta + \Delta_o$ , but the force developed in the bracing spring is simply  $\beta \Delta$ . Therefore, moment equilibrium for a given applied load level  $\Sigma P$  requires

$$\Sigma P (\Delta + \Delta_o) = (\beta \Delta) L_b \quad (2-4)$$

Upon dividing both sides of this equation by  $L_b$  and substituting Equation (2-3), this equation may be written as

$$\beta_i (\Delta + \Delta_o) = (\beta \Delta) \quad (2-5)$$

Given this relationship, one can solve for the displacement  $\Delta$  to obtain

$$\Delta = \frac{\beta_i}{(\beta - \beta_i)} \Delta_o \quad (2-6)$$

and the total lateral displacement can be written as

$$\Delta_{total} = \Delta + \Delta_o = \left[ \frac{\beta_i}{(\beta - \beta_i)} + 1 \right] \Delta_o \quad (2-7)$$

After some algebra, this expression can be simplified to the form

$$\Delta_{total} = \left[ \frac{\beta}{(\beta - \beta_i)} \right] \Delta_o \quad (2-8)$$

and finally to

$$\Delta_{total} = \left[ \frac{1}{\left(1 - \frac{\beta_i}{\beta}\right)} \right] \Delta_o \quad (2-9)$$

If one recognizes that the shear panel stiffness is defined fundamentally as the internal shear

force in the panel,  $H$ , divided by the panel shear racking displacement due to this internal shear

force,  $\Delta_H$ , that is,

$$\beta = \frac{H}{\Delta_H} \quad (2-10)$$

and if Equation (2-3) is substituted for  $\beta_i$  and the column height is expressed as  $L = L_b$ , then

Equation (2-9) may be expressed as

$$\Delta_{total} = \left[ \frac{1}{\left( 1 - \frac{\Sigma P}{HL / \Delta_H} \right)} \right] \Delta_o \quad (2-11)$$

The term within the brackets in Equation (2-11) is exactly the same as the equation for the sidesway amplification of a building story provided in Appendix 8 of the ANSI/AISC 360-10 Specification, but with the  $R_M$  term, which represents P-small delta effects on the story drift, taken equal to 1.0. ( $R_M = 1.0$  corresponds to zero P-small delta effects, which is correct for the above idealized model in which the column is pinned at each of the brace locations.) That is, in the context of AISC Appendix 8, the above equation for the total relative lateral displacement between the column ends within the unbraced length under consideration may be written as

$$\Delta_{total} = \left[ \frac{1}{\left( 1 - \frac{P_{story}}{P_{e story}} \right)} \right] \Delta_o = B_2 \Delta_o \quad (2-12)$$

where  $P_{story} = \Sigma P$  is the load on the story (stabilized in this case by the shear panel bracing system), and

$$P_{e story} = \frac{HL}{\Delta_H} \quad (2-13)$$

is the buckling load of the story.

Given the above solution for  $\Delta$ , the shear panel bracing force is determined basically by using the force-deformation relationship for the panel

$$V_{br} = \beta \Delta \quad (2-14)$$

which, upon substituting Equation (2-6) for  $\Delta$ , becomes

$$V_{br} = \beta \frac{\beta_i}{(\beta - \beta_i)} \Delta_o \quad (2-15)$$

This expression can then be rearranged to write

$$V_{br} = \frac{1}{\left(1 - \frac{\beta_i}{\beta}\right)} (\beta_i \Delta_o) = B_2 \left( \frac{\Sigma P}{L_b} \Delta_o \right) \quad (2-16)$$

which basically states that the brace force required for equilibrium, if the brace is rigid and the

brace point displacement under load is  $\Delta = 0$ ,  $\frac{\Sigma P}{L_b} \Delta_o$ , is magnified by the same amplification

factor that specifies the relationship between  $\Delta_{total}$  and  $\Delta_o$  (i.e., Equations 2-9, 2-11 or 2-12).

AISC Appendix 6 requires that at least twice the ideal bracing stiffness shall be used for the relative bracing stiffness, i.e.,  $\beta = 2\beta_i$ . Given this minimum required value of the shear panel bracing stiffness, then from Equation (2-6),

$$\Delta = \Delta_o$$

from Equation (2-9),

$$\Delta_{total} = 2\Delta_o$$

and from Equation (2-15),

$$V_{br} = 2 \frac{\Sigma P}{L_b} \Delta_o$$

Furthermore, if  $\Delta_o$  is taken as  $0.002L_b$ , based on the maximum nominal out-of-plumbness specified in the AISC Code of Standard Practice, then

$$V_{br} = 0.004\Sigma P \quad (2-17)$$

which is the base AISC Appendix 6 required strength for a shear panel brace. In many situations, a bracing stiffness larger than the above minimum required value is used. In these cases, if the minimum requirement is defined as

$$\beta_{req} = 2\beta_i$$

and if the actual provided bracing stiffness is defined as

$$\beta = \beta_{act}$$

then from Equation (2-16), one can write

$$V_{br} = \frac{1}{\left(1 - \frac{\beta_{req}}{2\beta_{act}}\right)} (\beta_i \Delta_o) = \frac{1}{\left(1 - \frac{\beta_{req}}{2\beta_{act}}\right)} \left(\frac{\Sigma P}{L_b} \Delta_o\right) = \frac{1}{\left(1 - \frac{\beta_{req}}{2\beta_{act}}\right)} \left(\frac{\Sigma P}{L_b} 0.002L_b\right) \quad (2-18)$$

If this expression is then divided by the base bracing strength requirement from Equation (2-17)

$V_{br.base} = 0.004 \Sigma P$ , one obtains the relationship

$$\frac{V_{br}}{V_{br.base}} = \frac{1}{\left(1 - \frac{\beta_{req}}{2\beta_{act}}\right)} \left(\frac{1}{2}\right) = \frac{1}{\left(2 - \frac{\beta_{req}}{\beta_{act}}\right)} \quad (2-19)$$

This equation is specified in the AISC Appendix 6 Commentary as a modifier on the base brace strength requirement to obtain the required brace strength corresponding to the actual brace stiffness.

In summary, the AISC Appendix 6 Commentary required minimum bracing stiffness is

$$\beta_{req} = 2\beta_i = \frac{2\Sigma P}{L_b} \quad (2-20)$$

not considering any resistance factors  $\phi$  or safety factors  $\Omega$  and the required bracing strength is

$$V_{br} = \frac{0.004\Sigma P}{\left(2 - \frac{\beta_{req}}{\beta_{act}}\right)} \quad (2-21)$$

The AISC Specification gives Equation (2-21) (or actually just the base value in the numerator of this equation) without any summation shown on the axial load term; however, the commentary emphasizes that the load to be used in this equation is the sum of all the axial forces in the columns being stabilized by the bracing system. The Specification applies  $1/\phi = 1/0.75$  to the above stiffness requirement in LRFD and  $\Omega = 2$  to this requirement in ASD, given the required force from the design analysis calculations,  $\Sigma P = \Sigma P_r$ .

Several attributes of the above equations that are important to recognize are as follows:

- The bracing stiffness and strength requirements are independent of the number of brace points along the column length. The requirements are localized to each shear panel and depend only on the  $\Sigma P$  and  $L_b$  of each unbraced length.
- Different shear panels can have different stiffness, different  $L_b$  and different  $\Sigma P$ . That is, the shear panel bracing equations accommodate unequal shear panel bracing stiffness, unequal brace spacing, and non-constant axial load from unbraced length to unbraced length along the column.

- As the unbraced length  $L_b$  becomes very short, the bracing stiffness requirement increases substantially. This is due to the fact that the shear panel (relative) bracing model does not consider the beneficial effect of any continuity of the column across the brace points.

The idealized model upon which the relative bracing equations are based assumes that the column has a pin in it at each bracing location.

## 2.2 Extension of the Basic Relative Bracing Case to Beams

AISC Appendix 6 extends the above column equations to shear panel (relative) lateral bracing of beams, where the shear panel is assumed to be located at the level of the compression flange in the direction through the depth of the member cross-section, by substituting  $\Sigma P = \frac{\Sigma M}{h_o}$ , where  $\Sigma M$  is the sum of the internal moments in the beams that are being stabilized by a given shear panel, and  $h_o$  is the distance between the flange centroids. Note that if multiple beams are stabilized by a given shear panel, the moments in all of the beams must be summed. For instance if a shear panel is placed between the compression flanges of two beams, then the moments in the two beams must be summed in determining the shear panel bracing requirements. In this research,  $\Sigma M$  is written just as  $M$  for simplicity, similar to the practice in Appendix 6 of the AISC Specification. In general, this is a dangerous simplification of the notation, since this tends to focus the engineer's attention on the moment in just one of the beams being stabilized rather than considering the overall structural system requirements.

In addition to the above substitution, two additional adjustment factors,  $C_{iR}$  and  $C_d$ , are applied in general based on the research by Yura (2005). These parameters account for the influence of load height as well as larger demands in the vicinity of inflection points that occur in certain cases. These terms and their proper application are summarized in detail by White et al.

(2011). This research focuses on the basic case of uniform bending, for which these parameters are both equal to 1.0.

Given all of the above developments, the resulting most general equation for the AISC minimum shear panel (relative) bracing stiffness requirement for beams can be written nominally as

$$\beta_{br} = \frac{2(M / h_o)}{L_b} C_{tR} C_d \quad (2-22)$$

and for design as

$$\beta_{br\ des} = \psi \frac{2(M_r / h_o)}{L_b} C_{tR} C_d \quad (2-23)$$

where  $M_r$  is the total sum of all the required moments in the beams being stabilized by the shear panel, and  $\psi$  is equal to  $1/\phi = 1/0.75$  in LRFD and  $\Omega = 2$  in ASD.

Furthermore, the most general expression for the AISC beam shear panel (relative) bracing strength requirement can be written nominally as

$$V_{br} = \frac{0.004(M / h_o)}{\left(2 - \frac{\beta_{br}}{\beta_{act}}\right)} C_{tR} C_d \quad (2-24)$$

and for design as

$$V_{br\ des} = \frac{0.004(M_r / h_o)}{\left(2 - \frac{\beta_{br}}{\beta_{act}}\right)} C_{tR} C_d \quad (2-25)$$

The following observations can be made from Equations (2-22) through (2-25):

- Their focus is on shear panel stiffness and shear force requirements within a given unbraced length. The shear force being considered is a shear force orthogonal to the axis of the column; hence, if one is considering diagonal bracing of a truss panel, the force in the diagonal must be resolved statically from this panel shear force.
- The derivation is general and applies to any variable unbraced length as well as variable shear panel stiffnesses, within the limits of the assumption that the shear panels are backed up by a rigid support system (i.e., there is no “flexing” of the bracing system with the members that are being braced, and therefore the bracing system undergoes only shear deformation), and within the limits of the assumption that the beam compression flange is basically “pinned out” at each of the brace locations.
- As  $L_b$  approaches zero, the stiffness requirement goes to infinity. This is due to the fact that the underlying model for shear panel bracing does not recognize the influence of continuity across the brace point locations.
- The above equations are independent of the member section properties. The equations neglect the help of the  $EI_y$ ,  $EC_w$  and  $GJ$  of the member in resisting the brace point displacements.
- The equations indicate that there is no impact of moment gradient effects other than via the inflection point “double-curvature” parameter  $C_d$ .
- Although AISC requires a minimum relative bracing stiffness of  $\beta_{req} = \beta_{br} = 2\beta_i$ , the above equations are applicable for bracing stiffnesses less than this value, albeit with the approximation that continuity effects across the brace point are neglected. When considering combined shear panel and torsional bracing stiffnesses, discussed

subsequently, it can be very beneficial to account for a significant reduction in torsional brace stiffness requirements due to a relatively small shear panel bracing stiffness. In addition, in cases where the shear panel bracing stiffness requirement becomes excessive because of the positioning of two brace points that are very close together (typically due to framing considerations unrelated to strength), it can be beneficial to consider the bracing response for  $\beta < 2\beta_i$ . However, in these cases, it would be beneficial to also consider the influence of the continuity of the member across the brace point(s). Therefore, the behavior for  $\beta < 2\beta_i$  as well as  $\beta \geq 2\beta_i$  is considered in the subsequent test simulation studies of this research.

### 2.3 Point (Nodal) Lateral Bracing Requirements

The base column idealization for nodal lateral bracing starts with the assumption of rigid lateral bracing at the member ends (note that this assumption is not part of the shear panel bracing requirements discussed in Section 2.2). Furthermore, the development of the AISC nodal lateral bracing equations stems from an analysis of the elastic stability response of a prismatic column subjected to uniform axial compression, braced by equally-spaced equal-stiffness discrete grounded braces (i.e., glorified elastic springs) along the length of the column. In addition, in contrast to the shear panel (relative) bracing idealization, the fundamental nodal bracing model includes the influence of continuity of the column across each of the brace locations. An example of a column with a single intermediate nodal brace at its mid-height is shown in Figure 2.4. The point where the nodal lateral brace meets the member is signified by the box with an “x” through it.

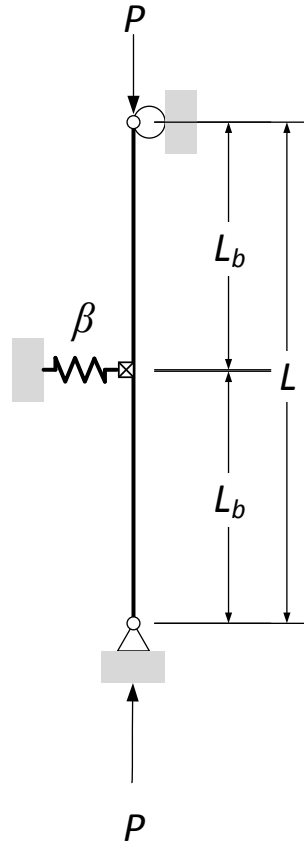


Fig. 2.4. Nodal lateral bracing at the mid-height of a column

Timoshenko and Gere (1961) provide the eigenvalue buckling solution to the governing ordinary differential equation (ODE) for this idealization of a perfectly straight member. The corresponding ideal bracing stiffness solution for “full bracing,” that is the bracing stiffness required to develop the column load corresponding to buckling between the brace points with an inflection point at the brace locations, is closely approximated for any number of intermediate brace points by the equation

$$\beta_{iF} = \frac{\left(4 - \frac{2}{n}\right) P_{eL_b}}{L_b} \quad (2-26)$$

where:

$\beta_{iF}$  = ideal full bracing stiffness for the nodal brace(s),

$n$  = number of intermediate brace points,

$L_b$  = unbraced length, or spacing between the brace points, and

$$P_{eLb} = \frac{\pi^2 EI}{L_b^2} = \text{elastic buckling load corresponding to the unbraced length } L_b.$$

It can be noted from Equation (2-26) that in the limit that the number of intermediate braces,  $n$ , approaches infinity, the required (ideal)\_bracing stiffness is doubled when compared to the requirement for  $n = 1$ . One can understand this behavior as an attribute of having brace points that are located far away from the rigidly braced ends of the member when  $n$  becomes large.

When the member has braces that are located far away from the rigidly-braced ends, the stiffness requirement on these braces is larger. In fact, one can show that for a “non-standard” column case with end lateral braces having one-half the stiffness of the intermediate braces, the ideal full bracing stiffness is the same as that for  $n = \infty$ .

Winter (1958) showed that the above full bracing solution can be reproduced by inserting pins at each of the brace locations and solving for the buckling of the corresponding idealized system. In the case of an initially imperfect column, the ODE solution yields a complicated function for the displacements and internal forces in the column and its bracing system. The specifics of this solution depend on the geometric imperfection assumed in the column. By assuming hinges at each of the brace point locations and assuming an initial imperfect geometry that has the same shape as the governing buckling mode of the idealized column and its bracing system, Winter (1958) developed the following commonly used approximation for calculating

the nodal brace response for situations where the brace stiffness is close to being sufficient to develop the member buckling strength  $P_{eLb}$ :

$$\beta_{act} = \beta_{iF} \left( 1 + \frac{\Delta_o}{\Delta} \right) \quad (2-27)$$

where  $\beta_{act}$  is the actual (or provided) bracing stiffness.

Equation (2-27) also can be expressed as

$$\frac{\Delta}{\Delta_o} = \frac{1}{\left( \frac{\beta_{act}}{\beta_{iF}} - 1 \right)} \quad (2-28)$$

which provides a more direct quantification of the maximum brace point movement under load,  $\Delta$ , given an initial offset  $\Delta_o$  of the brace point from the perfectly straight column position. Given the displacement  $\Delta$ , then similar to the relationships for shear panel bracing, the maximum brace force magnitude is simply

$$P_{br} = \beta_{act} \Delta \quad (2-29)$$

By substituting the above Equation (2-27) for  $\beta_{act}$  into this equation for the brace force, one obtains

$$P_{br} = \beta_{iF} (\Delta_o + \Delta) = \frac{\beta_{iF} \Delta_o}{\left( 1 - \frac{\beta_{iF}}{\beta_{act}} \right)} \quad (2-30)$$

which is the same form as derived previously for the shear panel bracing force.

Given the above equations, then if  $\beta_{act}$  is taken as  $2\beta_{iF}$ , which is the commonly used practice for design of full bracing (i.e., bracing that is capable of developing the theoretical buckling load of the column between the brace points, with an inflection point in the buckling mode at each of the brace locations), then  $\Delta = \Delta_o$ . In this case, for the single intermediate brace case,

$$P_{br} = \beta_{iF} (2\Delta_o) = \frac{2P_{eL_b}}{L_b} (2\Delta_o) \quad (2-31)$$

and if  $\Delta_o$  is taken as  $0.002L_b$ , one obtains

$$P_{br} = 0.008P_{eL_b} \quad (2-32)$$

Based on studies by Plaut (1993) and others, the required brace force for  $n = 1$  has been shown to be slightly larger than  $0.008P_{eL_b}$  due to the P-small delta effects from column curvature and continuity across the brace point location. Based on these solutions,  $0.01P_{eL_b}$  is taken as an acceptable approximation by AISC Appendix 6. For  $n > 1$ , larger brace forces than the above are obtained if  $\Delta_o$  is taken as  $0.002L_b$  in Equation (2-31); however, the above solutions are based on the assumption of an initial imperfection having the same shape as the buckling mode of the column and its bracing system. If the maximum offset of the initial imperfect geometry from the perfectly straight column position is taken as  $0.002L$ , the corresponding maximum out-of-alignment of the column unbraced lengths (given the buckling mode shape of the column and its bracing system) will be much larger than  $0.002L_b$ . Hence, AISC Appendix 6 uses  $0.001P_{eL_b}$  as the brace force requirement approximation for all values of  $n$ .

If one defines the base bracing stiffness requirement as  $\beta_{req} = 2\beta_i$ , and the base brace force requirement as  $0.01P_{eLb}$ , then the brace force requirement for other values of the nodal bracing stiffness is approximated as

$$P_{br} = \frac{0.01P_{eLb}}{\left(2 - \frac{\beta_{req}}{\beta_{act}}\right)} \quad (2-33)$$

using Winter's idealized model (with pins inserted in the column at each of the brace locations). One can observe that Equation (2-33) is very similar to Equation (2-21) for the shear panel brace force.

All of the above equations contain the column elastic buckling load  $P_{eLb}$ . These equations are extended to expressions for the bracing design of any elastic or inelastic column in AISC Appendix 6 basically by setting  $P_{eLb}$  equal to the applied load  $P$ . The assumption behind this substitution is that, in the limit that  $P$  approaches the column inelastic buckling load, the bracing behavior for the inelastic column is similar to that of an elastic column loaded up to  $P_{eLb}$ , but with a reduced effective column flexural rigidity  $EI$ .

In addition, for cases where  $P$  is smaller than the elastic or inelastic buckling load capacity based on  $L_b$ , AISC Appendix 6 allows a substitution for  $L_b$  in the bracing stiffness requirement  $2\beta_{iF}$ , with  $\beta_{iF}$  defined by Equation (2-26). The 2005 AISC Specification Appendix 6 provided a specific variable name,  $L_q$ , for this substitution, where  $L_q$  was defined as the unbraced length that makes the column strength equal to the value of the applied load  $P$ . Mention of the  $L_q$  parameter has been removed from the ANSI/AISC 360-10 Specification, but the same concept is explained within a sentence. The substitution of the term  $L_q$  provides a coarse approximation of

the bracing requirements necessary for the partially braced column strength (i.e., the reduced column strength due to the bracing stiffness being smaller than the full bracing stiffness requirements) to be approximately equal to  $P$ . The AISC Commentary references Lutz and Fisher (1985) for a more refined solution accounting for partial bracing. The Lutz and Fisher developments provide a direct consideration of the influence of column inelasticity in addition to direct calculations of the reduced column strength associated with smaller bracing stiffness values.

The relative bracing column model discussed in Section 2.2 does not make use of the  $L_q$  parameter. This is because the relative bracing model assumes that the column is pinned out at the brace points, and therefore this model does not capture any effects of member continuity across the bracing locations.

#### 2.4 Extension Of Basic Nodal Lateral Bracing Case To Beams

The extension of the column nodal lateral bracing case to beams is obtained simply by substituting

$$P = \frac{M}{h_o} \tag{2-34}$$

in the equations from Section 2.3. In addition, based on the research by Yura (2001), two additional adjustment factors,  $C_{tN}$  and  $C_d$ , are applied in general. These parameters account for the influence of load height as well as the larger demands in the vicinity of inflection points. Their definitions and proper application are summarized in detail by White et al. (2011). This research focuses on the basic case of uniform bending, for which these parameters are both equal

to 1.0. Therefore, the resulting most general equation for the AISC required minimum point (nodal) lateral bracing stiffness is obtained nominally as

$$\beta_{br} = 2 \left( 4 - \frac{2}{n} \right) \frac{(M / h_o)}{L_q} C_{tN} C_d \quad (2-35)$$

and for design as

$$\beta_{br\ des} = \psi \left[ 2 \left( 4 - \frac{2}{n} \right) \frac{(M_r / h_o)}{L_q} \right] C_{tN} C_d \quad (2-36)$$

where  $M_r$  is the total sum of all the required moments in the beams being stabilized by the nodal braces, and  $\psi$  is equal to  $1/\phi = 1/0.75$  in LRFD and  $\Omega = 2$  in ASD.

Furthermore, the most general expression for the AISC beam point (nodal) bracing strength requirement can be written nominally as

$$P_{br} = \frac{0.01(M / h_o)}{\left( 2 - \frac{\beta_{br}}{\beta_{act}} \right)} C_{tN} C_d \quad (2-37)$$

and for design as

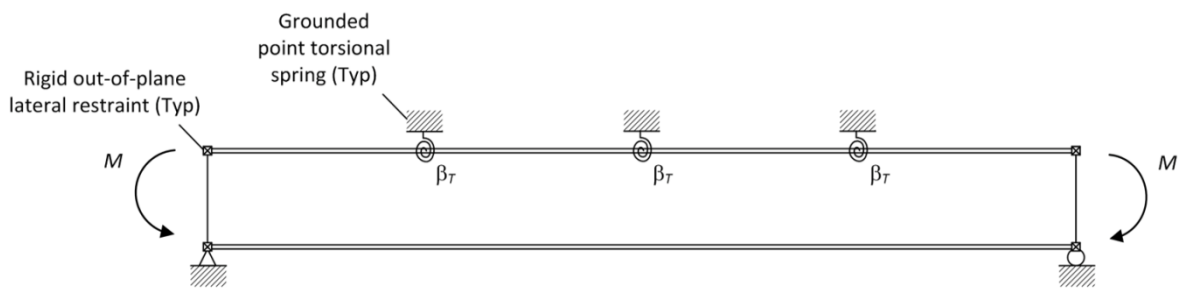
$$P_{br\ des} = \frac{0.01(M_r / h_o)}{\left( 2 - \frac{\beta_{br}}{\beta_{act}} \right)} C_{tN} C_d \quad (2-38)$$

The following observations can be made from Equations (2-35) through (2-38):

- Their focus is on direct nodal lateral bracing stiffness and force requirements normal to the brace points.
- The equations include the help from the  $EI_y$ ,  $EC_w$  and  $GJ$  of the member implicitly and approximately via the  $L_q$  parameter.

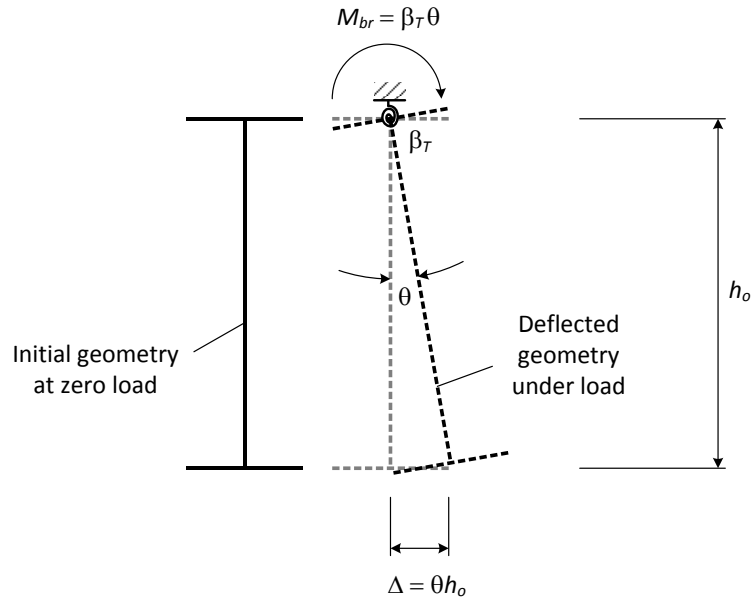
## 2.5 Torsional Bracing Requirements

The base idealization for the AISC torsional bracing requirements is an elastic I-section beam with a continuous torsional restraint on the compression flange (Figure 2.5). The continuous torsional bracing stiffness is lumped based on a tributary length to determine the point (nodal) torsional bracing requirements. The beam is rigidly restrained against twisting and lateral displacement at its ends, but the ends are otherwise free to bend laterally and the flanges are free to warp at the ends. The torsional bracing springs only restrain twisting at the brace points, that is, the beam is free to translate laterally out of the plane of the loading at all of the brace points.



(a) Elevation view

Fig. 2.5. Torsional bracing of an I-beam



(b) Cross-section view

Fig.2.5 (continued). Torsional bracing of an I-beam

Yura (1995) and others have shown that restraint of the relative lateral displacement of the top and bottom flanges of a beam, i.e., restraint of twisting, is sufficient for a point torsional brace location to be considered as a brace point (assuming that the brace has sufficient strength and stiffness). At each of the brace locations, the profile of the beam cross-section is assumed to remain unchanged upon any torsional deflections of the member; that is, distortion of the beam cross-section is assumed to be prevented. Generally, the torsional bracing system must be attached to both flanges of the beam, or the beam cross-section must be sufficiently restrained against distortion by transverse stiffening of the web, for this idealization to be sufficient. Yura (1995) provides important equations that address the influence of beam cross-section distortion by considering the cross-section distortional stiffness as a spring located in series with the spring

representing the actual torsional bracing. Given these caveats, the location of the idealized point torsional springs through the depth of the cross-section is immaterial to the solution.

The derivation of the point torsional bracing stiffness requirements starts with the following equation from Yura et al. (1992) and Yura (2001)

$$M_{cr} = \sqrt{(C_{bu}M_o)^2 + \frac{C_{bb}^2 EI_{eff} \bar{\beta}_T}{C_{iT}}} \quad (2-39)$$

which is an extension of an equation derived by Taylor and Ojalvo (1966) for elastic lateral torsional buckling of a doubly-symmetric I-section member subjected to uniform moment and having continuous torsional bracing along its axis. The above extended equation accounts for moment gradient effects along the member length as well top flange loading effects and single-symmetry of the I-beam cross-section. The terms in this equation are as follows:

$M_{cr}$  = elastic critical moment of the braced beam;

$C_{bu} = C_b$  factor for the unbraced beam, i.e., neglecting any of the torsional bracing along the member length;

$M_o$  = elastic lateral torsional buckling moment of the I-section member without any torsional bracing present along the member length;

$C_{bb} = C_b$  factor for the critical unbraced length of the braced beam, i.e., the unbraced length that governs the elastic lateral torsional buckling moment for the beam, assuming that the torsional bracing is fully effective at each of the brace locations;

$I_{eff} = I_y$  for doubly-symmetric sections and  $I_{yc} + t I_{yt} / c$  for singly-symmetric sections, where

$c$  = the distance between cross-section centroid and the centroid of compression flange,

$t$  = is the distance between cross-section centroid and the centroid of the tension flange,

$I_y$  = weak-axis moment of inertia of a doubly-symmetric section, approximately equal to

$2I_{yc}$  for this type of section,

$I_{yc}$  = lateral moment of inertia of the compression flange,

$I_{yt}$  = lateral moment of inertia of the tension flange;

$\bar{\beta}_T$  = equivalent (or actual) continuous torsional bracing stiffness; and

$C_{iT}$  = torsional bracing factor accounting for the effects of transverse load height.

For cases involving equally-spaced, equal-stiffness, point (nodal) torsional bracing along the member length, Yura et al. (1992) recommend that  $\bar{\beta}_T$  may be expressed in terms of the point torsional bracing stiffness  $\beta_T$  as

$$\bar{\beta}_T = \frac{\beta_T n_T}{\alpha L} \quad (2-40)$$

where:

$\beta_T$  = torsional stiffness of the point (nodal) torsional braces;

$n_T$  = the number of intermediate point torsional braces along the beam length;

$\alpha$  = a calibration factor, equal to 0.75 for a single mid-span torsional brace in beams subjected to centroidal transverse loading, i.e., for beams with a single mid-span torsional brace and in which there are no load height effects, and equal to 1.0 for all other cases; and

$L$  = overall length of the beam between its end rigid lateral braces.

Upon substituting Equation (2-40) for  $\bar{\beta}_T$ , Equation (2-39) may be written as

$$M_{cr} = \sqrt{(C_{bu}M_o)^2 + \frac{C_{bb}^2 EI_{eff}}{C_{iT}} \frac{\beta_T n_T}{\alpha L}} \quad (2-41)$$

This equation can then be solved for the ideal torsional bracing stiffness required to develop a given maximum moment in the beam,  $M_{cr} = M$ :

$$\beta_{Ti} = (M^2 - C_{bu}^2 M_o^2) \frac{C_{iT}}{C_{bb}^2 EI_{eff}} \frac{\alpha L}{n_T} \quad (2-42)$$

The subscript “ $i$ ” is introduced on the torsional bracing stiffness in Equation (2-38) to emphasize that this is the ideal torsional bracing stiffness and the critical moment  $M_{cr}$  is changed to just  $M$  to emphasize that  $M$  is the maximum applied moment level that member and its bracing system need to develop. To obtain the AISC Appendix 6 torsional bracing stiffness requirement, Equation (2-42) is manipulated further by conservatively assuming  $M_o = 0$ , taking  $\alpha = 1$ , recognizing that  $C_{bb} = C_b$ , i.e., the common notation for the beam moment gradient factor, taking

$$L = (n_T + 1)L_b \quad (2-42)$$

and writing

$$\beta_{Tbr} = 2\beta_{Ti} \quad (2-43)$$

Upon substituting and solving for the required torsional bracing stiffness, one can write the AISC Appendix 6 required torsional bracing stiffness nominally as

$$\beta_{Tbr} = \pi^2 h_o^2 \left[ \frac{M/C_b h_o}{P_{ef. eff}} \right] \left[ \frac{M/C_b h_o}{L_b} \right] \frac{(n_T + 1)}{n_T} C_{iT} \quad (2-44)$$

where:

$h_o$  = distance between the centroids of the compression and tension flanges;

$\frac{M}{C_b}$  = equivalent uniform moment for the critical unbraced length within the member span;

$C_b$  = equivalent uniform moment factor for the critical unbraced length;

$\frac{M}{C_b h_o}$  = effective required flange axial force;

$P_{ef. eff} = \frac{\pi^2 E (I_{eff} / 2)}{L_b^2}$  = effective elastic lateral buckling resistance of the beam compression

flange based on the unbraced length between the torsional braces, equal to  $\frac{\pi^2 E I_{yc}}{L_b^2}$  for a doubly-

symmetric I-section, where  $I_{yc}$  is the lateral moment of inertia of the compression flange;

$n_T$  = number of intermediate torsional braces along the beam length; and

$C_{iT}$  = torsional bracing factor accounting for the effects of the height of any transverse loads relative to the depth of the member cross-section.

For design, the moment  $M$  is replaced by the required resistance,  $M_r$ , determined from a structural analysis for the LRFD or ASD load combinations, and Equation (2-44) is pre-multiplied by  $\psi = 1/\phi = 1/0.75$  for LRFD and  $\psi = \Omega = 3.0$  for ASD ( $\Omega$  is usually taken as  $1.5 / \phi$ ;

however, it is taken as  $1.5^2 / 0.75 = 3.0$  in this case since the moment term appears twice in the equation). The resulting design equation is

$$\beta_{T\ br\ des} = \psi \pi^2 h_o^2 \left[ \frac{M_r / C_b h_o}{P_{ef,eff}} \right] \left[ \frac{M_r / C_b h_o}{L_b} \right] \frac{(n_T + 1)}{n_T} C_{iT} \quad (2-45)$$

Equation (2-45) for  $\beta_{T\ br\ des}$  gives identical results to a corresponding equation presented in the AISC Appendix 6 Commentary. However, the format of Equations (2-44) and (2-45) emphasizes an important characteristic of the required torsional bracing stiffness. The required stiffness is highly dependent on elastic continuity effects of the beam across the brace points, which are assumed in the underlying derivation. The influence of these effects is captured within the term  $P_{ef,eff}$ . For relatively short unbraced lengths, such as those associated with beams that fail by inelastic buckling or by “plastic buckling” (where the beam strength is equal to the “plateau resistance,”  $M_p$  for compact I-section members),  $P_{ef,eff}$  becomes relatively large. This results in a significantly reduced torsional bracing stiffness requirement. An appropriate academic question is: how does member inelasticity influence the accuracy of this equation?

The torsional brace stiffness requirement may be expressed as an equivalent required *relative* or *shear panel* brace stiffness (between the flanges of the I-section) by dividing  $\beta_{T\ br}$  by  $h_o^2$ . This equivalence is demonstrated in Figure 2.6. This equivalent relative brace stiffness is utilized throughout this research, since it facilitates various considerations related to the behavior of torsional bracing versus lateral bracing as well as assessment of the interaction between combined torsional and lateral bracing.

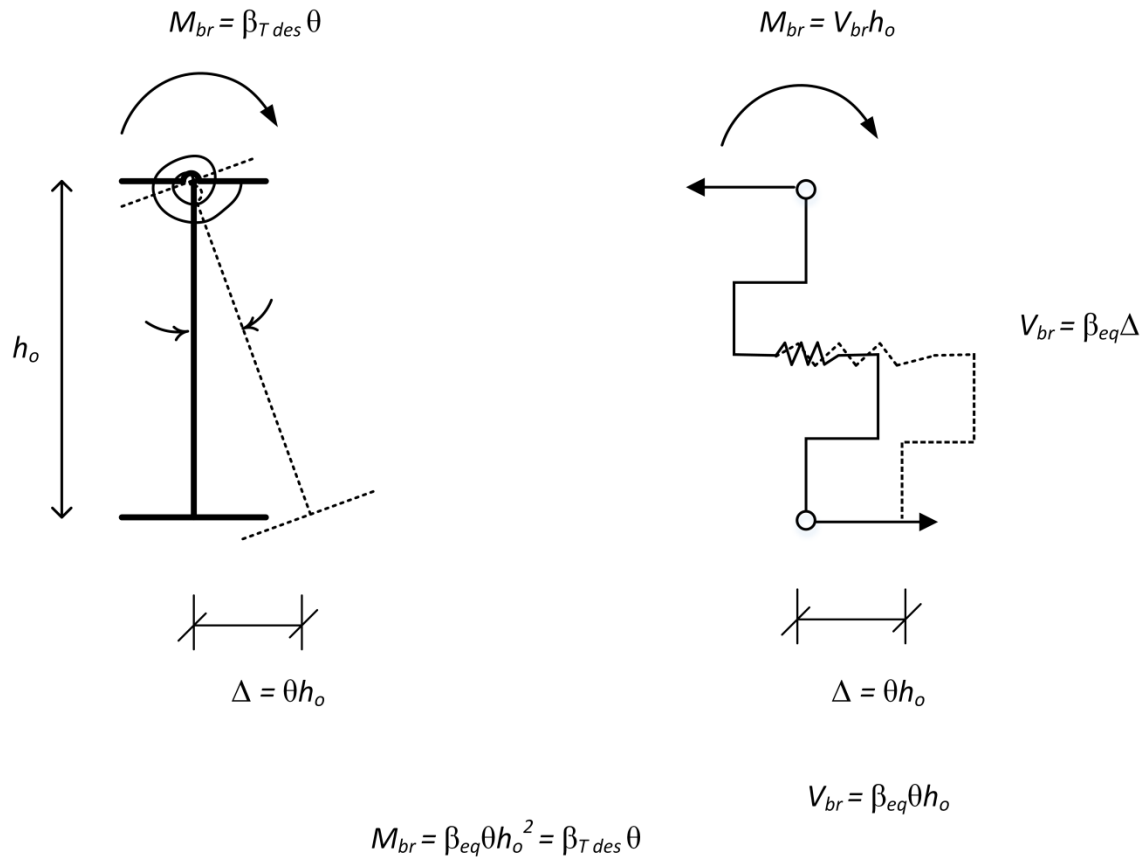


Fig. 2.6. Relative brace between the top and bottom flanges equivalent to a torsional brace

Given the required nominal torsional bracing stiffness from Equation (2-44), the corresponding torsional brace force (moment) requirement is determined by assuming that the twist rotation at the torsional brace is  $\theta = \theta_o$ . This is an ad hoc assumption, consistent with the assumptions commonly used for full bracing design when a minimum required bracing stiffness equal to two times the ideal bracing stiffness is used. However, the torsional bracing behavior generally is not identical to the relative or nodal lateral bracing response. Therefore, the nature of this approximation merits further investigation, which is one of the goals of this research.

By invoking the above assumption of  $\theta = \theta_o$  and using the basic linear elastic constitutive relationship between the maximum torsional brace moment and the maximum torsional brace rotation, one obtains

$$M_{br} = \beta_{Tbr} \theta_o \quad (2-46)$$

in terms of the required nominal brace stiffness, or

$$M_{br des} = \frac{\beta_{Tbr des}}{\psi} \theta_o \quad (2-47)$$

in terms of the required design brace stiffness. The ANSI/AISC 360-10 Appendix 6 Commentary uses these expressions along with the definition of the initial maximum imperfection at any of the torsional braces of

$$\theta_o = \frac{L_b}{500h_o} \quad (2-48)$$

for the most refined calculation of the required strength of the torsional braces. Conservative approximations are introduced to obtain the expression listed for the required torsional bracing strength in the body of the Specification. For short unbraced lengths representative of inelastic or plastic buckling conditions, the required brace strength obtained from the above Commentary provisions can be substantially smaller than the required brace strength obtained using the corresponding Specification equation.

It should be emphasized that, in general, it is essential to consider the influence of cross-section distortion on the effectiveness of torsional bracing. Yura (2001) proposes an approach in which the distortional stiffness of the web and the torsional brace stiffness are considered as springs in series. If the distortional flexibility of the beam cross-section is excessive, this model

can indicate appropriately that no amount of physical torsional bracing stiffness is adequate to brace the beam. In these cases, the beam cross-section must be stiffened at the brace points to alleviate the distortional flexibility problem. The reader is referred to Yura (2001) for details of these calculations.

In this research, it is assumed that the torsional bracing is attached to both the tension and the compression flanges of the beam, as would be the case with direct attachment of diagonal bracing and girts or purlins to each of the flanges. As such, the torsional bracing responses can be evaluated directly using the above equations, without any consideration of cross-section distortion effects. It should be noted that, in general, all sources of torsional bracing flexibility (e.g., bending flexibility of girts or purlins, axial flexibility of flange diagonals, and flexibility of the connections of the girts/purlins and flange diagonals to the member that is being braced) must be considered in assessing a given bracing system.

## 2.6 Fundamental Definition of Terms

At this stage, given the detailed summaries of the various approximate equations used by Appendix 6 of the ANSI/AISC 360-10 Specification, it is useful to review and emphasize the definitions of several key terms associated with stability bracing behavior and design:

- *Full bracing* = bracing that has sufficient stiffness and strength to develop the maximum member buckling resistance based on a buckling effective length equal to the unbraced length between the brace points. For prismatic members braced by equal-stiffness, equally-spaced point (nodal) braces, full bracing produces a buckling mode in which the member buckles in alternate directions in adjacent unbraced lengths and has inflection points at each of the brace locations. Full bracing can refer to an ideal member buckling

resistance, or it can refer to the nominal or design buckling resistance of the physical member having generally unavoidable initial imperfections.

- *Partial bracing* = bracing that does not have sufficient stiffness to ensure development of the maximum member buckling resistance based on an effective length equal to the unbraced length between the brace points.
- *Ideal bracing stiffness* = the bracing stiffness at which the member and its bracing system will buckle at the specified applied load level, assuming an ideal situation in which the member is perfectly straight in its initial geometry under zero load.

Depending on the nature of the approximations inherent in the basic bracing models, the ideal bracing stiffness may or may not depend on the actual cross-section rigidities (e.g.,  $EI$ ,  $EC_w$ ,  $GJ$ ) of the member being braced. For shear panel (relative) bracing, the ideal bracing stiffness (equal to one-half of the required bracing stiffness in Equation (2-22)) is independent of the member cross-section rigidities. Also, for full nodal bracing, the ideal bracing stiffness (equal to one-half of the required bracing stiffness in Eq (2-35), and with  $L_q$  taken as  $L_b$ ) is independent of the member cross-section rigidities. However, for torsional bracing, the ideal bracing stiffness for full bracing, which is equal to one-half of the required stiffness given by Equation (2-44) depends on the equivalent lateral rigidity of the cross-section,  $EI_{eff}$ , where  $I_{eff}$  is defined just after Equation (2-39). The ideal bracing stiffness is typically not considered sufficient to develop the full bracing resistance of a physical, geometrically imperfect member.

- *Ideal full bracing stiffness* = the ideal bracing stiffness sufficient to develop the buckling resistance of the ideal geometrically perfect member based on an effective length equal to the unbraced length between the brace points. This buckling resistance is often taken

as a theoretical elastic buckling resistance in the derivation of the bracing equations; however, the underlying ideal full bracing stiffnesses in Appendix 6 of the ANSI/AISC 360-10 Specification correspond to the hypothetical theoretical elastic or inelastic buckling resistance of the member.

- *Ideal partial bracing stiffness* = an ideal bracing stiffness sufficient to develop a given applied load level smaller than that corresponding to the fully-braced member buckling load just prior to the onset of buckling of the member and its bracing system.

Traditional shear panel (relative), point (nodal) and torsional bracing developments require that a bracing stiffness of 2x the ideal full bracing stiffness be used to ensure development of the full bracing strength of physical members. However, studies by Tran (2009) and by Bishop (2013) have shown that in certain situations, the full bracing strength of a physical geometrically imperfect member can be achieved using bracing stiffnesses that are approximately equal to or only slightly larger than the full ideal bracing stiffness. The studies conducted in this research delve more deeply into these bracing stiffness requirements and the general behavior of the different types of bracing over a wide range of stiffness values.

## 2.7 Bracing Stiffness Interaction

The impact of using both beam nodal lateral and nodal torsional bracing in combination, thus restraining both the lateral movement of the compression flange as well as the overall twisting of the member cross-section at the brace locations, has been considered in a few isolated studies in prior research. Yura et al. (1992) reviewed previous research solutions and showed that combined nodal lateral and nodal torsional bracing is more effective than when either of the bracing types are implemented independently with regard to enhancing the elastic buckling

strength of beams. They showed that a linear interaction between the nodal lateral and nodal torsional brace stiffnesses provides a conservative representation of the combined ideal full bracing stiffness requirements for elastic beam members. In addition, they generalized equations from prior research by considering the influence of cross-section distortion. However, the impact of the combined bracing on the bracing strength requirements was not considered. Furthermore, the lateral bracing was assumed to be placed on the compression flange. As noted previously in Section 1.1, it is common for lateral bracing to be located on the tension flange when members supporting wall or roof systems, and in which lateral bracing is provided from the wall or roof system, are subjected to moments causing flexural compression on the member's "inside" flange.

Tran (2009) conducted elastic eigenvalue buckling studies on several representative beam members having combined nodal lateral and nodal torsional bracing and subjected to both "positive" and "negative" bending. He showed that the bracing stiffness interactions are indeed very different depending on the sign of the bending moment. Tran (2009) also conducted a number of test simulation studies on example beam members with combined nodal lateral and nodal torsional bracing and having initial geometric imperfections, considering the physical elastic and inelastic load-deflection response of the members. He found that light lateral bracing in combination with torsional bracing can be very effective in reducing the torsional bracing demands. However, the studies were not extensive enough to provide any substantive design recommendations.

To the knowledge of the author, none of the prior research investigations have considered combined shear panel (relative) lateral and nodal torsional bracing.

The current research seeks to study the behavior of combined point (nodal) lateral and point torsional bracing, as well as combined shear panel (relative) lateral and point torsional bracing for both positive and negative uniform moment loadings for a reasonably complete range of beam cases. Recommendations are provided for the combined bracing stiffness and strength requirements based on these studies.

## 2.8 Maximum Strength Knuckle Curves and Brace Force versus Brace Stiffness Curves

The “knuckle curve” is one of the primary characterizations used in prior research for assessing the behavior of stability bracing. Knuckle curves are basically plots of member strength versus a stiffness of the bracing system. The term “knuckle curve” was first coined by Horne and Grayson (1983). This terminology stems from the shape of the curve – flat or horizontal when the bracing stiffnesses are sufficiently large, but showing a dip in strength, i.e., a “knuckle,” as the bracing stiffnesses are reduced.

In much of the prior research, knuckle curves are often used to convey a theoretical elastic or inelastic buckling resistance as a function of the brace stiffness, although they are not always referred to by this name. However, knuckle curves showing the maximum strength or limit load of physical members having initial geometric imperfections and initial residual stresses are potentially of greater value to the assessment of the impact of different characteristics of stability bracing for design. This is because, for strength limit states design, one is ultimately interested in the maximum strength behavior of the physical geometrically imperfect elastic/inelastic member or structure.

Direct experimental assessment of physical members and their bracing systems is important to establish the qualities and limitations of different theoretical developments. However, direct and comprehensive experimental assessment of stability bracing behavior is

difficult. This is because the force demands on stability bracing are largely dependent on the geometric imperfection pattern in the member or structure that is being braced. It is difficult and relatively expensive to construct stability bracing tests with the critical geometric imperfections fabricated into the member or structure. Refined finite element methods provide a more economical and practical means of simulating these types of physical tests. Maximum strength knuckle curves can be produced readily using carefully constructed models and advanced finite element tools.

Maximum strength knuckle curves are generally more laborious to produce compared to knuckle curves based on theoretical buckling loads. This is because determining the maximum strength of a geometrically imperfect member or structure having initial residual stresses and finite yield strength requires a full nonlinear load-deflection analysis. In contrast, knuckle curves for the theoretical buckling strength only require a simpler eigenvalue buckling analysis. However, test simulation load-deflection analyses also provide a direct assessment of the internal force demands induced in the bracing system; eigenvalue buckling analyses do not provide any direct information about the bracing system strength demands.

Figure 2.7 shows an example maximum strength knuckle curve. The specific numerical values for the abscissa and ordinate are immaterial to the discussion at this point. Generally, maximum strength knuckle curves always asymptote to a horizontal line, corresponding to the maximum resistance of the “rigidly braced” structure, as the bracing stiffness is increased. Depending on the specific bracing characteristics, the “knuckle” can involve a very gradual or a more abrupt asymptotic approach to the “rigidly braced strength.” At the other end of the knuckle curve, that is, as the bracing stiffness approaches zero, the knuckle curve gives the

maximum strength of the member or structure in the absence of any of the bracing being considered in the problem solution.

Given the above characteristics of the maximum strength knuckle curves, the question can be raised as to what is the “full bracing strength” and what is “full bracing stiffness.” Upon a first look at the problem, one might consider that the full bracing strength is the strength corresponding to rigid bracing.

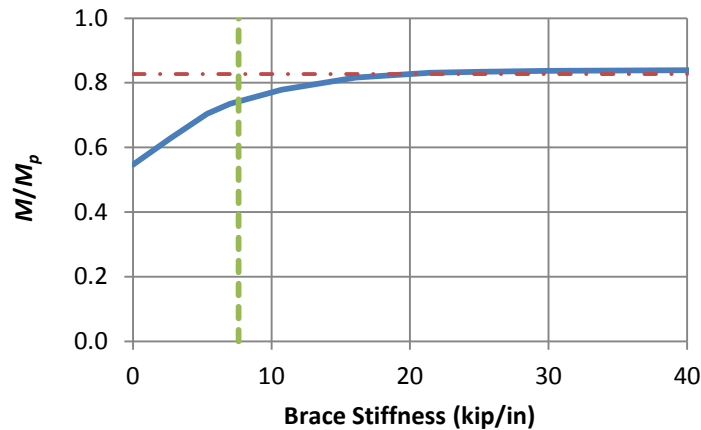


Fig. 2.7. Example maximum strength knuckle curve

However, this definition would then mean that the brace stiffness must be infinite in order to develop the full bracing resistance. A more appropriate definition of the full bracing strength, in the context of the maximum strength knuckle curves, is the strength corresponding to a particular fraction of the resistance of the rigidly braced member or structure. Values for this limit that have been considered in the literature range as low as 0.9, or 90 % of the resistance corresponding to the use of rigid bracing (e.g., see Stanway et al. (1992a & b)). In addition, depending on the specific type of bracing (i.e., lateral on just the compression flange, torsional, or combined lateral and torsional, providing lateral restraint to both the compression and tension flanges), and depending on attributes such as the number of unbraced lengths or the number of

intermediate braces within the member span, the rigidly braced member strengths can be slightly different. In this research, full bracing is defined in the context of a range of maximum strength knuckle curves as 98 % of the rigidly braced member resistance for the bracing configuration giving the smallest rigidly braced strength. For the beam cases studied, this bracing configuration is commonly torsional bracing with only one intermediate brace location.

It is useful to consider the ideal bracing stiffness associated with the above rigid bracing strength as an important index for bracing design. That is, given the above rigid bracing strength, what value is obtained by substituting the corresponding moment into the previously derived Equations (2-22), (2-35), and (2-44), divided by a factor of 2.0 (to convert from the base required stiffness to the ideal bracing stiffness). This stiffness may be shown by a vertical line on the knuckle curve plot (e.g., the dashed green vertical line in Figure 2.7). One can then ascertain what multiple of this so called “ideal bracing stiffness” is required to achieve the defined “full bracing strength.”

In addition to the use of maximum strength knuckle curves, it is common to consider companion plots of the brace force at the limit load of the member or structure versus the bracing stiffness in the literature. Figure 2.8 shows an example plot of this type. The brace force is commonly expressed as a percentage of the equivalent compression flange force ( $M/h_o$ ) in beam-type problems. Similar to the discussions of Figure 2.7, the specific numerical values in Figure 2.8 are immaterial to the present discussion. It is useful to locate the ideal brace stiffness on this plot, shown as the left-most vertical line in Figure 2.8, and to consider the magnitude of the brace forces as a function of different fractions or multiples of this stiffness. The right-hand vertical line in Figure 2.8 corresponds to two times the ideal bracing stiffness. Estimated base strength requirements, such as obtained from Equations (2-24), (2-37) and (2-46), can be compared to the

force requirements indicated from the test simulations. The horizontal line in Figure 2.8 shows an example calculation obtained from Equation (2-46).

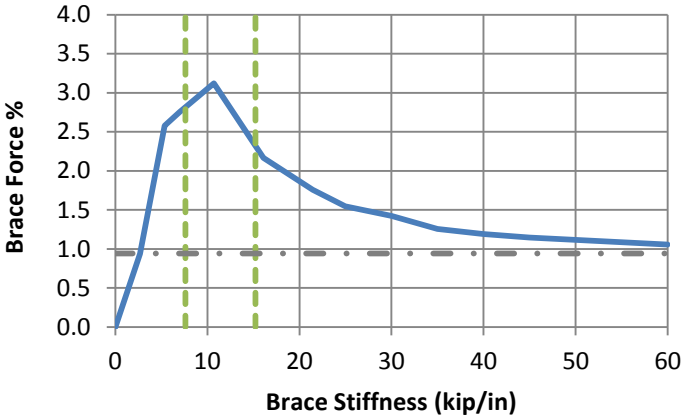


Fig. 2.8. Example brace force versus brace stiffness curve

## CHAPTER 3

### FINITE ELEMENT PROCEDURES

#### 3.1 General Modeling Considerations

The test simulation studies conducted in this research are directed at modeling the overall load-deflection response up to and beyond the peak load capacity of various member and bracing configurations, considering the influence of initial geometric imperfections, residual stress effects, and the overall spread of plasticity throughout the volume of the members. The members are modeled using shell finite elements, and thus the FEA models are capable of capturing general overall member buckling, local buckling and distortional buckling influences as applicable for the cases studied. The different bracing components are modeled generally using elastic spring elements.

Figure 3.1 shows a representative example of a particular study case, case A110, described in more detail in the Chapter 4 presentation of the overall study design. This member has a single intermediate lateral brace at its mid-span ( $n = 1$ ), subdividing the member into two unbraced lengths with  $L_b = 5$  ft. The axial load applied to the member is zero in this example ( $P=0$ ), as well as in all the cases studied in this research. However, the broader research program in which this study is a part considers the bracing behavior for members subjected to combined bending and axial load. Equal and opposite bending moments are applied at the ends of the beam by concentrated longitudinal axial forces located at the web-flange juncture. Multi-point constraints are applied at the member end cross-sections to enforce Vlasov kinematics at these locations. That is, plane sections are constrained to remain plane in the web as well as in the

flanges at the member ends, but the flanges are allowed to rotate freely and independently about a vertical axis through the web. Therefore, warping of the flanges is completely unrestrained at the member ends. The specific multi-point constraint equations are specified in detail by Kim (2010). Because of the application of the multi-point constraints at the member ends, the application of the loads as shown in Figure 3.1 does not result in any stress concentrations.

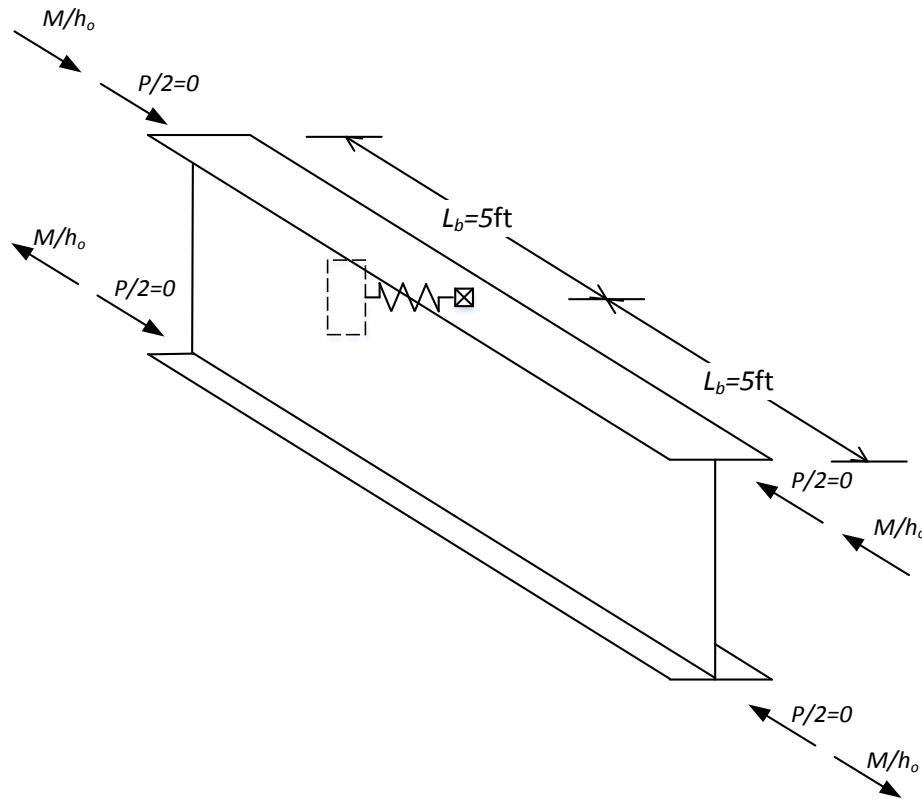


Fig. 3.1. Representative example beam study case, case A110, a 10ft long I-section member with a single intermediate nodal lateral brace ( $n = 1$ ) at the mid-span of the top flange creating two equal unbraced lengths of  $L_b = 5$  ft

The above member is supported at one end in the plane of bending by constraining the vertical and longitudinal displacements to zero at the bottom web-flange juncture, and at the other end in the plane of bending by constraining just the vertical displacement to zero. The lateral (out-of-plane) displacements at the member ends are constrained to zero at each web-

flange juncture and throughout the height of the web. The vertical displacement of all points on the top and bottom flange are constrained to be equal to the vertical displacement at the corresponding web-flange juncture at each end of the member, such that there is no distortion of the cross-section profile at the member ends. The mid-span lateral bracing is modeled by an elastic grounded spring attached to the beam at the top web-flange juncture. Self-weight of the member is not included in the analysis.

The general purpose finite element software system ABAQUS version 6.13 (Simulia 2013) is used throughout these studies. The four-node S4R shell element is used to model both the flanges and the web of the member. The S4R element is a general purpose large strain quadrilateral element which uses a single point numerical integration over its area combined with an algorithm for stabilization of the corresponding spurious zero-energy modes. Twelve elements are used across the width of the flange and sixteen elements are used through the depth web. An aspect ratio of 1 to 1 is implemented for all the elements in the web. The flange elements maintain the same length dimensions as the web elements along the longitudinal direction of the member. Specific benchmark studies conducted at the beginning of this research indicate that this mesh density is sufficient to provide a converged solution for all the attributes of the nonlinear responses considered in this work. A five point Simpson's rule is applied for integration of the stresses through the thickness of the shell element. Early benchmark studies have shown that this discretization also is sufficient for convergence of the test simulation results. The Riks method is used to perform the incremental-iterative non-linear load-deflection analyses.

Residual stresses are implemented via a user-defined Fortran subroutine. Geometric imperfections are introduced by performing a pre-analysis on the member in which displacements corresponding to the desired geometric imperfection pattern are imposed at various control points and the member is allowed to elastically deform between these points, The deflections from the pre-analysis are then applied as an initial imperfection on the geometry of the member at the zero load condition in the subsequent test simulation load-deflection analysis. The member is taken as stress- and strain-free in this initial imperfect geometry, with the exception of the residual stresses, at the beginning of the test simulation. Force equilibrium is not strictly maintained when the residual stresses are introduced on the imperfect member geometry. The residual stresses are self-equilibrating only on the perfect geometry of the member. As such, a first step of the test simulation analysis is conducted in which the residual stresses are allowed to equilibrate. This is followed by a second step of the test simulation analysis in which load is applied to the member.

Generally, it is essential that the load increment size in the vicinity of the member limit loads is relatively small such that the displacements at the braced member limit load can be accurately determined. The load-displacement response is by definition relatively flat in the vicinity of the limit load. Generally, it is desired to recover the various brace displacements (and hence the brace forces, since the brace forces are proportional to the brace displacements) at the limit of resistance of the braced member. This is so that the maximum brace force required to develop the member limit load can be determined as a function of bracing configurations and bracing stiffness values. The Riks algorithm in ABAQUS employs a wide range of internal heuristics that vary the increment size as a function of the problem nonlinearity. It was determined generally that, to ensure a “very close” set of equilibrium solution data points in the

vicinity of the limit load, using ABAQUS version 6.12, it is necessary to use a starting size of the load incrementation on the order of 1.5 % of the expected member limit load. This results in a large number of increments that are essentially elastic, but leads to a reliable small increment size for determining the brace forces at the member limit load. Procedures could be implemented to avoid the initial small elastic load increments, such as by dividing the application of the load into two steps and using a larger initial load increment size for the first of these steps; however, the author opted for the simplicity of just having ABAQUS quickly increment through these elastic steps in this research.

### 3.2 Modeling of Braces

Abaqus provides two types of spring elements which are used to simulate the behavior on a member caused by bracing elements in the study. All the bracing spring elements are modeled as linear elastic in this research. Point (nodal) lateral bracing is simulated with the spring type 1 in ABAQUS, which is a grounded spring element. Shear panel (relative) bracing is simulated with the spring type 2 in ABAQUS, which is a spring element that resists relative displacements in a specified lateral direction between different points on the FEA model. In addition, nodal torsional bracing is implemented via the use of the spring type 2 element. As illustrated in Figure 2.6, torsional bracing may be modeled efficiently by using this type of spring element.

### 3.3 Material Properties

The material properties of the steel are modeled in all the test simulation studies of this research using the stress-strain curve shown in Figure 3.2. All the members are assumed to be homogenous and the yield stress of the steel,  $F_y$ , is taken as 50 ksi. The modulus of elasticity,  $E$  is taken as 29000 ksi. The material is modeled with a small tangent stiffness within the yield plateau region of  $E/1000$  up to a strain-hardening strain of  $\epsilon_{sh} = 10\epsilon_y$ , where  $\epsilon_y$  is the yield strain

of the material. Beyond this strain, a constant strain-hardening modulus of  $E_{sh} = E/50$  is used up to the ultimate stress level of  $F_u = 65$  ksi. The material is modeled as perfectly plastic beyond this point. The maximum stress reached at the limit load in the test simulations is generally significantly less than the ultimate stress of the steel, therefore justifying this common simplified representation of the stress-strain response.

Since the S4R element in ABAQUS is a large strain formulation, this element actually interprets the input stress versus plastic strain curve associated with Figure 3.2 as the true stress versus log strain response. However, for the maximum strains commonly experienced at the limit load of the test simulation solutions, the difference between the uniaxial true-stress log strain and engineering stress versus engineering strain is small. The stress-strain curve shown in Figure 3.2 is a reasonable representation of the true-stress true-strain response of structural steel for stresses up to the level of  $F_u$ .

### 3.4 Residual Stresses

Residual stresses are introduced into structural steel members by uneven cooling after rolling operations, as well as after flame cutting and welding. Residual stresses are also introduced by operations such as cold straightening of members at the steel mill. One of the most commonly accepted models for the nominal residual stresses in hot-rolled structural steel I-section members is the Lehigh residual stress pattern shown in Figure 3.3.

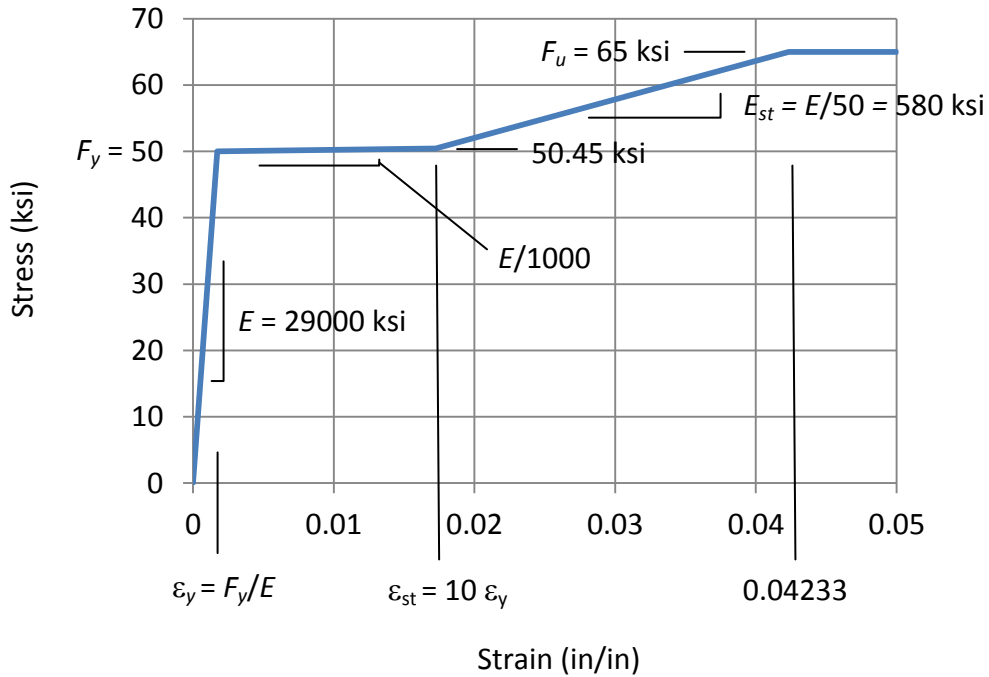


Fig. 3.2. Steel stress-strain curve assumed in the structural analysis

This pattern has a constant residual tension in the web and a self-equilibrating stress distribution in the flanges with a maximum residual compression of  $0.3F_y$  at the tips of the flanges and a linear variation in stress between the flange tips and the above residual tension value at the web-flange juncture. The residual stresses are constant through the thickness of the flange and web plates. The Lehigh residual stress pattern is typically considered to provide an accurate to relatively conservative assessment of the residual stress effects on the inelastic buckling response of rolled wide flange members.

This is due to the attribute that the flanges contain a net compressive residual force that is balanced by the web residual tension. The Lehigh residual stress pattern is assumed in all of the studies conducted in this research.

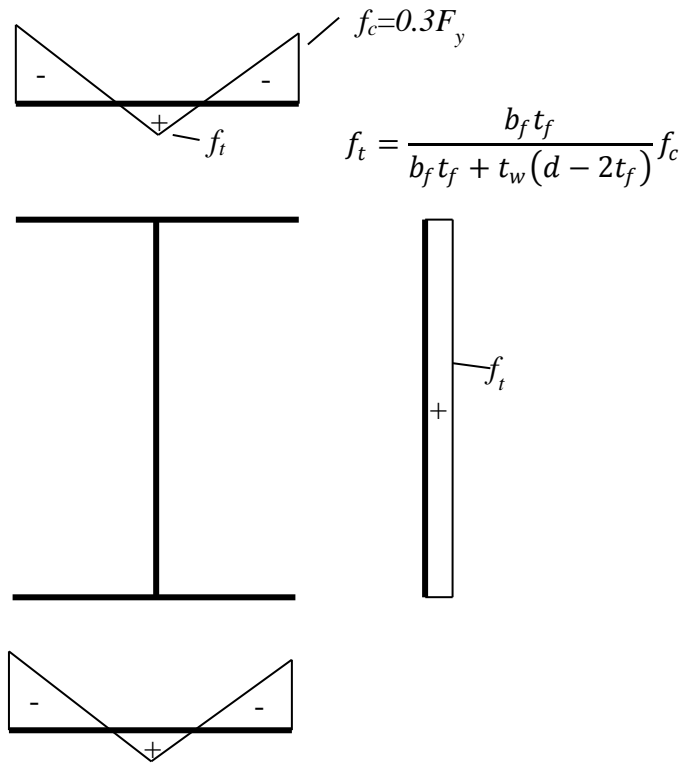


Fig. 3.3. Lehigh residual stress pattern (Galambos and Ketter, 1959)

### 3.6 Geometric Imperfections

Wang and Helwig (2005) found that the largest brace forces in fully-braced beams are produced for all practical purposes by giving the compression flange at the brace point having the largest internal moment an out-of-plane initial displacement, leaving the other brace points at their perfect geometry position and leaving the tension flange straight. Furthermore, to create a maximum out-of-alignment along the compression flange equal to the maximum value of 1/500

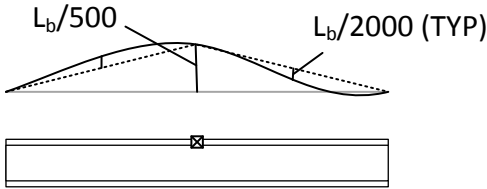
specified in the AISC Code of Standard Practice, this out of plane initial displacement should be  $L_b/500$ . This imperfection is employed for all of the beam studies conducted in this research.

In addition to the above out-of-alignment of the brace points, an out-of-straightness of the compression flange of  $L_b/2000$  is imposed in opposite directions on each side of the above critical brace location in this work. This additional “sweep” of the compression flange is applied to avoid cases where the imperfect geometry is completely symmetric about the critical brace location, thus ensuring that the beam fails ultimately in an “S” shape with an inflection point at the brace locations in the test simulations (assuming full bracing). Cases in which the geometry is completely symmetric about the critical brace point and in which this type of additional out-of-straightness is not modeled can fail in an unrealistic symmetrical mode about the brace, resulting in larger member strengths and brace force demands than would be expected for the physical member. The value  $L_b/2000$  is selected as a reasonable value for the compression flange out-of-straightness that is less than the AISC Code of Standard Practice maximum of  $L_b/1000$  and for which the overall imperfection in the unbraced length where the out-of-alignment and the out-of-straightness are additive is only slightly larger than that obtained if the compression flange were simply allowed to bend between the brace points based on the offset of  $L_b/500$  imposed at the critical brace location.

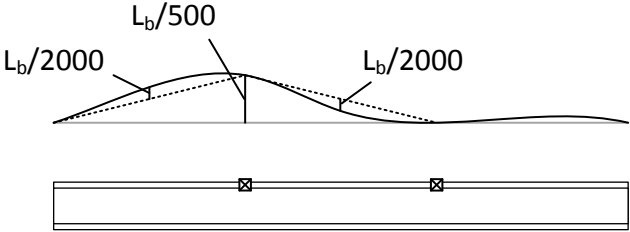
Figure 3.4 shows the resulting lateral imperfection imposed on the beam compression flange for cases with one, two and three intermediate braces considered in this research. As described in Section 3.1, these imperfections are imposed in a pre-analysis by specifying the desired initial lateral displacements of the compression flange at the critical brace point and at the middle of the unbraced lengths on each side of the brace point. In addition, zero lateral displacement is specified at the corresponding locations on the tension flange in this pre-analysis.

In the cases with  $n = 2$  and 3, the compression flange lateral displacement at the middle of the unbraced lengths further removed from the critical brace location are determined from an elastic frame analysis of a prismatic beam with the above displacements imposed at the brace location and the middle of the unbraced lengths on each side of this brace in that analysis. The values for the elastic deflection obtained at the middle of these additional unbraced lengths are imposed on the compression flange of the beam in these unbraced lengths in the ABAQUS pre-analysis.

Figure 3.5 shows the magnified imperfect geometry at the end of the pre-analysis for a member with two intermediate brace points. The contours on the deformed finite element mesh correspond to the magnitude of the lateral displacements.

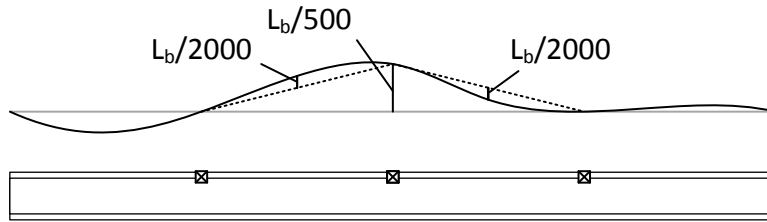


(a) Compression flange imperfection for  $n = 1$



(b) Compression flange imperfection for  $n = 2$

Fig. 3.4. Beam compression flange imperfections utilized in this research



(c) Compression flange imperfection for  $n = 3$

Fig. 3.5. (continued). Beam compression flange imperfections utilized in this research

It should be noted that the above imperfections are focused on cases in which the members are fully-braced, or in which the members are partially braced but the brace stiffness is approaching the full bracing stiffness. For the members with  $n = 2$  or  $3$  and relatively flexible partial bracing, the critical geometric imperfections are generally different. For instance, in the limit that the intermediate brace stiffnesses are zero, the critical geometric imperfection would involve a single sweep of the compression flange along the entire length of the member. The studies in this research are focused predominantly on cases with full or near full bracing.

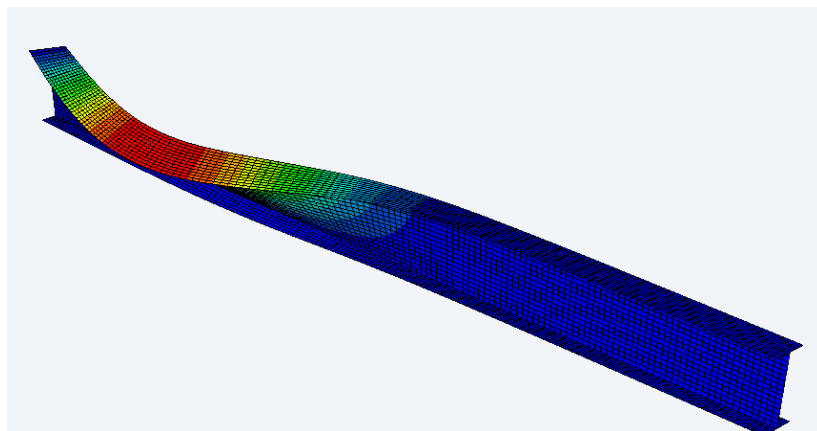


Fig. 3.5. Imperfect geometry for a beam with two intermediate brace points

The above imperfections correspond to beams, which is the sole focus of the studies conducted in this work. However, the bracing of beam-columns is being considered in the broader research program of which this study is a part. Therefore, it is useful to consider how the above geometric imperfections might change when the members are subjected to axial force in combination with bending. For a member subjected solely to concentric axial compression, and assuming full or near-full bracing, the maximum brace forces for column bracing are produced for all practical purposes by giving the brace point the same out-of-plane initial displacement at both flanges (Wang and Helwig, 2005). Generally, the beam lateral bracing checks in AISC Appendix 6 are based on treating the flanges as effective columns subjected to an axial force of  $M/h_o$ . For column bracing, each of the flanges can be idealized as a column subjected to a force of  $P/2$ . Therefore, for positive bending, the “top flange” axial force from combined axial compression and bending, based on the above idealization, is  $P_{f1} = M/h_o + P/2$  (positive in compression), and the corresponding bottom flange axial force is  $P_{f2} = -M/h_o + P/2$ . For members subjected solely to bending (zero axial force),  $P_{f1}/P_{f2} = -1$ . For members subjected solely to concentric axial compression (zero bending moment),  $P_{f1}/P_{f2} = 1$ . Generally, for a beam-column member, one must select an out-of-alignment imperfection for the “bottom flange” (i.e., the flange subjected to flexural tension) that is equal to one or the other of the above imperfections, or is some intermediate value between these imperfections. Figure 3.5 illustrates the possible “paths” for the offset of the bottom flange at the critical brace point in a beam-column.

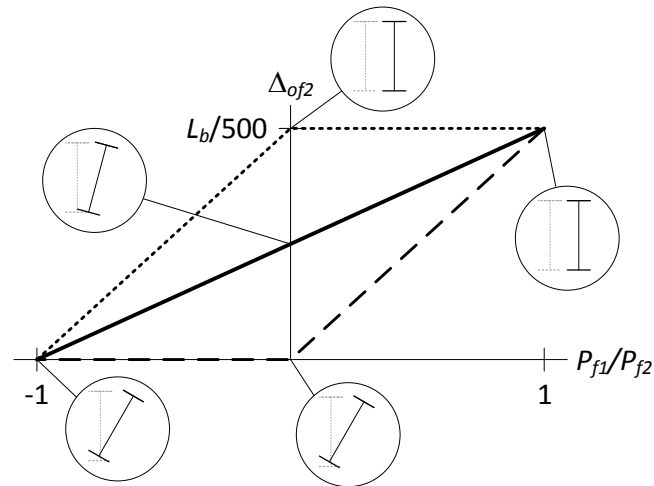


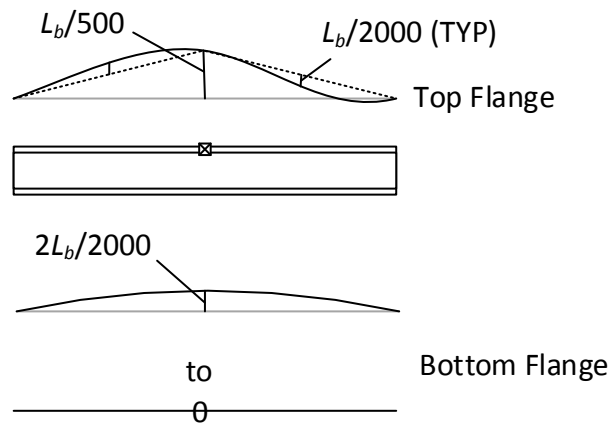
Fig. 3.6. Possible selections for the imperfection in the bottom flange of a beam-column,  $\Delta_{of2}$ , based on the ratio of the flange loads  $P_{f1}/P_{f2}$

The most logical variation in the flange geometric imperfections between the above extremes for a beam member (on the far left of the plot in Figure 3.6) and for a column member (on the far right) is as follows: As long as a flange is in tension under the combined axial force and moment loading, then  $P_{f1}/P_{f2}$  is negative and the flange should be taken to be straight in the initially imperfect geometry. Once the combination of the axial force and bending effects results in a net compression in the flange (i.e., for points to the right of the origin in the above plot), the geometric imperfections should be varied linearly between zero and  $L_b/500$  as a function of  $P_{f1}/P_{f2}$ . These selections correspond to the “path” illustrated by bold dashed line in Figure 3.6.

The rationale for keeping the flange straight as long as it is subjected to a net tension is that the tension force will tend to straighten the flange, if the flange were to have an initial geometric imperfection. The twisting imperfection at a given cross-section is maximized by specifying that the tension flange is straight in the initially imperfect member geometry. This logic can be applied also to specify the out-of-straightness of the flanges.

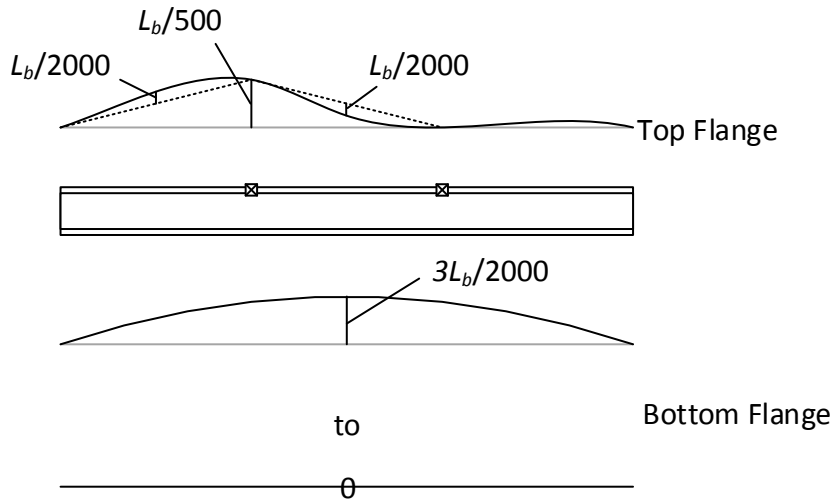
Figure 3.7 illustrates the extension from the beam geometric imperfections shown in Figure 3.4 to the case of general beam-columns subjected to “positive” bending moment, causing compression on the top flange and lateral bracing only on the “top” (compression) flange. Figure 3.7 (a) illustrates the imperfection patterns and magnitudes for members that have a single intermediate brace point. The pattern shown above the member illustrates the imperfection of the top flange. The bottom flange has its imperfection swept as a function of the overall unbraced length of the flange.

Figure 3.7 (b) shows the imperfection pattern used for the above type of member with two intermediate brace points. The left brace is selected arbitrarily as the critical brace location. The right brace point is specified to have zero displacement. Figure 3.7 (c) shows the imperfection pattern for the above type of member with three intermediate brace points. The critical brace point is chosen as the middle brace.

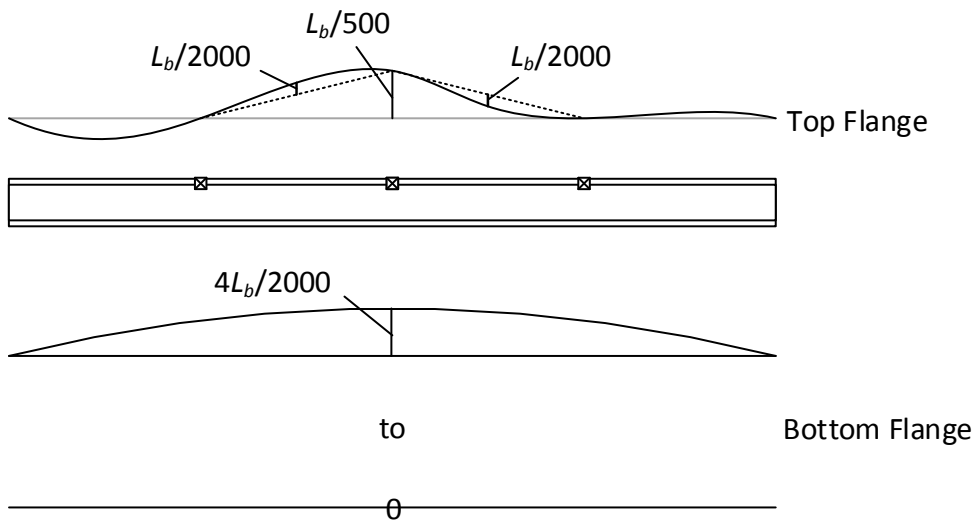


(a) Imperfection pattern for a member with single intermediate brace,  $n = 1$

Fig. 3.7 Imperfection patterns for members with  $n = 1, 2,$  or  $3$



(b) Imperfection pattern for a member with two intermediate brace points,  $n = 2$



(c) Imperfection pattern for a member with three intermediate brace points,  $n = 3$

Fig. 3.7 (continued). Imperfection patterns for members with  $n = 1, 2$ , or  $3$

The top flange is loaded in flexural compression in all of the cases illustrated in Figure 3.7. For cases with moments causing flexural compression on the bottom flange, similar concepts

apply but the patterns are different. Basically, the flange subjected to flexural tension always has its geometric imperfections reduced to zero as the total compression force from combined axial compression and flexure approaches zero in that flange. The flange subjected to flexural compression uses the same out-of-alignment and out-of-straightness imperfection for all values of axial force and moment.

The top flange is assumed to have lateral bracing and the bottom flange does not have any intermediate bracing in the examples shown in Figure 3.7. For cases involving torsional bracing or combined torsional and lateral bracing, the bottom flange imperfection pattern differs from that shown in this figure. In these beam-column cases, assuming the bottom flange is subjected to flexural tension, the geometric imperfection on this flange varies from zero to the imperfection pattern shown on the top flange as  $P_{f1}/P_{f2}$  varies from 0.0 to 1.0. If the bottom flange is in flexural compression, then the bottom flange geometric imperfection pattern is the same for all loadings and the top flange geometric imperfection is varied.

The above bracing imperfections are reasonable values that can be assumed to determine the maximum required strength demands at the critical brace location for full bracing (i.e., bracing that is stiff enough to maximize the member strengths) and for partial bracing approaching full bracing values. For partial bracing situations and two or more intermediate brace points, the critical member imperfections producing the maximum required strength demands at the critical brace location for full bracing can be different, since the failure mode can involve significant brace point displacements. The primary focus of this research is on the behavior for full bracing and for partial bracing approaching full bracing.

# CHAPTER 4

## STUDY DESIGN

### 4.1 Overview

This chapter explains the overall design of a beam bracing test simulation study aimed at addressing the research objectives outlined in Section 1.2. The basic study process is to conduct load-deflection test simulations of a wide range of beam cases with different unbraced lengths, bracing types, bracing configurations and bracing stiffness values. For each of the many test simulations, load versus deflection and load versus brace force curves are generated. The limit load of the different tests and the brace forces at the limit load are collected and plotted as a function of the bracing stiffness for the different cases. The first of these types of plots is commonly referred to as the “knuckle curves,” as discussed in Section 2.8.

The overall study is organized at its highest level according the different major types of bracing to be considered:

Category A: Nodal lateral bracing

Category B: Relative lateral bracing

Category C: Torsional bracing

Category D: Torsional and nodal lateral bracing *in combination*

and

Category E: Torsional and relative bracing *in combination*

The results for Categories A, B and C are addressed subsequently in the individual Chapters 5 through 7, and the results for Categories D and E are addressed in Chapter 8. Within each of these categories, three different member unbraced lengths are considered corresponding to

plastic member buckling (i.e., lateral-torsional buckling after the development of extensive member yielding), inelastic member buckling (lateral-torsional buckling within the intermediate range of the corresponding AISC strength curves), and elastic member buckling. In addition different numbers of intermediate braces are considered to evaluate the effects of member continuity across the brace locations within each of the categories. For Categories D and E, a range of lateral and torsional bracing stiffness ratios is evaluated and bracing stiffness interaction curves are prepared corresponding to the achievement of full bracing. In Categories A and B, the lateral bracing is always placed on the compression flange. Furthermore, in Category C, the sign of the moment is immaterial (assuming a doubly-symmetric I-section member) and therefore only one sign of moment is considered. However, in Categories D and E, both “positive” and “negative” bending are considered, where positive bending corresponds to lateral bracing on the compression flange and negative bending corresponds to lateral bracing on the tension flange.

The next section discusses the study “constants.” This is followed in Section 4.3 by a summary of the main variables considered and the conventions for naming of the different portions of the studies, and Section 4.4, which explains the notation used to identify the different test cases considered in this research. Section 4.5 then presents benchmark studies conducted at the start of the research to ascertain the member lateral-torsional buckling strengths predicted by the test simulation models for uniform moment loading and simply-supported boundary conditions. Lastly, Section 4.6 summarizes the rigid bracing strengths obtained for all of the different bracing conditions, unbraced lengths, and bracing configurations studied in this research. These results are used to establish reference values for assessment of the results in the subsequent chapters.

## 4.2 Study Constants

The constants in the study design of the current research are as follows:

- The steel material is assumed to be A992 Grade 50. The curve shown in Figure 3.2 is representative of the stress-strain characteristics for this material.
- A W21x44 section is adopted as a representative “beam-type” wide flange section (i.e., W sections with  $d/b_f$  greater than about 1.7) for this study. In general, it may be useful to consider the behavior of column-type wide flange sections as well; however, the present studies focus on the bracing of beam-type sections. It is possible that the bracing stiffness and strength requirements will not be sensitive to whether the cross-section is a beam or a column type. The key dimensions and properties of the W21x44 section are  $h_o = 20.25$  in,  $b_f = 6.5$  in,  $t_w = 0.35$  in,  $d = 20.7$  in,  $t_f = 0.45$  in,  $A = 13$  in<sup>2</sup>. (Note that the web elements extend over the depth  $h_o$  between the centroids of the flanges in the FEA model of the W21x44; the overlap of the web elements with the flange elements at the web-flange junctures is approximately equal to the area of the web-flange fillets of the W21x44 section.)
- Rigid out-of-plane bracing is assumed at the member ends (i.e., zero lateral displacement and zero twisting of the member at the ends). Lateral bending and warping of the flanges are free at the member ends.
- Positive or negative uniform-moment is applied to the members in all the cases considered in this research.
- Representative residual stresses are modeled using the Lehigh residual stress pattern as discussed in Section 3.4.
- Representative critical geometric imperfections are modeled as discussed in Section 3.5. For the beam cases studied in this research, this basically involves offsetting the compression

flange laterally relative to the perfect member geometry by  $L_b/500$  at a selected “critical” brace location and imposing a sweep in the compression flange of  $L_b/2000$  in opposite directions on each side of the critical brace location in addition to the above out-of-alignment imperfection. The tension flange of the member is held straight in this imperfect geometry.

- Equally-spaced and equal-stiffness braces are used throughout this work such that the fundamental bracing behavior targeted by Appendix 6 of the ANSI/AISC 360-10 Specification can be assessed.

### 4.3 Study Variables

#### 4.3.1 Unbraced Length and Member Inelasticity

The following unbraced lengths are considered in this study:

- 5 ft ( $\cong L_p = 4.45$  ft),  $L/r_y = 47.6$
- 10 ft (intermediate between  $L_p$  &  $L_r$ ),  $L/r_y = 95.2$
- 15 ft (slightly larger than  $L_r = 13.0$  ft),  $L/r_y = 128.7$

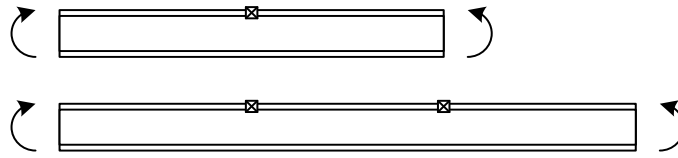
The member is heavily plastified at its ultimate strength condition for  $L_b = 5$  ft. As such, the tests using this length are referred to as plastic buckling tests. The member experiences significant distributed yielding due to residual stress and geometric imperfection effects, in combination with the stability behavior, for  $L_b = 10$  ft. The tests using this length are referred to as inelastic buckling tests. The member stability behavior is dominated by the elastic stability behavior for  $L_b = 15$  ft. However, it should be recognized that the physical test behavior of the geometrically imperfect members is a general three-dimensional load-deflection amplification problem. Members having this length fail after the onset of a relatively minor amount of distributed yielding, which is influenced by the bending of the flanges caused by second-order

amplification of the member initial geometric imperfections. The tests using this length are referred to as elastic buckling tests.

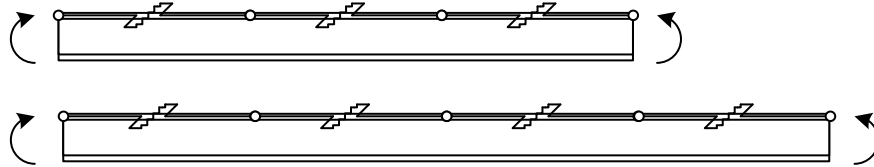
Prior research addressing the effects of member inelastic behavior on the stability bracing requirements is relatively limited. By conducting studies at each of the above unbraced lengths, a more comprehensive understanding of the influence of member inelasticity on the bracing behavior can be achieved.

#### 4.3.2 Number of Intermediate Brace Locations and Member Continuity Effects

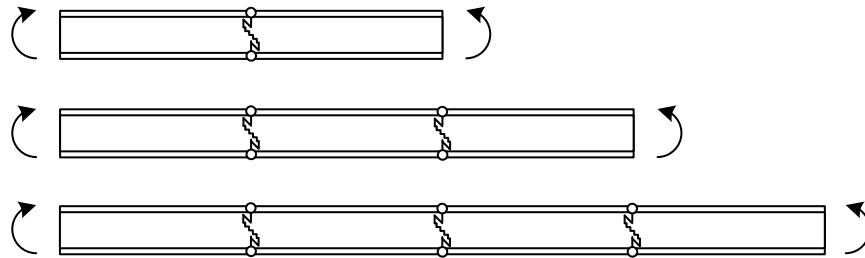
In order to ascertain the impact of member continuity across the brace point locations in the current research, tests with one, two and three intermediate brace points are studied (i.e.,  $n = 1, 2$  and  $3$ ). However, only a partial set of these three values of  $n$  are considered, in general, in the different test categories discussed in Section 4.1. Figure 4.1 illustrates the bracing configurations and the applied moment loadings considered for each category. Figure 4.2 gives a “bracing graphics key” defining the symbols used in Figure 4.1 to illustrate the different types of bracing. Point (nodal) braces are represented by a box with an x through it, shear panel (relative) braces, which resist the relative out-of-plane movement between adjacent brace points along the length of the beam are represented by a graphic illustration of a shear spring, and torsional braces, which resist the relative out-of-plane movement of the top and bottom flanges of the member, are depicted by a similar shear spring graphic but in which the shear spring is oriented vertically. Figure 4.1(a) shows the bracing configurations considered for Category A (nodal lateral bracing). Values of  $n = 1$  and  $2$  are studied for this category. Based on Equation (2-35), one can observe that the largest change in the value of the required bracing stiffness, per AISC Appendix 6, corresponds to varying  $n$  between these values. Figure 4.1(b) shows the bracing configurations considered for Category B of the current research (shear panel lateral bracing).



(a) Category A models



(b) Category B models

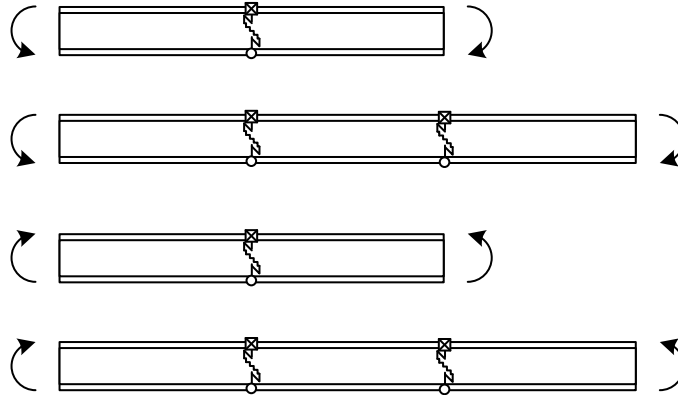


(c) Category C models

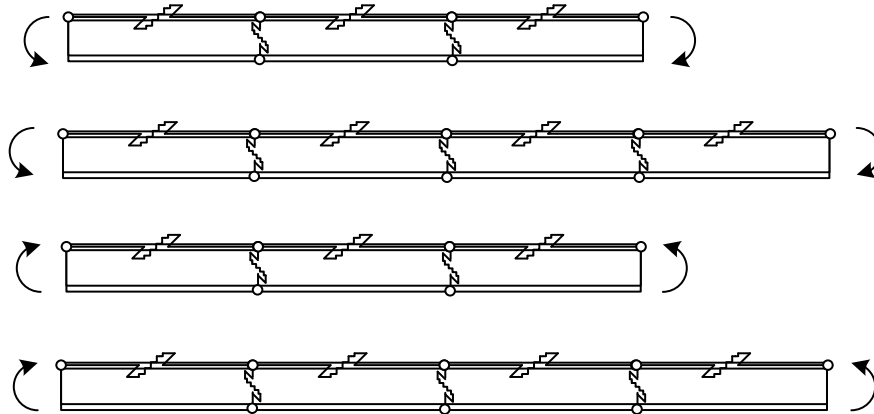
Fig. 4.1. Overview of bracing configurations considered within each test category

Values of  $n$  equal to 2 and 3 are considered for this category. There is no need to consider  $n = 1$  in Category B since the Category A case with  $n = 1$  is fully representative of either nodal lateral bracing or shear panel lateral bracing with  $n = 1$ . For the equivalent shear panel bracing with  $n = 1$ , the shear panels would be specified with one-half of the value of the nodal lateral bracing stiffness. Given the equal stiffness shear panel braces, and given the fact that the shear panel displacements will be equal on each side of the brace location, each of the

shear panel forces must be the same. These forces are always simply one-half of the nodal lateral bracing force for this case.



(d) Category D models



(e) Category E models

Fig. 4.1 (continued). Overview of bracing configurations considered within each test category


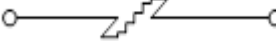

- Nodal Lateral Brace 
- Relative Brace 
- Torsional Brace 

Fig. 4.2. Bracing graphics key

By considering  $n = 2$  and 3 for the shear panel bracing, the test simulation studies can provide an assessment of the influence of member continuity across the brace locations for  $n = 1$ , 2 and 3 relative to the Appendix 6 shear panel bracing equations, which assume that the member is “pinned-out” at each of the brace positions and thus neglect the influence of any member continuity on the bracing response.

Figure 4.1(c) shows the bracing configurations considered for Category C of the current research (torsional bracing). All three values of  $n$  are considered for this category.

Lastly, Figures 4.1(d) and (e) show the bracing configurations as well as the moment loadings considered for Categories D and E, which evaluate the influence of combined nodal lateral and nodal torsional bracing as well as shear panel lateral and nodal torsional bracing. The number of intermediate braces considered in these categories parallels that for the lateral bracing configurations considered in Categories A and B. Both positive and negative bending moments are considered for these cases, whereas only positive bending moment, causing flexural compression on the top flange, is considered for Categories A through C.

### 4.3.3 Ratios of Combined Lateral to Torsional Bracing Stiffnesses and Bracing Lateral versus Torsional Stiffness Interaction

Figure 4.3 shows the selection of the lateral to torsional bracing stiffness ratios for Categories D and E of this research. Basically, the ratios of the lateral and torsional bracing stiffnesses are set at several different values in these Categories, and then the bracing stiffnesses are varied proportionally so that the stiffnesses “fan out” along the dashed radial lines shown in the figure. For the positive bending cases, the results from Categories A through C serve as another set of “ratios” that plot along the horizontal and vertical axes of the plots in Figure 4.3. However, for the negative moment cases, lateral bracing on the tension flange is essentially ineffective as the torsional brace stiffness approaches zero, and therefore, there is no effective point on the vertical axis of these plots for negative moment loading.

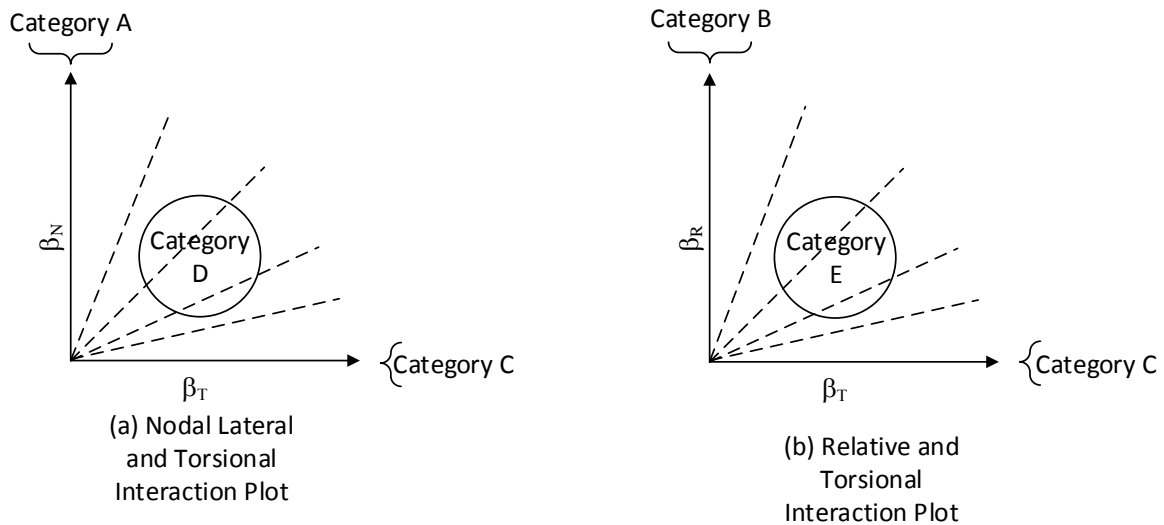


Fig. 4.3. Test design selection of lateral to torsional stiffness ratios for Categories D and E

#### 4.4 Naming Convention for Test Cases

The following naming convention is adopted to identify the different test cases considered in this research:

- The test name starts with a letter designation corresponding to the test categories described in Section 4.1.
- The second character of the name is the number, 1, 2 or 3. This number denotes the unbraced length, 1 for  $L_b = 5$  ft, 2 for  $L_b = 10$  ft and 3 for  $L_b = 15$  ft.
- The third character of the name is the number 1, 2 or 3. This number denotes the number of intermediate brace points considered in the test.
- The fourth character of the name is generally 0 in all of the test cases considered in this research. This character is reserved for the designation of axial load levels in the beam-column studies being conducted in the broader research program of which this study is a part.

The above constructions constitute the full test case names for all of the Category A, B and C studies.

For the Category D and E studies, the following additional characters are added to the end of the above naming constructions:

- The fifth character of the name is a number ranging from 0 to the maximum number of lateral to torsional bracing stiffness ratios considered, and
- The sixth character is either the letter p or the letter n, indicating whether the test case corresponds to positive or negative bending moment.

Numerous individual test simulations are conducted for each of the test cases in which the bracing stiffnesses are varied from small values, less than the ideal bracing stiffness, up

through values that are relatively large multiples of the ideal bracing stiffness. Given the results from the many different test simulations for a given test case, the maximum strength knuckle curves and the brace force versus brace stiffness curves can be generated for the test case. In addition, for Categories D and E, the knuckle curve results are then synthesized into lateral-torsional bracing stiffness interaction plots corresponding to full bracing of the members.

#### 4.5 Benchmark Studies

Benchmark studies were performed to develop confidence in the models used for the study. These studies consisted of members which had an unbraced length,  $L_b = 5, 10,$  and  $15$  ft and no intermediate brace points. Three benchmark cases with an unbraced length,  $L_b,$  of  $5, 10,$  and  $15$  ft were used. Only one load-deflection analysis was performed for each of these members as there were no brace stiffness to vary. The modeling approach was exactly the same as that used for all of the categories in the study, but with no intermediate brace points. A sweep of the compression flange with a maximum amplitude of  $L_b/1000$  at the mid-span was used for all of these models. In Figure 4.4, the maximum strengths determined from the test simulations ( $M_{max}$ ) are compared to the elastic buckling capacity, capped by the plastic moment of the W21x44 cross-section, as well as to the ANSI-AISC 360-10 and the Eurocode 3 (CEN 2005) predicted strengths in. Two curves are shown from the Eurocode 3 provisions, one corresponding to “general I-section members” and the second providing an enhanced strength estimated intended for application with rolled I-section members and members with cross-sections similar to rolled I-sections.

Table 4.1 summarizes the numerical values from the benchmark results for each of the unbraced lengths considered. The test simulation strengths are closest to the EC3-1 curve. This is

to be expected since the EC3-1 strength curve was developed largely from extensive test simulation studies similar to the studies conducted here, but with a nominal (deterministic) residual stress pattern that is not quite as damning as the Lehigh residual stress pattern. The use of the Lehigh residual stress pattern reduces the member capacity slightly in comparison to the EC3-1 curve. The EC3-2 and AISC strength curves were developed considering extensive collections of experimental data. Generally, the maximum strengths obtained from test simulations, using typical nominal residual stress patterns along with geometric imperfections set at maximum construction tolerances, tend to be smaller on average compared to the strengths from experimental tests.

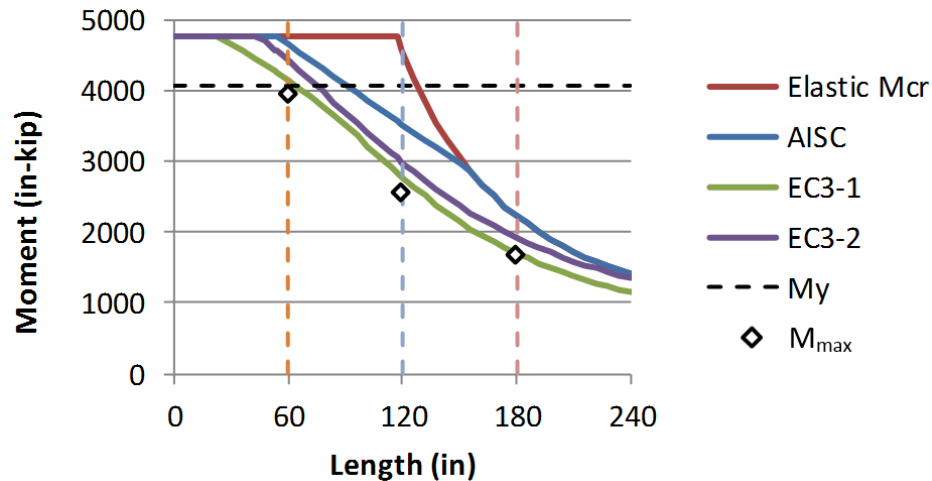


Fig. 4.4. Comparison of maximum test simulations strengths ( $M_{max}$ ) for W21x44 members with 5, 10, and 15 ft unbraced lengths to the elastic buckling, yield and plastic moment resistances ( $M_{cr}$ ,  $M_y$  and  $M_p$ ) as well as nominal strengths from the AISC Specification and the Eurocode 3 Standard

Table 4.1. Benchmark case results and comparisons

$L_b$ (ft)	$M_{max}$ (kip-in)	Min ( $M_{cr}$ , $M_p$ ) (kip-in)	$M_n$ AISC (kip-in)	$M_n$ EC3-1 (kip-in)	$M_n$ EC3-2 (kip-in)
5	3950	4770	4650	4160	4420
10	2560	4560	3530	2780	2980
15	1670	2230	2230	1700	1930

#### 4.6 Rigidly Braced Member Strengths

Table 4.2 shows the maximum rigidly braced member strengths achieved in the test simulations for the various test cases considered in this research. Table 4.3 shows the strengths specifically for the Category C cases where  $n=1$  which provide the base rigidly braced strengths for all of the knuckle curves produced in the study. Figure 4.5 shows the percentage increase in the rigidly braced strength of each case with respect to Category C ( $n = 1$ ) for the respective 5, 10, and 15 ft unbraced lengths. One can observe that generally the strengths are slightly different for the different combinations of bracing configurations and number of intermediate brace points. This behavior is due to the slight additional restraint induced by using lateral bracing of the compression flange, compared to the use of torsional bracing (which restrains twist but does not provide any restraint to overall lateral movement at the brace point), as well as the extra lateral restraint of both flanges by using combined lateral and torsional bracing. Furthermore, some additional incidental warping and lateral bending restraint at the ends of the critical unbraced length tends to be generated in a number of the test cases with  $n = 2$  and 3 compared to the test cases with  $n = 1$ . This is due to the less critical unbraced lengths (less critical because of the initial geometric imperfections imposed on the member) providing some resistance to the cross-section lateral bending and warping deformations at the end of the critical unbraced length.

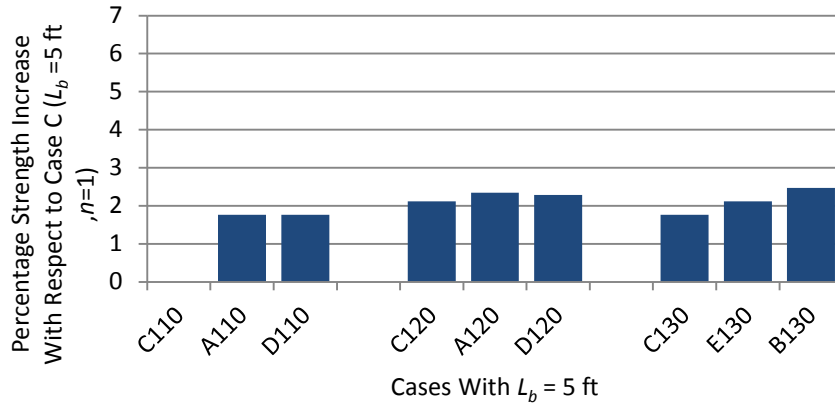
Table 4.2. Rigidly braced strengths

$L_b=5$ ft		$L_b=10$ ft		$L_b=15$ ft	
Case	$M_{max}/M_p$	Case	$M_{max}/M_p$	Case	$M_{max}/M_p$
A110	0.842	A210	0.581	A310	0.380
A120	0.848	A220	0.599	A320	0.394
B120	0.848	B220	0.599	B320	0.394
B130	0.842	B230	0.595	B330	0.393
C110	0.827	C210	0.570	C310	0.370
C120	0.845	C220	0.577	C320	0.377
C130	0.842	C230	0.581	C330	0.382
D110	0.842	D210	0.581	D310	0.38
D120	0.845	D220	0.599	D320	0.394
E120	0.845	E220	0.599	E320	0.394
E130	0.845	E230	0.595	E330	0.393

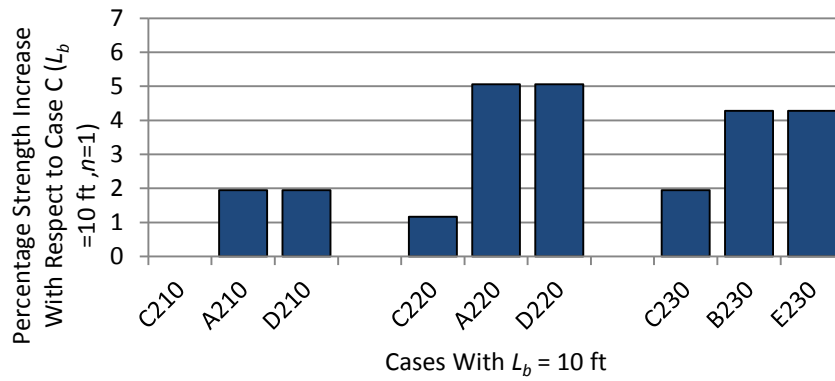
Table 4.3.  $M_{max}$  numerical values for the governing Cases C110, C210 and C310

Case	$M_{max}$ (kip-in)
C110	3950
C210	2720
C310	1770

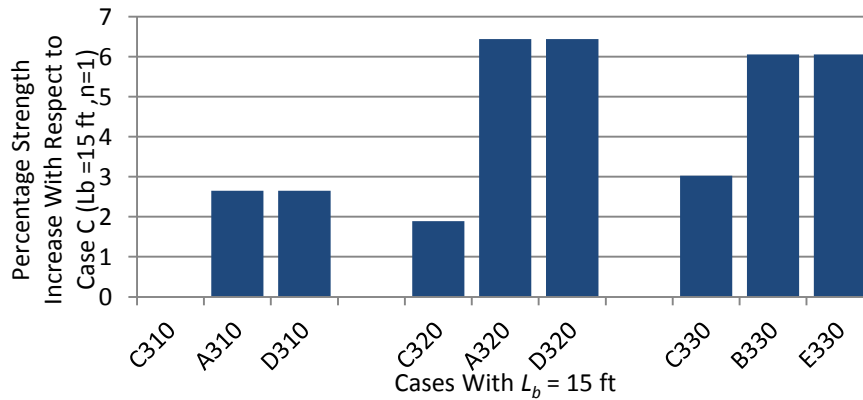
The subsequent knuckle curves developed for each test case are compared to the corresponding rigidly braced member strengths from Category C with  $n = 1$  (Cases C110, C210 and C310), which always give the smallest strength for of the test cases for the corresponding  $L_b$ . One can compare these Case C resistances to the benchmark resistances in Table 4.1 to ascertain that the previous benchmark cases have even slightly smaller resistances. The full bracing strengths considered in the subsequent studies are taken as 98 % of the rigidly braced strengths from Cases C110, C210 and C310 in all of these studies. In the combined bracing studies discussed in Chapter 8, the use of 96 % of these rigidly braced strengths also is considered.



(a) Percentage strength increase with respect to Case C110 ( $L_b = 5$  ft,  $n=1$ )



(b) Percentage strength increase with respect to case C210 ( $L_b = 10$ ft,  $n = 1$ )



(c) Percentage strength increase with respect to case C310 ( $L_b = 15$  ft,  $n = 1$ )

Fig. 4.5. Comparison of rigidly braced strengths for all categories



# CHAPTER 5

## NODAL LATERAL BRACING REQUIREMENTS

### 5.1 Category A: Nodal Lateral Bracing Results

Table 5.1 shows the base nominal bracing stiffness ( $\beta_{br} = 2\beta_{iF.AISC}$ ) required from the AISC Appendix 6 Commentary, where  $\beta_{iF.AISC}$  is the conceptual AISC ideal full (nodal lateral) bracing stiffness for beams based on the applied moment  $M$  (rather than a theoretical member elastic buckling capacity). The values of  $\beta_{br}$  are calculated using Equation (2-35) with  $L_q$  taken equal to  $L_b$  and  $C_{iN}$  and  $C_d$  both taken equal to 1.0. Furthermore, in the calculation of  $\beta_{br}$ , the values of  $M$  are taken as the rigidly-braced strengths  $M_{max}$  from Table 4.3. These are the moment capacities from the simulations for the rigid torsional bracing cases with  $n = 1$ , which are the smallest rigidly braced strengths.

Table 5.1. Category A rigidly-braced strengths and base nominal bracing stiffnesses

Case	$L_b$ (ft)	$n$	$M_{max}$ (kip-in)	$\beta_{br}$ (kip/in)
A110	5	1	3945	12.99
A210	10		2720	4.48
A310	15		1767	1.94
A120	5	2	3945	19.48
A220	10		2720	6.72
A320	15		1767	2.91

Figure 5.1 shows two nodal lateral bracing configurations that are representative of the cases A\*10 (A110, A210, A310) and A\*20 (A120, A220, A320) respectively. Figures 5.2 to 5.4 show the “knuckle” curve (on the left side of the figure) and the brace force as a percentage of

flange force vs brace stiffness plots (on the right side of the figure) for all of the cases from category A.

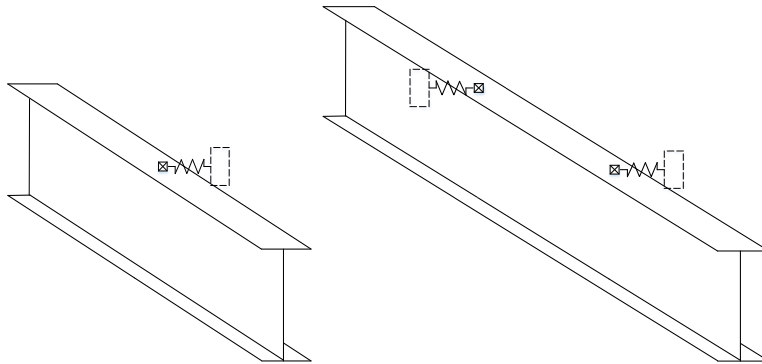
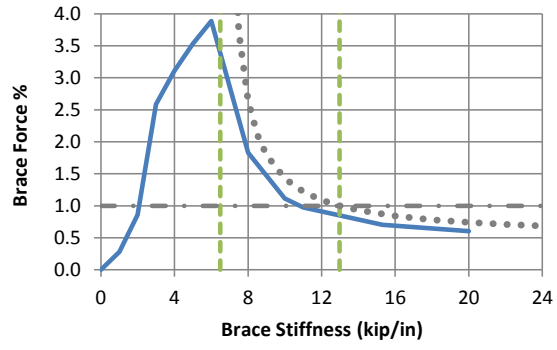
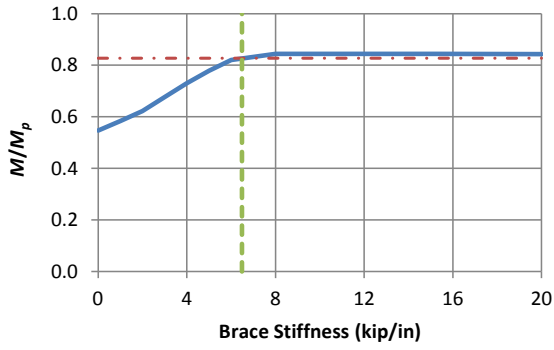
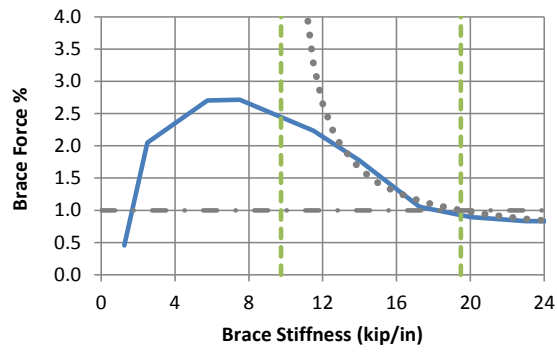
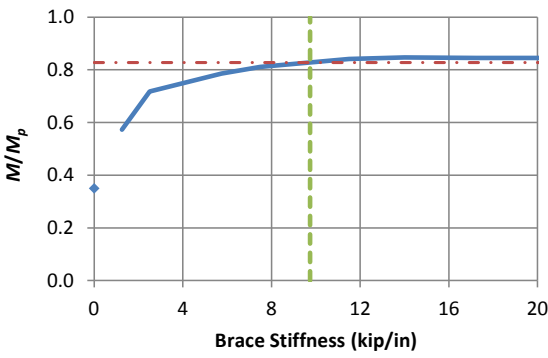


Fig. 5.1. Representative nodal lateral model for cases A\*10 and A\*20

Figure 5.2 shows the cases with an  $L_b = 5$  ft . These make up the plastic buckling cases of category A. Figure 5.3 shows the cases with an  $L_b = 10$  ft. These make up the inelastic buckling cases of category A. Figure 5.4 shows the cases with an  $L_b = 15$  ft. These make up the elastic buckling cases of category A. Figures 5.2a and b show the plastic buckling case knuckle curves and brace force vs brace stiffness plots for  $n = 1$  and 2. The vertical green dashed line in the knuckle curve plots represents the AISC ideal bracing stiffness. The brace force vs brace stiffness plot also shows this stiffness as well as the base required brace stiffness,  $\beta_{br} = 2\beta_{iF.AISC}$ . The dash-dot horizontal line in the knuckle curve plot is the base rigid bracing strength as defined in Section 2.8. Since the cases that make up category A usually have a larger rigidly braced strength than the base torsional rigidly braced strengths, the knuckle curve plots tend to asymptote towards a slightly larger loading.



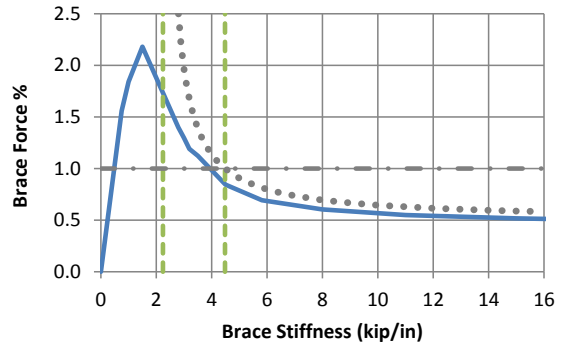
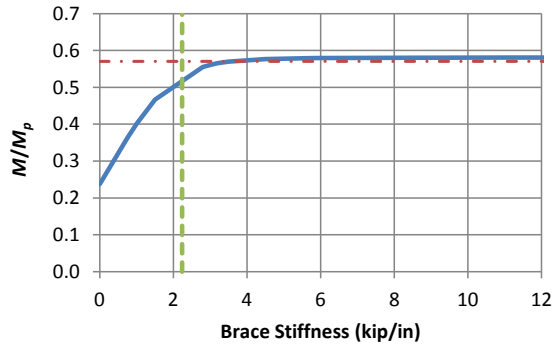
(a) A110 ( $n = 1$ ,  $\beta_{iF.AISC} = 6.5$  kip/in)



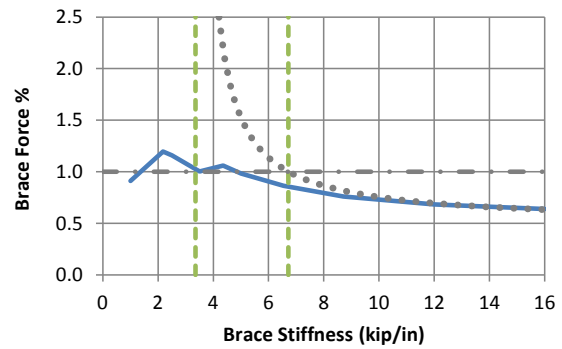
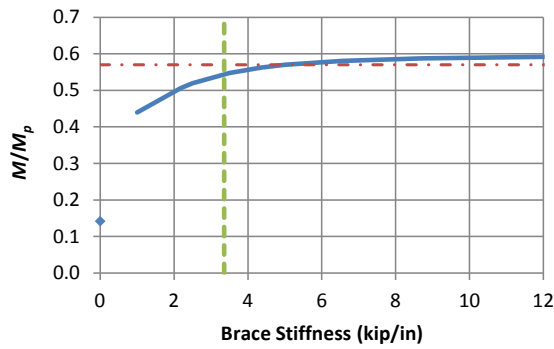
(b) A120 ( $n = 2$ ,  $\beta_{iF.AISC} = 9.7$  kip/in)

- Test Simulation Results
- ◆ Test Simulation Strength at Zero Brace Stiffness (Case A120)
- · - Rigid Bracing Strength
- - - 1 and 2x AISC Ideal Bracing Stiffness ( $\beta_{iF.AISC}$  and  $2\beta_{iF.AISC}$ )
- · · Base AISC Required Strength Corresponding to  $\beta = 2\beta_{iF.AISC}$
- · · Refined Estimate of Required Strength from AISC Commentary

Fig. 5.2. Case A1\*0 knuckle and brace force vs. brace stiffness curves (Compression flange nodal lateral bracing,  $L_b = 5$  ft)



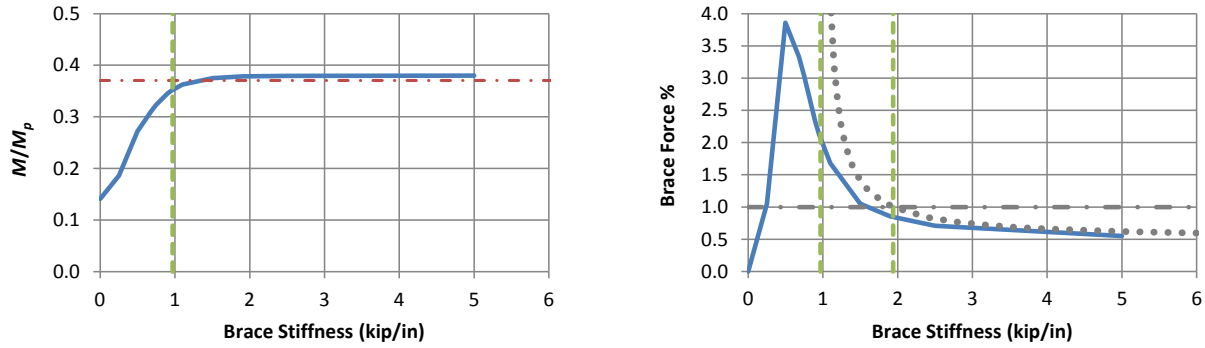
(a) A210 ( $n = 1$ ,  $\beta_{iF.AISC} = 2.2$  kip/in)



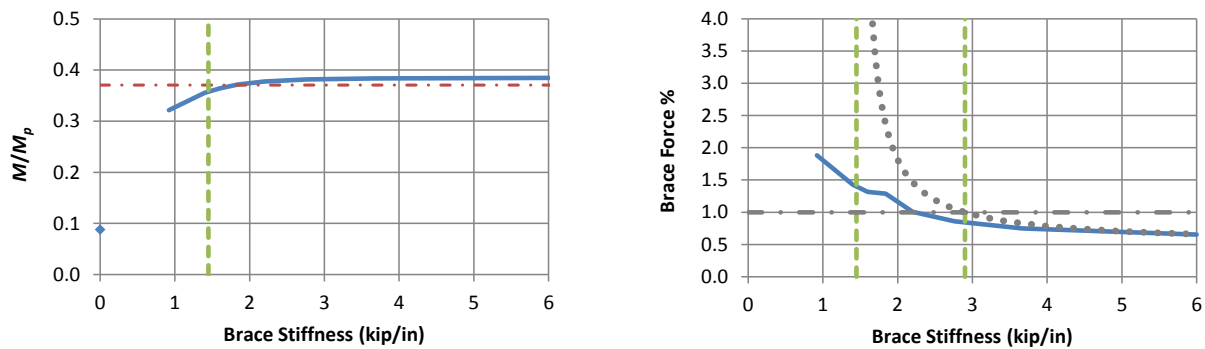
(b) A220 ( $n = 2$ ,  $\beta_{iF.AISC} = 3.4$  kip/in)

- Test Simulation Results
- ◆ Test Simulation Strength at Zero Brace Stiffness (Case A220)
- - - Rigid Bracing Strength
- - - 1 and 2x AISC Ideal Bracing Stiffness ( $\beta_{iF.AISC}$  and  $2\beta_{iF.AISC}$ )
- · - Base AISC Required Strength Corresponding to  $\beta = 2\beta_{iF.AISC}$
- · · Refined Estimate of Required Strength from AISC Commentary

Fig. 5.3. Case A2\*0 knuckle and brace force vs. brace stiffness curves  
(Compression flange nodal lateral bracing,  $L_b = 10$  ft)



(a) A310 ( $n = 1$ ,  $\beta_{iF.AISC} = 0.97$  kip/in)



(b) A320 ( $n = 2$ ,  $\beta_{iF.AISC} = 1.5$  kip/in)

- Test Simulation Results
- ◆ Test Simulation Strength at Zero Brace Stiffness (Case A320)
- - - Rigid Bracing Strength
- - - 1 and 2x AISC Ideal Bracing Stiffness ( $\beta_{iF.AISC}$  and  $2\beta_{iF.AISC}$ )
- · - Base AISC Required Strength Corresponding to  $\beta = 2\beta_{iF.AISC}$
- · · Refined Estimate of Required Strength from AISC Commentary

Fig. 5.4. Case A3\*0 knuckle and brace force vs. brace stiffness curves  
(Compression flange nodal lateral bracing,  $L_b = 15$  ft)

Figure 5.2(a)'s knuckle curve A110 has stiffness values that include zero and values close to zero. This is because the member only has one brace point and the member failure mode associated with any brace point movement is affine to the out-of-alignment imperfection shown in Figure 3.4(a) for any given brace stiffness. This is in contrast to the Figure 5.2(b) case, A120,

which has a distinct break in the knuckle curve as the knuckle curve “falls off”. This break corresponds to a change in the shape of the failure mode associated with any brace point movement from one similar to the out-of-alignment imperfection shown in Figure 3.4(b) to a failure mode that involves substantial movement of both brace points. For cases with  $n = 2$ , no stiffness values below 80% of the rigidly braced strength were considered due to the possibility of a change in the shape of the failure mode. Some jumps appear in the plots due to the discretization of the analysis in the knuckle curves. The category A knuckle curves tend to have a near constant slope for partial bracing stiffness values until they reach approximately the AISC ideal bracing stiffness, where a reasonably sharp turn in the curve occurs and the curve then asymptotes to its rigidly braced strength. The bracing stiffness value at which the knuckle curve crosses 98 % of the base rigid bracing strength is referred to as the full bracing stiffness in this work and is denoted subsequently by the symbol  $\beta_{F98}$ .

Figures 5.5 and 5.6 synthesize the results shown in Figures 5.2 through 5.4 by giving bar graph comparisons or line plots of the ideal full bracing stiffness values versus full bracing stiffness values based on developing 98% of the rigidly braced member strength ( $\beta_{F98}$ ) and compare them with the AISC required stiffness ( $\beta_{iF.AISC}$ ) for Category A (compression flange nodal lateral bracing). Figures 5.5(a) , 5.5(b), and 5.5(c) compare the brace stiffnesses  $\beta_{iF.AISC}$  (colored grey) and  $\beta_{F98}$  (colored blue) for Category A. Figure 5.6 shows the same data as Figure 5.5 with line plots to show comparisons. Figure 5.7 gives the required bracing strength estimate from AISC Appendix 6 and the required bracing estimate found from test simulations. The following general observations can be made in regards to Figures 5.5 to 5.7:

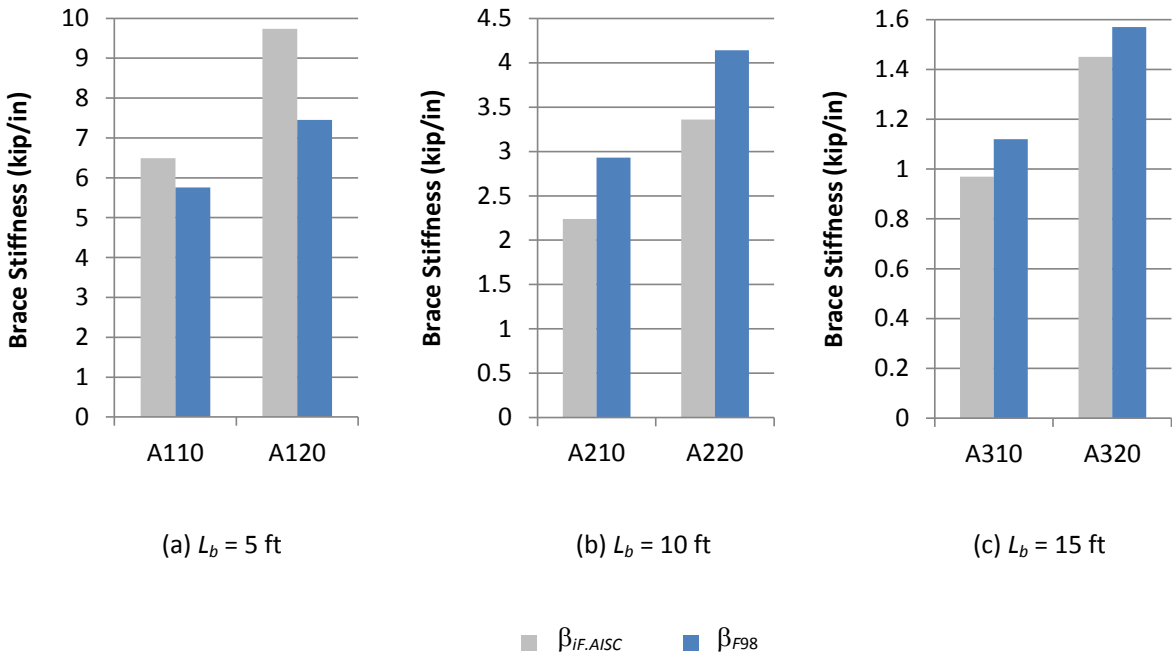


Fig. 5.5. Bar graph comparison of ideal full bracing stiffness values,  $\beta_{IF,AISC}$ , versus full bracing stiffness values based on developing 98 % of the rigidly braced member strength,  $\beta_{F98}$ , for Category A (Compression flange nodal lateral bracing)

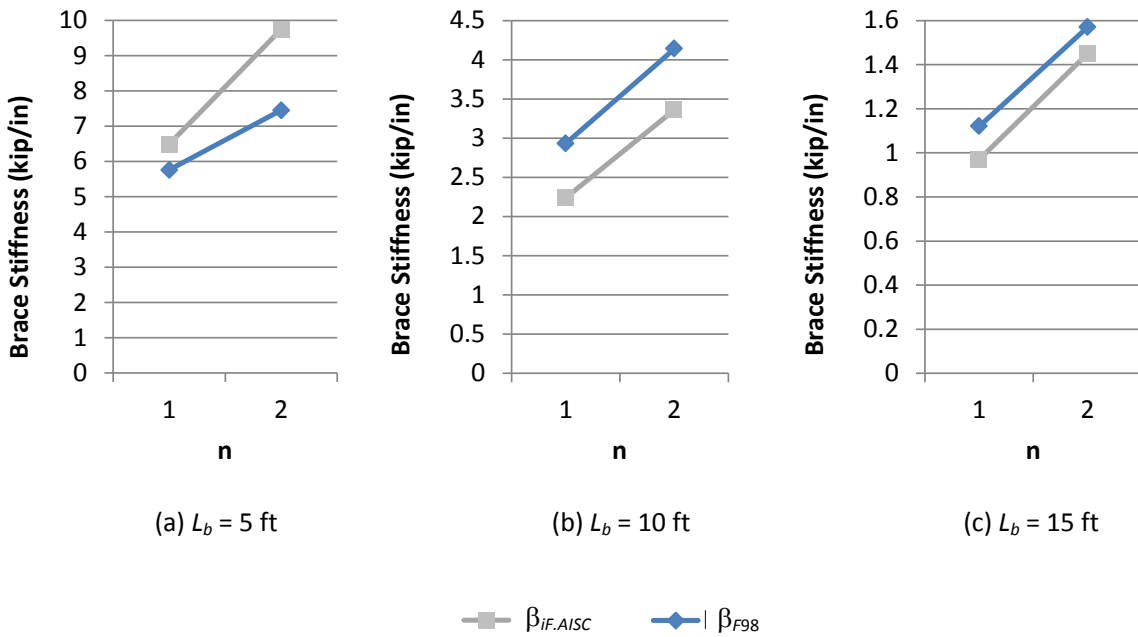


Fig. 5.6. Line plot comparison of ideal full bracing stiffness values,  $\beta_{IF,AISC}$ , versus full bracing stiffness values based on developing 98 % of the rigidly braced member strength,  $\beta_{F98}$ , for Category A (Compression flange nodal lateral bracing)

- The increase in  $\beta_{F98}$  as a function of  $n$  is closely correlated with the increase in  $\beta_{iF.AISC}$  (as a function of  $n$ ), which is a fit to the requirements obtained from the analytical solution of the elastic buckling problem. The AISC Appendix 6 Commentary equation suggests that the ratio of the stiffness requirements for  $n = 2$  to those for  $n = 1$  is

$$\frac{\left(4 - \frac{2}{2}\right)}{\left(4 - \frac{2}{1}\right)} = \frac{3}{2} = 1.5. \text{ The ratio of } \beta_{F98} \text{ for } n = 2 \text{ versus } n = 1 \text{ is 1.29, 1.41 and 1.40 for}$$

the plastic, inelastic and elastic buckling cases considered.

- Compared to the behavior for  $n = 1$ , the bracing cases with  $n = 2$  have an additional reduction in the required brace strength relative to the refined (modified) AISC Commentary predictions in the partial bracing range of the response (i.e., for  $\beta < \beta_{F98}$ ). This is due to additional incidental restraint coming from the member unbraced length on one side of the critical brace location, as localization of the member deformations occurs in the unbraced length on the other side of the critical brace point.

The partial bracing member resistance can be approximated accurately to somewhat conservatively in all cases by drawing a straight line between the member full bracing resistance at  $\beta = \beta_{F98}$  and the strength of the member for zero bracing stiffness at  $\beta = 0$ . The conservatism of this approximation is greater for  $n = 2$  compared to  $n = 1$ . For all of the Category A cases, there is no significant drop in beam strength until the brace stiffness becomes less than  $\beta_{F98}$ . The brace forces tend to increase significantly for bracing stiffnesses less than approximately  $2\beta_{iF.AISC}$ .

The AISC estimate of the ideal full bracing stiffness ( $\beta_{iF.AISC}$ ) captures the minimum required full bracing stiffness ( $\beta_{F98}$ ) with some slight conservatism for the plastic buckling case. The ratio  $\beta_{F98}/\beta_{iF.AISC}$  ranges from 0.76 to 0.89 for this case.

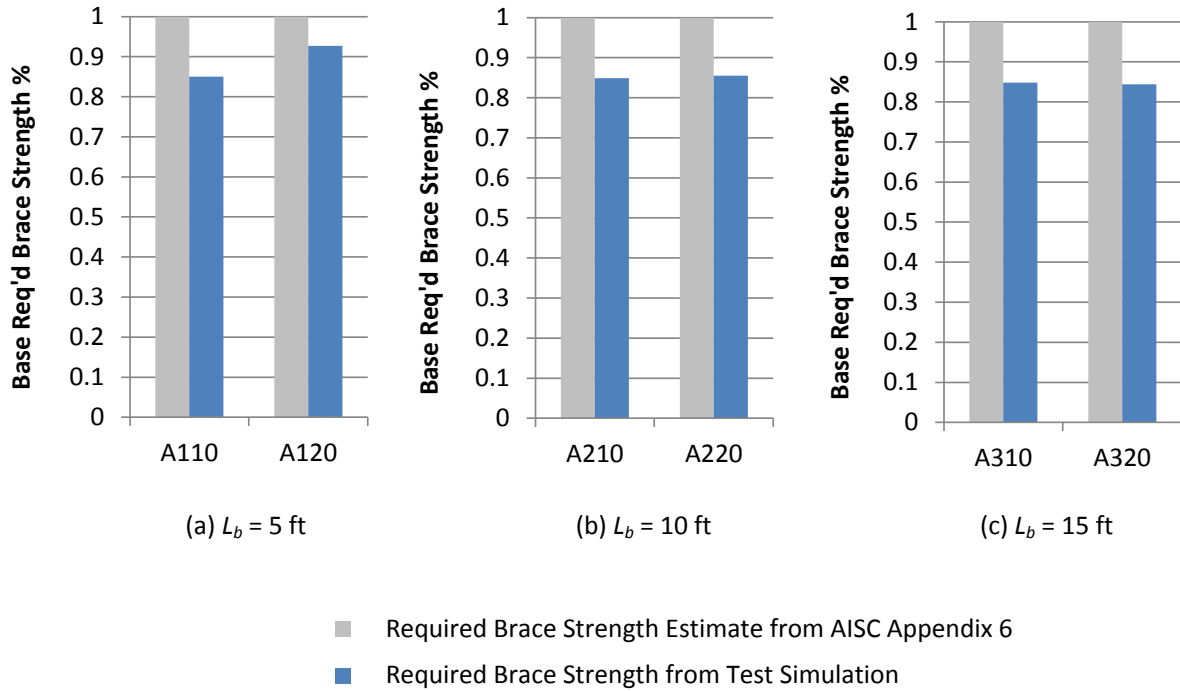


Fig. 5.7. Bar graph comparison of base AISC required strength corresponding to  $\beta = 2\beta_{iF.AISC}$  versus the test simulation required brace strength at the member limit load, using this brace stiffness (Category A, compression flange nodal lateral bracing)

The  $\beta_{iF.AISC}$  of the plastic buckling cases is somewhat smaller than  $\beta_{F98}$  for the inelastic and elastic buckling cases.  $\beta_{F98}/\beta_{iF.AISC}$  ranges from 1.23 to 1.31 for the inelastic buckling cases considered shown in Figure 5.3. It ranges from 1.08 to 1.15 for the elastic buckling cases shown in Figure 5.4.

It is generally expected that the brace stiffness needs to be larger than  $\beta_{iF.AISC}$  to develop a member's fully-braced strength. However, the above values are significantly less than the basic multiple of 2.0 used commonly in bracing design. It can also be gleaned that the effect of the bracing stiffness on the member strength is negligible in all cases for brace stiffnesses greater than  $1.31 \beta_{iF.AISC}$  for all the cases studied.

Regarding the brace force vs. brace stiffness plot behavior in Figures 5.2 through 5.4, the AISC brace force estimate corresponding to  $\beta = 2\beta_{iF.AISC}$  is quite accurate compared to the test simulation strength requirements at this stiffness. The test simulation strength requirements range from 0.84 % to 0.93 % at  $\beta = 2\beta_{iF.AISC}$  for all of the category A test simulations, compared to the base AISC strength requirement of 1.0 %. The Appendix 6 modifier on the base brace strength requirement given in Equation (2-37), with  $\beta_{br}$  taken as  $2\beta_{iF.AISC}$ , does an excellent to somewhat conservative job of estimating the variation in the brace strength requirement to achieve the member limit load in all cases for  $\beta$  values larger than approximately  $1.5 \beta_{iF.AISC}$ . The refined AISC estimate of the brace strength requirement, given by Equation (2-37), is illustrated by the dotted curve in the brace force vs brace stiffness plots. One can observe in these plots that modifier on the base brace strength requirement, as well as the underlying amplification of the brace point displacements, becomes unbounded as  $\beta$  approaches  $\beta_{iF.AISC}$ .

The reasons why the physical brace forces do not become unbounded as  $\beta$  approaches  $\beta_{iF.AISC}$  are as follows:

- The physical member participates in resisting the brace point displacements more and more with decreasing  $\beta$ , from essentially no participation (since the member is buckling between the brace points) for large  $\beta$ , to substantial participation for

very flexible partial bracing. The idealized second-order elastic model on which

the modifier  $\frac{1}{2 - \frac{2\beta_{iF.AISC}}{\beta_{act}}}$  is based does not account for any participation of the

member in resisting the brace point displacements.

- As the member lateral displacements commence due to buckling of the member between the brace points (for full bracing), or the member and its bracing system (for partial bracing), yielding soon starts (if it has not started already) and the yielding continues to spread through the member cross-section and along the member length. This results in the member, or the member and its bracing system, reaching a limit load at finite brace point displacements (and thus at finite brace forces). This limits the magnitude of the brace forces that need to be resisted to develop the member (or system) limit load.

- At a point significantly before the brace point displacements become infinite, the member deflections no longer satisfy the small rotation assumption implicit in the derivation of the magnifier  $\frac{1}{2 - \frac{2\beta_{iF.AISC}}{\beta_{act}}}$ . This results in an increased strength of

the physical geometrically imperfect member, for cases involving stable postbuckling response, or a limit load response at a finite brace point displacement, for cases involving unstable postbuckling response.

For smaller  $\beta$  values, the above modifier from the AISC commentary becomes very conservative. This conservatism is due to the fact that  $\frac{1}{2 - \frac{2\beta_{iF.AISC}}{\beta_{act}}}$  is derived from a simplified second-order elastic analysis model that does not account for the influence of continuity of the member across the brace locations. As the brace stiffness approaches  $\beta_{iF.AISC}$ , the modifier from the AISC Commentary goes to infinity, whereas the actual brace forces are well bounded. The simplified second-order elastic analysis model gives the same second-order amplification as the  $B_2$  equation in AISC Appendix 8 with  $R_M$  taken equal to 1.0 (see Sections 2.2 and 2.3 for a discussion of these equivalencies).

The required brace strengths are larger for partial bracing cases, compared to the requirements with full bracing. However, the current AISC Specification Appendix 6 does not explicitly address this behavior. The AISC Commentary suggests that the modifier on the

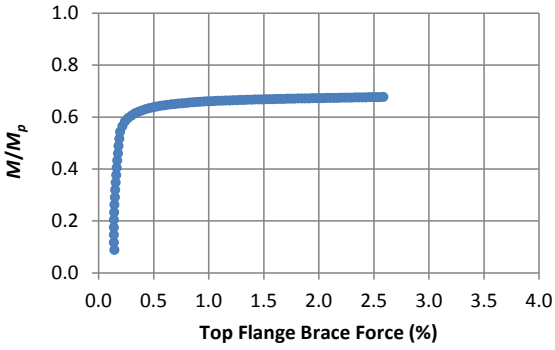
required brace strength,  $\frac{1}{2 - \frac{2\beta_{iF.AISC}}{\beta_{act}}}$  should be applied only for brace stiffnesses larger than

$\frac{2\beta_{iF.AISC}}{\phi}$ . The results in Figures 5.2 to 5.4 show that this modifier works reasonably well in all

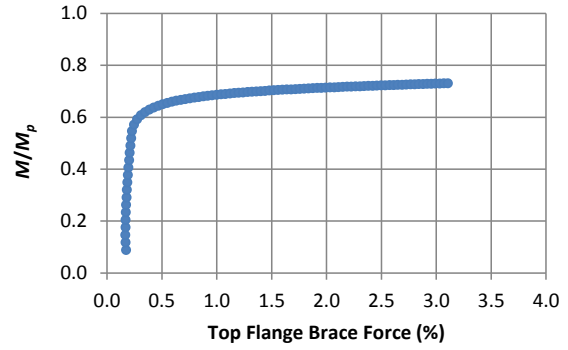
cases for roughly  $\beta \geq 1.5 \beta_{iF.AISC}$ . This limit is somewhat close to  $\beta_{F98}$ .

Figures 5.8 through 5.13 show  $M/M_p$  versus the critical lateral brace force for selected stiffness values of the cases from Category A. The plots are shown in the order of increasing brace stiffness. The following observations can be made from Figures 5.8 through 5.13:

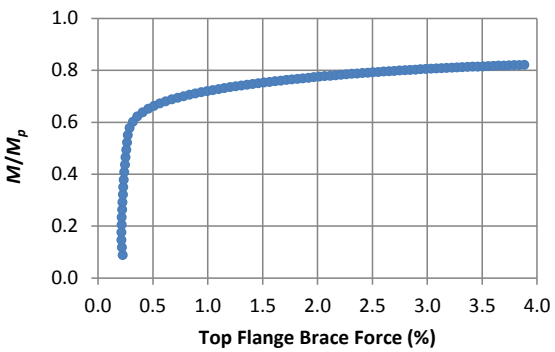
- For partial bracing of members that fail by plastic buckling, the brace forces are relatively small until the member starts to yield, at which point they increase rapidly. The brace forces at the member limit load are substantially larger than the base AISC design values (corresponding to  $2\beta_{iF.AISC}$ ) for these partial bracing cases.
- For partial bracing of members that fail by inelastic or elastic buckling, the  $M/M_p$  vs. brace force curves are very round-house when  $n = 1$ ; however, for  $n = 2$ , this round-house nature of the curves is reduced (i.e., the brace forces are a little smaller at the larger  $M/M_p$  values up to near to the limit load of the member).
- For the partially-braced member cases, the second-order amplification of the brace forces (and brace point displacements) is evidenced by a more significant round house nature of the  $M/M_p$  vs. brace force curves, particularly for the longer unbraced lengths.
- By reviewing the load-deflection plots, one can observe that a maximum nodal lateral bracing force of 2 % is sufficient to develop approximately 95 % of the strength of the fully or partially braced member for all the test simulations conducted.
- The largest brace forces for any brace stiffness (at the development of the member limit load) are less than 4 % for the plastic and elastic LTB cases; they are only slightly larger than 2 % for the inelastic LTB case.
- The maximum overall brace force (at the development of the member limit load), considering partial bracing, typically occurs very close to  $\beta_{iF.AISC}$  or at slightly smaller values than  $\beta_{iF.AISC}$ .



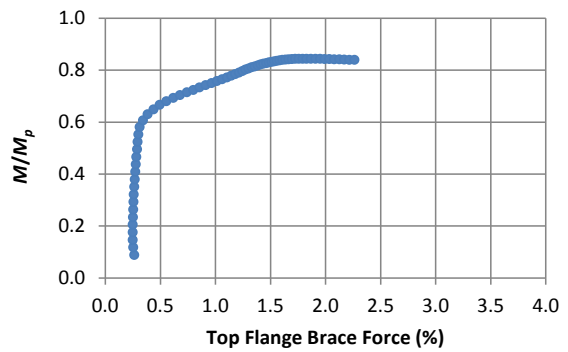
(a)  $\beta = 3.0$  kip/in ( $0.46 \beta_{iF.AISC}$ )



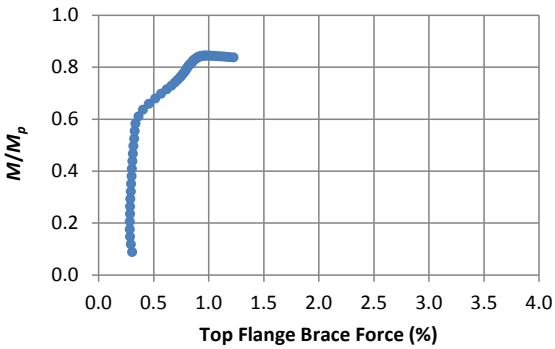
(b)  $\beta = 4.0$  kip/in ( $0.62 \beta_{iF.AISC}$ )



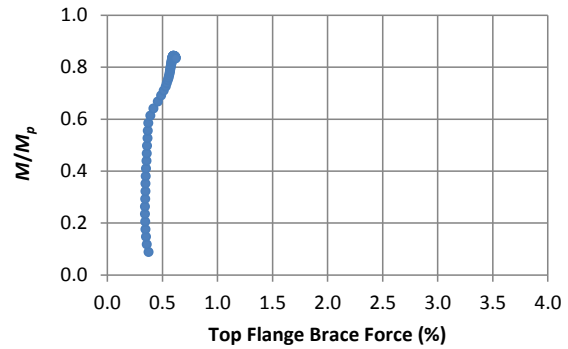
(c)  $\beta = 6.0$  kip/in ( $0.92 \beta_{iF.AISC}$ )



(d)  $\beta = 8.0$  kip/in ( $1.2 \beta_{iF.AISC}$ )

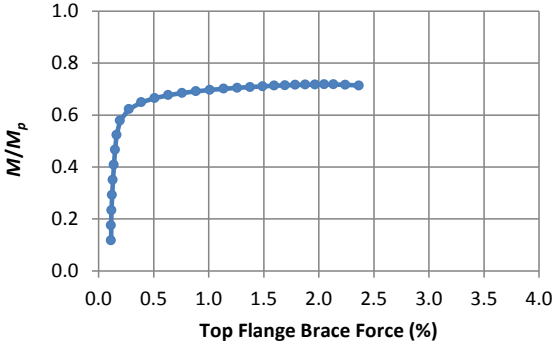


(e)  $\beta = 11.0$  kip/in ( $1.7 \beta_{iF.AISC}$ )

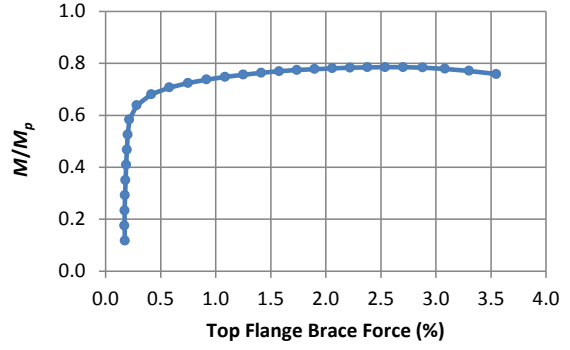


(f)  $\beta = 20.0$  kip/in ( $3.1 \beta_{iF.AISC}$ )

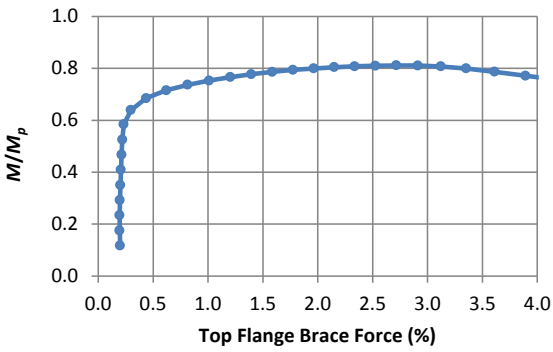
Fig. 5.8. Case A110  $M/M_p$  vs. % brace force curves for a progression of increasing brace stiffnesses (Compression (top) flange nodal lateral bracing,  $L_b = 5$  ft,  $n = 1$ ,  $\beta_{iF.AISC} = 6.5$  kip/in)



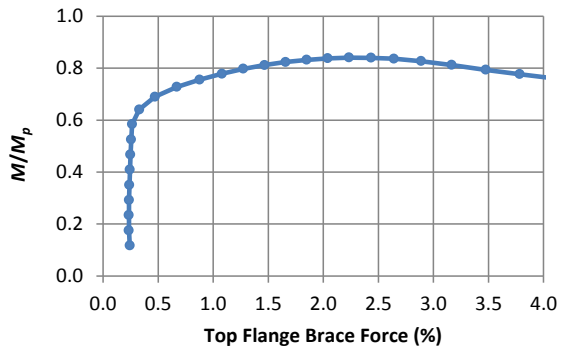
(a)  $\beta = 2.5$  kip/in ( $0.26 \beta_{iF.AISC}$ )



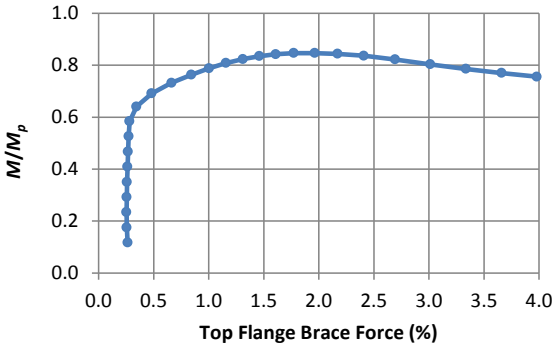
(b)  $\beta = 5.8$  kip/in ( $0.60 \beta_{iF.AISC}$ )



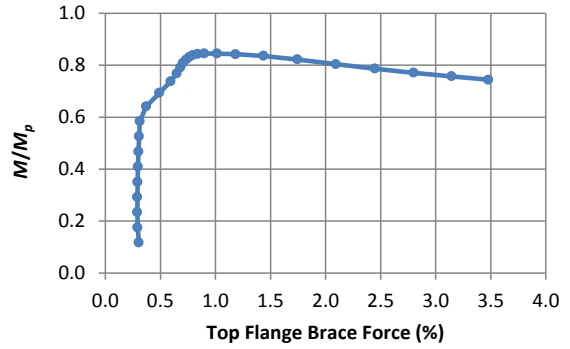
(c)  $\beta = 7.5$  kip/in ( $0.77 \beta_{iF.AISC}$ )



(d)  $\beta = 11.5$  kip/in ( $1.2 \beta_{iF.AISC}$ )

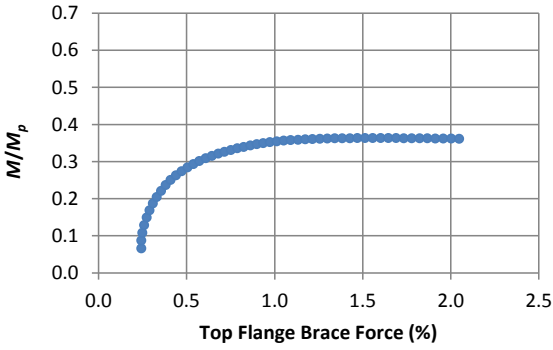


(e)  $\beta = 14.0$  kip/in ( $1.4 \beta_{iF.AISC}$ )

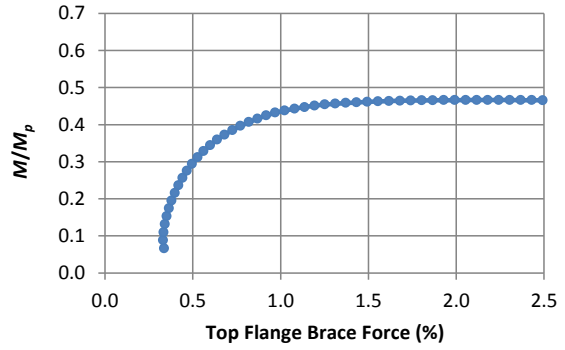


(f)  $\beta = 20.0$  kip/in ( $2.1 \beta_{iF.AISC}$ )

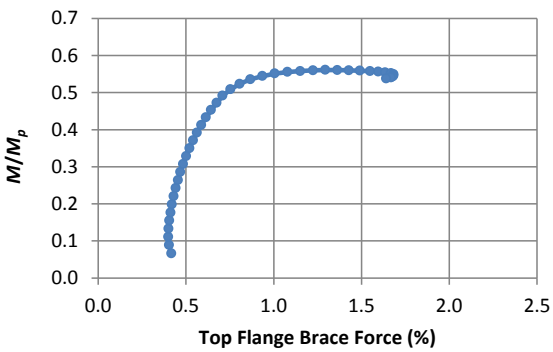
Fig. 5.9. Case A120  $M/M_p$  vs. % brace force curves for a progression of increasing brace stiffnesses (Compression (top) flange nodal lateral bracing,  $L_b = 5$  ft,  $n = 2$ ,  $\beta_{iF.AISC} = 9.7$  kip/in)



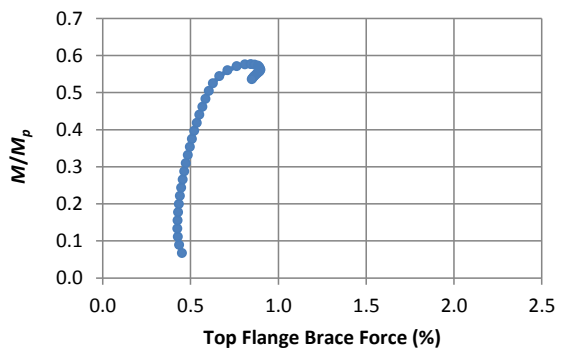
(a)  $\beta = 0.75$  kip/in ( $0.33 \beta_{iF.AISC}$ )



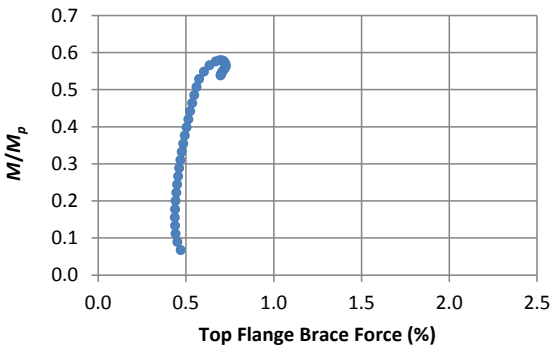
(b)  $\beta = 1.5$  kip/in ( $0.67 \beta_{iF.AISC}$ )



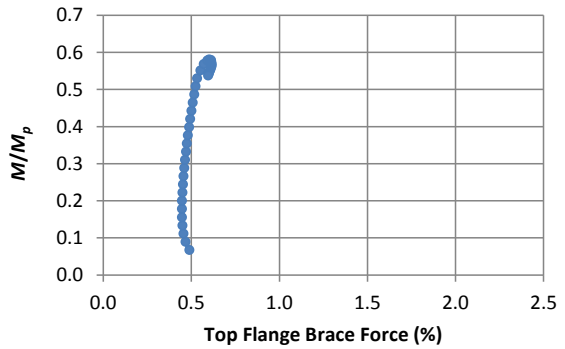
(c)  $\beta = 3.0$  kip/in ( $1.3 \beta_{iF.AISC}$ )



(d)  $\beta = 4.5$  kip/in ( $2.0 \beta_{iF.AISC}$ )

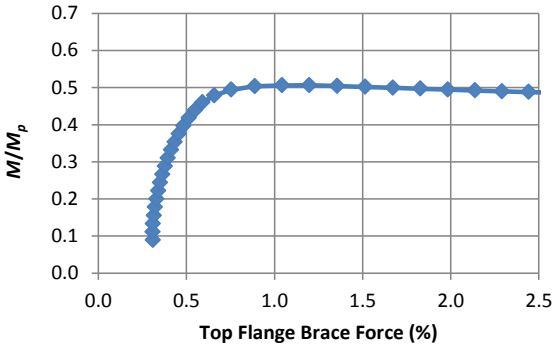


(e)  $\beta = 5.8$  kip/in ( $2.6 \beta_{iF.AISC}$ )

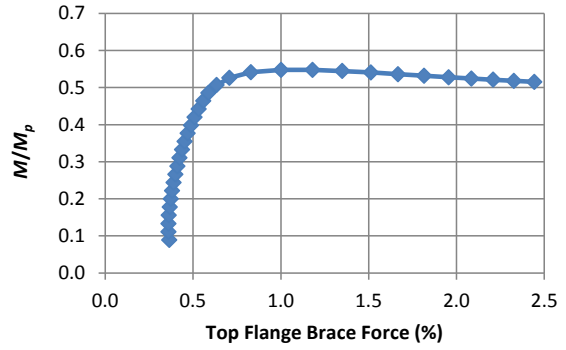


(f)  $\beta = 8.0$  kip/in ( $3.6 \beta_{iF.AISC}$ )

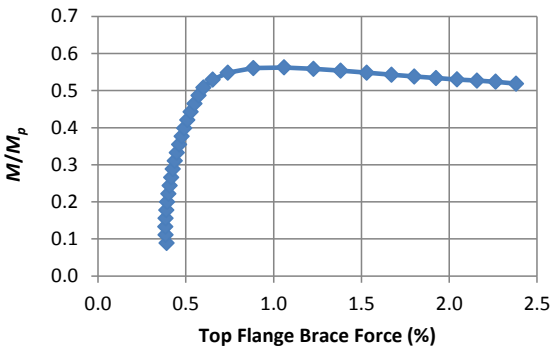
Fig. 5.10. Case A210  $M/M_p$  vs. % brace force curves for a progression of increasing brace stiffnesses (Compression (top) flange nodal lateral bracing,  $L_b = 10$  ft,  $n = 1$ ,  $\beta_{iF.AISC} = 2.2$  kip/in)



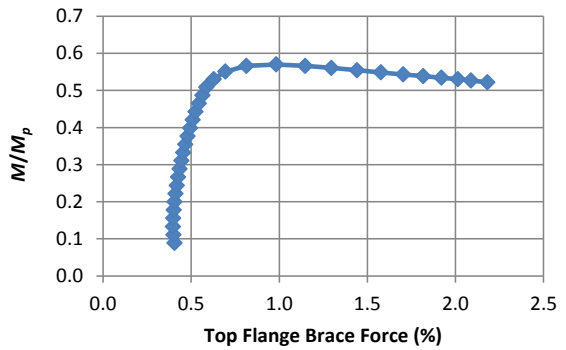
(a)  $\beta = 2.2$  kip/in ( $0.65 \beta_{iF.AISC}$ )



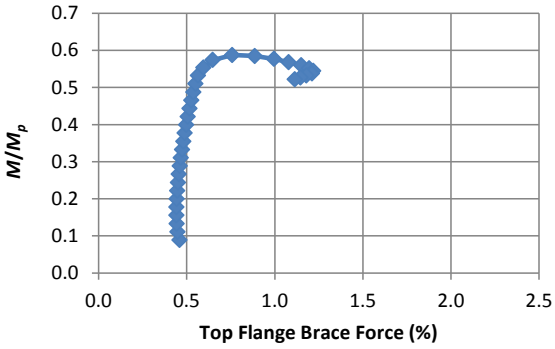
(b)  $\beta = 3.5$  kip/in ( $1.0 \beta_{iF.AISC}$ )



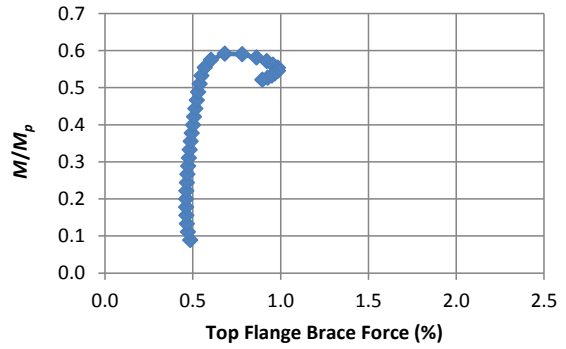
(c)  $\beta = 4.4$  kip/in ( $1.3 \beta_{iF.AISC}$ )



(d)  $\beta = 5.0$  kip/in ( $1.5 \beta_{iF.AISC}$ )

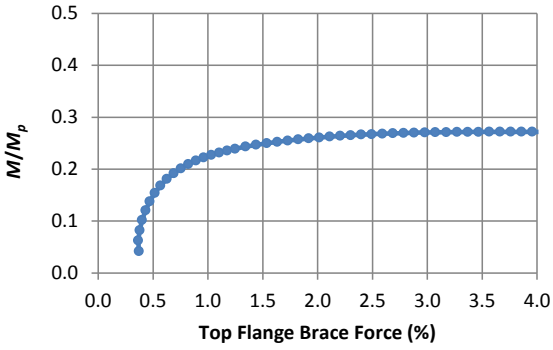


(e)  $\beta = 8.7$  kip/in ( $2.6 \beta_{iF.AISC}$ )

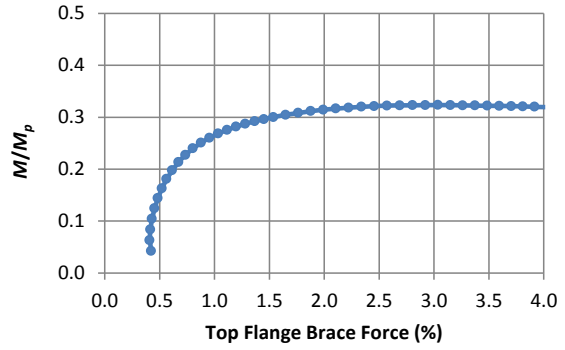


(f)  $\beta = 12.0$  kip/in ( $3.6 \beta_{iF.AISC}$ )

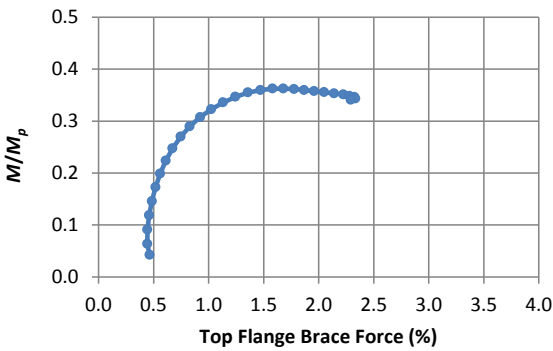
Fig. 5.11. Case A220  $M/M_p$  vs. % brace force curves for a progression of increasing brace stiffnesses (Compression (top) flange nodal lateral bracing,  $L_b = 10$  ft,  $n = 2$ ,  $\beta_{iF.AISC} = 3.4$  kip/in)



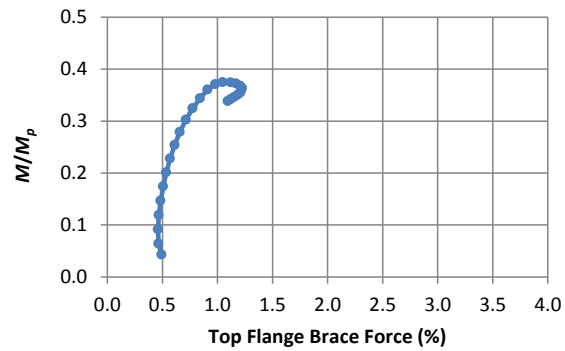
(a)  $\beta = 0.50$  kip/in ( $0.52 \beta_{iF.AISC}$ )



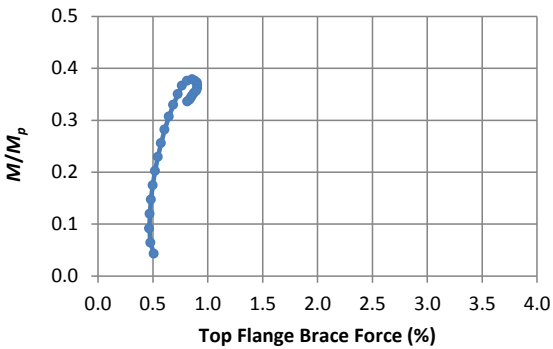
(b)  $\beta = 0.75$  kip/in ( $0.77 \beta_{iF.AISC}$ )



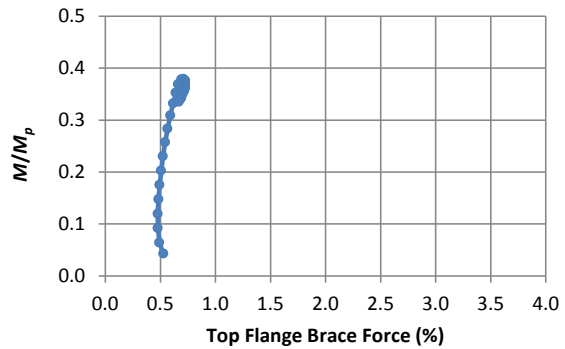
(c)  $\beta = 1.1$  kip/in ( $1.1 \beta_{iF.AISC}$ )



(d)  $\beta = 1.5$  kip/in ( $1.5 \beta_{iF.AISC}$ )

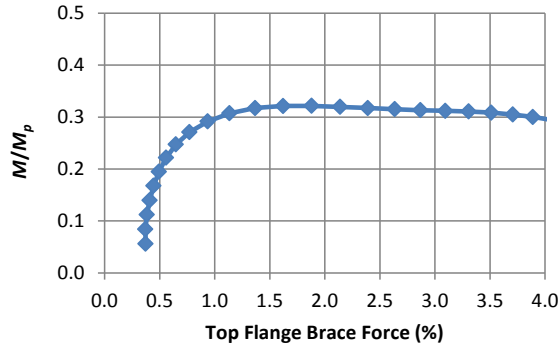


(e)  $\beta = 1.9$  kip/in ( $1.9 \beta_{iF.AISC}$ )

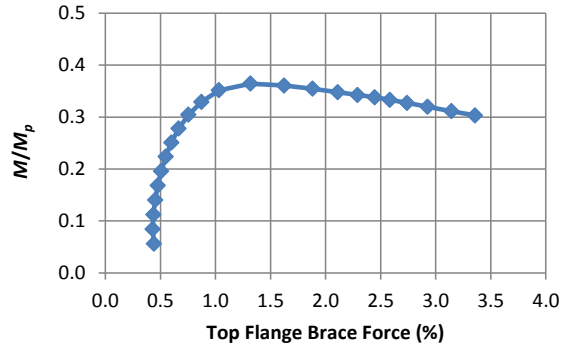


(f)  $\beta = 2.5$  kip/in ( $2.6 \beta_{iF.AISC}$ )

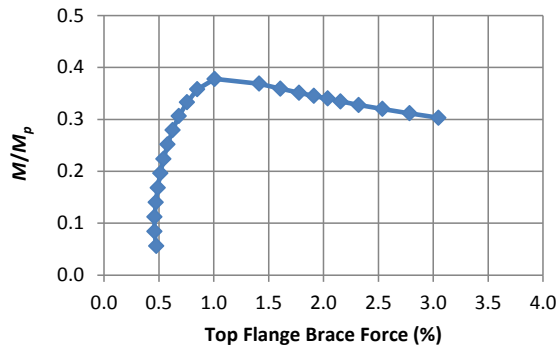
Fig. 5.12. Case A310  $M/M_p$  vs. % brace force curves for a progression of increasing brace stiffnesses (Compression (top) flange nodal lateral bracing,  $L_b = 15$  ft,  $n = 1$ ,  $\beta_{iF.AISC} = 0.97$  kip/in)



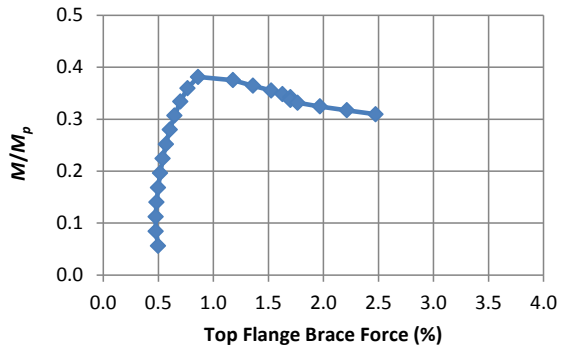
(a)  $\beta = 0.92$  kip/in ( $0.63 \beta_{iF.AISC}$ )



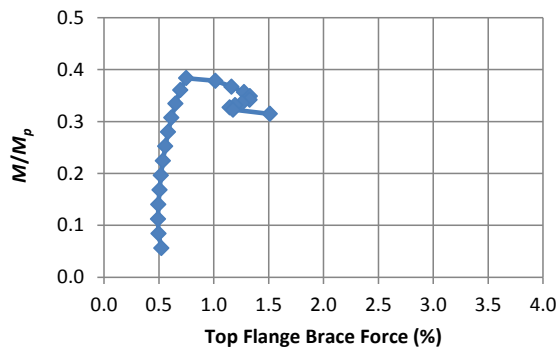
(b)  $\beta = 1.6$  kip/in ( $1.1 \beta_{iF.AISC}$ )



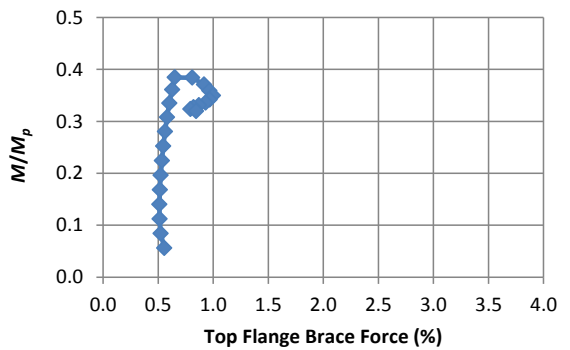
(c)  $\beta = 2.2$  kip/in ( $1.5 \beta_{iF.AISC}$ )



(d)  $\beta = 2.8$  kip/in ( $1.9 \beta_{iF.AISC}$ )



(e)  $\beta = 3.7$  kip/in ( $2.6 \beta_{iF.AISC}$ )



(f)  $\beta = 6.0$  kip/in ( $4.1 \beta_{iF.AISC}$ )

Fig. 5.13. Case A320  $M/M_p$  vs. % brace force curves for a progression of increasing brace stiffnesses (Compression (top) flange nodal lateral bracing,  $L_b = 15$  ft,  $n = 2$ ,  $\beta_{iF.AISC} = 1.5$  kip/in)



## CHAPTER 6

### RELATIVE (SHEAR PANEL) LATERAL BRACING REQUIREMENTS

#### 6.1 Category B: Relative (Shear Panel) Lateral Bracing Results

Table 6.1 shows the base nominal bracing stiffness ( $\beta_{br} = 2\beta_{iF.AISC}$ ) required from the AISC Appendix 6 Commentary, where  $\beta_{iF.AISC}$  is the conceptual AISC ideal full (relative) bracing stiffness for beams based on the applied moment  $M$  (rather than a theoretical member elastic buckling capacity). The values of  $\beta_{br}$  are calculated in this case by Equation (2-22) with  $C_{tN}$  and  $C_d$  both taken equal to 1.0. Furthermore, in the calculation of  $\beta_{br}$ , the values of  $M$  are taken as the rigidly-braced strengths  $M_{max}$  from Table 4.3. These are the moment capacities from the simulations for the rigid torsional bracing cases with  $n = 1$ , which are the smallest rigidly braced strengths. Figure 6.1 shows two relative braced member models which are respectively representative for cases B\*10 (B120, B210, B310) and B\*20 (B120, B220, B320).

Table 6.1. Category B rigidly-braced strengths and base nominal bracing stiffnesses

Case	$L_b$ (ft)	$n$	$M_{max}$ (kip-in)	$\beta_{br}$ (kip/in)
B120	5	2	3945	3.25
B220	10		2720	1.12
B320	15		1767	0.48
B130	5	3	3945	3.25
B230	10		2720	1.12
B330	15		1767	0.48

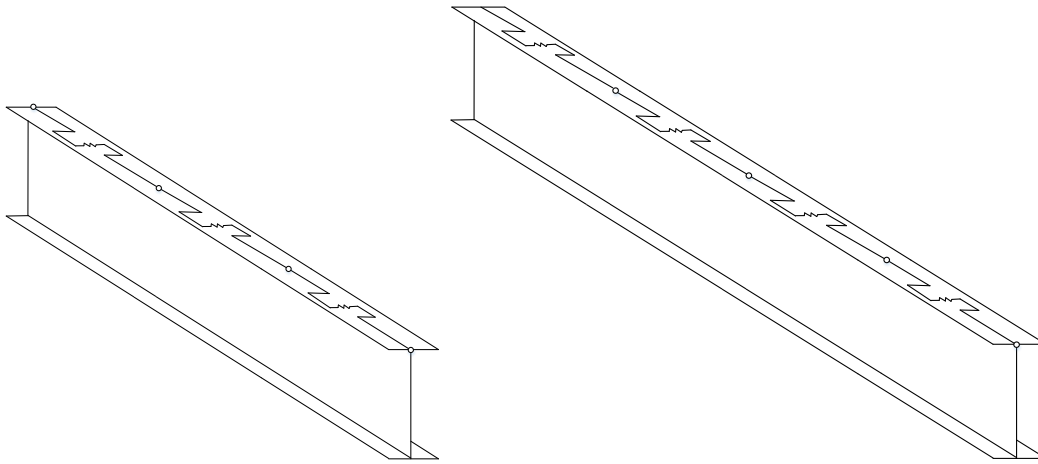


Fig. 6.1. Representative relative bracing model for cases B\*20 and B\*30

Figures 6.2 through 6.7 are similar to those shown for category A's Figures 6.2 through 6.7. The vertical green dashed line in the knuckle curve plots represents the AISC ideal bracing stiffness. The dash-dot horizontal line in the knuckle curve plot is the base rigid bracing strength as defined in Section 2.8. Since the cases that make up category A usually have a larger rigidly braced strength than the base torsional rigidly braced strengths, the knuckle curve plots tend to asymptote towards a slightly larger loading. Since these plots represent relative bracing, the right-hand panel shear force adjacent to the critical brace and the left-hand panel shear force adjacent to the critical brace are to be considered since they are expected to exhibit the largest demands in the system near the limit load. These are captured in the brace force vs brace stiffness plots as curves respective to each shear panel brace.

Since Category B consists of cases with only  $n = 2$  and 3, no stiffness values below 80% of the rigidly braced strength were considered due to the possibility of a change in the shape of the failure mode. Some jumps appear in the plots due to the discretization of the analysis in the

knuckle curves . The category B knuckle curves tend to have a near constant slope for partial bracing stiffness values until they reach approximately the AISC ideal bracing stiffness, where a reasonably sharp turn in the curve occurs and the curve then asymptotes to its rigidly braced strength. The bracing stiffness value at which the knuckle curve crosses 98 % of the base rigid bracing strength is referred to as the full bracing stiffness in this work and is denoted by the symbol  $\beta_{F98}$ . The AISC estimate of the ideal full bracing stiffness ( $\beta_{iF.AISC}$ ) captures the minimum required full bracing stiffness ( $\beta_{F98}$ ) with some slight conservatism for the plastic buckling case . The ratio  $\beta_{F98}/\beta_{iF.AISC}$  ranges from 0.89 to 0.96 for the plastic buckling cases considered. The  $\beta_{iF.AISC}$  is somewhat smaller than  $\beta_{F98}$  for the inelastic and elastic buckling cases.  $\beta_{F98}/\beta_{iF.AISC}$  ranges from 1.14 to 1.33 for the inelastic buckling cases considered. It ranges from 1.08 to 1.17 for the elastic buckling cases considered. It is generally expected that the brace stiffness needs to be larger than  $\beta_{iF.AISC}$  to develop a member's fully-braced strength. However, the above values are significantly less than the basic multiple of 2.0 used commonly in bracing design.

The partial bracing member resistance can be approximated with reasonable accuracy in all cases by drawing a straight line between the rigidly-braced strength at  $\beta = \beta_{F98}$  and the strength of the member for zero bracing stiffness at  $\beta = 0$ .

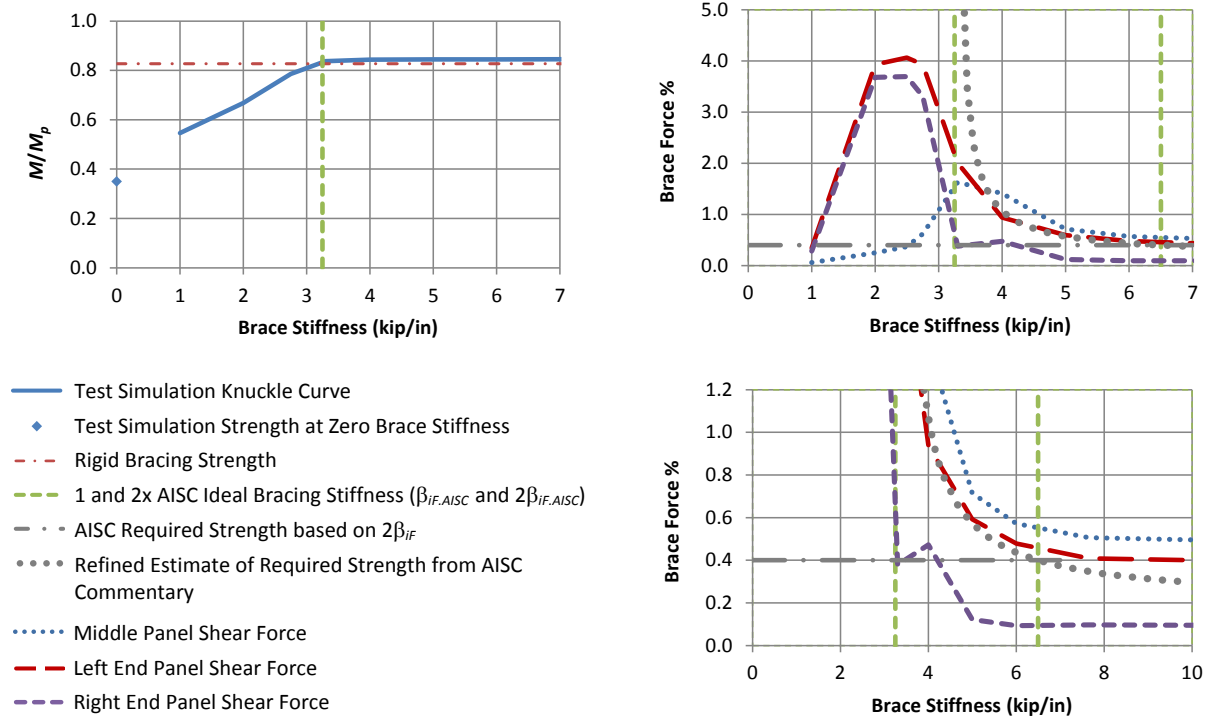


Fig. 6.2. Case B120 knuckle and brace force vs. brace stiffness curves (Compression flange shear panel (relative) lateral bracing,  $L_b = 5$  ft,  $n = 2$ ,  $\beta_{iF,AISC} = 3.2$  kip/in)

The following observations can be made from Figures 6.2 through 6.7:

- The effect of the bracing stiffness on the member strength is negligible in all cases for brace stiffnesses greater than  $1.33 \beta_{iF,AISC}$  for all the cases studied.
- There is no significant drop in beam strength until the brace stiffness becomes less than  $\beta_{F98}$ . The brace forces increase significantly with decreasing brace stiffness below this value.
- The largest shear panel brace forces for any brace stiffness (at the development of the member limit load) are as high as 4 % for the plastic LTB case with  $n = 1$ ; they are only slightly larger than 2 % at most for the other LTB cases.

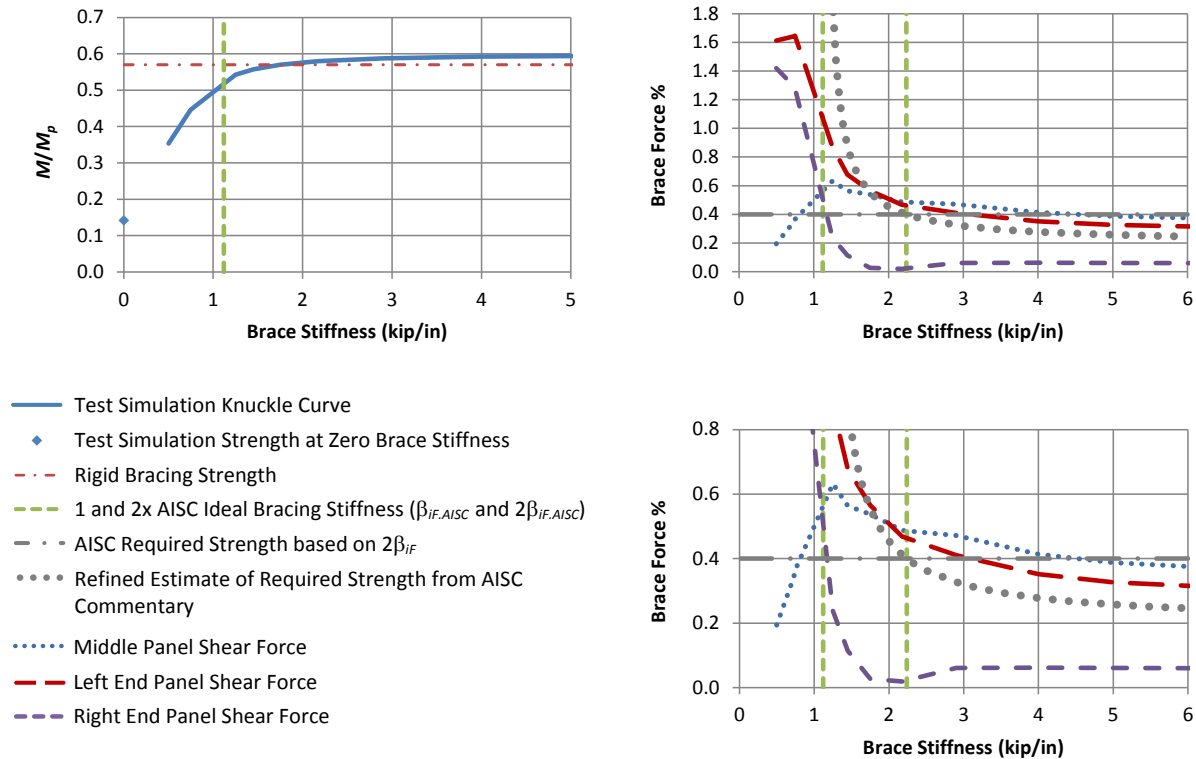


Fig. 6.3. Case B220 knuckle and brace force vs. brace stiffness curves  
 (Compression flange shear panel (relative) lateral bracing,  $L_b = 10$  ft,  $n = 2$ ,  $\beta_{iF.AISC} = 1.1$  kip/in)

- The maximum overall brace force (at the development of the member limit load), considering partial bracing, typically occurs very close to  $\beta_{iF.AISC}$  or at slightly smaller values than  $\beta_{iF.AISC}$ .
- The AISC brace strength estimate corresponding to  $\beta = 2\beta_{iF.AISC}$  is slightly low compared to the test simulation strength requirements at this stiffness. The test simulation strength requirements range from 0.42 % to 0.55 % at  $\beta = 2\beta_{iF.AISC}$  for all of the Category B test simulations. Given that the base AISC bracing strength requirement for nodal lateral bracing is 1 %, there is no reason why the base relative bracing requirement should not be

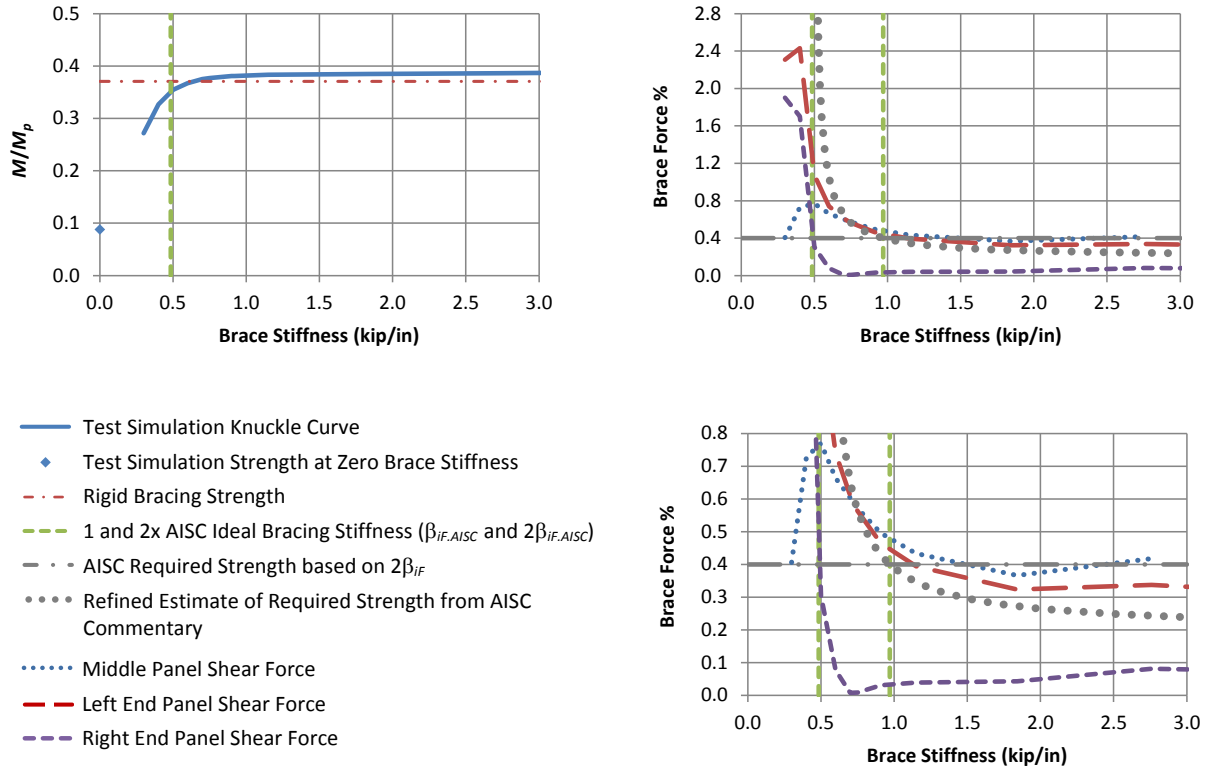


Fig. 6.4. Case B320 knuckle and brace force vs. brace stiffness curves (Compression flange shear panel (relative) lateral bracing,  $L_b = 15$  ft,  $n = 2$ ,  $\beta_{iF,AISC} = 0.48$  kip/in)

0.5 %. For Cases with  $n = 1$ , the relative bracing strength requirement theoretically must be one half of the nodal bracing strength requirement. A base shear panel bracing strength requirement of 0.5 % fits better with the overall mean of the test simulation data, compared to the 0.4 % value currently recommended by AISC Appendix 6. This shift in the base required strength value avoids undershooting of the required bracing strength

when using the modifier  $\frac{1}{2 - \frac{\beta_{req}}{\beta}}$  recommended in the commentary (with  $\beta_{req}$  taken equal

to  $2\beta_{iF,AISC}$  for  $\beta_{req}$  when comparing to test simulation, or physical test, results). This leads to the following observations:

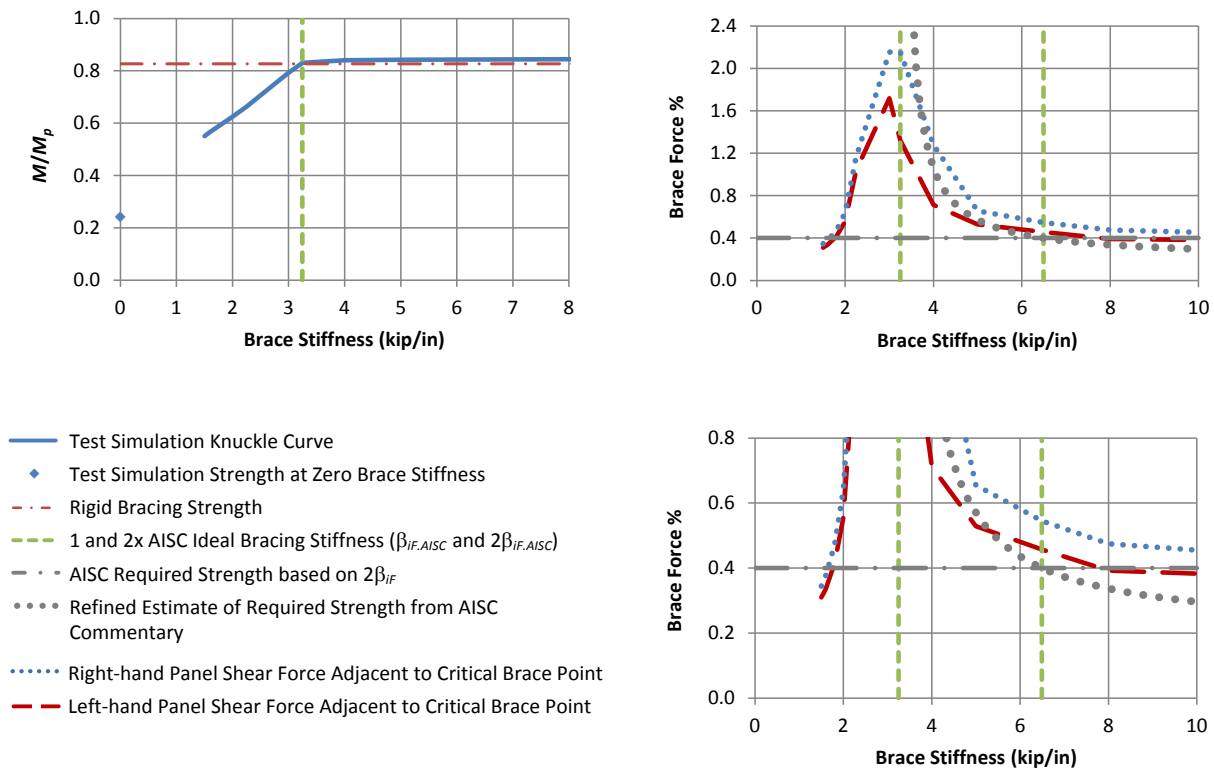


Fig. 6.5. Case B130 knuckle and brace force vs. brace stiffness curves  
 (Compression flange shear panel (relative) lateral bracing,  $L_b = 5$  ft,  $n = 3$ ,  $\beta_{IF,AISC} = 3.2$  kip/in)

- With the change in the base AISC strength requirement, the modifier on the brace strength requirement recommended in the AISC Appendix 6 Commentary provides a reasonably accurate (slightly low for large shear panel stiffnesses) to conservative estimate (increasingly conservative as  $\beta$  approaches  $\beta_{IF,AISC}$  from above) of the maximum shear panel strength requirement obtained from the test simulations.

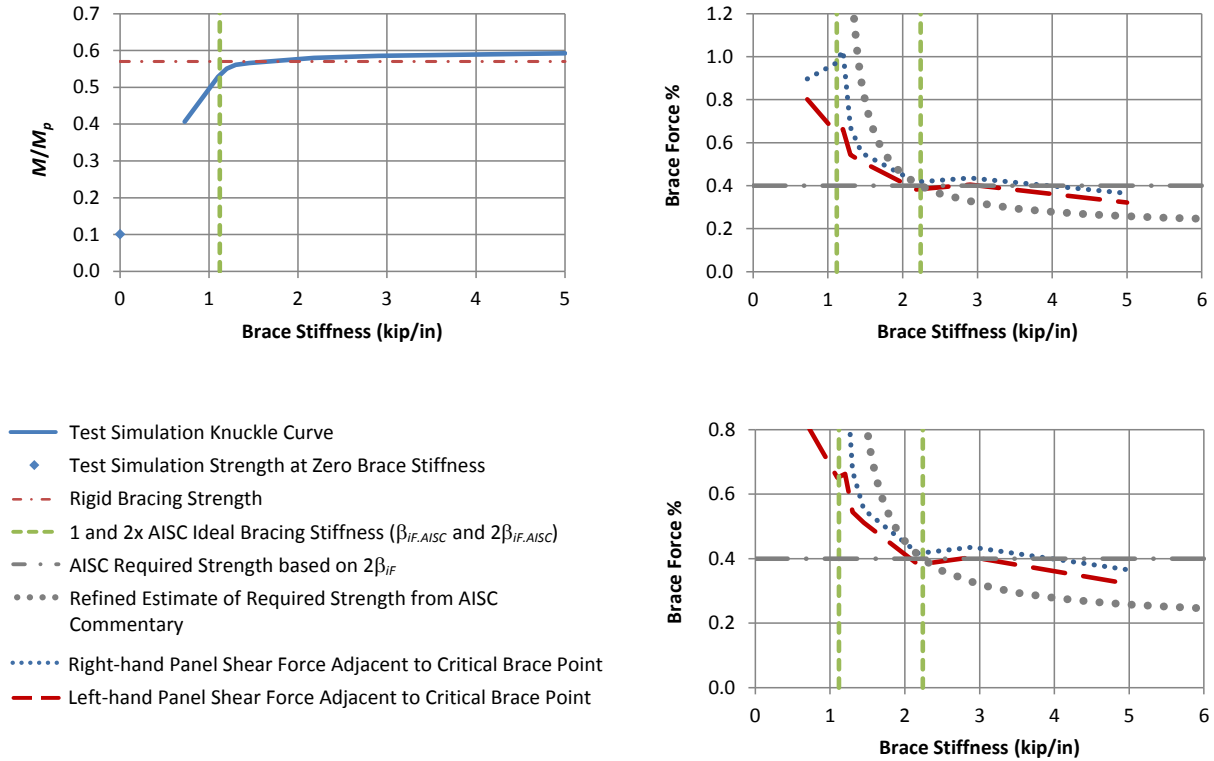


Fig. 6.6. Case B230 knuckle and brace force vs. brace stiffness curves  
 (Compression flange shear panel (relative) lateral bracing,  $L_b = 10$  ft,  $n = 3$ ,  $\beta_{iF,AISC} = 1.1$  kip/in)

- For smaller  $\beta$  values, the above refined estimate from the AISC commentary

becomes very conservative. This conservatism is due to the fact that  $\frac{1}{2 - \frac{\beta_{req}}{\beta}}$  is

derived from a simplified second-order elastic analysis model that does not account for the influence of continuity of the member across the brace locations.

As the brace stiffness approaches  $\beta_{iF,AISC}$ , the modifier from the AISC

Commentary goes to infinity, whereas the actual brace forces are well bounded.

The simplified second-order elastic analysis model gives the same second-order amplification as the  $B_2$  equation in AISC Appendix 8 with  $R_M$  taken equal to 1.0.

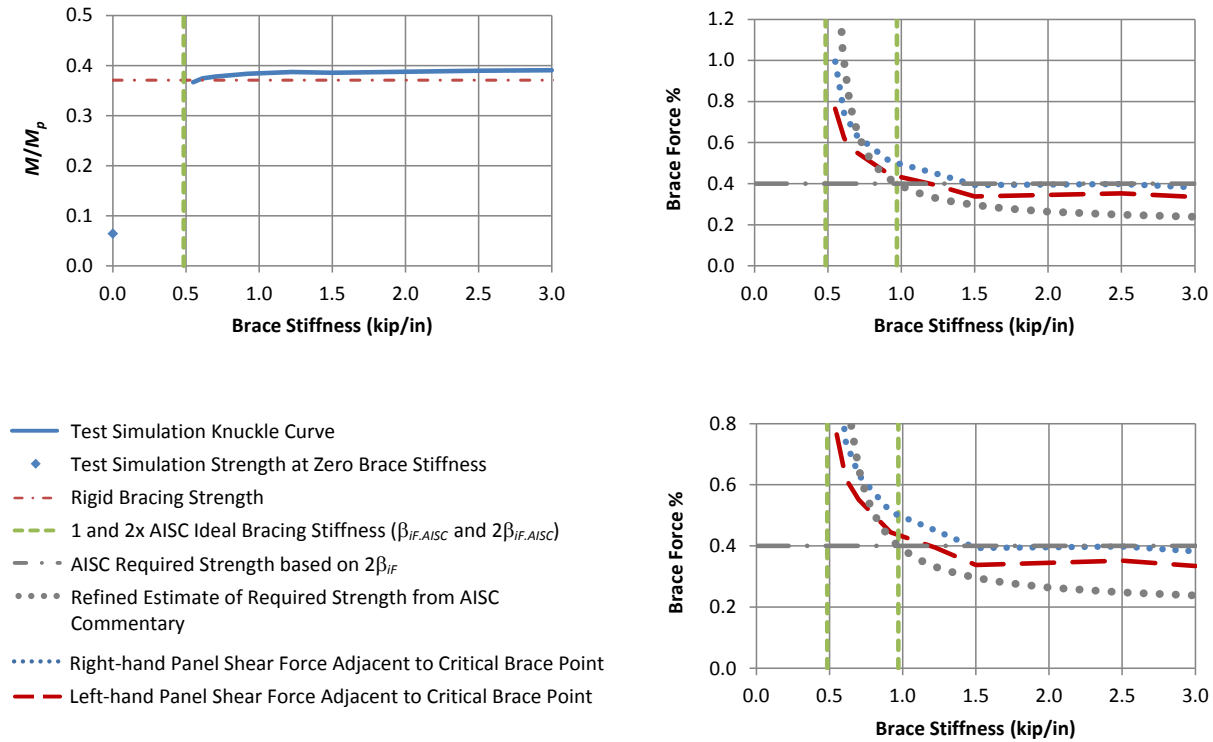


Fig. 6.7. Case B330 knuckle and brace force vs. brace stiffness curves (Compression flange shear panel (relative) lateral bracing,  $L_b = 15$  ft,  $n = 3$ ,  $\beta_{iF,AISC} = 0.48$  kip/in)

- The required brace strengths are larger for partial bracing cases, compared to the requirements for full bracing; the current AISC Specification Appendix 6 does not explicitly address this behavior. The AISC Commentary suggests that the

modifier on the required brace strength,  $\frac{1}{2 - \frac{2\beta_{iF,AISC}}{\beta}}$  should be applied only for

brace stiffnesses larger than  $2\beta_{iF,AISC}/\phi$ . The results in Figures 6.2 to 6.7 show that this modifier works reasonably well in all cases for roughly  $\beta \geq 1.5\beta_{iF,AISC}$ .

This limit is somewhat close to  $\beta_{F98}$ .

- The modifier on the brace strength from the AISC Commentary, as well as the underlying  $B_2$  amplification factor, becomes unbounded as  $\beta$  approaches  $\beta_{iF,AISC}$ .

The reasons why the physical brace forces do not become unbounded as  $\beta$  approaches  $\beta_{iF.AISC}$  are as follows:

- The physical member participates in resisting the brace point displacements more and more with decreasing  $\beta$ , from essentially no participation (since the member is buckling between the brace points) for large  $\beta$ , to substantial participation for very flexible partial bracing. The idealized second-order elastic model on which the modifier  $\frac{1}{2 - \frac{2\beta_{iF.AISC}}{\beta}}$  is based does not account for any participation of the member in resisting the brace point displacements. In addition, the model upon which the AISC shear panel bracing equations are based does not account for any participation of the member in resisting the brace point displacements; this model assumes pins at each of the brace point locations.
- As the member lateral displacements commence due to buckling of the member between the brace points (for full bracing), or the member and its bracing system (for partial bracing), yielding soon starts (if it has not started already) and the yielding continues to spread through the member cross-section and along the member length. This results in the member, or the member and its bracing system, reaching a limit load at finite brace point displacements (and thus at finite brace forces). This limits the magnitude of the brace forces that need to be resisted to develop the member (or system) limit load.
- At a point significantly before the brace point displacements become infinite, the member deflections no longer satisfy the small rotation assumption implicit in the derivation of the magnifier  $\frac{1}{2 - \frac{2\beta_{iF.AISC}}{\beta}}$ . This results in an increased strength of the physical

geometrically imperfect member, for cases involving stable post buckling response, or a limit load response at a finite brace point displacement, for cases involving unstable post buckling response.

Figures 6.8 through 6.10 give bar graph comparisons of the ideal full bracing stiffness values versus full bracing stiffness values based on developing 98% of the rigidly braced member strength for Category B (compression flange relative bracing).

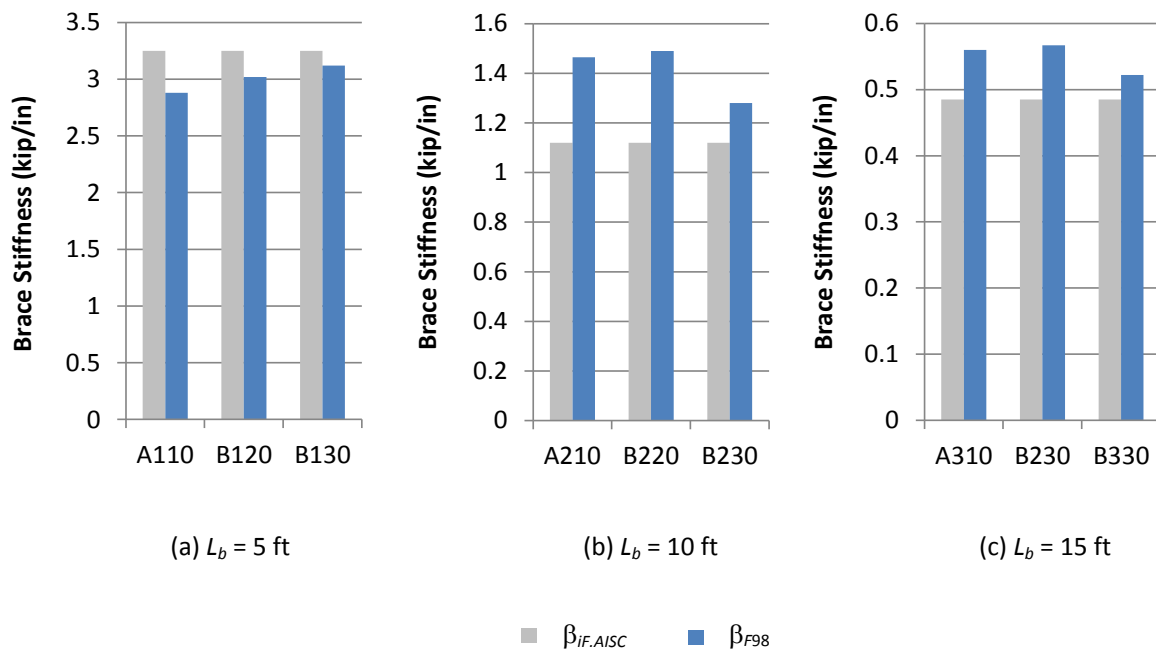


Fig. 6.8. Bar graph comparison of ideal full bracing stiffness values,  $\beta_{IF,AISC}$ , versus full bracing stiffness values based on developing 98 % of the rigidly braced member strength,  $\beta_{F98}$ , for Case B (Compression flange shear panel (relative) lateral bracing)

It is observed that the  $\beta_{F98}$  is essentially unaffected by the number of intermediate brace locations, as predicted by the AISC relative bracing model. This stiffness value changes by only 8 % as  $n$  is increased from one to three for the plastic buckling cases, it changes by only +2 to -13

% as  $n$  is increased from one to three for the inelastic buckling cases, and it changes by only +1 to -7 % as  $n$  is increased from one to three for the elastic buckling cases. This is very different

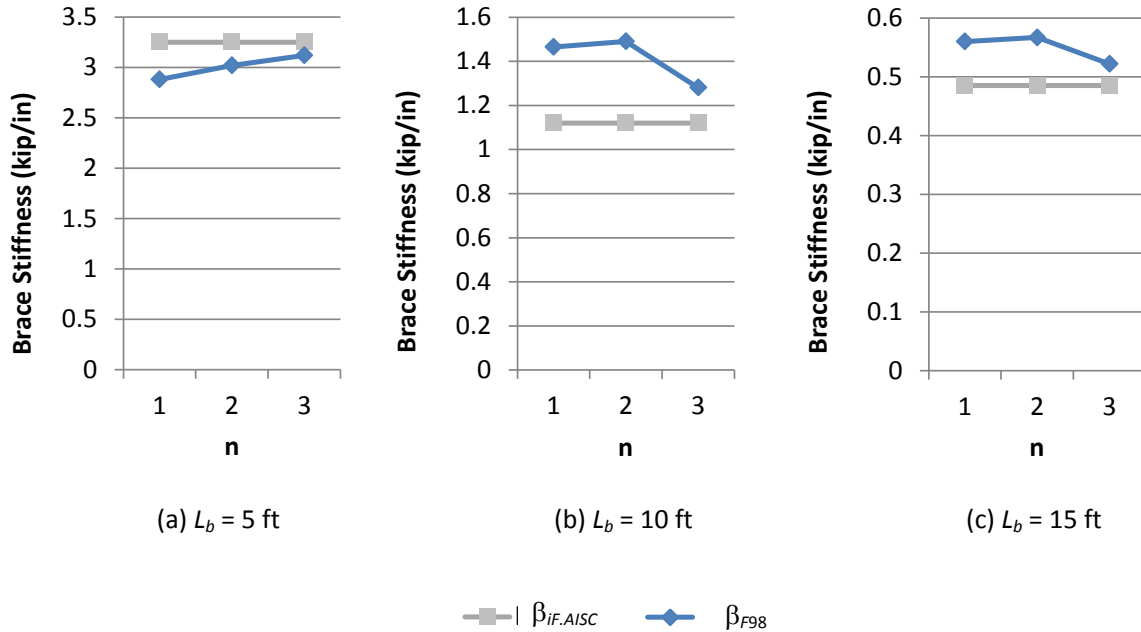


Fig. 6.9. Line plot comparison of ideal full bracing stiffness values,  $\beta_{iF.AISC}$ , versus full bracing stiffness values based on developing 98 % of the rigidly braced member strength,  $\beta_{F98}$ , for Case B (Compression flange shear panel (relative) lateral bracing)

from the behavior for nodal lateral bracing, which shows increases in the bracing stiffness requirements of 1.29 to 1.41 as the number of intermediate braces is increased from 1 to 2. Contrary to the nodal bracing cases, there is no significant reduction in the brace strength requirement relative to the refined (modified) AISC Commentary predictions with increases in  $n$ .

Figures 6.11 through 6.16 shows the  $M/M_p$  vs. the top flange brace force for selected stiffness values of the cases in category B. Plots are shown in increasing brace stiffness order.

The following observations are made from Figures 6.11 through 6.16 for partial bracing of members that fail by plastic buckling:

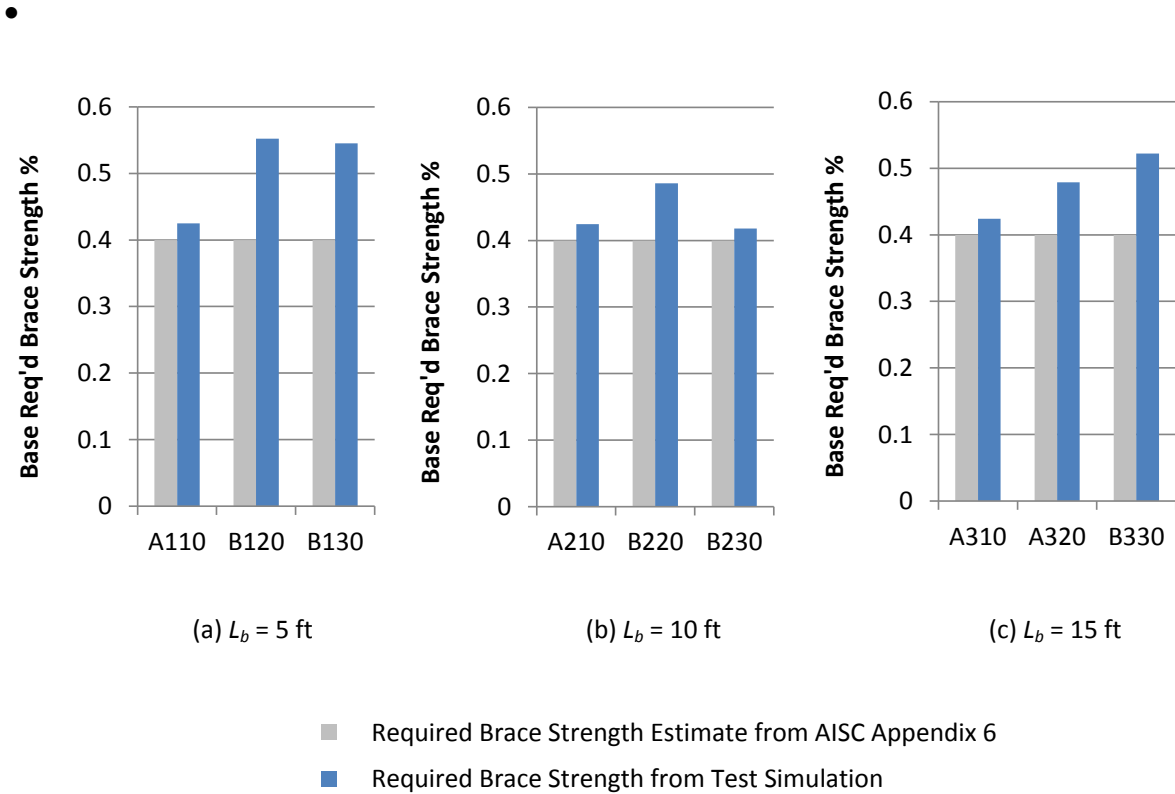
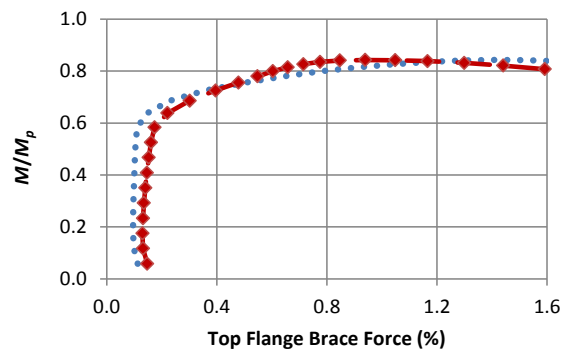
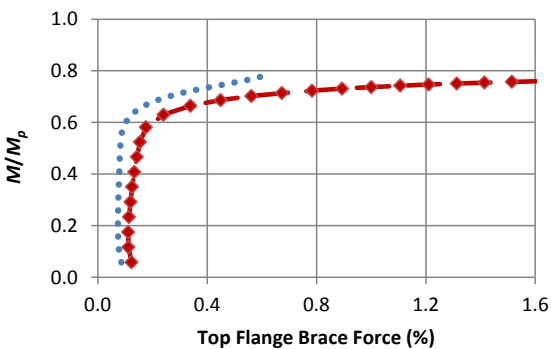


Fig. 6.10. Bar graph comparison of base AISC required strength corresponding to  $\beta = 2\beta_{iF.AISC}$  versus the test simulation required brace strength at the member limit load, using this brace stiffness (Case B, compression flange shear panel (relative) lateral bracing)

- The brace forces are relatively small until the member starts to yield, at which point they increase rapidly. The brace forces at the member limit load are substantially larger than the base AISC design values (corresponding to  $2\beta_{iF.AISC}$ ) for these partial bracing cases.

- The  $M/M_p$  vs. brace force curves are very round-house when  $n = 2$ ; however, for  $n = 3$ , this round-house nature of the curves is reduced (i.e., the brace forces are a little smaller at the larger  $M/M_p$  values up to near to the limit load of the member).
- 
- The second-order amplification of the brace forces (and brace point displacements) is evidenced by a more significant round house nature of the  $M/M_p$  versus brace force curves, particularly for the longer unbraced lengths. For the partially-braced member cases, the second-order amplification of the brace forces (and brace point displacements) is evidenced by a more significant round house nature of the  $M/M_p$  vs. brace force curves, particularly for the longer unbraced lengths.

One can observe that a maximum shear panel force of 1 % is sufficient to develop approximately 95 % of the strength of the fully or partially braced member for all the test simulations conducted. By reviewing the load-deflection plots, one can observe that a maximum shear panel force of 1 % is sufficient to develop approximately 95 % of the strength of the fully or partially braced member for all the test simulations conducted.



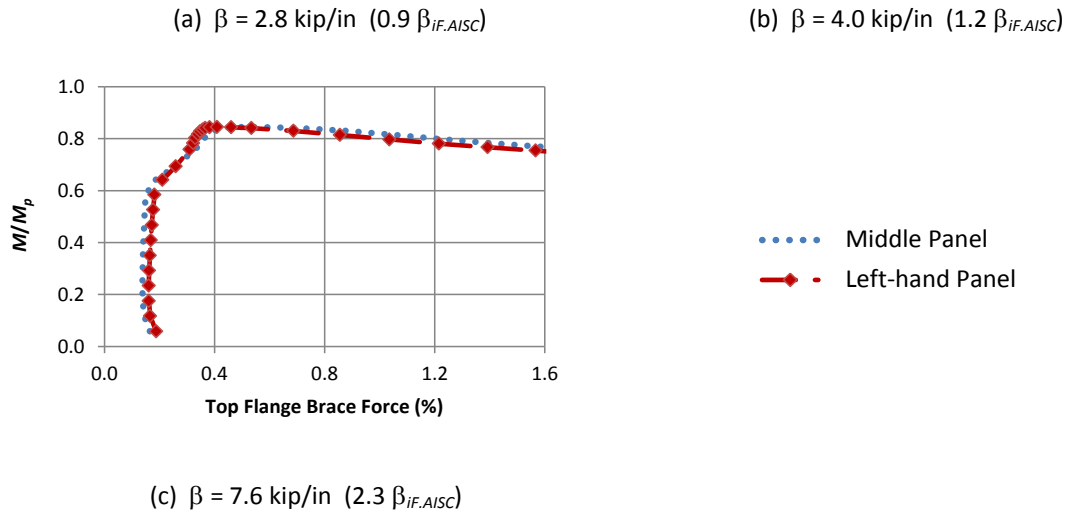


Fig. 6.11. Case B120  $M/M_p$  vs. % brace force curves for a progression of increasing brace stiffnesses (Compression flange shear panel (relative) bracing,  $L_b = 5 \text{ ft}$ ,  $n = 2$ ,  $\beta_{iF.AISC} = 3.2 \text{ kip/in}$ )

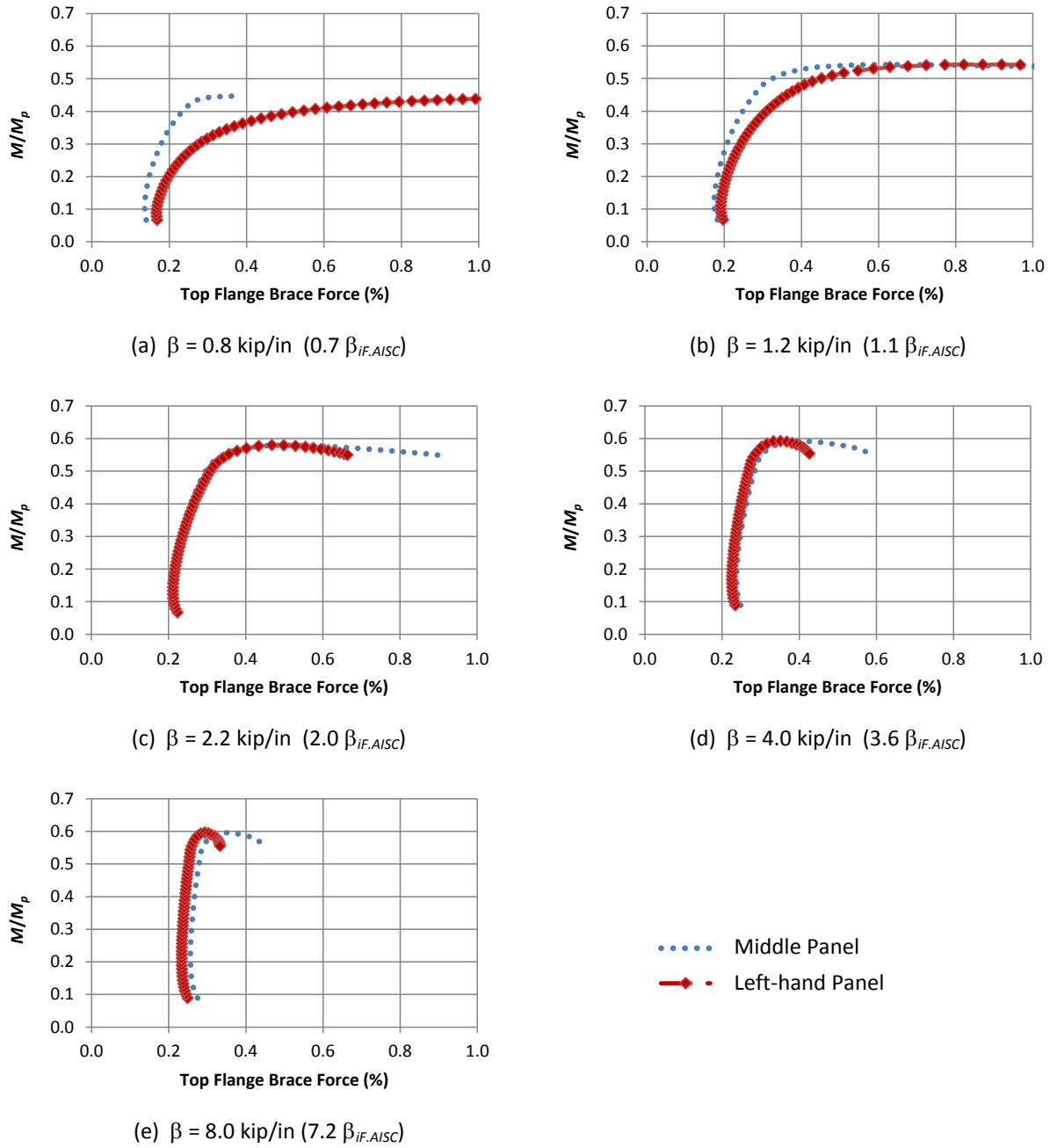
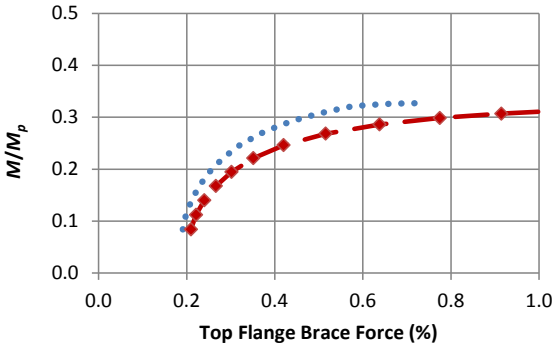
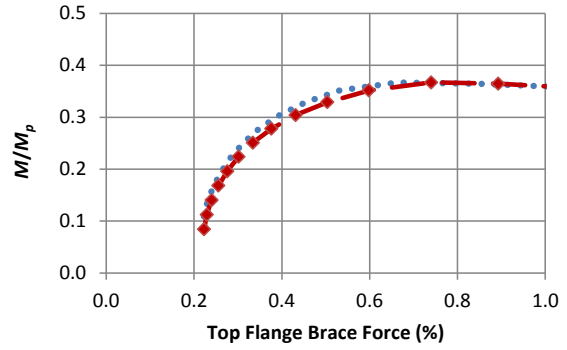


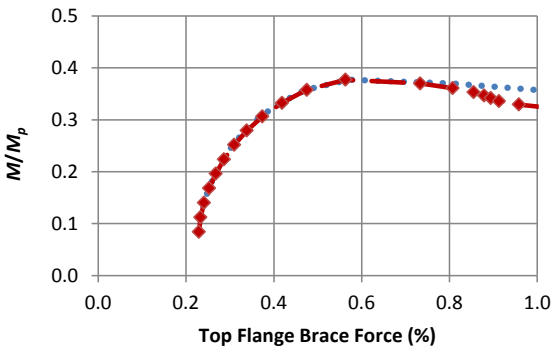
Fig. 6.12. Case B220  $M/M_p$  vs. % brace force curves for a progression of increasing brace stiffnesses (Compression flange shear panel (relative) bracing,  $L_b = 10$  ft,  $n = 2$ ,  $\beta_{iF.AISC} = 1.1$  kip/in)



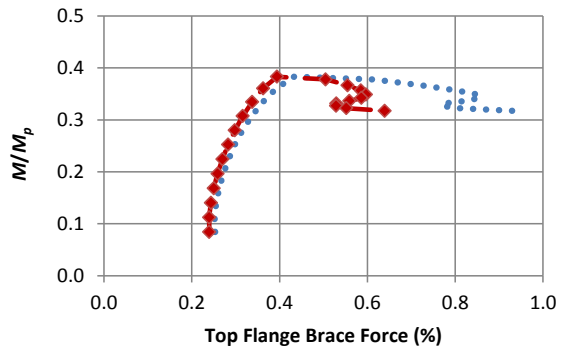
(a)  $\beta = 0.40$  kip/in ( $0.8 \beta_{IF.AISC}$ )



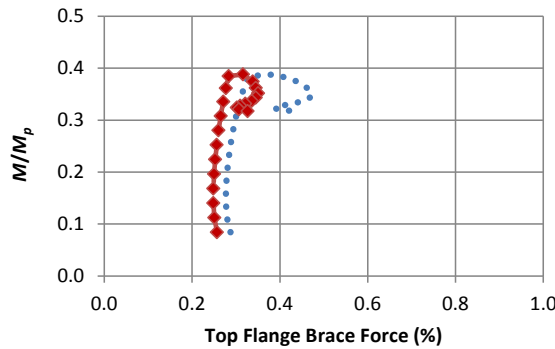
(b)  $\beta = 0.60$  kip/in ( $1.2 \beta_{IF.AISC}$ )



(c)  $\beta = 0.75$  kip/in ( $1.5 \beta_{IF.AISC}$ )



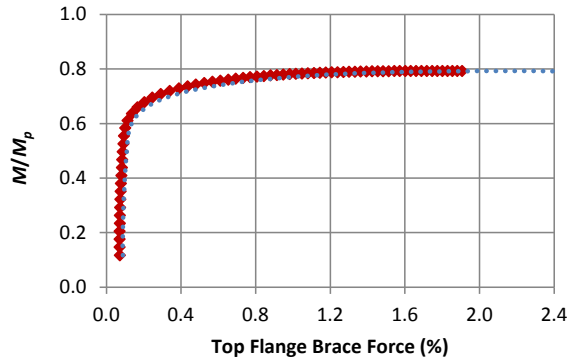
(d)  $\beta = 1.2$  kip/in ( $2.5 \beta_{IF.AISC}$ )



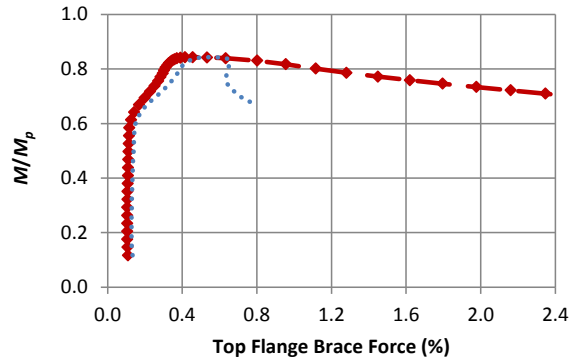
(e)  $\beta = 3.7$  kip/in ( $7.6 \beta_{IF.AISC}$ )

● Middle Panel  
◆ Left-hand Panel

Fig. 6.13. Case B320  $M/M_p$  vs. % brace force curves for a progression of increasing brace stiffnesses (Compression flange shear panel (relative) bracing,  $L_b = 15$  ft,  $n = 2$ ,  $\beta_{IF.AISC} = 0.48$  kip/in)



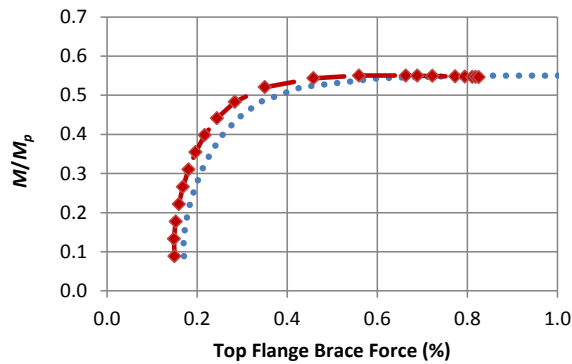
(a)  $\beta = 3.0$  kip/in ( $0.9 \beta_{iF,AISC}$ )



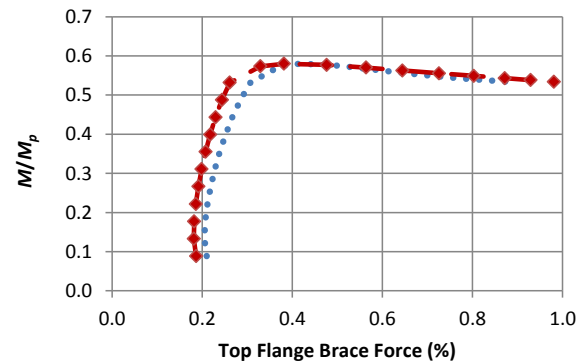
(b)  $\beta = 6.5$  kip/in ( $2.0 \beta_{iF,AISC}$ )

- Right-hand Panel Adjacent to Critical Brace Point
- ◆— Left-hand Panel Adjacent to Critical Brace Point

Fig. 6.14. Case B130  $M/M_p$  vs. % brace force curves for a progression of increasing brace stiffnesses (Compression flange shear panel (relative) bracing,  $L_b = 5$  ft,  $n = 3$ ,  $\beta_{iF,AISC} = 3.2$  kip/in)



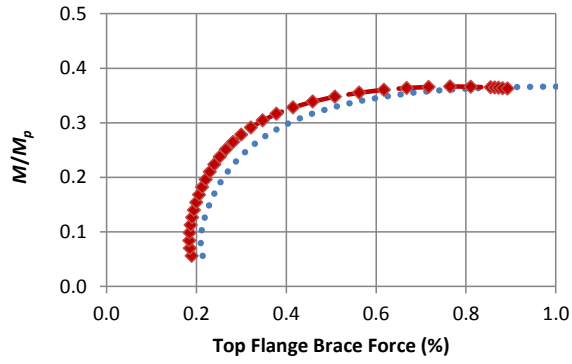
(a)  $\beta = 1.2$  kip/in ( $1.1 \beta_{iF,AISC}$ )



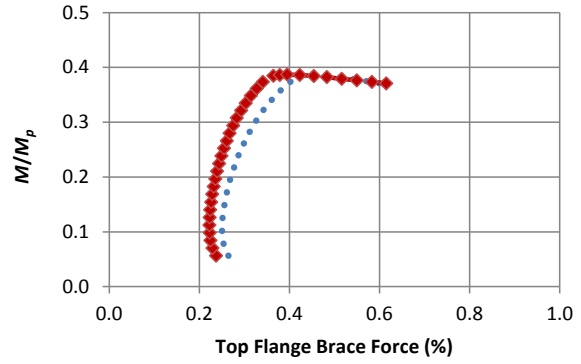
(b)  $\beta = 2.2$  kip/in ( $2.0 \beta_{iF,AISC}$ )

- Right-hand Panel Adjacent to Critical Brace Point
- ◆— Left-hand Panel Adjacent to Critical Brace Point

Fig. 6.15. Case B230  $M/M_p$  vs. % brace force curves for a progression of increasing brace stiffnesses (Compression flange shear panel (relative) bracing,  $L_b = 10$  ft,  $n = 3$ ,  $\beta_{iF,AISC} = 1.1$  kip/in)



(a)  $\beta = 0.55$  kip/in ( $1.1 \beta_{iF,AISC}$ )



(b)  $\beta = 1.2$  kip/in ( $2.5 \beta_{iF,AISC}$ )

- Right-hand Panel Adjacent to Critical Brace Point
- ◆— Left-hand Panel Adjacent to Critical Brace Point

Fig. 6.16. Case B330  $M/M_p$  vs. % brace force curves for a progression of increasing brace stiffnesses (Compression flange shear panel (relative) bracing,  $L_b = 15$  ft,  $n = 3$ ,  $\beta_{iF,AISC} = 0.48$  kip/in)



## CHAPTER 7

### TORSIONAL BRACING REQUIREMENTS

#### 7.1 Category C: Nodal Torsional Bracing Results

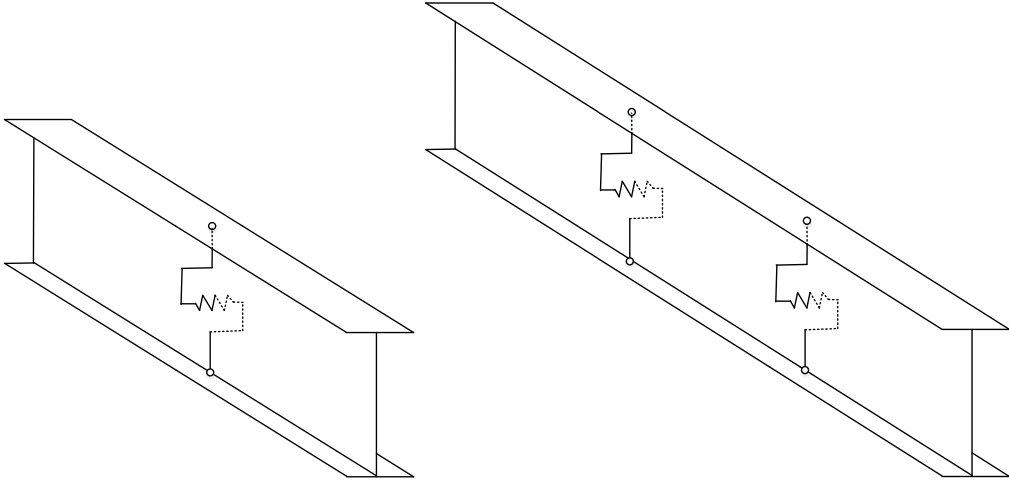
Table 7.1 shows the base nominal bracing stiffness ( $\beta_{Tbr} = 2\beta_{iF.AISC}$ ) required from the AISC Appendix 6 Commentary, where  $\beta_{iF.AISC}$  is the conceptual AISC ideal full (torsional) bracing stiffness for beams based on the applied moment  $M$  (rather than a theoretical member elastic buckling capacity). This is given by Equation (2-44) with  $C_{iT}$  taken equal to 1.0. Furthermore, in the calculation of  $\beta_{Tbr}$ , the values of  $M$  are taken as the rigidly-braced strengths  $M_{max}$  from Table 4.3. These are the moment capacities from the simulations for the rigid torsional bracing cases with  $n_T = 1$ , which are the smallest rigidly braced strengths.

Table 7.1. Category C maximum strengths with required bracing stiffness

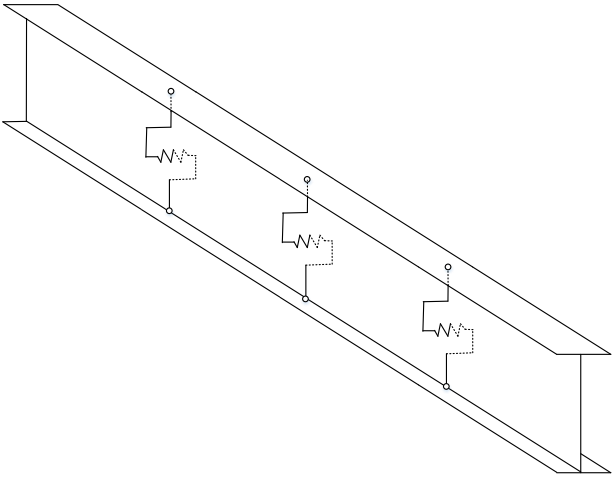
Case	$L_b$ (ft)	$n$	$P_{ef\_eff}$	$M_{max}$ (kip-in)	$\beta_{Treq}$ (kip/in)
C110	5	1	819	3945	15.25
C210	10		205	2720	14.50
C310	15		91	1767	9.18
C120	5	2	819	3945	11.44
C220	10		205	2720	10.87
C320	15		91	1767	6.88
C130	5	3	819	3945	10.16
C230	10		205	2720	9.66
C330	15		91	1767	6.12

Figure 7.2 shows the models to be used for category C. They are C\*10 (C110, C210, C310), C\*20 (C120, C220, C320), and C\*30 (C130, C230, C330). Figures 7.2 through 7.4 are similar to those shown for Category A's Figures 5.2 through 5.4. The exception being that the

behavior of the results are different due to the relative stiffness between the top and bottom flange. Category C tends to have more gradual development of the fully rigid bracing strength in comparison with Categories A and B.

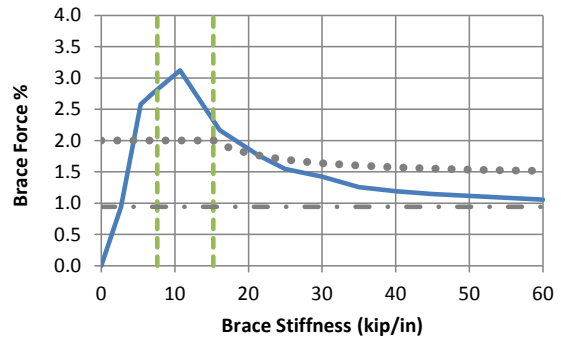
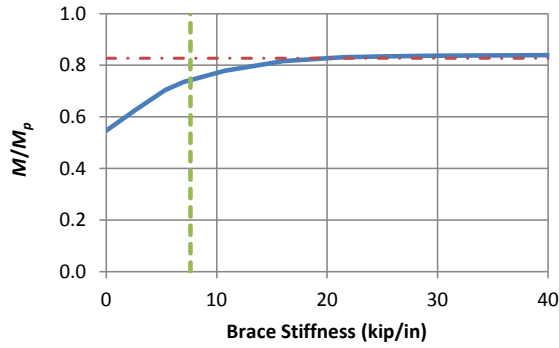


(a) Representative torsional bracing model for cases C\*10, C\*20

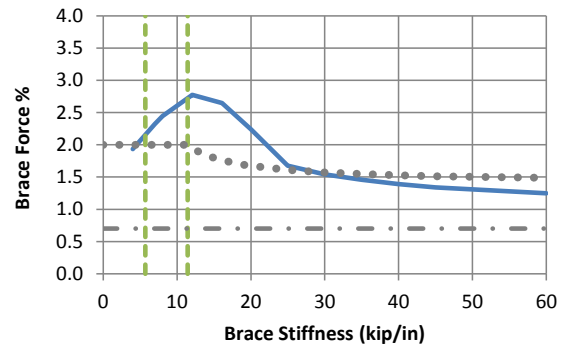
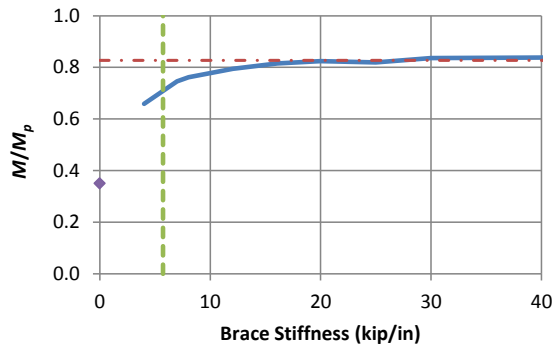


(b) Representative torsional bracing model for cases C\*30

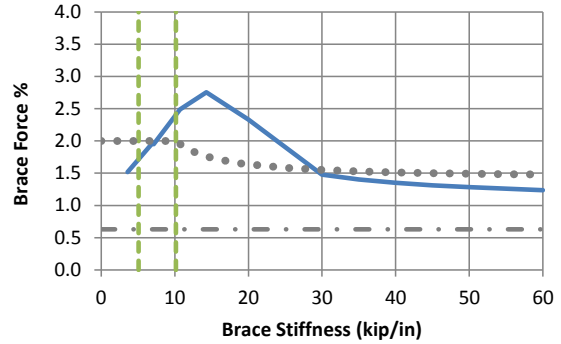
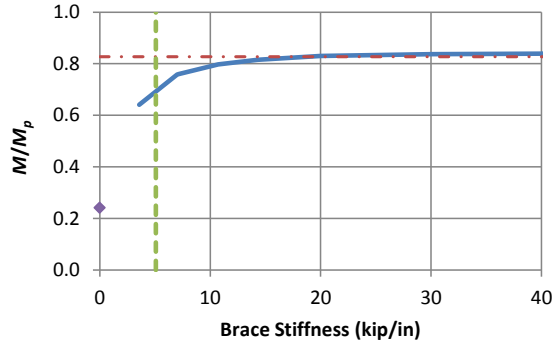
Fig. 7.1. Representative torsional bracing model for cases C\*10, C\*20, and C\*30



(a) C110 ( $n = 1$ ,  $\beta_{iF.AISC} = 7.6$  kip/in,  $V_{br.AISC} = 0.94$  %)



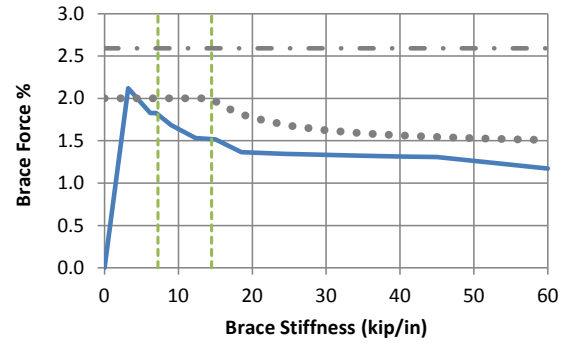
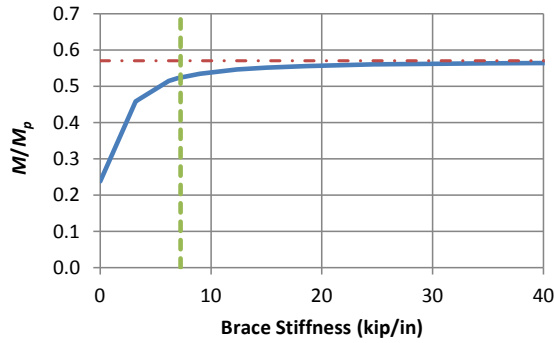
(b) C120 ( $n = 2$ ,  $\beta_{iF.AISC} = 5.7$  kip/in,  $V_{br.AISC} = 0.70$  %)



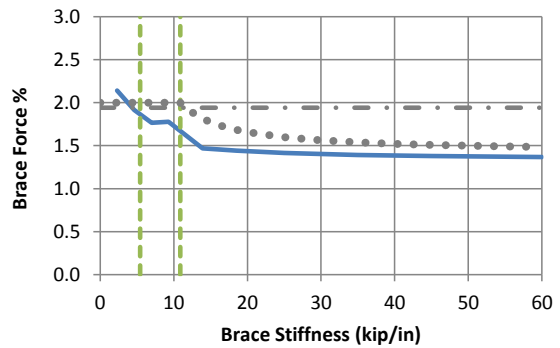
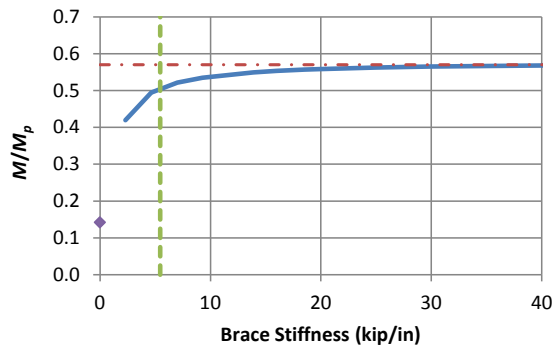
(c) C130 ( $n = 3$ ,  $\beta_{iF.AISC} = 5.1$  kip/in,  $V_{br.AISC} = 0.63$  %)

- Test Simulation Results
- ◆ Test Simulation Strength at Zero Brace Stiffness
- - - Rigid Bracing Strength
- - - 1 and 2x AISC Ideal Bracing Stiffness ( $\beta_{iF.AISC}$  and  $2\beta_{iF.AISC}$ )
- · - Base AISC Required Strength Corresponding to  $\beta = 2\beta_{iF.AISC}$
- · · Recommended Refined Estimate of Required Strength

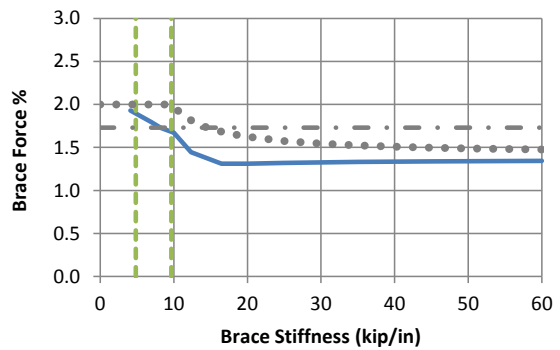
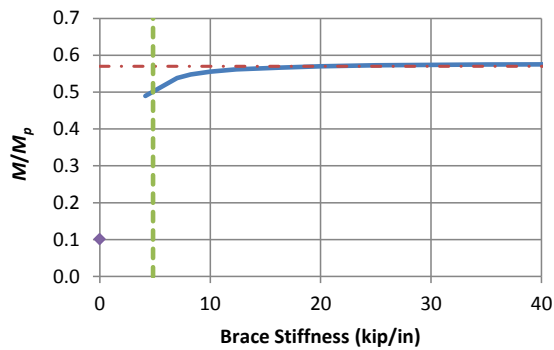
Fig. 7.2. Case C1\*0 knuckle and brace force vs. brace stiffness curves (Nodal torsional bracing,  $L_b = 5$  ft)



(a) C210 ( $n = 1$ ,  $\beta_{iF.AISC} = 7.2$  kip/in,  $V_{br.AISC} = 2.6$  %)



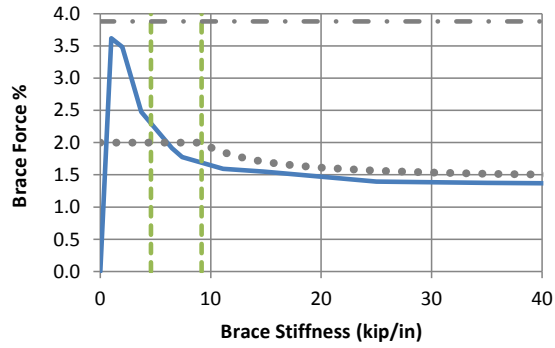
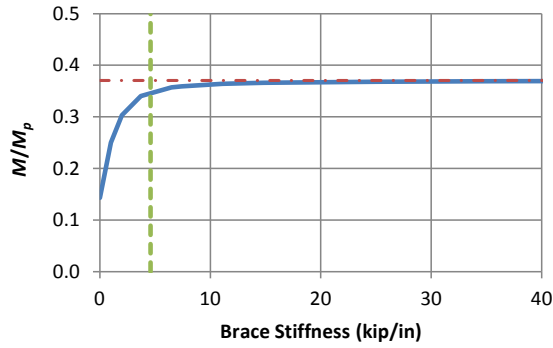
(b) C220 ( $n = 2$ ,  $\beta_{iF.AISC} = 5.4$  kip/in,  $V_{br.AISC} = 1.9$  %)



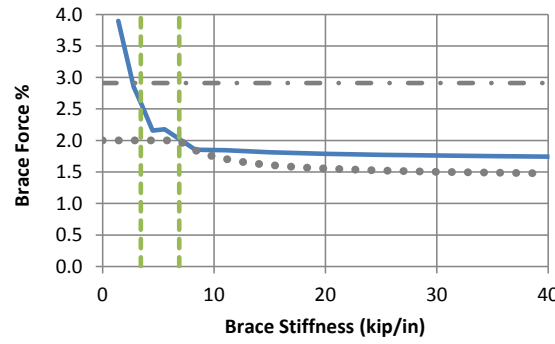
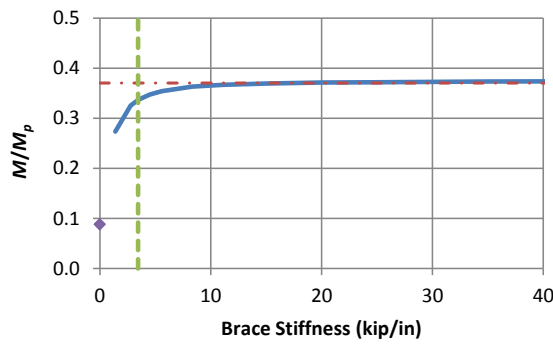
(c) C230 ( $n = 3$ ,  $\beta_{iF.AISC} = 4.8$  kip/in,  $V_{br.AISC} = 1.7$  %)

- Test Simulation Results
- ◆ Test Simulation Strength at Zero Brace Stiffness
- - - Rigid Bracing Strength
- - - 1 and 2x AISC Ideal Bracing Stiffness ( $\beta_{iF.AISC}$  and  $2\beta_{iF.AISC}$ )
- · - Base AISC Required Strength Corresponding to  $\beta = 2\beta_{iF.AISC}$
- · · Recommended Refined Estimate of Required Strength

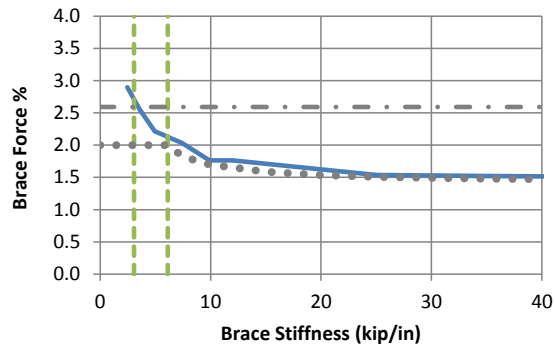
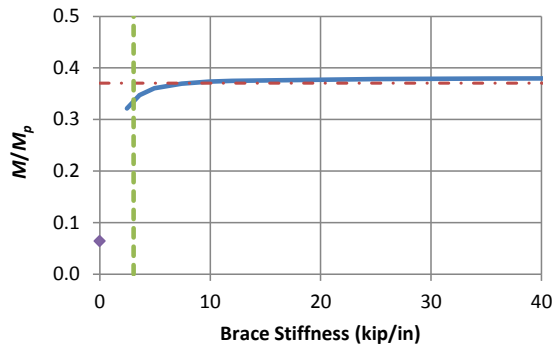
Fig. 7.3. Case C2\*0 knuckle and brace force vs. brace stiffness curves (Nodal torsional bracing,  $L_b = 10$  ft)



(a) C310 ( $n = 1$ ,  $\beta_{iF.AISC} = 4.6$  kip/in,  $V_{br.AISC} = 3.9$  %)



(b) C320 ( $n = 2$ ,  $\beta_{iF.AISC} = 3.4$  kip/in,  $V_{br.AISC} = 2.9$  %)



(c) C330 ( $n = 3$ ,  $\beta_{iF.AISC} = 3.2$  kip/in,  $V_{br.AISC} = 2.6$  %)

- Test Simulation Results
- ◆ Test Simulation Strength at Zero Brace Stiffness
- - - Rigid Bracing Strength
- - - 1 and 2x AISC Ideal Bracing Stiffness ( $\beta_{iF.AISC}$  and  $2\beta_{iF.AISC}$ )
- · - Base AISC Required Strength Corresponding to  $\beta = 2\beta_{iF.AISC}$
- · · Recommended Refined Estimate of Required Strength

Fig. 7.4. Case C3\*0 knuckle and brace force vs. brace stiffness curves (Nodal torsional bracing,  $L_b = 15$  ft)

The following observations can be made from Figures 7.2 through 7.4 for category C (nodal torsional bracing):

- The ideal full bracing stiffness values from AISC Appendix 6 ( $\beta_{iF.AISC}$ ) are considerably smaller than the minimum required full bracing stiffnesses  $\beta_{F98}$  and  $\beta_{F96}$ , the minimum required full bracing stiffness set at 96% of the rigidly brace strength. The mean of the ratio  $\beta_{F96}/\beta_{iF.AISC}$  is 1.8, with maximum and minimum values of 2.5 and 1.4. The mean of the ratio  $\beta_{F98}/\beta_{iF.AISC}$  is 2.6, with maximum and minimum values of 3.8 and 1.8. The largest of these ratios occurs for the inelastic buckling cases.
- The  $\beta_{F98}$  values are substantially larger than the  $\beta_{F96}$  and  $\beta_{iF.AISC}$  values for the inelastic buckling cases. This is related to the fact that the base rigid bracing strength (taken as the minimum of the rigid bracing strengths for different specific bracing types) for  $L_b = 10$  ft is based on case C210, as well as the fact that the rigid bracing strengths for C220 are essentially the same as those for C210. As such, the intersection between the knuckle curves for these cases and the rigid bracing strength occurs well out within the flat portion of the knuckle curves for these cases, making the definition of the full bracing stiffness quite sensitive to minor variations in the curves.
- The knuckle curves for torsional bracing tend to be more rounded and approach the rigid bracing strength more gradually than the knuckle curves for the other types of bracing
- The partial bracing member resistance can be approximated accurately to somewhat conservatively in all cases by drawing a straight line between the rigidly-braced strength at  $\beta = \beta_{F98}$  and the strength of the member for zero bracing stiffness at  $\beta = 0$ . The nature of this approximation does not appear to vary significantly as a function of  $n$ .

- There is no significant drop in beam strength until the brace stiffness becomes less than  $\beta_{F98}$ . The brace forces increase more significantly with decreasing brace stiffness below this value.
- The largest brace forces for any brace stiffness (at the development of the member limit load) are less than about 3 % for the plastic LTB cases, 2 % for the inelastic LTB cases, and 4 % for the elastic LTB cases.
- The maximum overall brace force (at the development of the member limit load), considering partial bracing, typically occurs at  $\beta$  values slightly to significantly above  $\beta_{iF.AISC}$  for the plastic buckling cases. It occurs at  $\beta$  values ranging from close to significantly less than  $\beta_{iF.AISC}$  for the inelastic and elastic buckling cases.

The AISC brace force estimate corresponding to  $\beta = 2\beta_{iF.AISC}$  is generally rather inaccurate. The AISC estimate tends to substantially under-predict the required brace strength for short unbraced lengths involving LTB after developing substantial plasticity. The source of this under prediction can be observed clearly in the form of the equation for the required torsional bracing stiffness presented in this report. For short unbraced lengths, the term  $P_{ef,eff}$ , which represents an equivalent column lateral buckling capacity of the compression flange, becomes relatively large, which reduces the bracing stiffness requirement. For the intermediate unbraced length involving inelastic buckling, the AISC brace force estimate matches closely with the test simulation results for C230 ( $n = 3$ ) and becomes increasingly conservative for  $n = 2$  and 1. For the longer unbraced length involving predominantly elastic buckling, the AISC brace force estimate ranges from slightly conservative for  $n = 3$  to highly conservative for  $n = 1$ .

The Appendix 6 modifier on the base brace strength requirement,  $\frac{1}{2 - \frac{2\beta_{iF.AISC}}{\beta}}$ , does not

work well in predicting the variation in the torsional brace forces at the member strength limit as a function of the torsional brace stiffness. However, the ad-hoc modifier

$$\frac{1}{\left(2 - \frac{2\beta_{iF.AISC}}{\beta}\right)^{0.5}} \quad (7-1)$$

combined with a base torsional brace strength requirement of 2 %, gives a reasonably good estimate of the torsional brace forces for  $\beta \geq 2\beta_{iF.AISC}$ . For  $\beta < 2\beta_{iF.AISC}$ , it can be observed that a brace force requirement of 2 % provides an upper bound to the brace forces required to develop 95 % or greater of the load capacity from the test simulations in all cases (i.e., for all brace stiffness values). Therefore, it is recommended that 2 % can be used as the required torsional brace strength within this range. Similar to the behavior for nodal lateral and shear panel lateral bracing, the torsional brace forces are well bounded for all partial bracing cases.

Figures 7.5 through 7.7 give bar graph comparisons of the ideal full bracing stiffness values versus full bracing stiffness values based on developing 98% of the rigidly braced member strength for case C (compression flange nodal torsional bracing). The following observations can be made from these graphs:

- The AISC estimate for  $\beta_{iF.AISC}$  predicts that required stiffness reduces slightly with an increase in the number of intermediate braces,  $n$ . The test simulation values for  $\beta_{F98}$  and  $\beta_{F96}$  also show a slight decrease with increasing  $n$ , except that the values for  $\beta_{F98}$  are essentially unchanged between C110 and C120 and the values for  $\beta_{F96}$  are essentially unchanged between C210 and C220 and between C310 and C320.

- Unlike the nodal lateral and shear panel lateral bracing case, the number of intermediate braces,  $n$ , does not appear to have any significant influence on the bracing force requirements within the partial bracing range.

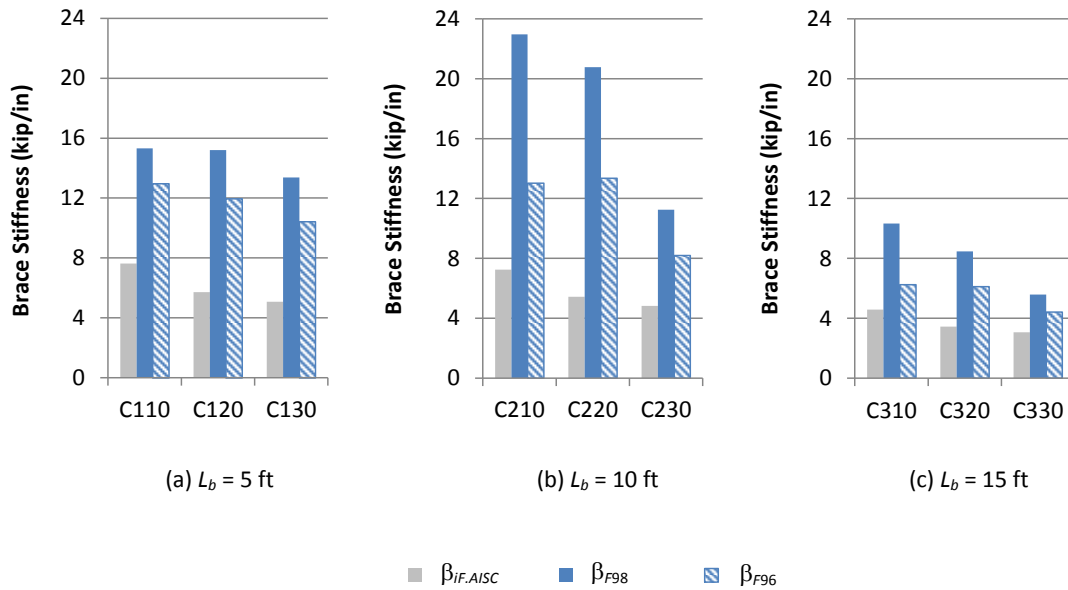


Fig. 7.5. Bar graph comparison of ideal full bracing stiffness values,  $\beta_{iF.AISC}$ , versus full bracing stiffness values based on developing 98 % of the rigidly braced member strength,  $\beta_{F98}$ , for Category C (Nodal torsional bracing)

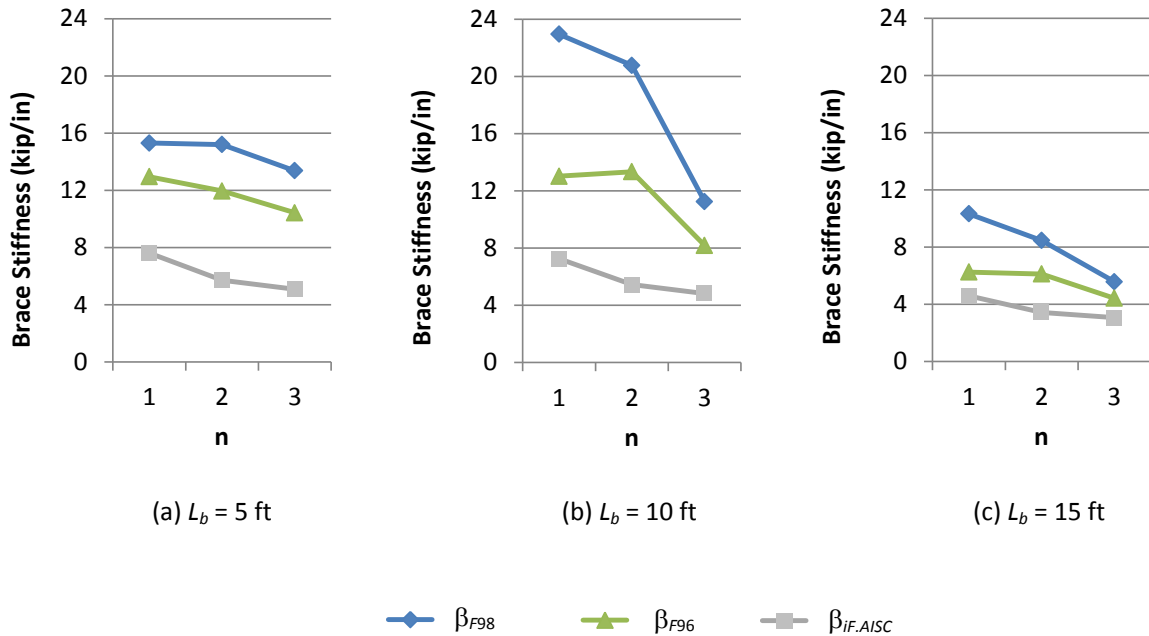


Fig. 7.6. Line plot comparison of ideal full bracing stiffness values,  $\beta_{IF.AISC}$ , versus full bracing stiffness values based on developing 98 % of the rigidly braced member strength,  $\beta_{F98}$ , for Category C (Nodal torsional bracing)

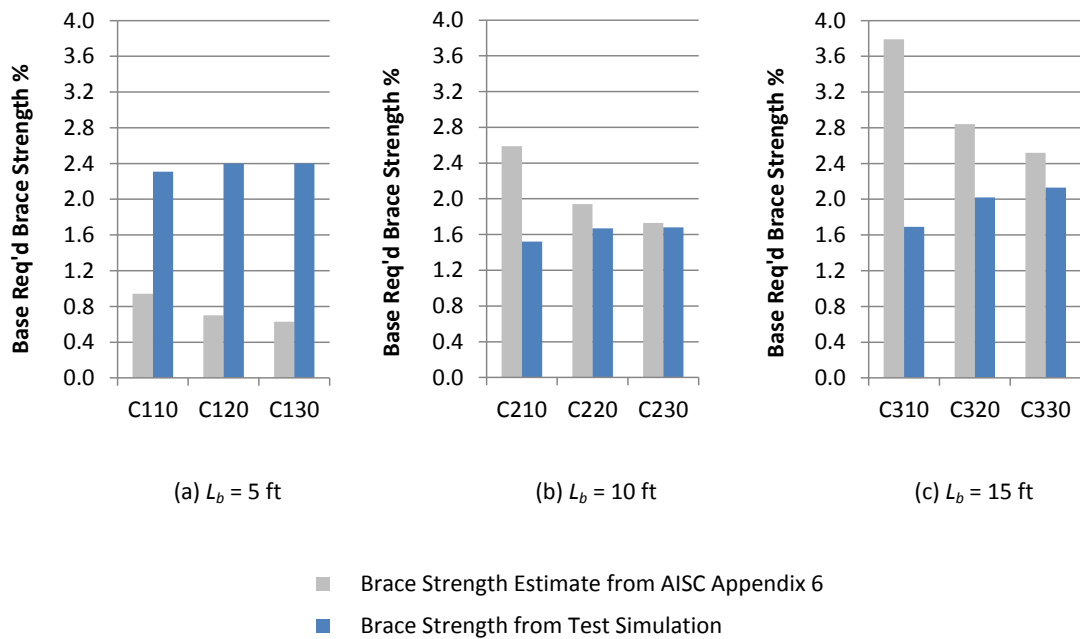
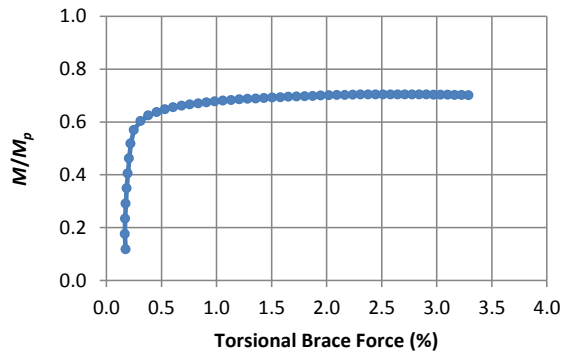


Fig. 7.7. Bar graph comparison of base AISC required strength corresponding to  $\beta = 2\beta_{IF.AISC}$  versus the test simulation required brace strength at the member limit load, using this brace stiffness (Category C, nodal torsional bracing)

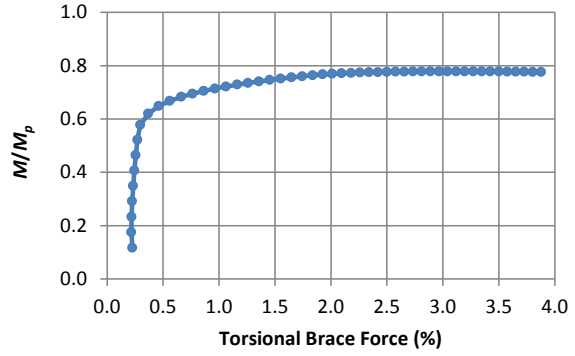
Figures 7.8 through 7.15 show the  $M/M_p$  vs the top flange brace force for selected stiffness values of the cases in category C. Plots are shown in increasing brace stiffness order.

The following observations are made from Figures 7.8 through 7.15:

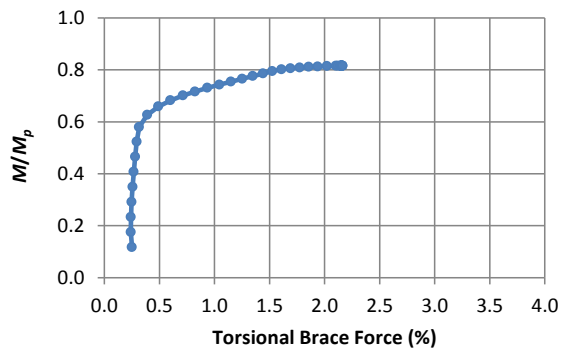
- For partial bracing of members that fail by plastic buckling, the brace forces are relatively small until the member starts to yield, at which point they increase rapidly. However, the brace forces for the partial bracing cases are not necessarily larger than the brace forces predicted by the current AISC torsional bracing estimates. This shows that plasticity reduces brace demands. The second-order amplification of the brace forces (and brace point displacements) is evidenced by a more significant round house nature of the  $M/M_p$  versus brace force curves for both the inelastic and elastic buckling cases. There does not appear to be a significant difference in the shape of these curves for inelastic versus elastic buckling however.
- As the brace stiffness is made larger and larger, the  $M/M_p$  versus torsional brace force curves tend to develop sharply defined “kinks”. These kinks correspond to the significant onset of yielding, as well as the development of the member maximum strength.
- From the  $M/M_p$  versus brace force curves, it can be observed that for partial bracing of members that fail by inelastic or elastic buckling, the  $M/M_p$  vs. brace force curves are very round-house for all the values of  $n$  considered.



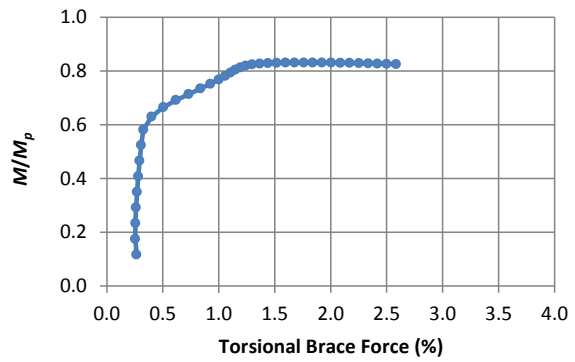
(a)  $\beta = 5.4$  ( $0.68 \beta_{iF.AISC}$ )



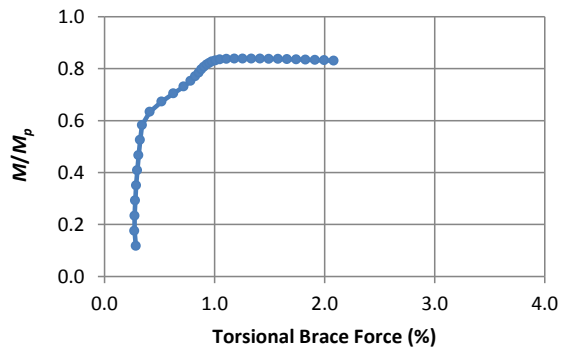
(b)  $\beta = 10.7$  ( $1.4 \beta_{iF.AISC}$ )



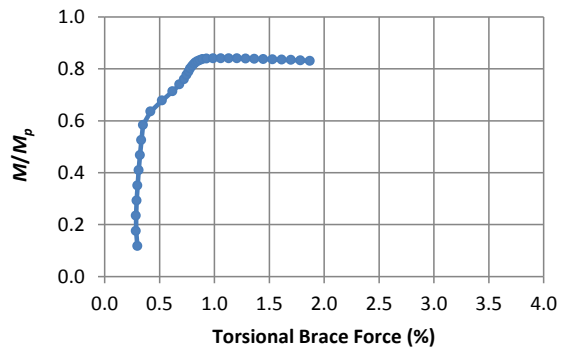
(c)  $\beta = 16.1$  ( $2.1 \beta_{iF.AISC}$ )



(d)  $\beta = 21.4$  ( $2.8 \beta_{iF.AISC}$ )

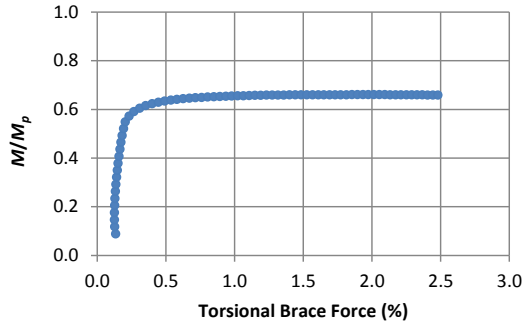


(e)  $\beta = 35.0$  ( $4.6 \beta_{iF.AISC}$ )

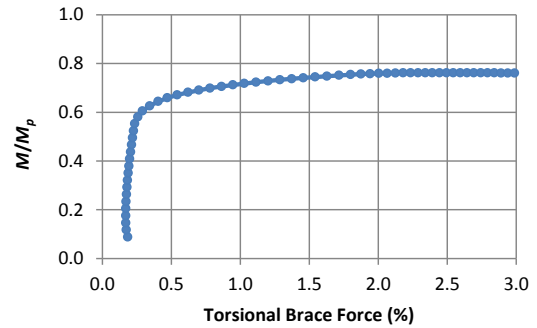


(f)  $\beta = 60.0$  ( $7.9 \beta_{iF.AISC}$ )

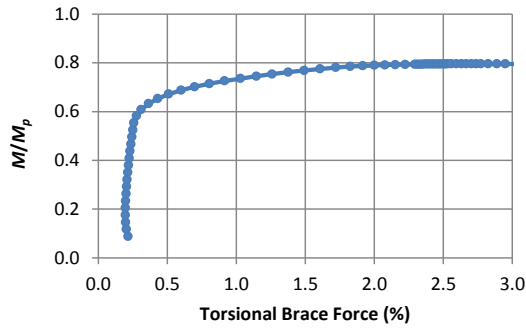
Fig. 7.8. Case C110  $M/M_p$  vs. % brace force curves for a progression of increasing brace stiffnesses (Nodal torsional bracing,  $L_b = 5$  ft,  $n = 1$ ,  $\beta_{iF.AISC} = 7.6$  kip/in)



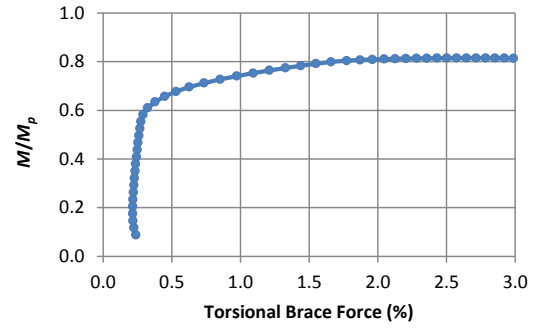
(a)  $\beta = 4.0$  ( $0.70 \beta_{iF.AISC}$ )



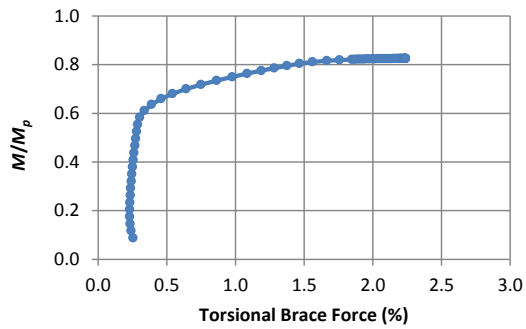
(b)  $\beta = 8.0$  ( $1.4 \beta_{iF.AISC}$ )



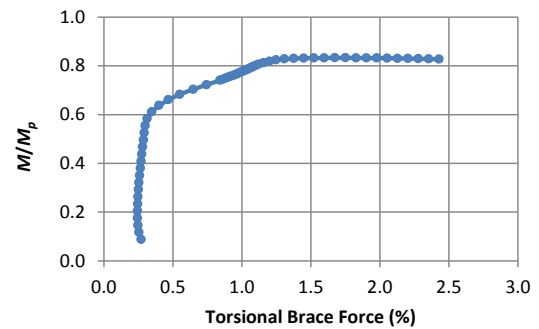
(c)  $\beta = 12.1$  ( $2.1 \beta_{iF.AISC}$ )



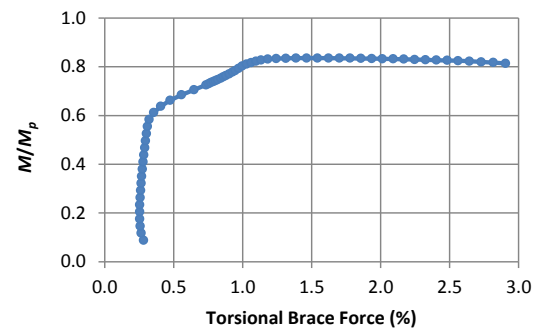
(d)  $\beta = 16.1$  ( $2.8 \beta_{iF.AISC}$ )



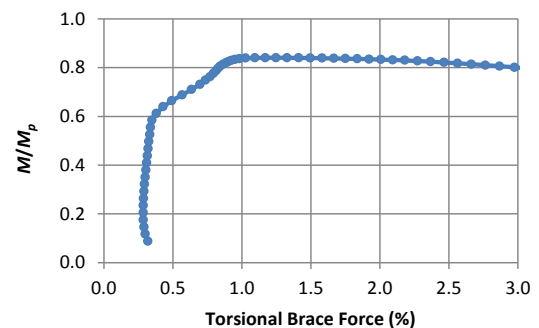
(e)  $\beta = 20.0$  ( $3.5 \beta_{iF.AISC}$ )



(f)  $\beta = 25.0$  ( $4.4 \beta_{iF.AISC}$ )

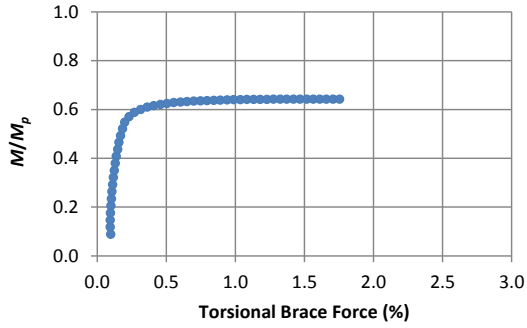


(g)  $\beta = 30.0$  ( $5.2 \beta_{iF.AISC}$ )

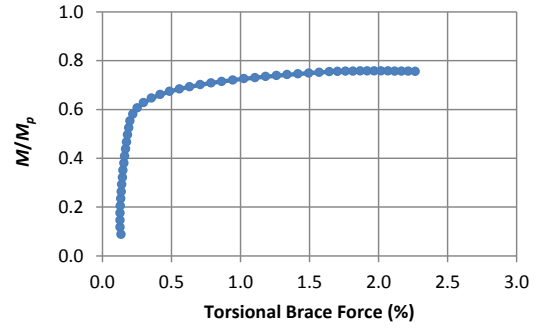


(h)  $\beta = 60.0$  ( $10.5 \beta_{iF.AISC}$ )

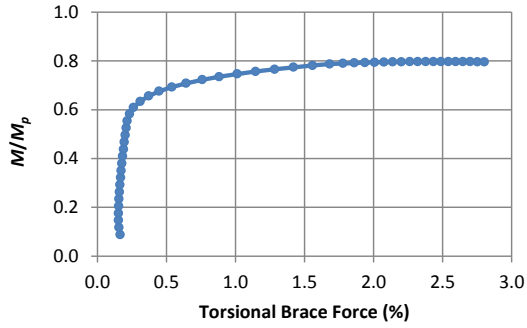
Fig. 7.9. Case C120  $M/M_p$  vs. % brace force curves for a progression of increasing brace stiffnesses (Nodal torsional bracing,  $L_b = 5$  ft,  $n = 2$ ,  $\beta_{iF.AISC} = 5.7$  kip/in)



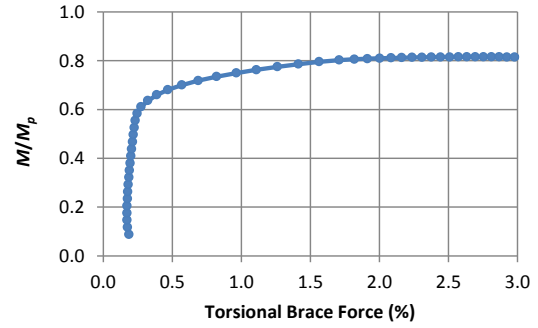
(a)  $\beta = 3.6$  ( $0.71 \beta_{iF.AISC}$ )



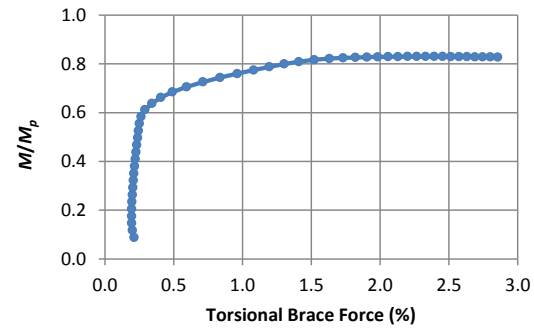
(b)  $\beta = 7.0$  ( $1.4 \beta_{iF.AISC}$ )



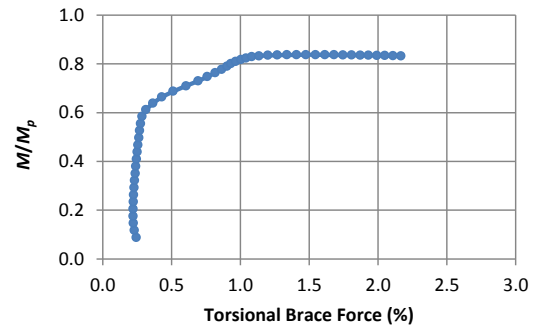
(c)  $\beta = 10.7$  ( $2.1 \beta_{iF.AISC}$ )



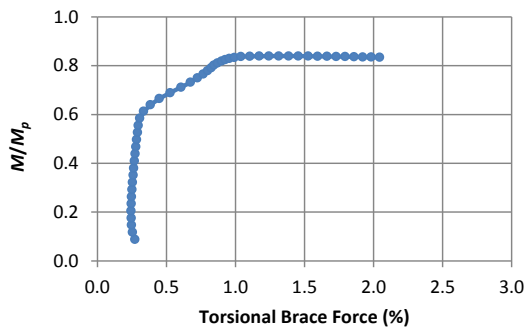
(d)  $\beta = 14.3$  ( $2.8 \beta_{iF.AISC}$ )



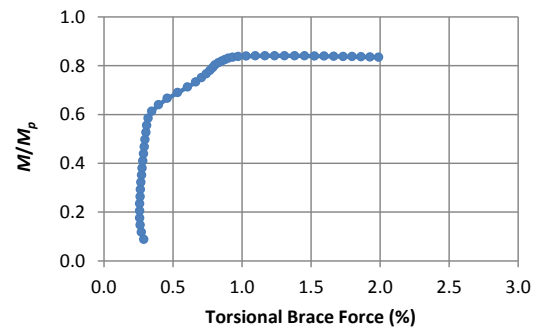
(e)  $\beta = 20.0$  ( $3.9 \beta_{iF.AISC}$ )



(f)  $\beta = 30.0$  ( $5.9 \beta_{iF.AISC}$ )

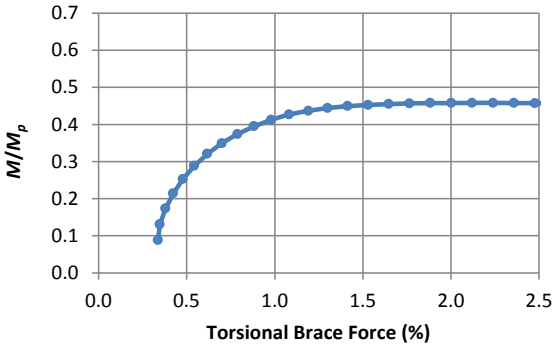


(g)  $\beta = 45.0$  ( $8.9 \beta_{iF.AISC}$ )

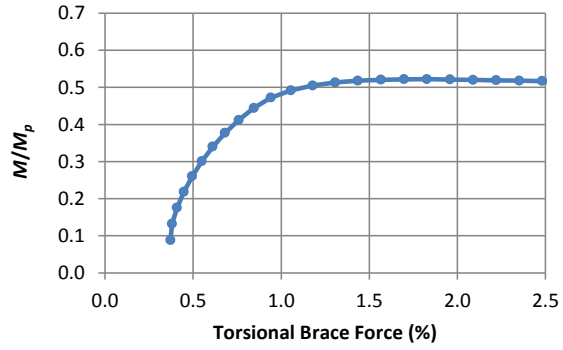


(h)  $\beta = 60.0$  ( $11.8 \beta_{iF.AISC}$ )

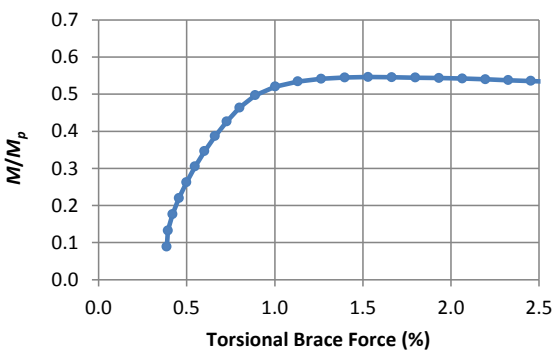
Fig. 7.10. Case C130  $M/M_p$  vs. % brace force curves for a progression of increasing brace stiffnesses (Nodal torsional bracing,  $L_b = 5$  ft,  $n = 3$ ,  $\beta_{iF.AISC} = 5.1$  kip/in)



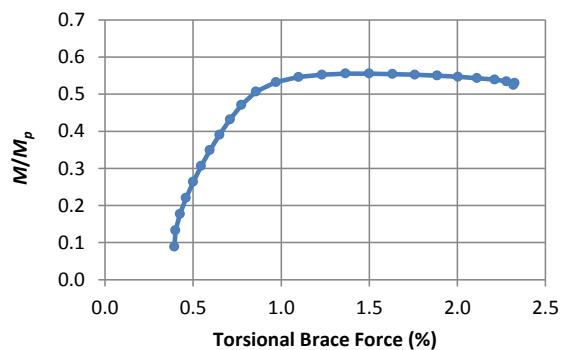
(a)  $\beta = 3.2$  ( $0.44 \beta_{iF.AISC}$ )



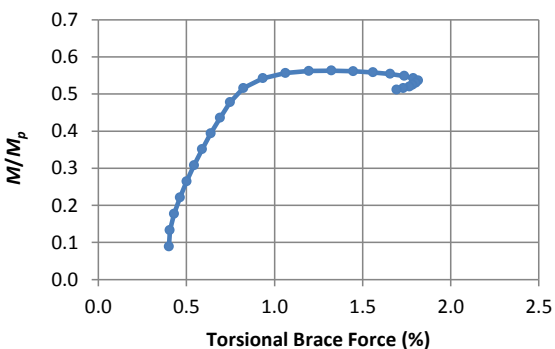
(b)  $\beta = 7.0$  ( $0.97 \beta_{iF.AISC}$ )



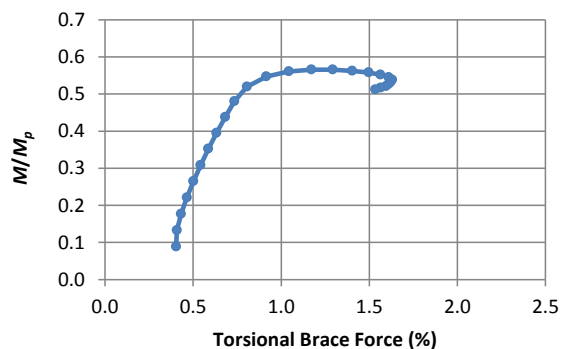
(c)  $\beta = 12.4$  ( $1.7 \beta_{iF.AISC}$ )



(d)  $\beta = 18.5$  ( $2.6 \beta_{iF.AISC}$ )

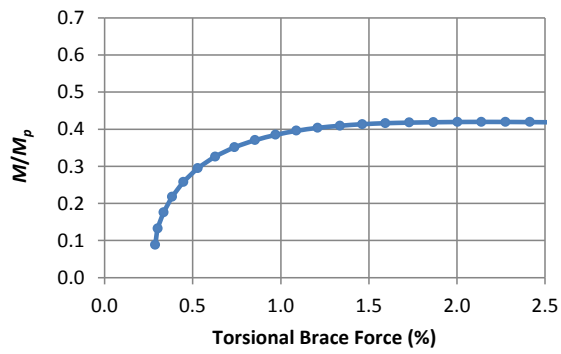


(e)  $\beta = 35.0$  ( $4.8 \beta_{iF.AISC}$ )

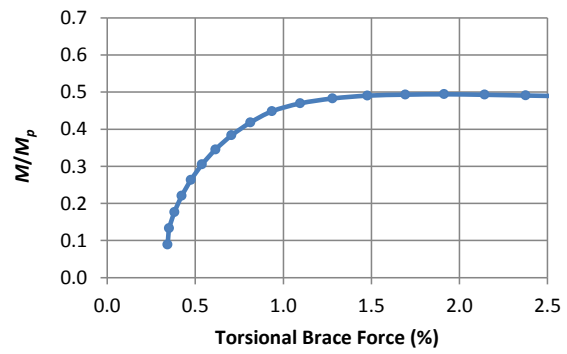


(f)  $\beta = 60.0$  ( $8.3 \beta_{iF.AISC}$ )

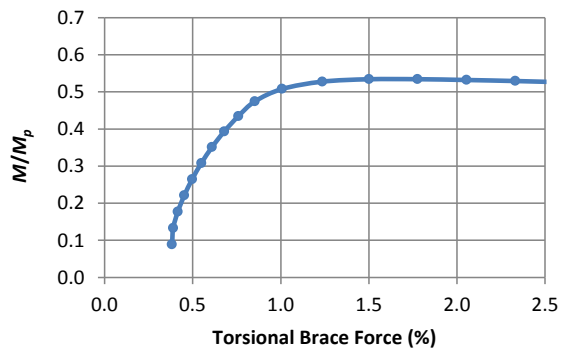
Fig. 7.11. Case C210  $M/M_p$  vs. % brace force curves for a progression of increasing brace stiffnesses (Nodal torsional bracing,  $L_b = 10$  ft,  $n = 1$ ,  $\beta_{iF.AISC} = 7.2$  kip/in)



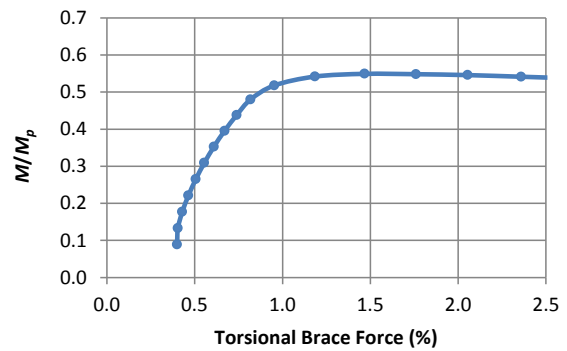
(a)  $\beta = 2.3$  ( $0.42 \beta_{iF.AISC}$ )



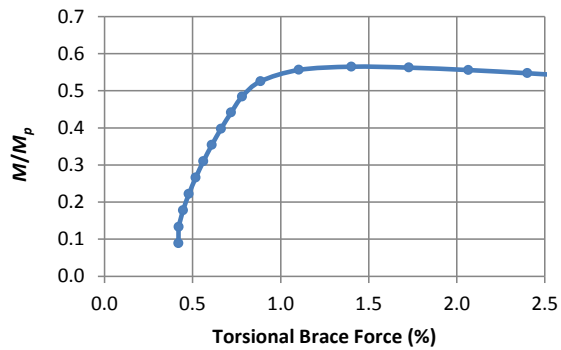
(b)  $\beta = 7.0$  ( $1.3 \beta_{iF.AISC}$ )



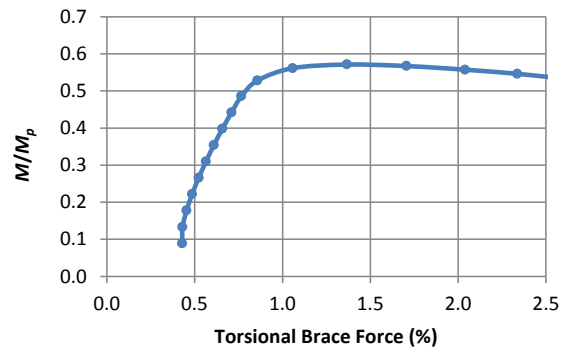
(c)  $\beta = 9.3$  ( $1.7 \beta_{iF.AISC}$ )



(d)  $\beta = 13.9$  ( $2.6 \beta_{iF.AISC}$ )

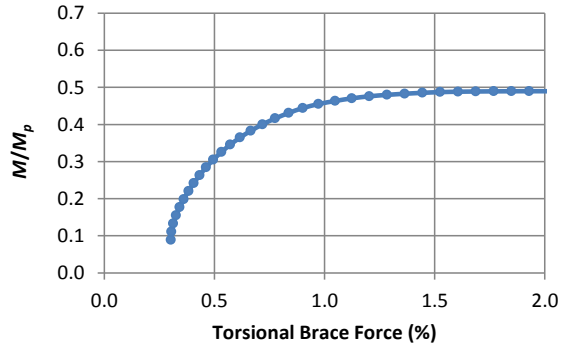


(e)  $\beta = 30.0$  ( $5.5 \beta_{iF.AISC}$ )

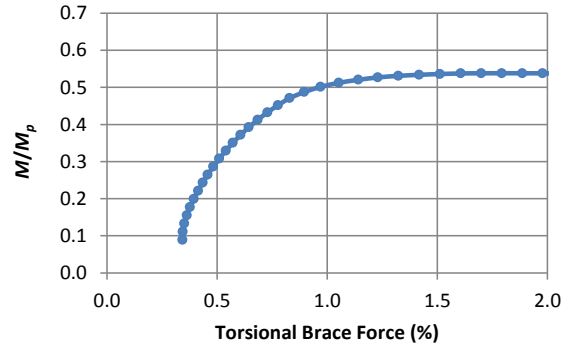


(f)  $\beta = 60.0$  ( $11 \beta_{iF.AISC}$ )

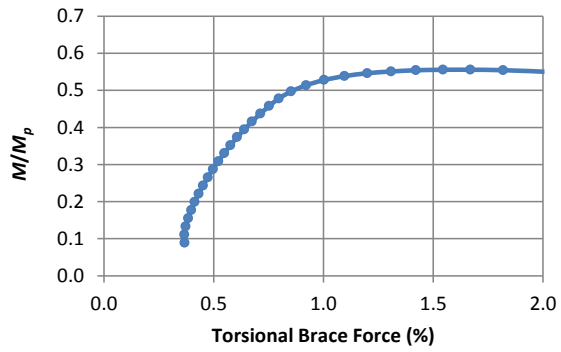
Fig. 7.12. Case C220  $M/M_p$  vs. % brace force curves for a progression of increasing brace stiffnesses (Nodal torsional bracing,  $L_b = 10$  ft,  $n = 2$ ,  $\beta_{iF.AISC} = 5.4$  kip/in)



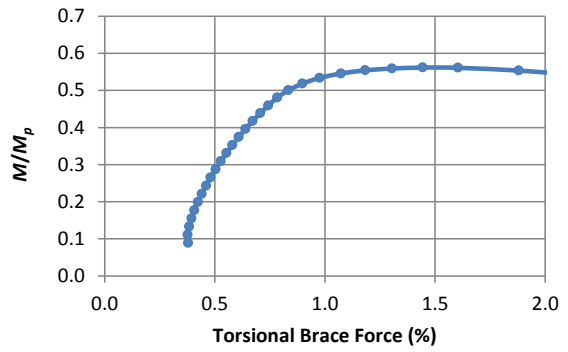
(a)  $\beta = 4.1$  ( $0.85 \beta_{iF.AISC}$ )



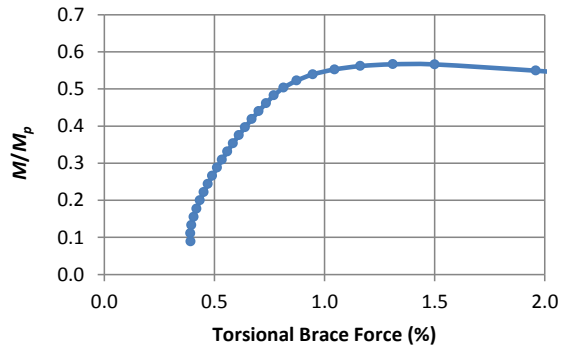
(b)  $\beta = 7.0$  ( $1.4 \beta_{iF.AISC}$ )



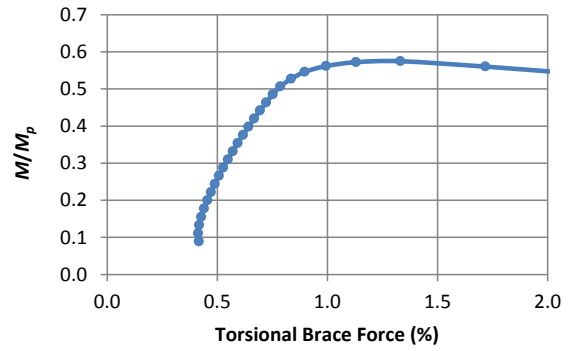
(c)  $\beta = 10.0$  ( $2.1 \beta_{iF.AISC}$ )



(d)  $\beta = 12.4$  ( $2.6 \beta_{iF.AISC}$ )

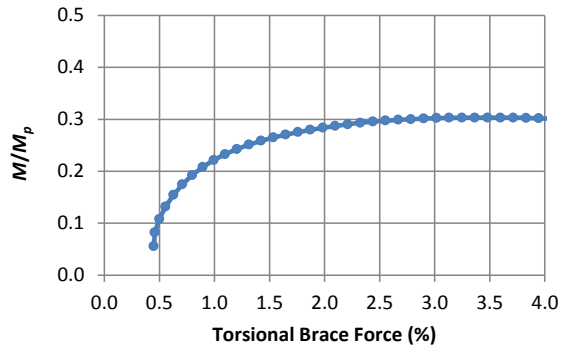


(e)  $\beta = 16.5$  ( $3.4 \beta_{iF.AISC}$ )

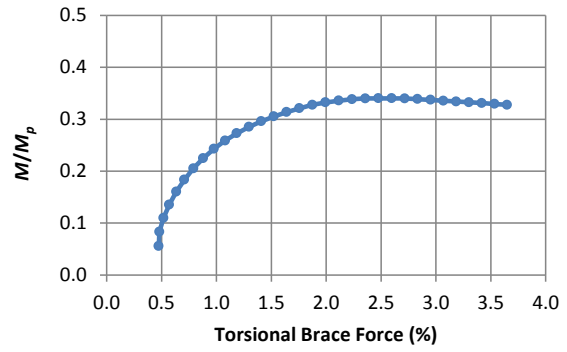


(f)  $\beta = 35.0$  ( $7.2 \beta_{iF.AISC}$ )

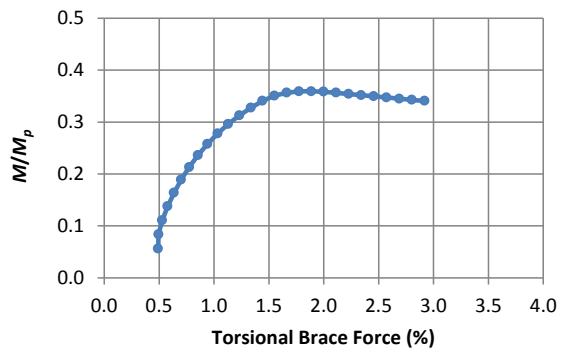
Fig. 7.13. Case C230  $M/M_p$  vs. % brace force curves for a progression of increasing brace stiffnesses (Nodal torsional bracing,  $L_b = 10$  ft,  $n = 3$ ,  $\beta_{iF.AISC} = 4.8$  kip/in)



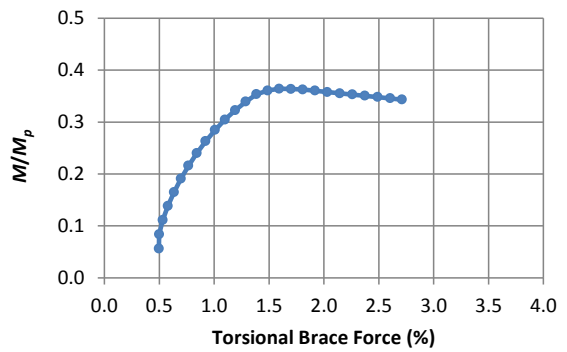
(a)  $\beta = 2.0$  ( $0.44 \beta_{iF.AISC}$ )



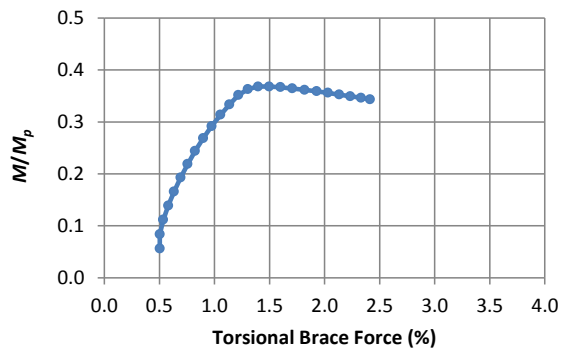
(b)  $\beta = 3.7$  ( $0.81 \beta_{iF.AISC}$ )



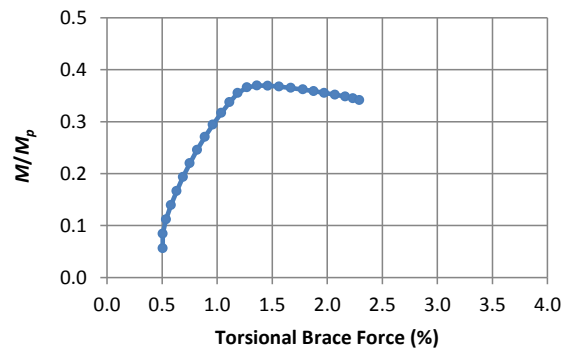
(c)  $\beta = 7.4$  ( $1.6 \beta_{iF.AISC}$ )



(d)  $\beta = 11.1$  ( $2.4 \beta_{iF.AISC}$ )

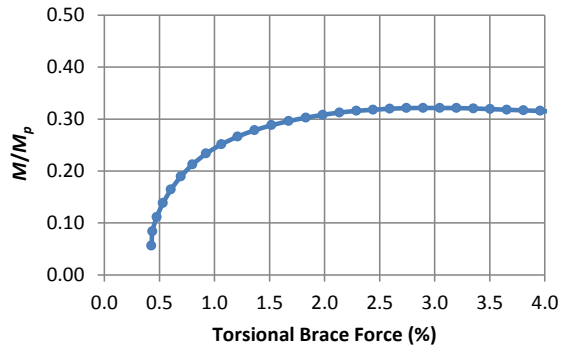


(e)  $\beta = 25.0$  ( $5.4 \beta_{iF.AISC}$ )

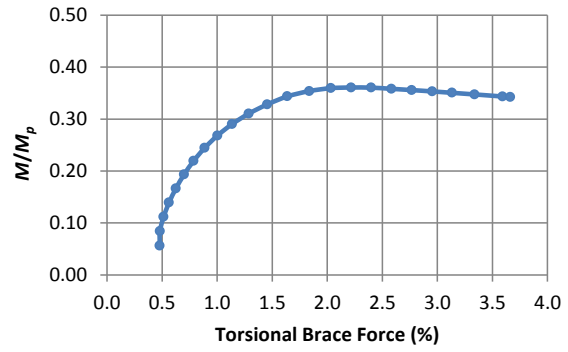


(f)  $\beta = 45.0$  ( $9.8 \beta_{iF.AISC}$ )

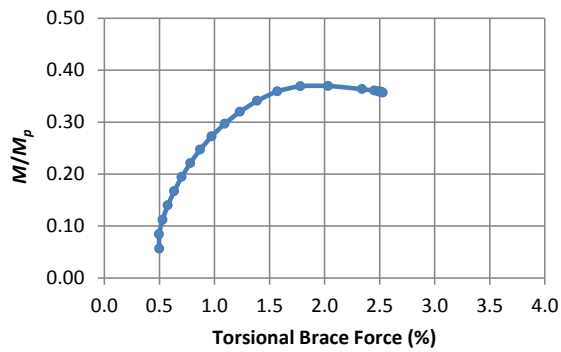
Fig. 7.14. Case C310  $M/M_p$  vs. % brace force curves for a progression of increasing brace stiffnesses (Nodal torsional bracing,  $L_b = 15$  ft,  $n = 1$ ,  $\beta_{iF.AISC} = 4.6$  kip/in)



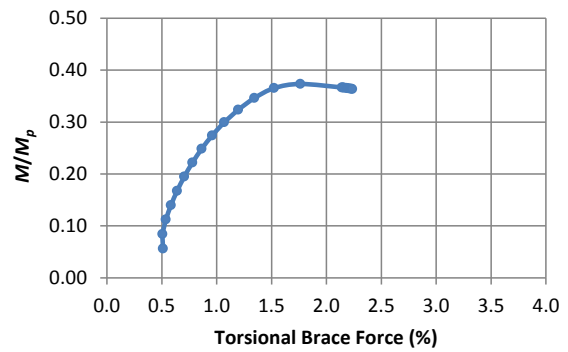
(a)  $\beta = 2.5$  ( $0.82 \beta_{iF.AISC}$ )



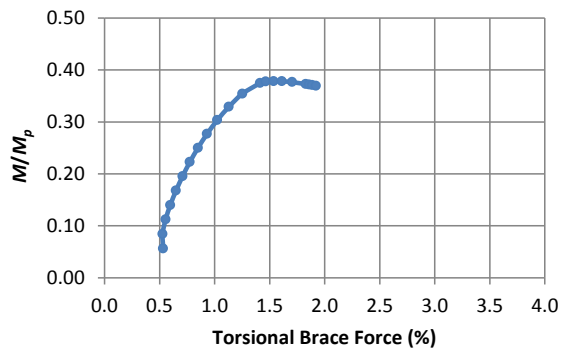
(b)  $\beta = 4.9$  ( $1.6 \beta_{iF.AISC}$ )



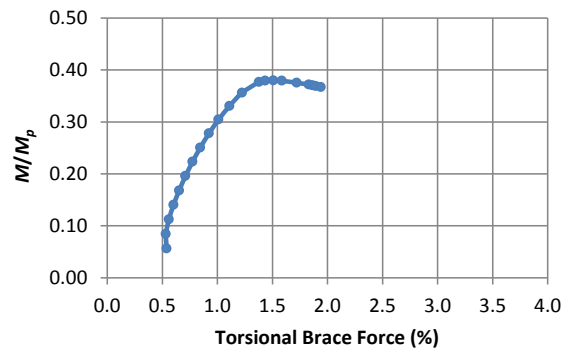
(c)  $\beta = 7.4$  ( $2.4 \beta_{iF.AISC}$ )



(d)  $\beta = 9.9$  ( $3.2 \beta_{iF.AISC}$ )



(e)  $\beta = 25.0$  ( $8.2 \beta_{iF.AISC}$ )



(f)  $\beta = 45.0$  ( $14.7 \beta_{iF.AISC}$ )

Fig. 7.15. Case C330  $M/M_p$  vs. % brace force curves for a progression of increasing brace stiffnesses (Nodal torsional bracing,  $L_b = 15$  ft,  $n = 3$ ,  $\beta_{iF.AISC} = 3.1$  kip/in)



# CHAPTER 8

## COMBINED BRACING REQUIREMENTS

### 8.1 Category D Nodal Lateral and Torsional Combined Bracing

Figure 8.1 shows the representative member models for cases D\*10\*\* and D\*20\*\*.

Figure 8.2 shows a cross-section view at one of the intermediate brace locations.

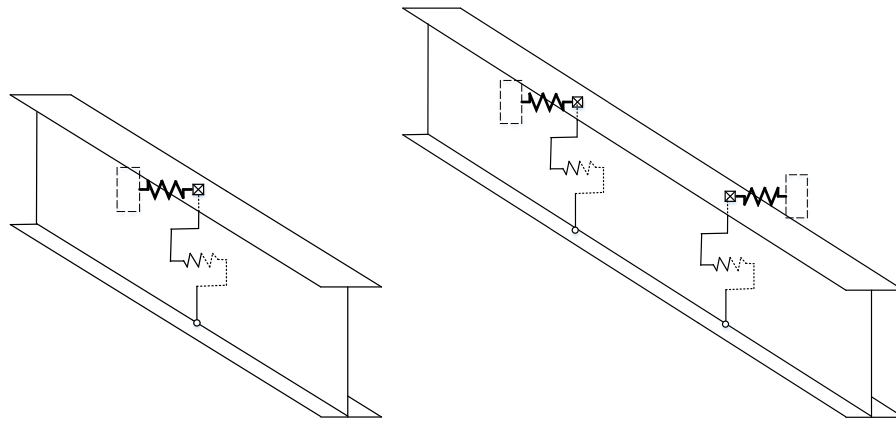


Fig. 8.1. Representative combined nodal lateral and torsional bracing model for cases D\*10\*\* and D\*20\*\*

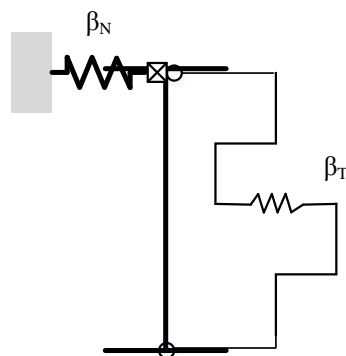
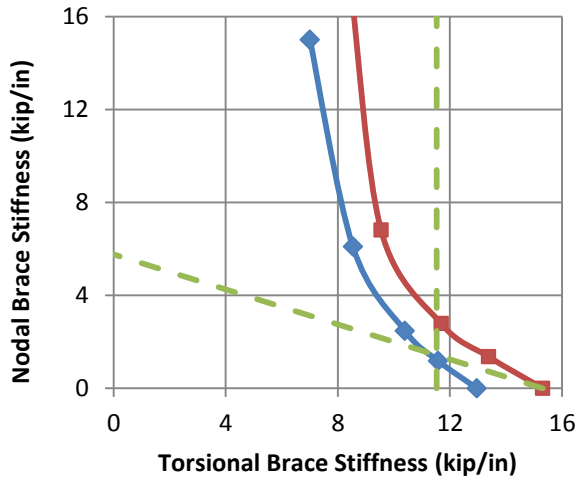


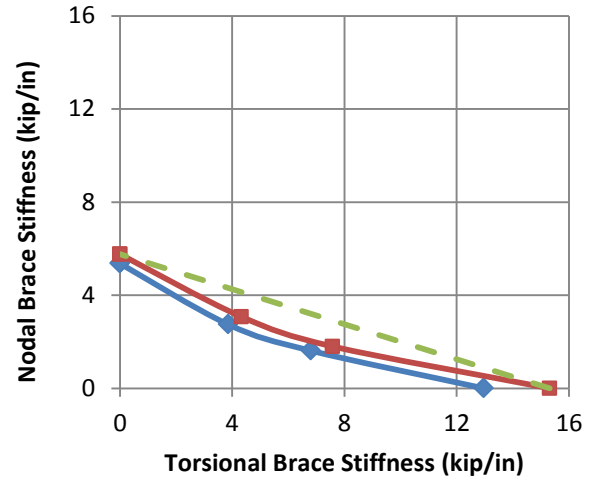
Fig. 8.2 Cross-section view of combined nodal lateral and nodal torsional bracing at an intermediate brace point

Figure 8.3 shows the combined stiffness interaction plots for the Category D (nodal lateral and torsional bracing) models with an unbraced length of 5 ft. These members are influenced the most by inelasticity. Figure 8.3(a) shows simulation-based stiffness interaction curves for negative bending and with a single intermediate brace point. Figure 8.3(b) shows the corresponding curves for positive bending with a single intermediate brace location. Two stiffness interaction curves are shown in each of the plots, one corresponding to 96% of the rigidly braced member strength (the blue curve with the diamond symbols) and one corresponding 98% of this strength (the red curve with the square symbols). These two curves are shown to capture the attributes of the asymptotic behavior of the knuckle curve near the rigidly braced strength. Figures 8.3(c) and 8.3(d) show the bracing stiffness interactions for  $L_b = 5$  ft but with two intermediate brace points. The difference between the 96% and 98% curves is slightly wider in these plots. Figures 8.3 and 8.4 show similar behavior to that shown in Figure 8.2 but with unbraced lengths of  $L_b = 10$  ft and 15 ft.

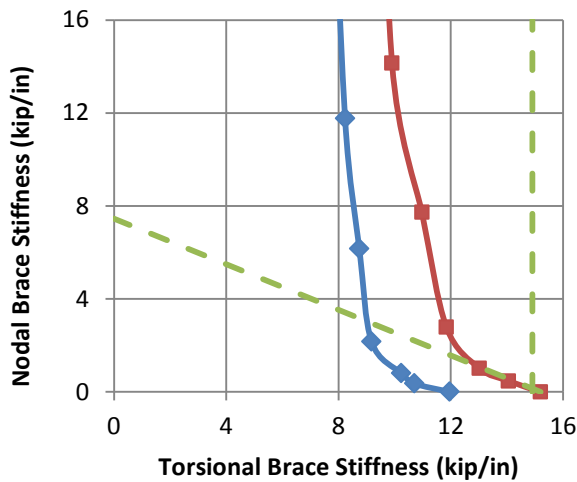
The bracing stiffness values plotted in Figure 8.3 have been determined by interpolation between the knuckle curve data points for the respective cases. The corresponding knuckle curve plots are shown in Appendix A.



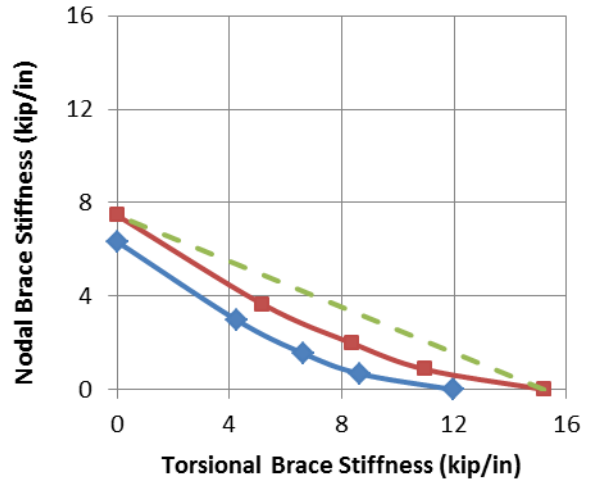
(a) D110\*n (negative moment,  $n = 1$ )



(b) D110\*p (positive moment,  $n = 1$ )



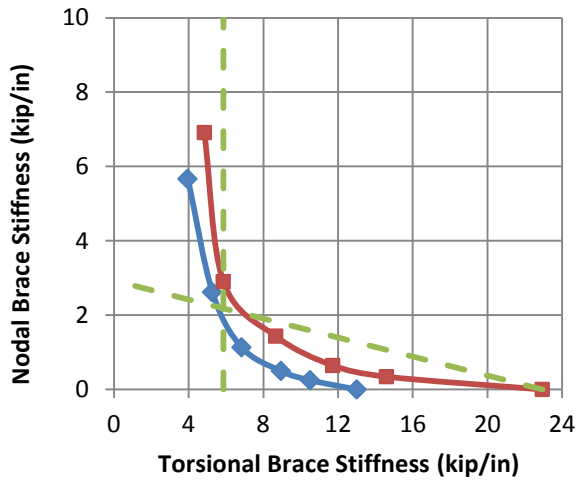
(c) D120\*n (negative moment,  $n = 2$ )



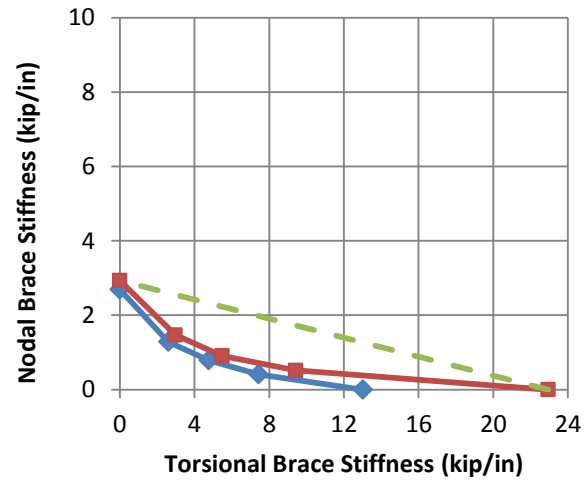
(d) D120\*p (positive moment,  $n = 2$ )

- ◆— Simulation-based stiffness interaction corresponding to 96 % of rigid bracing strength
- Simulation-based stiffness interaction corresponding to 98 % of rigid bracing strength
- - - Recommended design approximation

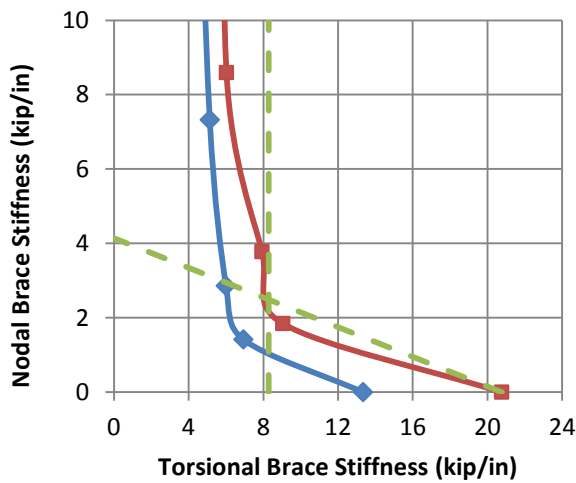
Fig. 8.3. Category D nodal lateral – nodal torsional brace stiffness interactions ( $L_b = 5$  ft)



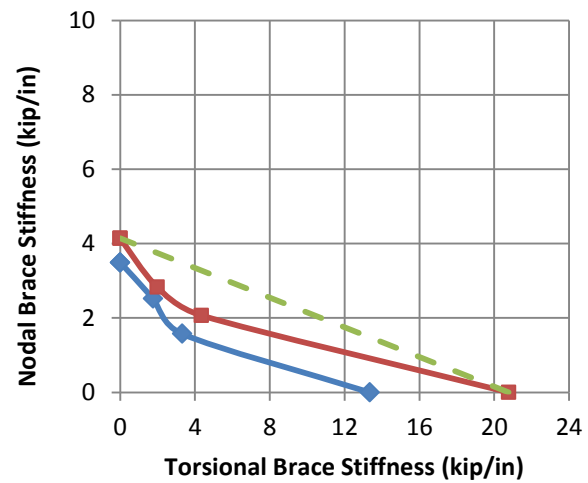
(a) D210\*n (negative moment,  $n = 1$ )



(b) D210\*p (positive moment,  $n = 1$ )



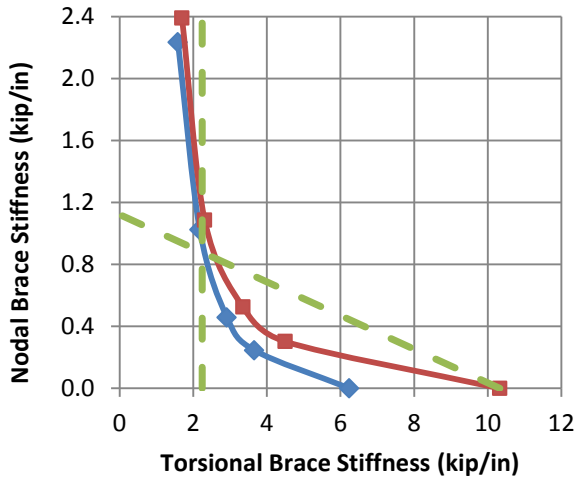
(c) D220\*n (negative moment,  $n = 2$ )



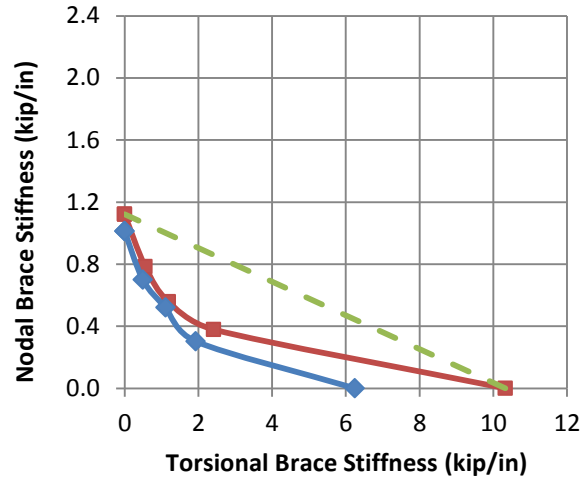
(d) D220\*p (positive moment,  $n = 2$ )

- ◆ Simulation-based stiffness interaction corresponding to 96 % of rigid bracing strength
- Simulation-based stiffness interaction corresponding to 98 % of rigid bracing strength
- - Recommended design approximation

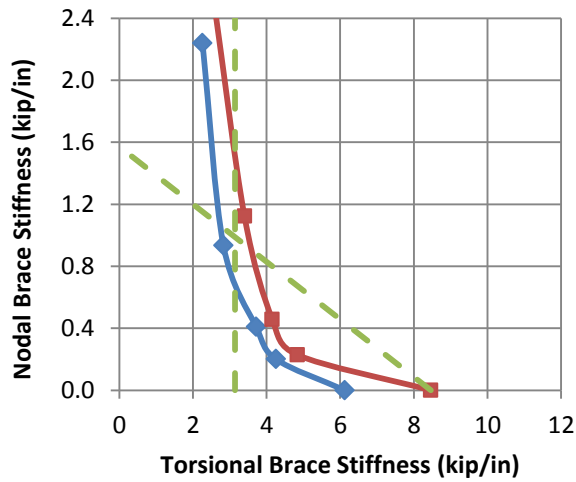
Fig. 8.4. Category D nodal lateral – nodal torsional brace stiffness interactions ( $L_b = 10$  ft)



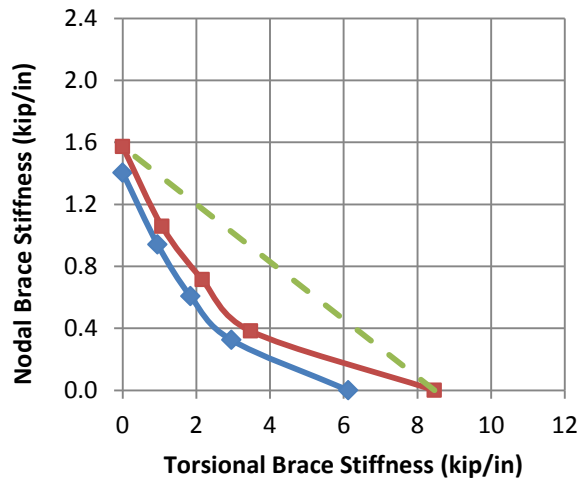
(a) D310\*n (negative moment,  $n = 1$ )



(b) D310\*p (positive moment,  $n = 1$ )



(c) D320\*n (negative moment,  $n = 2$ )



(d) D320\*p (positive moment,  $n = 2$ )

- ◆ Simulation-based stiffness interaction corresponding to 96 % of rigid bracing strength
- Simulation-based stiffness interaction corresponding to 98 % of rigid bracing strength
- Recommended design approximation

Fig. 8.5. Category D nodal lateral – nodal torsional brace stiffness interactions ( $L_b = 15$  ft)

In the above plots, when the member experiences positive bending, the interaction between the combined nodal and torsional bracing stiffness requirements is conservative compared to a linear interaction between the nodal and torsional bracing stiffness. However, when a member with combined nodal lateral and nodal torsional bracing is under negative bending, where the laterally-braced top flange is in tension and the bottom flange is in compression, the interaction between the two bracing stiffness requirements is different. In this case, the lateral brace to the tension flange provides negligible benefit to the stability behavior of the beam in the limit that the torsional brace stiffness approaches zero. However, in the limit that the lateral brace stiffness is rigid, the torsional brace (when modeled as a relative brace between the top and bottom flanges) effectively becomes a nodal lateral brace to the bottom compression flange. This is because the idealization for a nodal lateral brace is simply a grounded spring. In the limit that the lateral brace to the tension flange is rigid, the relative brace between the top and bottom flange is indeed such a grounded spring.

Upon establishing the above concept, then in the limit that the lateral bracing to the tension flange is rigid, one can surmise that the minimum torsional bracing stiffness requirement, expressed as an equivalent relative bracing (i.e., shear spring) stiffness between the top and bottom flange, can be expressed simply the nodal lateral bracing stiffness requirement  $\beta_{br}$  from Equation (2-35). Upon viewing the negative moment case stiffness interaction curves in Figures 8.3 through 8.5, it is apparent that the test simulation results tend to asymptote to a vertical line equal to this stiffness on the left-hand side of the plots. However, the nodal lateral bracing stiffness at the tension flange will need to be very large before the required torsional bracing stiffness becomes equal to the value from Eq. (2-35). Based on inspection of the complete set of negative moment cases in Figures 8.3 to 8.5, one can observe that a vertical line at two times the

$\beta_{br}$  from Equation (2-35), illustrated by the green dashed vertical line in the negative moment based plots, provides accurate to somewhat conservative minimum limit for the torsional bracing stiffness as the nodal lateral bracing stiffness becomes relatively large. In addition, it is observed that, with the exception of this minimum limit, the torsional bracing stiffness requirement can be reduced, by providing a relatively small lateral bracing stiffness, by the same linear interpolation function as shown for the positive moment based plots. One can observe that for some cases, e.g., the case shown in Figure 8.2(c), two times the  $\beta_{br}$  from Equation (2-35) is practically equal to the torsional bracing stiffness requirement from Equation (2-44). In fact, generally speaking, two times the  $\beta_{br}$  from Equation (2-35) can be greater than the torsional bracing stiffness requirement from Equation (2-44). When  $2\beta_{br}$  from Equation (2-35) exceeds the value from Equation (2-44), it is recommended that the torsional bracing stiffness from Eq. (2-44) should be used, and that no reduction in the torsional bracing stiffness should be taken accounting for benefits from lateral bracing at the tension flange.

It should be noted that the intercepts with the horizontal and vertical axes for the diagonal green dashed lines in Figures 8.3 through 8.5, representing a basic linear interaction between the torsional and lateral bracing stiffnesses, are taken as the 98 % of rigid bracing stiffness values. Given the results from Figure 5.5, one can conclude that  $\beta_{br}$  from Equation (2-35) is generally a conservative estimate of  $\beta_{F98}$  for the nodal bracing only case (corresponding to the intercept with the vertical axis). Based on the results from Figure 7.5, it can be seen that Eq. (2-44) is a slightly conservative to slightly unconservative estimate of  $\beta_{F96}$ . It tends to be a slightly conservative to unconservative (by approximately a factor of two) representation of  $\beta_{F98}$ .

## 8.2 Category E: Combined Relative (Shear Panel) Lateral and Torsional Bracing

Figure 8.6 shows the representative member models for cases E\*20\*\* and E\*30\*\*. These members are not to scale and only serve as an illustrative tool for understanding Category E.

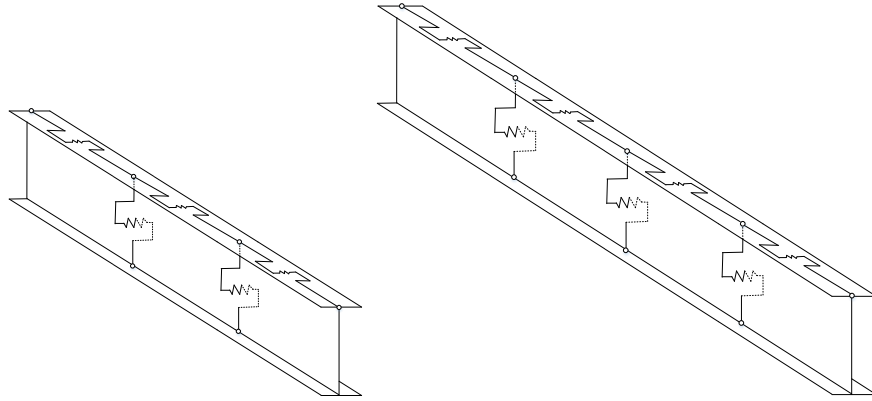
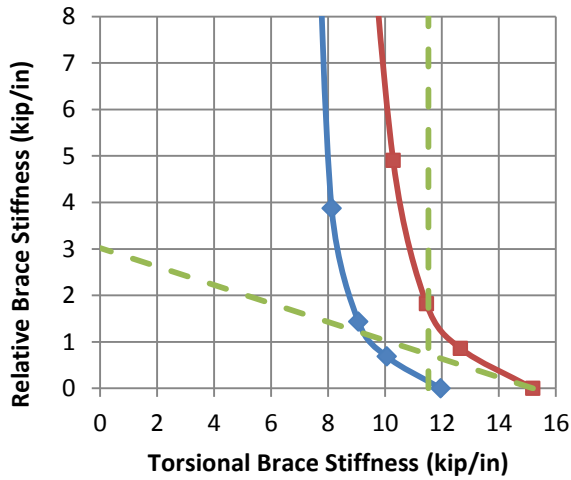
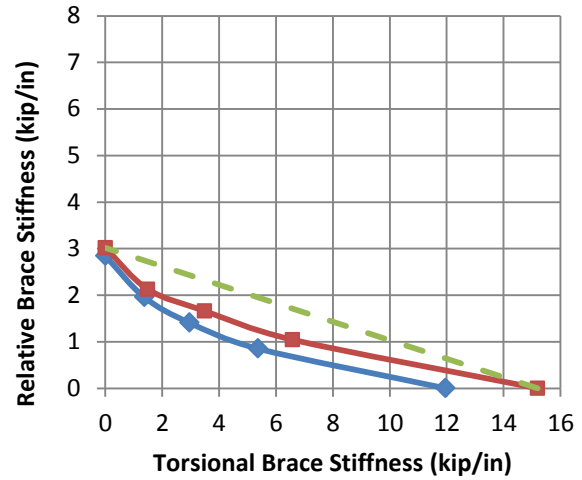


Fig. 8.6. Representative combined relative and torsional bracing model for cases E\*20\*\* and E\*30\*\*

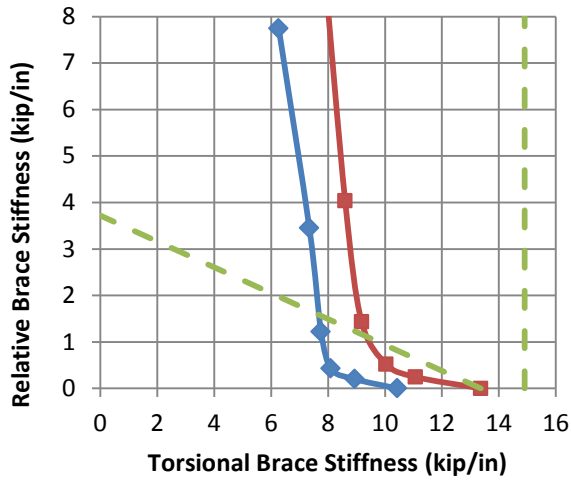
Figures 8.7 to 8.9 show the interaction behavior for relative bracing and torsional bracing in a similar manner as done in Figures 8.3 to 8.5 for Category D. The presentations in these plots directly parallel those in Figures 8.7 to 8.9, but the vertical axis in these plots corresponds to a relative bracing stiffness. In addition, these plots correspond to the use of two and three intermediate brace points ( $n = 2$  and  $3$ ) rather than  $n = 1$  and  $2$ . Similar to the presentation for the previous Category D, the knuckle curves corresponding to Figures 8.7 to 8.9 are shown in Appendix A.



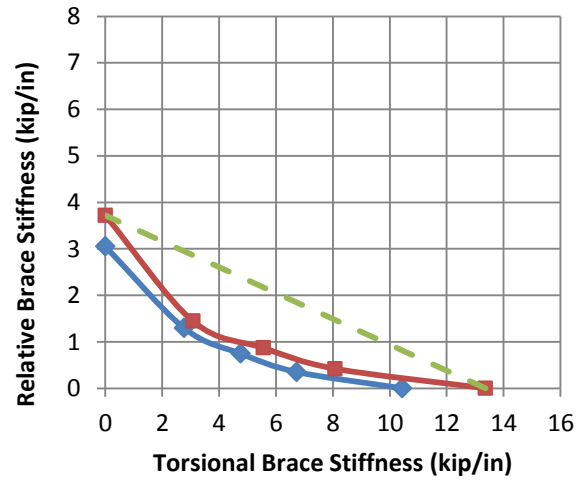
(a) E120\*n (negative moment,  $n = 2$ )



(b) E120\*p (positive moment,  $n = 2$ )



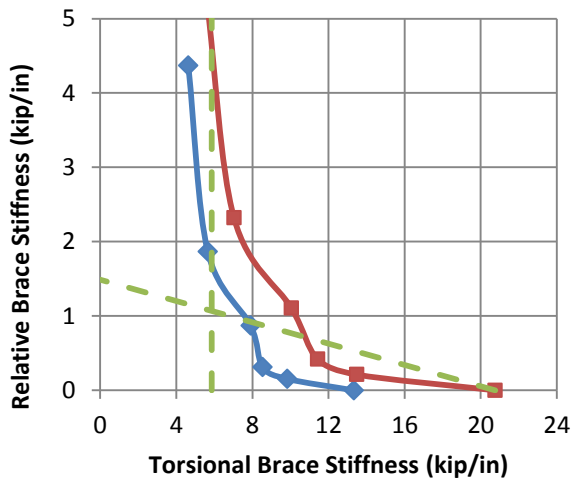
(c) E130\*n (negative moment,  $n = 3$ )



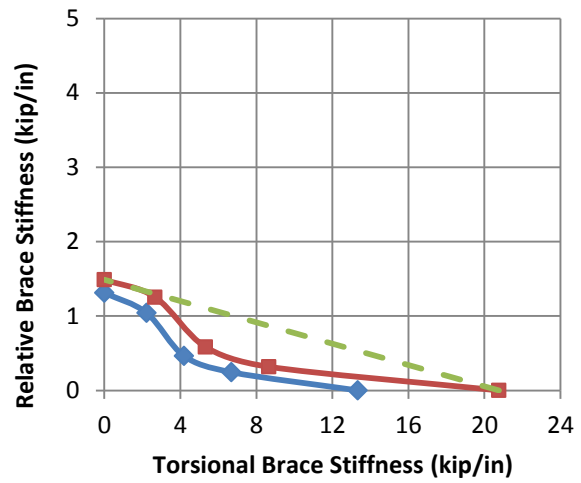
(d) E130\*p (positive moment,  $n = 3$ )

- ◆ Simulation-based stiffness interaction corresponding to 96 % of rigid bracing strength
- Simulation-based stiffness interaction corresponding to 98 % of rigid bracing strength
- - Recommended design approximation

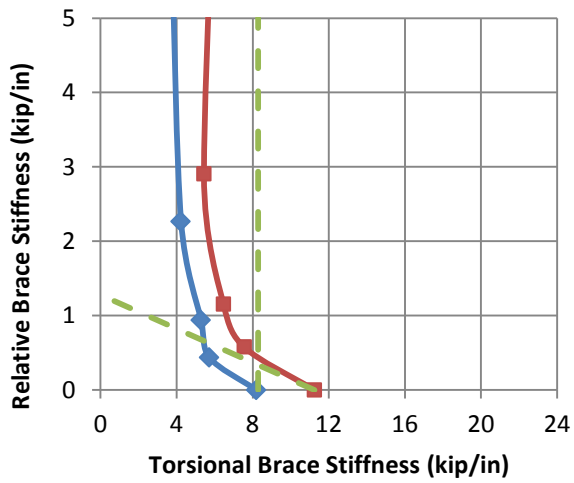
Fig. 8.7. Category E shear panel lateral – nodal torsional brace stiffness interactions ( $L_b = 5$  ft)



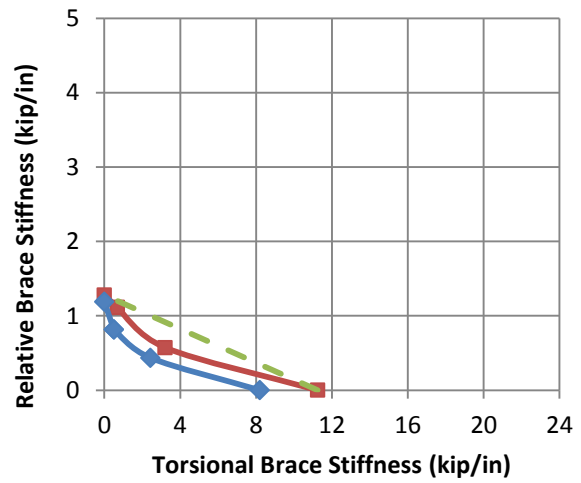
(a) E220\*n (negative moment,  $n = 2$ )



(b) E220\*p (positive moment,  $n = 2$ )



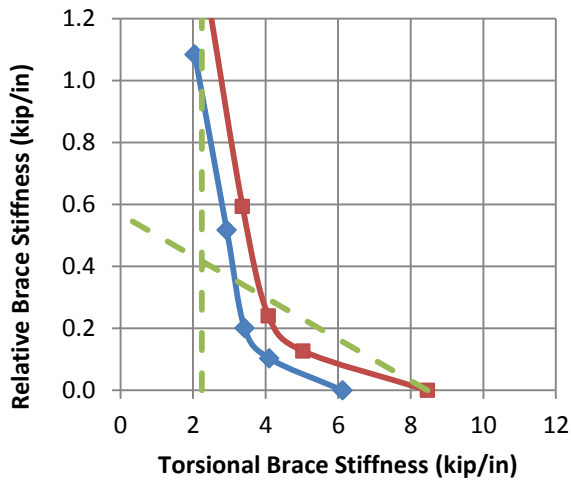
(c) E230\*n (negative moment,  $n = 3$ )



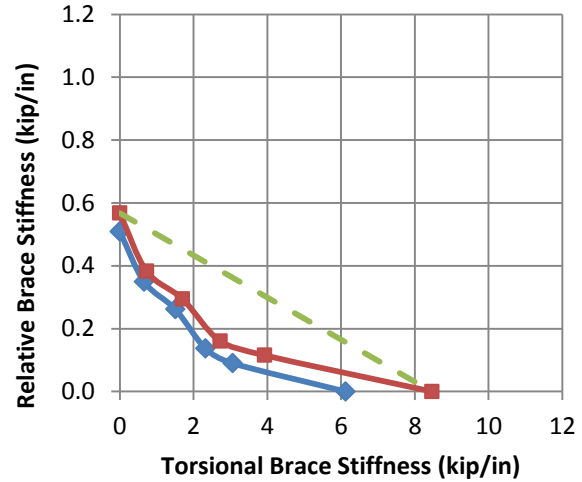
(d) E230\*p (positive moment,  $n = 3$ )

- ◆ Simulation-based stiffness interaction corresponding to 96 % of rigid bracing strength
- Simulation-based stiffness interaction corresponding to 98 % of rigid bracing strength
- - Recommended design approximation

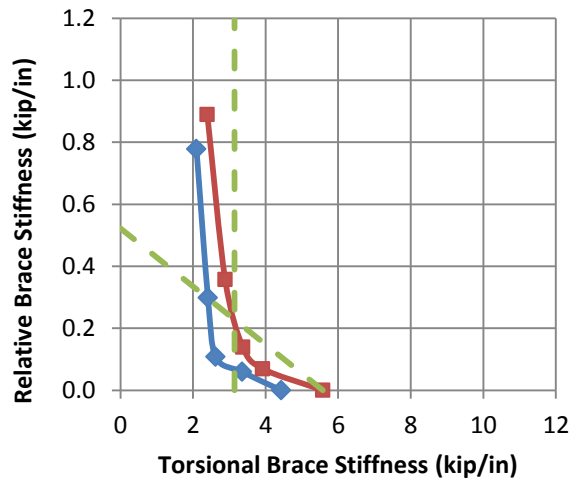
Fig. 8.8. Category E shear panel lateral – nodal torsional brace stiffness interactions ( $L_b = 10$  ft)



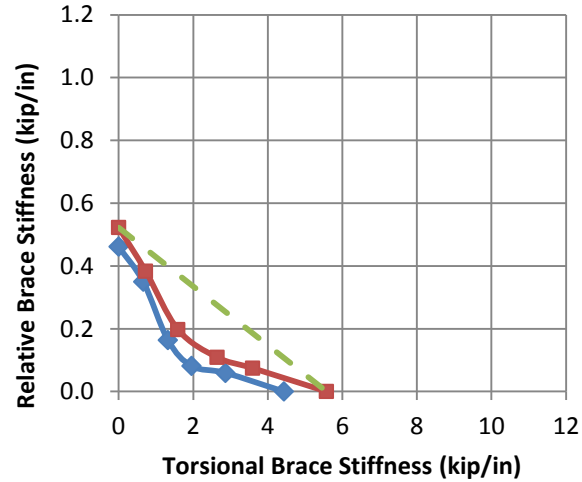
(a) E320\*n (negative moment,  $n = 2$ )



(b) E320\*p (positive moment,  $n = 2$ )



(c) E330\*n (negative moment,  $n = 3$ )



(d) E330\*p (positive moment,  $n = 3$ )

- ◆ Simulation-based stiffness interaction corresponding to 96 % of rigid bracing strength
- Simulation-based stiffness interaction corresponding to 98 % of rigid bracing strength
- Recommended design approximation

Fig. 8.9. Category E shear panel lateral – nodal torsional brace stiffness interactions ( $L_b = 15$  ft)

Similar to Category D, for the positive bending cases, the interaction between the shear panel and torsional bracing stiffnesses is represented conservatively by a linear equation. Furthermore, for the negative bending cases, the same concepts for estimating the required stiffnesses presented with Figures 8.3 to 8.5 apply also to Category E. The abscissa for the green dashed vertical line in Figures 8.7 to 8.9 is taken as  $2\beta_{br}$  from Eq. (2-35). The diagonal green dashed line is the same for both the negative and positive bending plots and is drawn between the horizontal and vertical axis intercepts of the 98 % of rigid bracing curves. Based on the results from Figure 6.8,  $\beta_{br}$  from Eq. (2-22) is a conservative estimate of  $\beta_{F98}$  corresponding to the intercept of the positive moment based curves with the vertical axis in Figures 8.7 to 8.9. The representation of  $\beta_{F98}$  by  $\beta_{Tbr}$  from Eq. (2-44) is the same as that discussed regarding the plots for Category D.

## CHAPTER 9

### SUMMARY AND CONCLUSIONS

In this research, a study of beam bracing with member inelasticity and combined bracing types is executed and the results are evaluated against the current AISC (2010) Appendix 6 provisions. These provisions generally do an excellent job of capturing the bracing responses and attributes corresponding to nodal (point) lateral, relative (shear panel) (lateral) and nodal torsional bracing of beams. However, a number of findings can be considered as potential improvements. The key findings are as follows:

- The base relative (shear panel) bracing strength requirement should be set to 0.5 % of the flange compressive load, which is fully consistent with the use of 1.0 % for nodal (point) bracing for cases with one intermediate brace point. The value 0.5 % is a better upper bound to the brace strength requirements corresponding to the use of shear panel braces with a brace stiffness of  $2\beta_{iF,AISC}$ .
- AISC Appendix 6 does not acknowledge any change in the brace strength requirements within the partial bracing realm. The test simulation studies clearly show that the brace strength requirements can be significantly higher in partial bracing situations.
- The basic second-order elastic amplifier inherent in the modification factor  $1/(2 - 2\beta_{iF,AISC}/\beta)$ , and much of the prior discussions in the literature corresponding to partial bracing, imply that as the partial bracing stiffness  $\beta$  approaches  $2\beta_{iF,AISC}$ , the brace point displacements and the brace forces will become unbounded. This behavior is true only for the idealized derivation where idealized frictionless pins are placed at each of the brace

points. The brace point displacements and brace forces at the limit load (capacity) of the member are well bounded in cases where:

- There is continuity across the brace points
  - The fact that yielding occurs in the member and
  - The fact that the basic amplifier derivation is based on small rotation assumptions, is recognized.
- In all the nodal lateral and shear panel lateral bracing cases studied,  $\beta = 1.33 \beta_{iF.AISC}$  is a sufficient upper-bound requirement for the bracing stiffness necessary to develop 98 % of the member's rigidly-braced strength (defined as the strength obtained for the case of one intermediate rigid torsional brace).
  - For torsional bracing alone,  $\beta = 3.8 \beta_{iF.AISC}$  is a sufficient upper bound for the bracing stiffness necessary to develop 98 % of the member's rigidly-braced strength. However, the strength vs. bracing stiffness curve is very flat at this limit;  $\beta = 2.5 \beta_{iF.AISC}$  is a sufficient upper bound to reach 96 % of the rigidly-braced strength for torsional bracing alone.
  - For torsional bracing, the elastic continuity effects inherent in the derivation of the torsional bracing stiffness equation, using the commentary equations, results in a low prediction of the torsional bracing strength requirements for members with shorter unbraced lengths representative of the "plastic buckling" range of member response.
  - Similarly, for members that fail by "elastic buckling," the torsional bracing stiffness estimates from AISC Appendix 6, using the commentary equations, are larger than indicated by the test simulations.

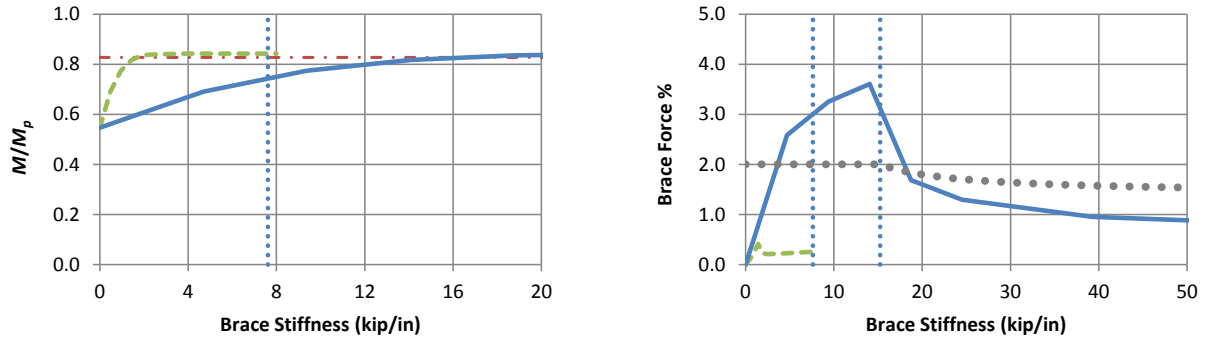
- A torsional bracing stiffness requirement of 2 % appears to be a good value that permits the development of approximately 95 % or more of the fully-braced member resistance in all cases. This value is approximately the mean of the estimates for the plastic, inelastic and elastic buckling estimates from the current AISC Appendix 6 equations.
- The test simulations indicate that within the range of partial bracing, 1 % shear panel lateral, 2 % nodal lateral and 2 % nodal torsional bracing strength requirements are sufficient to develop approximately 95 % or more of the partially braced member strengths in all cases.
- As observed in prior research by Yura and others, a basic linear interaction between the point (or shear panel) and nodal torsional brace stiffnesses is accurate to conservative for positive bending (bending causing compression on the flange that has the lateral brace).
- For “negative” moment cases and combined bracing, the above linear interaction works as long as it is “truncated” by a minimum torsional bracing stiffness requirement equal to 2x the full nodal lateral bracing stiffness value. The behavior behind this recommendation is that the torsional brace works essentially as a nodal lateral brace to the compression flange in the limit that the tension flange lateral bracing is rigid. However, the asymptotic approach of the interaction to this limit is very gradual, hence the requirement of 2x the full nodal lateral bracing stiffness.



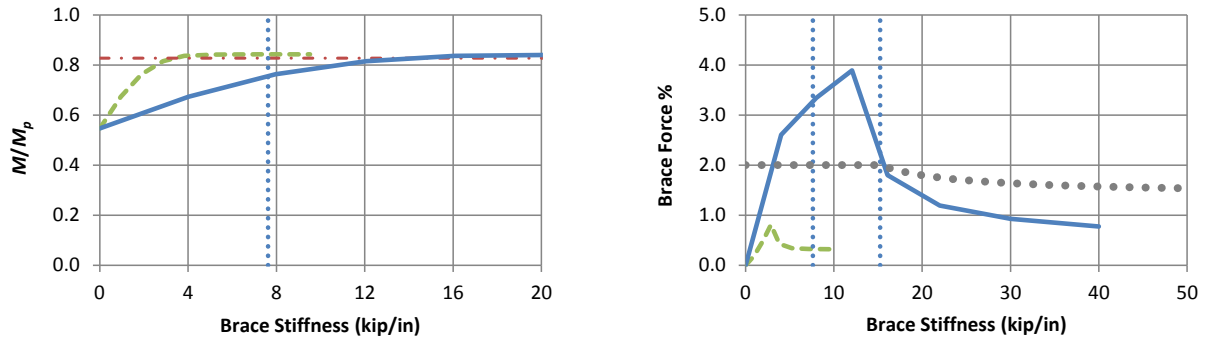
## APPENDIX A

Appendix A consists of knuckle curve and brace force vs brace stiffness plots for the interaction cases shown in Chapter 8 for the interaction bracing cases. Sections A.1 through A.4 consist of Category D negative loadings, Category D positive loadings, Category E negative loadings, and Category E positive loadings respectively. In Sections A.5 to A.7, the deformed geometries at the limit load from selected load-deflection analysis are shown for categories A, B, and C. The selected load-deflection analysis were chosen to illustrate the changes on behavior of the member for different brace stiffness values. The black shaded regions on the deformed geometries indicates where the Von Misses stress exceeds  $F_y = 50$  ksi.

### A.1 Category Dn



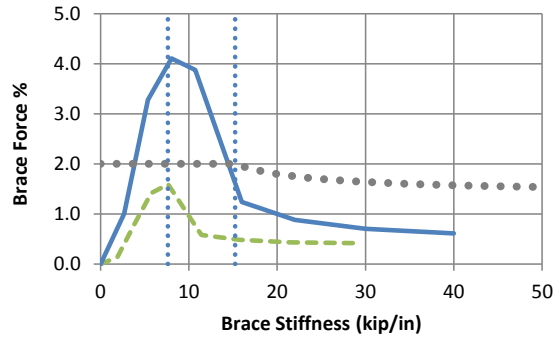
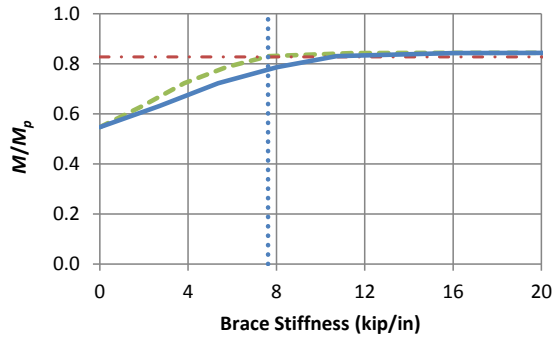
(a) D1100n ( $\beta_T/\beta_n = 9.81$ )



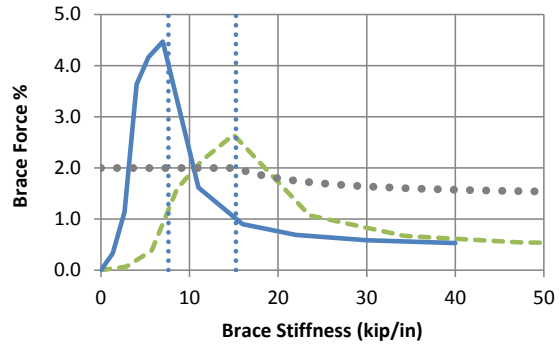
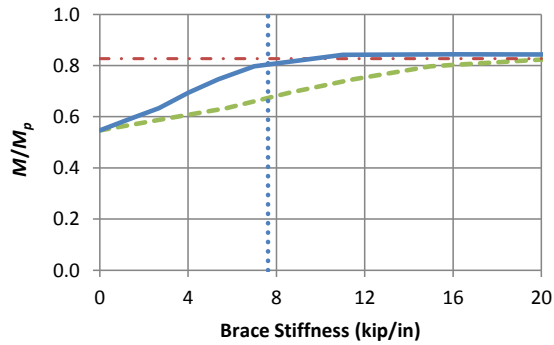
(b) D1101n ( $\beta_T/\beta_n = 4.20$ )

- Test Simulation Results, Torsional Bracing
- - - Test Simulation Results, Nodal Lateral Bracing
- · - Rigid Bracing Strength
- · · 1 and 2x AISC Ideal Torsional Bracing Stiffness ( $\beta_{IF,AISC}$  and  $2\beta_{IF,AISC}$ )
- · · Refined Estimate of Required Torsional Bracing Strength (not considering combined torsional and lateral bracing)

Fig. A.1. Case D110\*n knuckle and brace force vs. brace stiffness curves (Combined nodal lateral and nodal torsional bracing,  $L_b = 5$  ft,  $n = 1$ , negative bending)



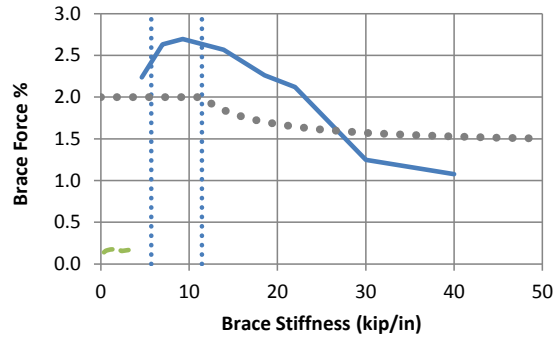
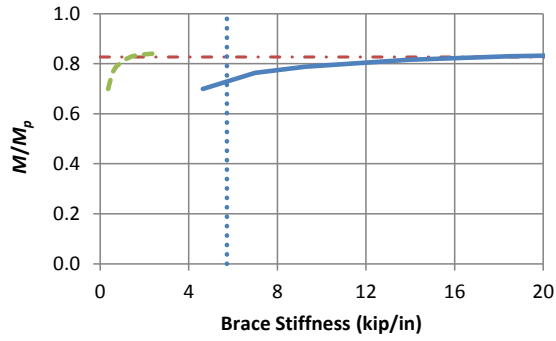
(c) D1102n ( $\beta_T/\beta_n = 1.40$ )



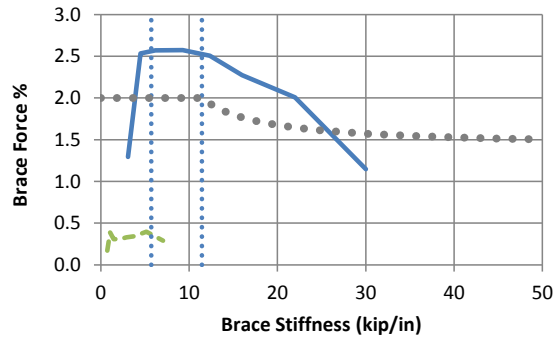
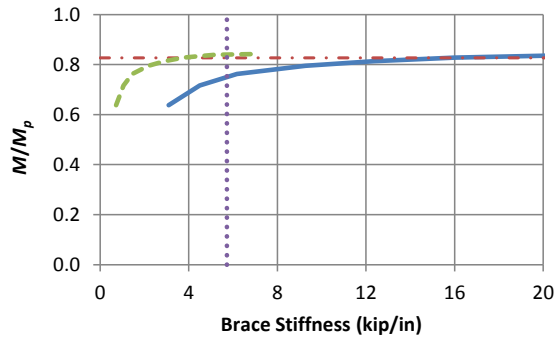
(d) D1103n ( $\beta_T/\beta_n = 0.467$ )

- Test Simulation Results, Torsional Bracing
- - - Test Simulation Results, Nodal Lateral Bracing
- - - Rigid Bracing Strength
- 1 and 2x AISC Ideal Torsional Bracing Stiffness ( $\beta_{IF,AISC}$  and  $2\beta_{IF,AISC}$ )
- Refined Estimate of Required Torsional Bracing Strength (not considering combined torsional and lateral bracing)

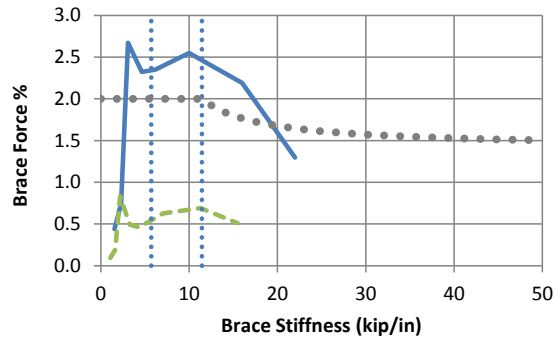
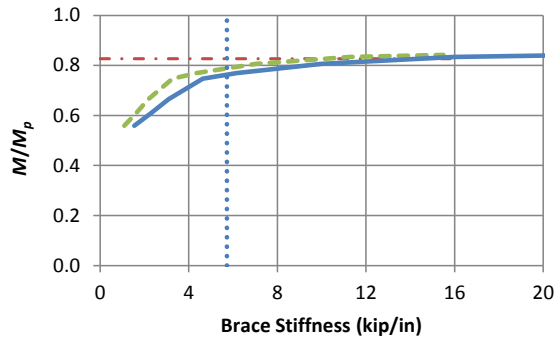
Fig. A.1 (continued). Case D110\*n knuckle and brace force vs. brace stiffness curves (Combined nodal lateral and nodal torsional bracing,  $L_b = 5$  ft,  $n = 1$ , negative bending)



(a) D1201n ( $\beta_T/\beta_n = 12.8$ )



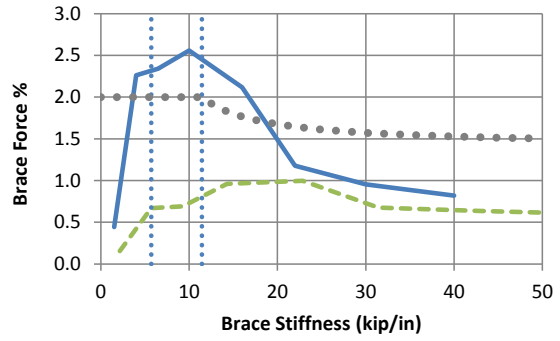
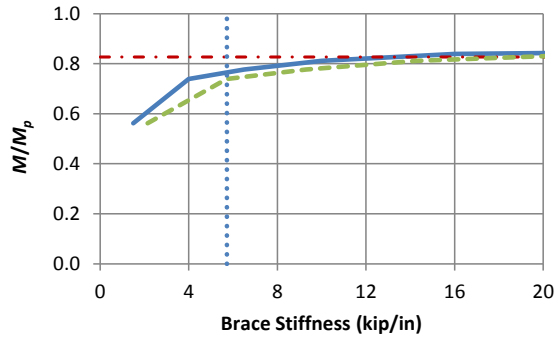
(b) D1202n ( $\beta_T/\beta_n = 4.25$ )



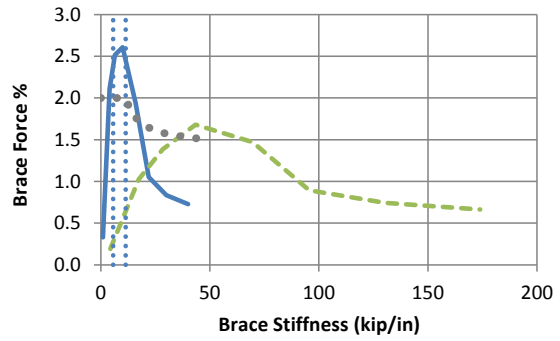
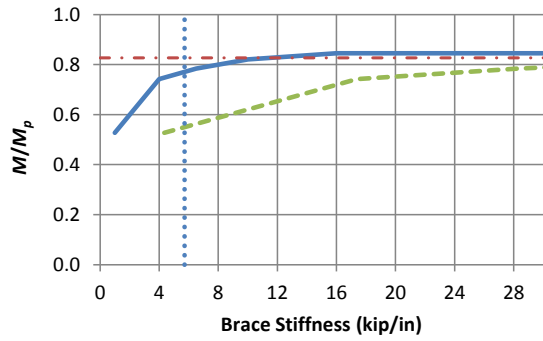
(c) D1203n ( $\beta_T/\beta_n = 1.42$ )

- Test Simulation Results, Torsional Bracing
- - - Test Simulation Results, Nodal Lateral Bracing
- - - Rigid Bracing Strength
- 1 and 2x AISC Ideal Torsional Bracing Stiffness ( $\beta_{IF,AISC}$  and  $2\beta_{IF,AISC}$ )
- Refined Estimate of Required Torsional Bracing Strength (not considering combined torsional and lateral bracing)

Fig. A.2. Case D120\*n knuckle and brace force vs. brace stiffness curves (Combined nodal lateral and nodal torsional bracing,  $L_b = 5$  ft,  $n = 2$ , negative bending)



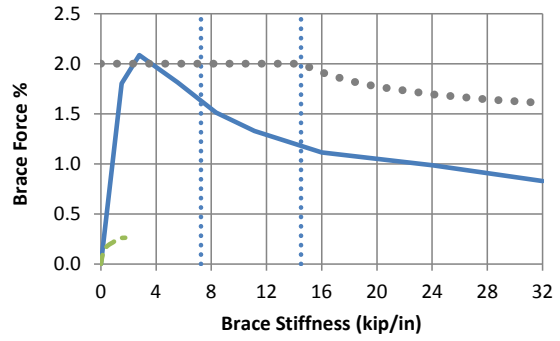
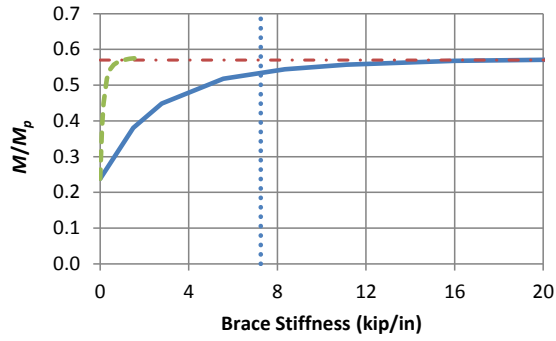
(d) D1204n ( $\beta_T/\beta_n = 0.70$ )



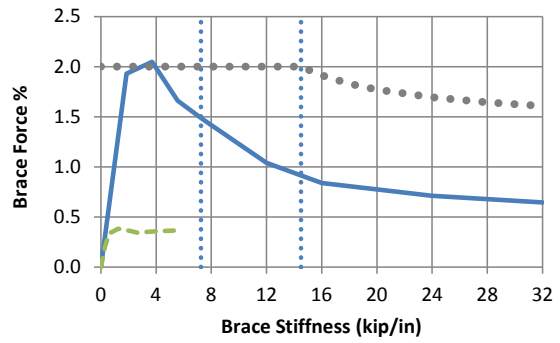
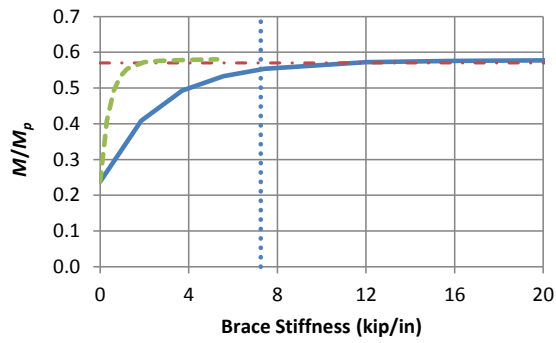
(e) D1205n ( $\beta_T/\beta_n = 0.23$ )

- Test Simulation Results, Torsional Bracing
- - - Test Simulation Results, Nodal Lateral Bracing
- · - Rigid Bracing Strength
- · · 1 and 2x AISC Ideal Torsional Bracing Stiffness ( $\beta_{IF,AISC}$  and  $2\beta_{IF,AISC}$ )
- · · Refined Estimate of Required Torsional Bracing Strength (not considering combined torsional and lateral bracing)

Fig. A.2 (continued). Case D120\*n knuckle and brace force vs. brace stiffness curves (Combined nodal lateral and nodal torsional bracing,  $L_b = 5$  ft,  $n = 2$ , negative bending)



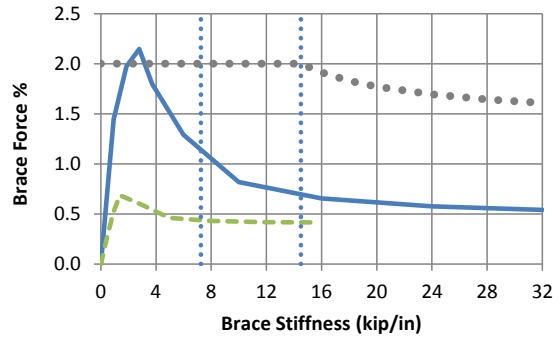
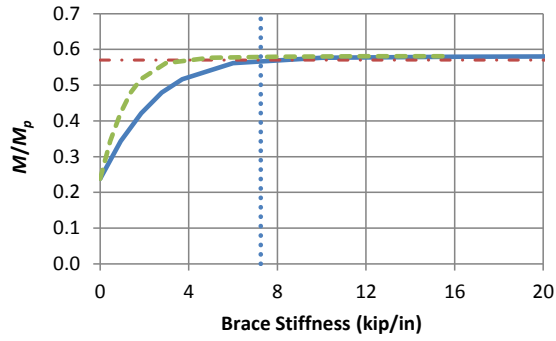
(a) D2101n ( $\beta_T/\beta_n = 18.2$ )



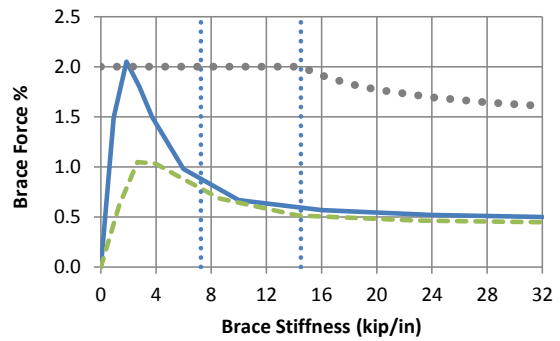
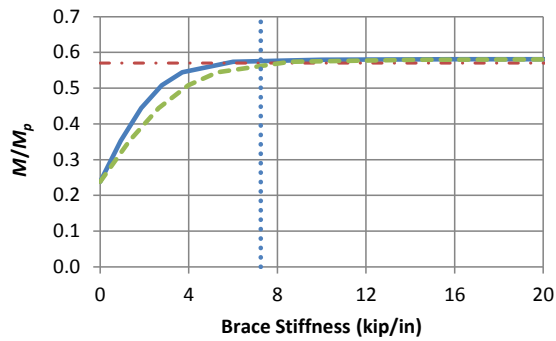
(b) D2102n ( $\beta_T/\beta_n = 6.06$ )

- Test Simulation Results, Torsional Bracing
- - - Test Simulation Results, Nodal Lateral Bracing
- · - Rigid Bracing Strength
- · · 1 and 2x AISC Ideal Torsional Bracing Stiffness ( $\beta_{IF,AISC}$  and  $2\beta_{IF,AISC}$ )
- · · Refined Estimate of Required Torsional Bracing Strength (not considering combined torsional and lateral bracing)

Fig. A.3. Case D210\*n knuckle and brace force vs. brace stiffness curves (Combined nodal lateral and nodal torsional bracing,  $L_b = 10$  ft,  $n = 1$ , negative bending)



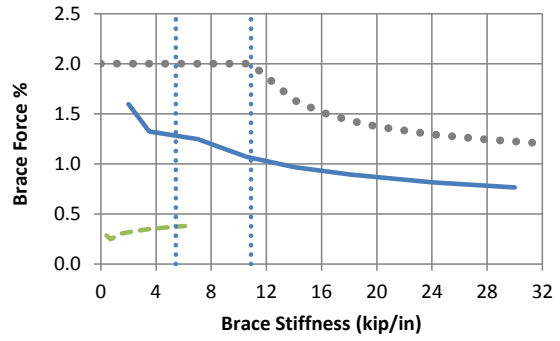
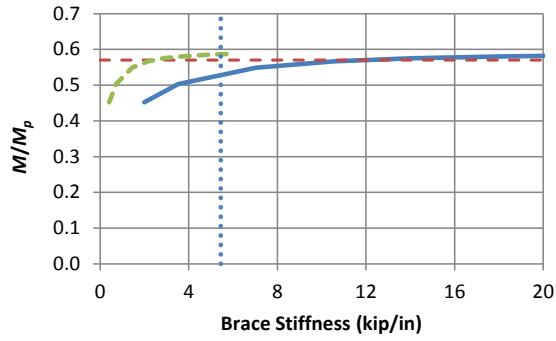
(c) D2103n ( $\beta_T/\beta_n = 2.02$ )



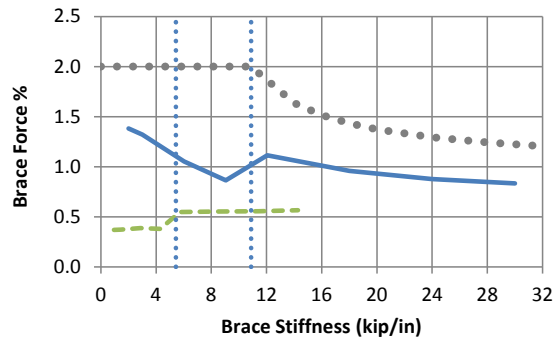
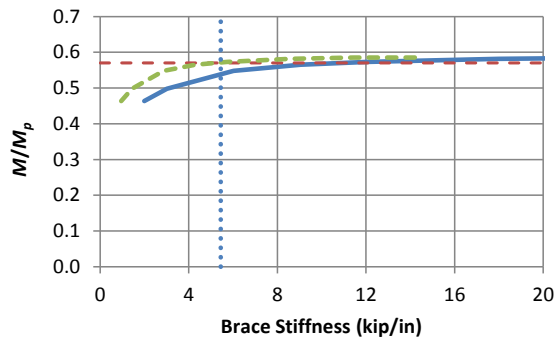
(d) D2104n ( $\beta_T/\beta_n = 0.70$ )

- Test Simulation Results, Torsional Bracing
- - - Test Simulation Results, Nodal Lateral Bracing
- - - Rigid Bracing Strength
- 1 and 2x AISC Ideal Torsional Bracing Stiffness ( $\beta_{IF,AISC}$  and  $2\beta_{IF,AISC}$ )
- Refined Estimate of Required Torsional Bracing Strength (not considering combined torsional and lateral bracing)

Fig. A.3 (continued). Case D210\*n knuckle and brace force vs. brace stiffness curves (Combined nodal lateral and nodal torsional bracing,  $L_b = 10$  ft,  $n = 1$ , negative bending)



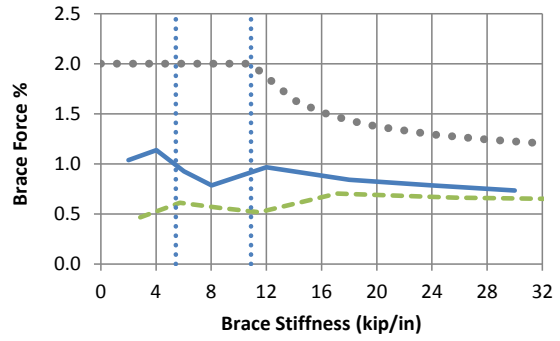
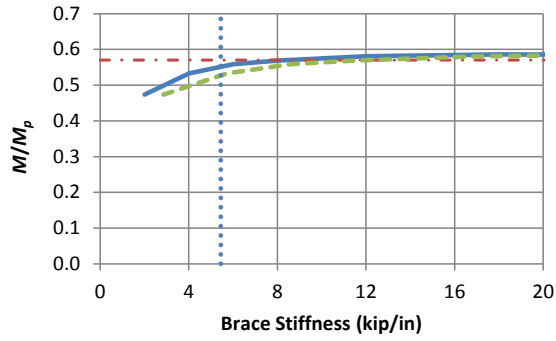
(a) D2200n ( $\beta_T/\beta_n = 4.90$ )



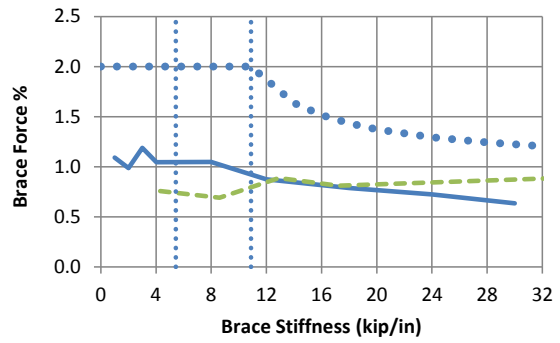
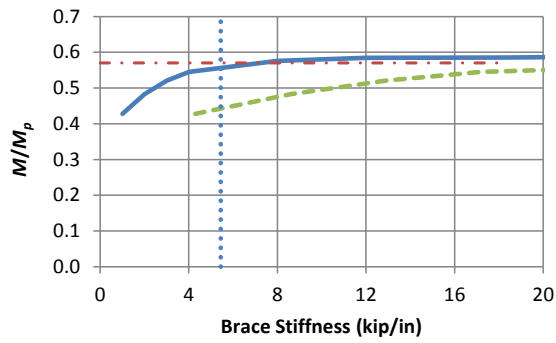
(b) D2201n ( $\beta_T/\beta_n = 2.10$ )

- Test Simulation Results, Torsional Bracing
- - - Test Simulation Results, Nodal Lateral Bracing
- . - . Rigid Bracing Strength
- · · · 1 and 2x AISC Ideal Torsional Bracing Stiffness ( $\beta_{IF,AISC}$  and  $2\beta_{IF,AISC}$ )
- · · · Refined Estimate of Required Torsional Bracing Strength (not considering combined torsional and lateral bracing)

Fig. A.4. Case D220\*n knuckle and brace force vs. brace stiffness curves (Combined nodal lateral and nodal torsional bracing,  $L_b = 10$  ft,  $n = 2$ , negative bending)



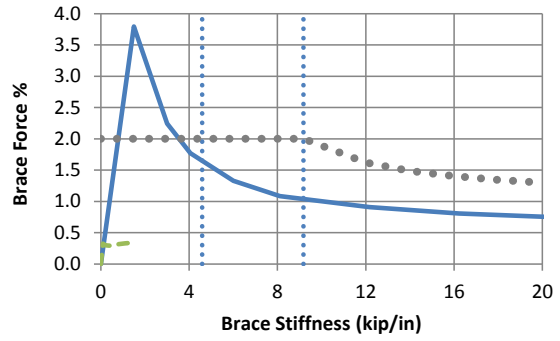
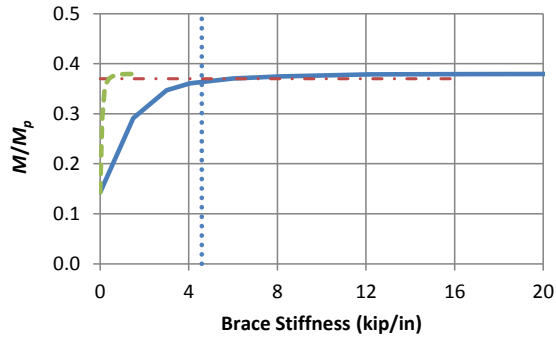
(c) D2202n ( $\beta_T/\beta_n = 0.70$ )



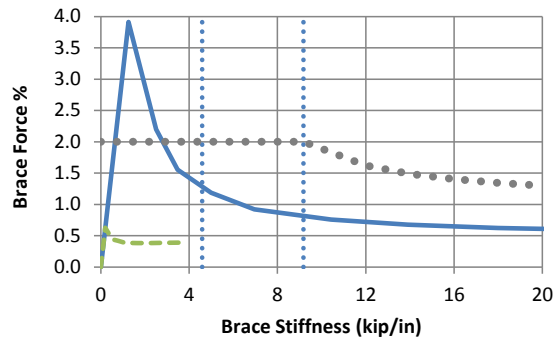
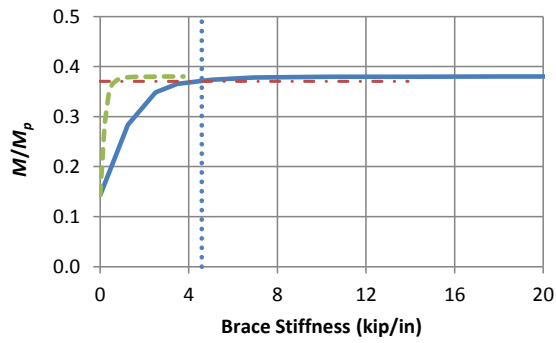
(d) D2203n ( $\beta_T/\beta_n = 0.23$ )

- Test Simulation Results, Torsional Bracing
- - - Test Simulation Results, Nodal Lateral Bracing
- . - . Rigid Bracing Strength
- 1 and 2x AISC Ideal Torsional Bracing Stiffness ( $\beta_{IF,AISC}$  and  $2\beta_{IF,AISC}$ )
- Refined Estimate of Required Torsional Bracing Strength (not considering combined torsional and lateral bracing)

Fig. A.4 (continued). Case D220\*n knuckle and brace force vs. brace stiffness curves (Combined nodal lateral and nodal torsional bracing,  $L_b = 10$  ft,  $n = 2$ , negative bending)



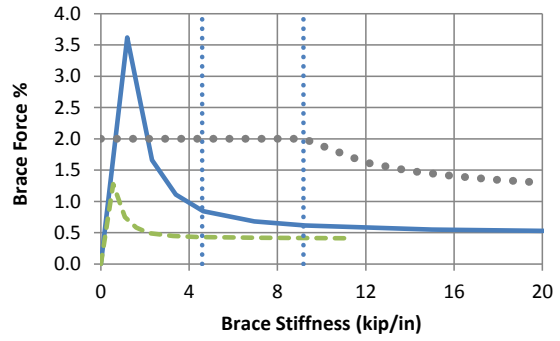
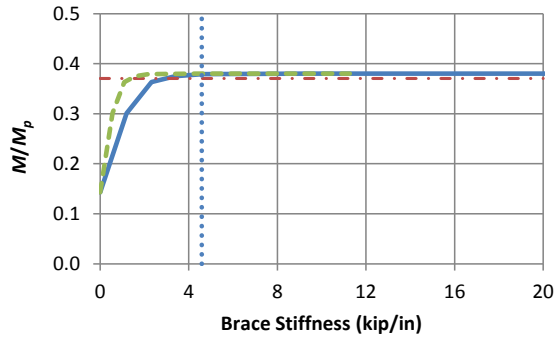
(a) D3100n ( $\beta_T/\beta_n = 14.9$ )



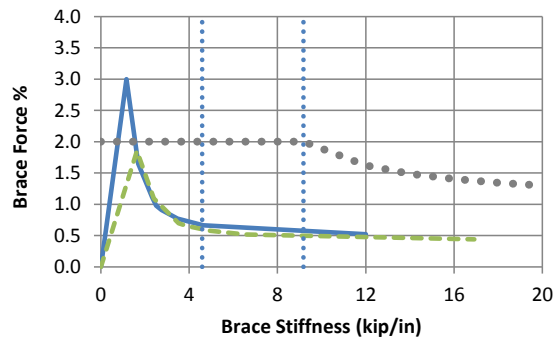
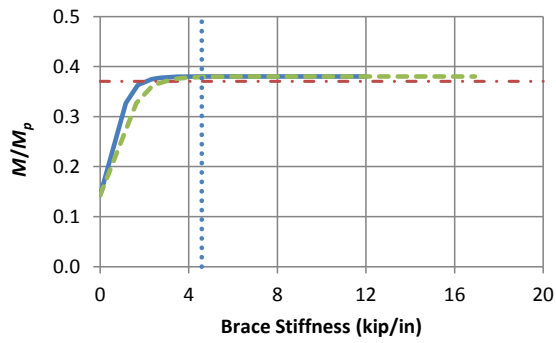
(b) D3101n ( $\beta_T/\beta_n = 6.38$ )

- Test Simulation Results, Torsional Bracing
- - - Test Simulation Results, Nodal Lateral Bracing
- . - Rigid Bracing Strength
- · · · 1 and 2x AISC Ideal Torsional Bracing Stiffness ( $\beta_{IF,AISC}$  and  $2\beta_{IF,AISC}$ )
- · · · Refined Estimate of Required Torsional Bracing Strength (not considering combined torsional and lateral bracing)

Fig. A.5. Case D310\*n knuckle and brace force vs. brace stiffness curves (Combined nodal lateral and nodal torsional bracing,  $L_b = 15$  ft,  $n = 1$ , negative bending)



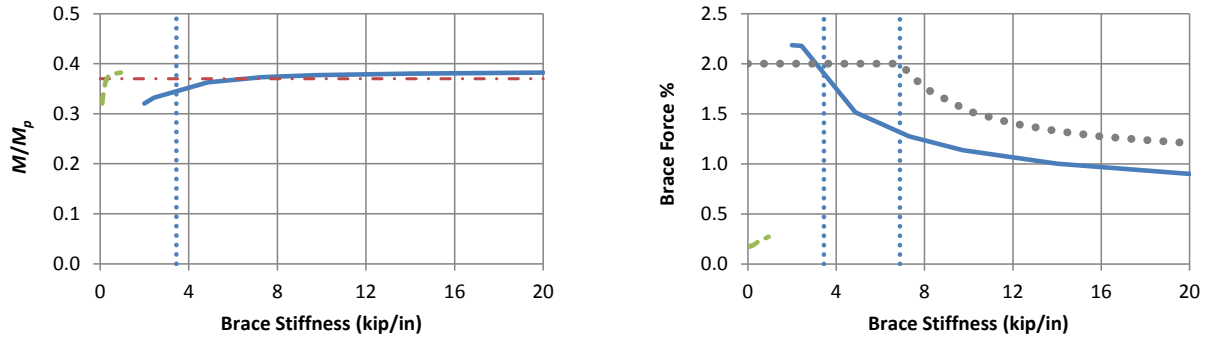
(c) D3102n ( $\beta_T/\beta_n = 2.13$ )



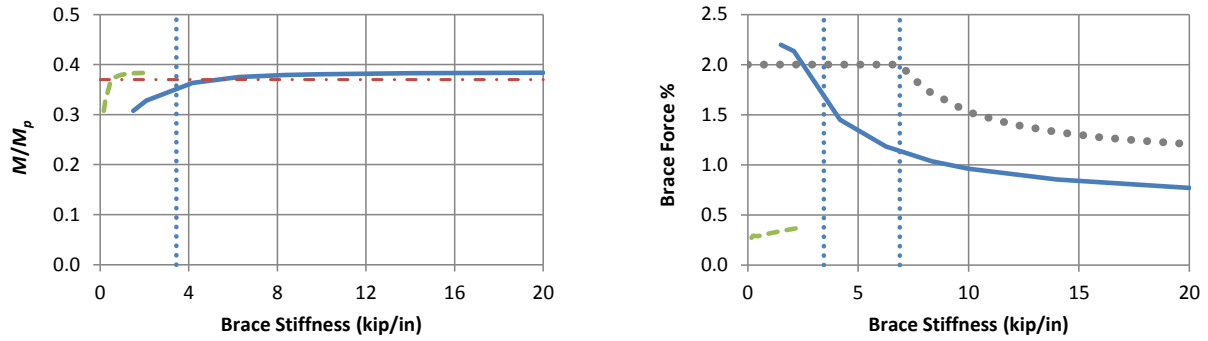
(d) D3103n ( $\beta_T/\beta_n = 0.71$ )

- Test Simulation Results, Torsional Bracing
- - - Test Simulation Results, Nodal Lateral Bracing
- . - . Rigid Bracing Strength
- · · · 1 and 2x AISC Ideal Torsional Bracing Stiffness ( $\beta_{IF,AISC}$  and  $2\beta_{IF,AISC}$ )
- · · · Refined Estimate of Required Torsional Bracing Strength  
(not considering combined torsional and lateral bracing)

Fig. A.5 (continued). Case D310\*n knuckle and brace force vs. brace stiffness curves (Combined nodal lateral and nodal torsional bracing,  $L_b = 15$  ft,  $n = 1$ , negative bending)



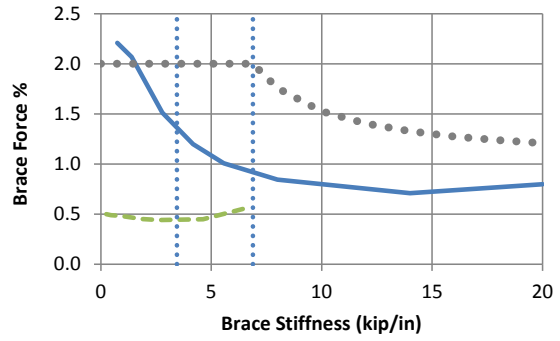
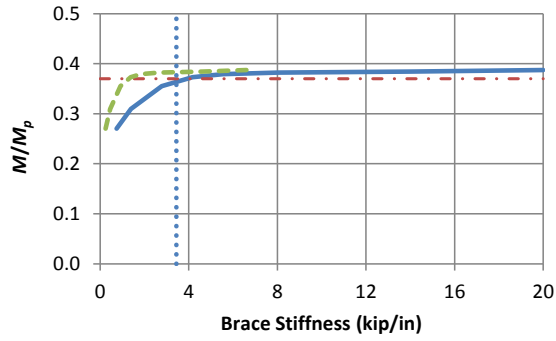
(a) D3200n ( $\beta_T/\beta_n = 21.2$ )



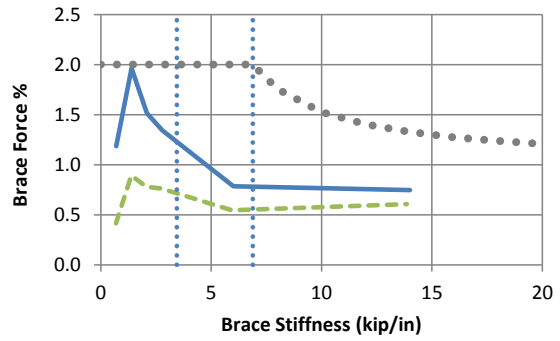
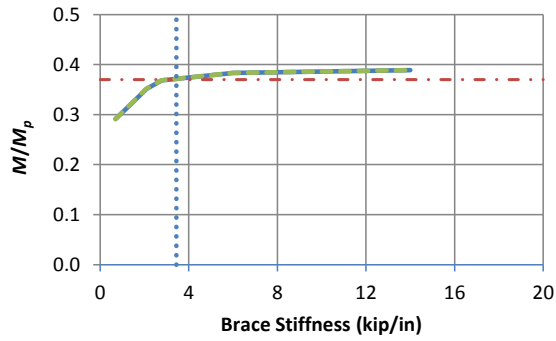
(b) D3201n ( $\beta_T/\beta_n = 9.08$ )

- Test Simulation Results, Torsional Bracing
- - - Test Simulation Results, Nodal Lateral Bracing
- . - Rigid Bracing Strength
- 1 and 2x AISC Ideal Torsional Bracing Stiffness ( $\beta_{IF,AISC}$  and  $2\beta_{IF,AISC}$ )
- Refined Estimate of Required Torsional Bracing Strength (not considering combined torsional and lateral bracing)

Fig. A.6. Case D320\*n knuckle and brace force vs. brace stiffness curves (Combined nodal lateral and nodal torsional bracing,  $L_b = 15$  ft,  $n = 2$ , negative bending)



(c) D3202n ( $\beta_T/\beta_n = 3.03$ )

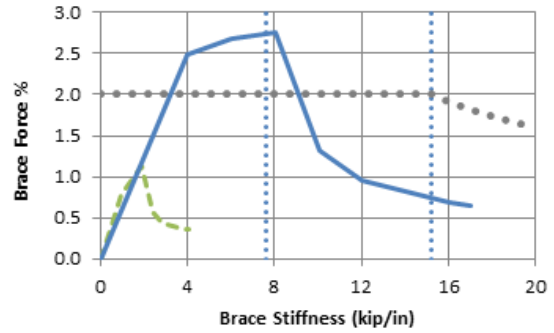
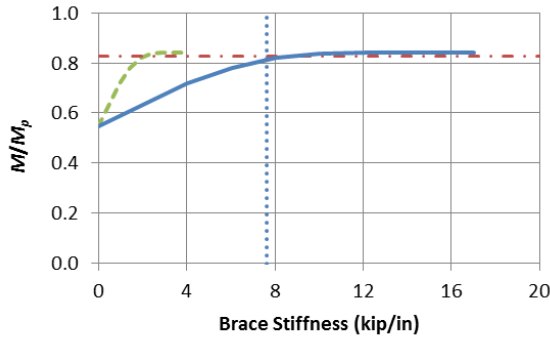


(d) D3203n ( $\beta_T/\beta_n = 1.01$ )

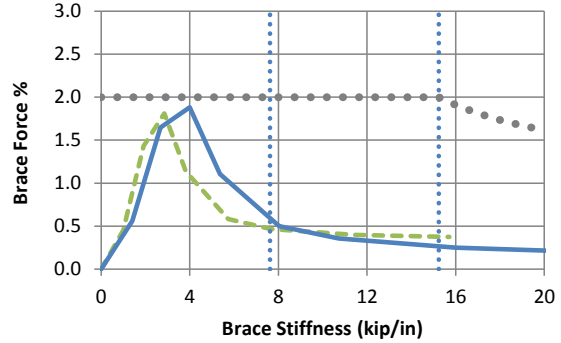
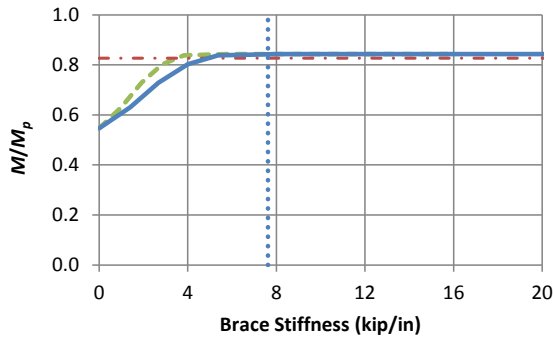
- Test Simulation Results, Torsional Bracing
- - - Test Simulation Results, Nodal Lateral Bracing
- . - . Rigid Bracing Strength
- · · · 1 and 2x AISC Ideal Torsional Bracing Stiffness ( $\beta_{IF,AISC}$  and  $2\beta_{IF,AISC}$ )
- · · · Refined Estimate of Required Torsional Bracing Strength  
(not considering combined torsional and lateral bracing)

Fig. A.6 (continued). Case D320\*n knuckle and brace force vs. brace stiffness curves (Combined nodal lateral and nodal torsional bracing,  $L_b = 15$  ft,  $n = 2$ , negative bending)

## A.2 Category Dp



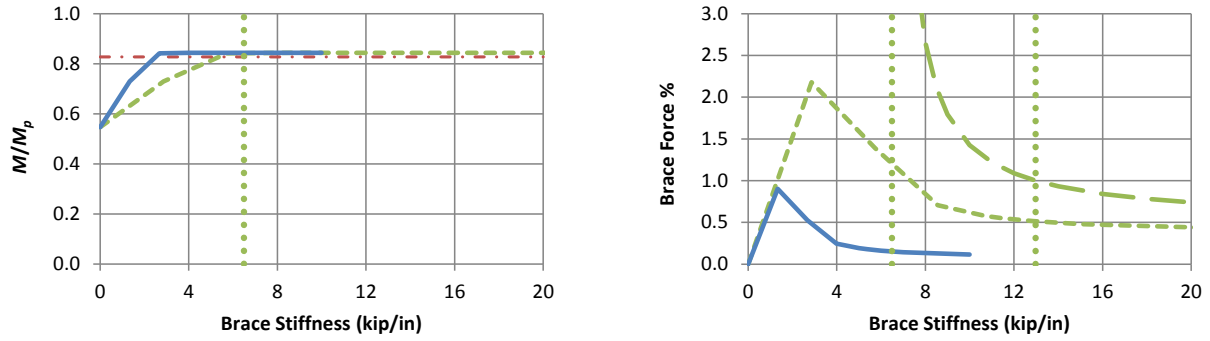
(a) D1100p ( $\beta_T/\beta_n = 4.20$ )



(b) D1101p ( $\beta_T/\beta_n = 1.40$ )

- Test Simulation Results, Torsional Bracing
- - - Test Simulation Results, Nodal Lateral Bracing
- · - Rigid Bracing Strength
- · · · 1 and 2x AISC Ideal Torsional Bracing Stiffness ( $\beta_{IF,AISC}$  and  $2\beta_{IF,AISC}$ )
- · · · Refined Estimate of Required Torsional Bracing Strength (not considering combined torsional and lateral bracing)
- · · · 1 and 2x AISC Ideal Nodal Lateral Bracing Stiffness ( $\beta_{IF,AISC}$  and  $2\beta_{IF,AISC}$ )
- · - Refined Estimate of Required Nodal Lateral Bracing Strength from AISC Commentary (not considering combined torsional and lateral bracing)

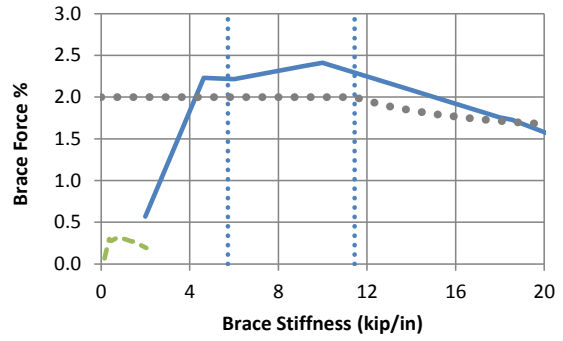
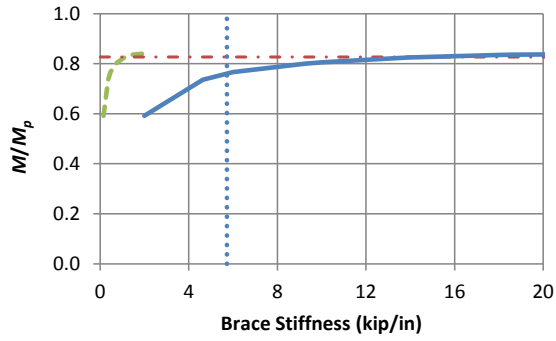
Fig. A.7. Case D110\*p knuckle and brace force vs. brace stiffness curves (Combined nodal lateral and nodal torsional bracing,  $L_b = 5$  ft,  $n = 1$ , positive bending)



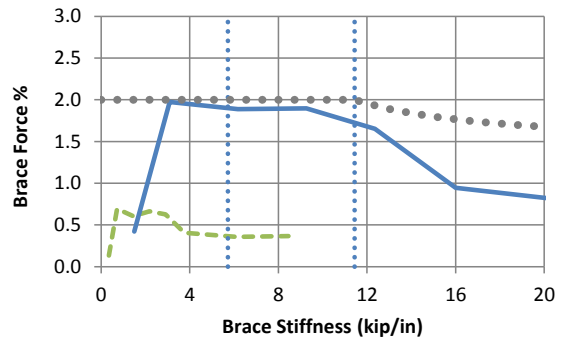
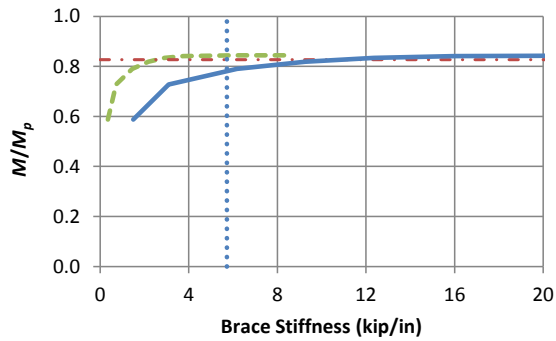
(c) D1102p ( $\beta_T/\beta_n = 0.47$ )

- Test Simulation Results, Torsional Bracing
- - - Test Simulation Results, Nodal Lateral Bracing
- · - Rigid Bracing Strength
- · · · 1 and 2x AISC Ideal Torsional Bracing Stiffness ( $\beta_{IF,AISC}$  and  $2\beta_{IF,AISC}$ )
- · · · Refined Estimate of Required Torsional Bracing Strength (not considering combined torsional and lateral bracing)
- · · · 1 and 2x AISC Ideal Nodal Lateral Bracing Stiffness ( $\beta_{IF,AISC}$  and  $2\beta_{IF,AISC}$ )
- - - Refined Estimate of Required Nodal Lateral Bracing Strength from AISC Commentary (not considering combined torsional and lateral bracing)

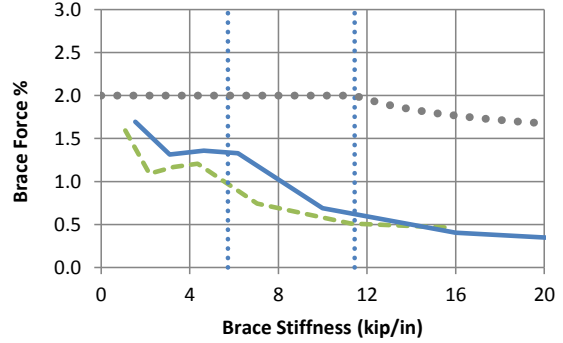
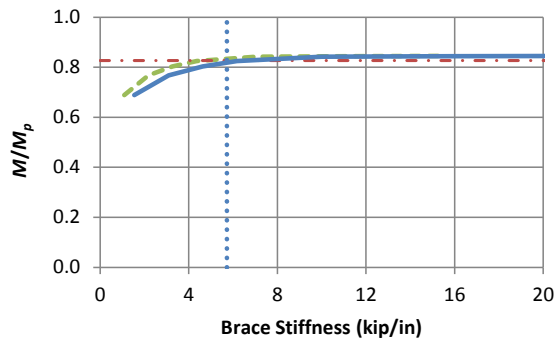
Fig. A.7 (continued). Case D110\*p knuckle and brace force vs. brace stiffness curves (Combined nodal lateral and nodal torsional bracing,  $L_b = 5$  ft,  $n = 1$ , positive bending)



(a) D1200p ( $\beta_T/\beta_n = 12.8$ )



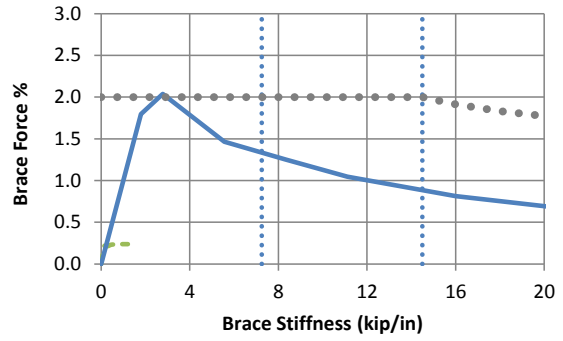
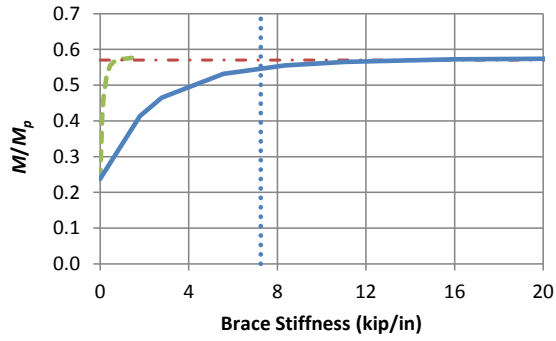
(b) D1201p ( $\beta_T/\beta_n = 4.26$ )



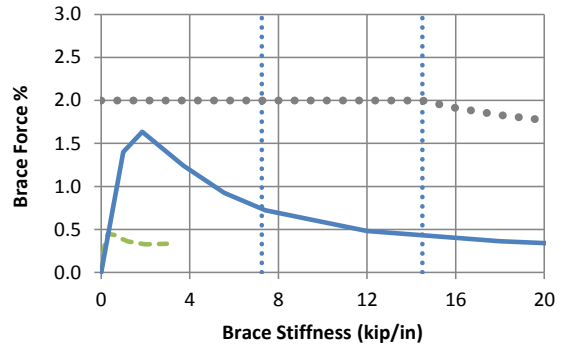
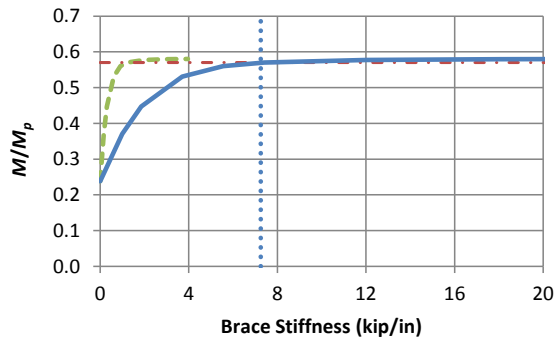
(c) D1202p ( $\beta_T/\beta_n = 1.42$ )

- Test Simulation Results, Torsional Bracing
- - - Test Simulation Results, Nodal Lateral Bracing
- . - Rigid Bracing Strength
- · · 1 and 2x AISC Ideal Torsional Bracing Stiffness ( $\beta_{IF,AISC}$  and  $2\beta_{IF,AISC}$ )
- · · Refined Estimate of Required Torsional Bracing Strength (not considering combined torsional and lateral bracing)

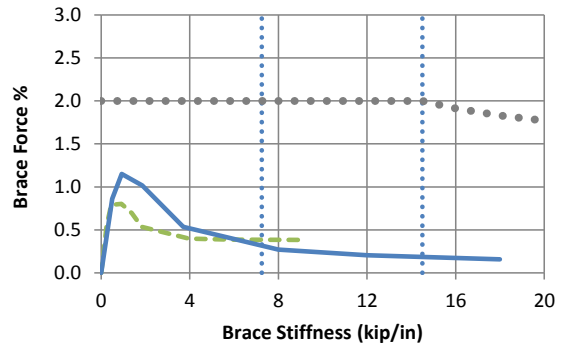
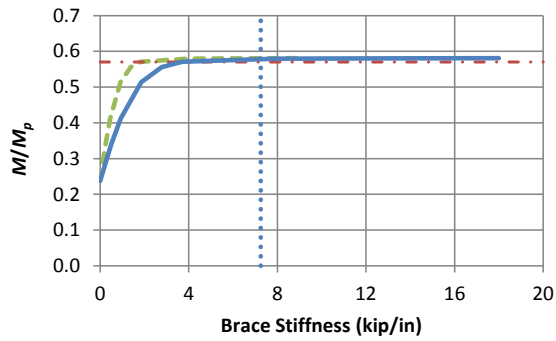
Fig. A.8. Case D120\*p knuckle and brace force vs. brace stiffness curves (Combined nodal lateral and nodal torsional bracing,  $L_b = 5$  ft,  $n = 2$ , positive bending)



(a) D2100p ( $\beta_T/\beta_n = 18.2$ )



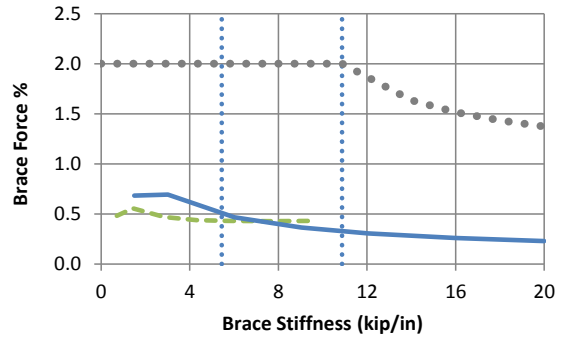
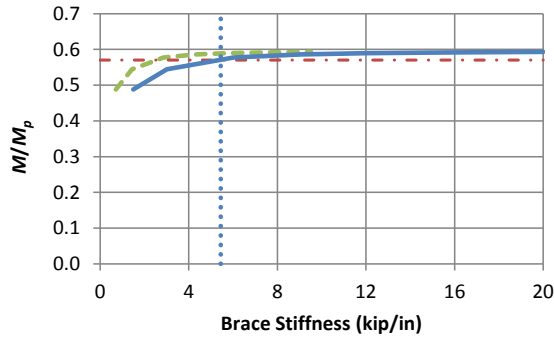
(b) D2101p ( $\beta_T/\beta_n = 6.06$ )



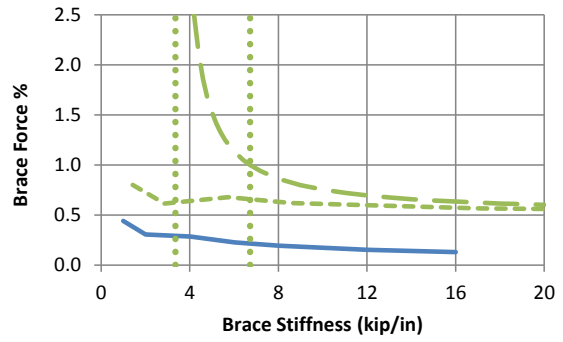
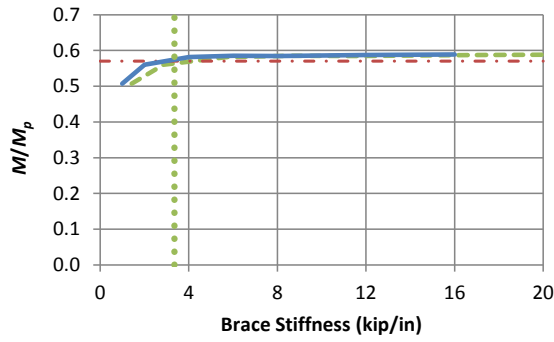
(c) D2102p ( $\beta_T/\beta_n = 2.02$ )

- Test Simulation Results, Torsional Bracing
- - - Test Simulation Results, Nodal Lateral Bracing
- · - · Rigid Bracing Strength
- · · · 1 and 2x AISC Ideal Torsional Bracing Stiffness ( $\beta_{IF,AISC}$  and  $2\beta_{IF,AISC}$ )
- · · · Refined Estimate of Required Torsional Bracing Strength (not considering combined torsional and lateral bracing)

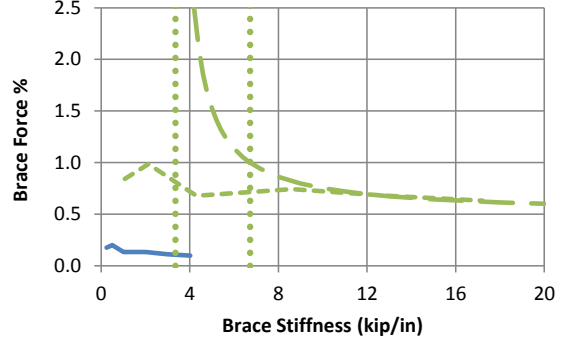
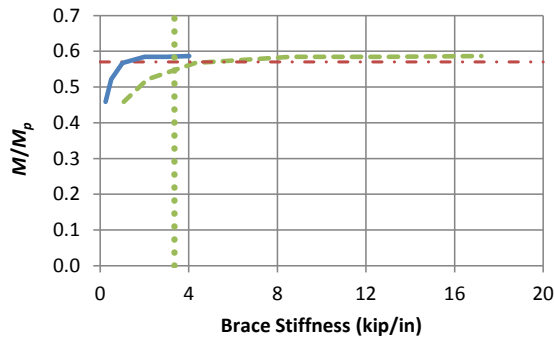
Fig. A.9. Case D210\*p knuckle and brace force vs. brace stiffness curves (Combined nodal lateral and nodal torsional bracing,  $L_b = 10$  ft,  $n = 1$ , positive bending)



(a) D2200p ( $\beta_T/\beta_n = 2.10$ )



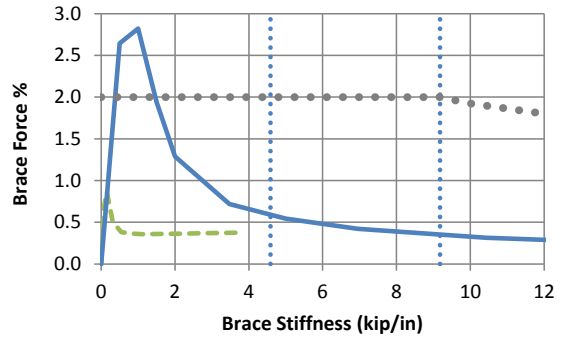
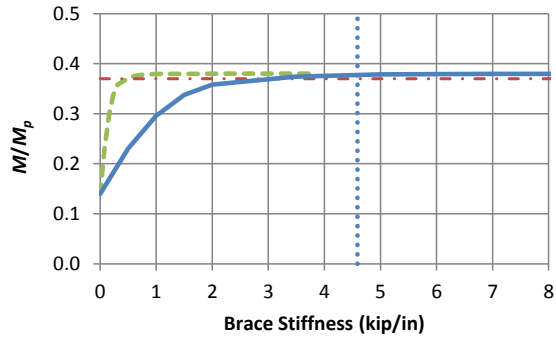
(b) D2201p ( $\beta_T/\beta_n = 0.701$ )



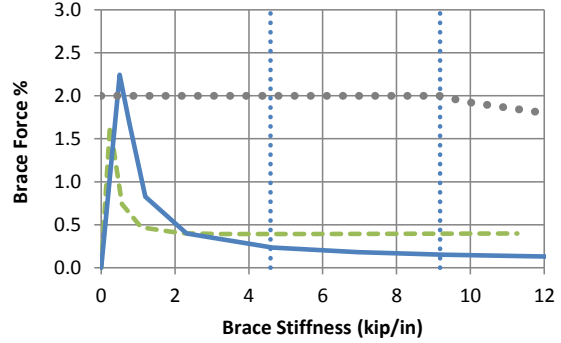
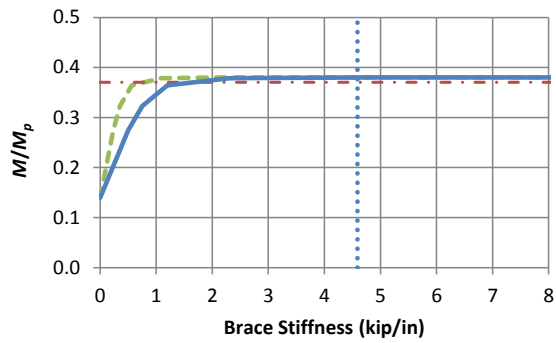
(c) D2202p ( $\beta_T/\beta_n = 0.234$ )

- Test Simulation Results, Torsional Bracing
- - - Test Simulation Results, Nodal Lateral Bracing
- · - Rigid Bracing Strength
- · · 1 and 2x AISC Ideal Torsional Bracing Stiffness ( $\beta_{IF,AISC}$  and  $2\beta_{IF,AISC}$ )
- · · Refined Estimate of Required Torsional Bracing Strength (not considering combined torsional and lateral bracing)
- · · 1 and 2x AISC Ideal Nodal Lateral Bracing Stiffness ( $\beta_{IF,AISC}$  and  $2\beta_{IF,AISC}$ )
- · - Refined Estimate of Required Nodal Lateral Bracing Strength from AISC Commentary (not considering combined torsional and lateral bracing)

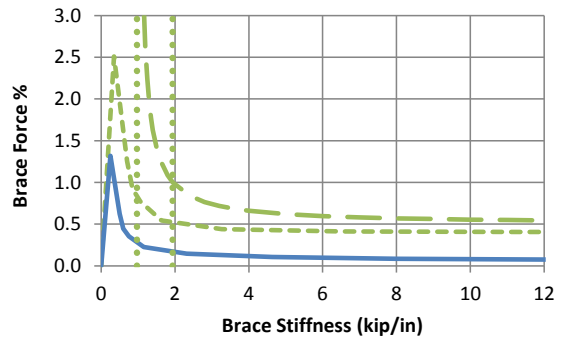
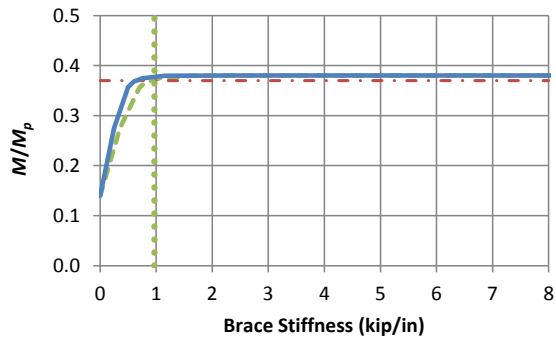
Fig. A.10. Case D220\*p knuckle and brace force vs. brace stiffness curves (Combined nodal lateral and nodal torsional bracing,  $L_b = 10$  ft,  $n = 2$ , positive bending)



(a) D3100p ( $\beta_T/\beta_n = 6.38$ )



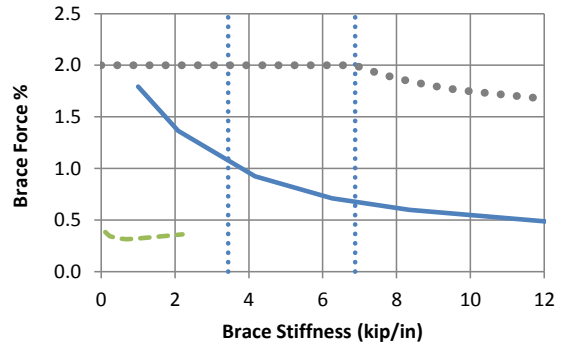
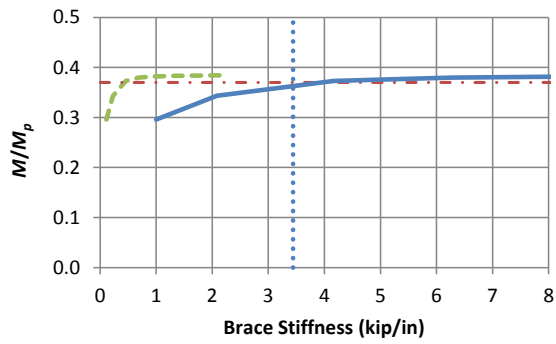
(b) D3101p ( $\beta_T/\beta_n = 2.13$ )



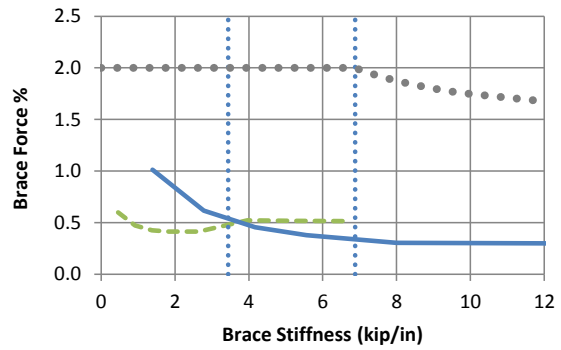
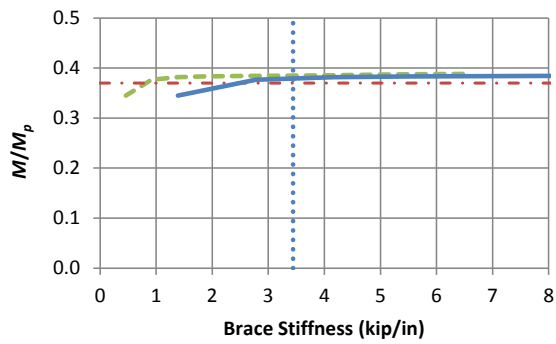
(c) D3102p ( $\beta_T/\beta_n = 0.709$ )

- Test Simulation Results, Torsional Bracing
- - - Test Simulation Results, Nodal Lateral Bracing
- · - Rigid Bracing Strength
- · · 1 and 2x AISC Ideal Torsional Bracing Stiffness ( $\beta_{IF,AISC}$  and  $2\beta_{IF,AISC}$ )
- · · Refined Estimate of Required Torsional Bracing Strength (not considering combined torsional and lateral bracing)
- · · 1 and 2x AISC Ideal Nodal Lateral Bracing Stiffness ( $\beta_{IF,AISC}$  and  $2\beta_{IF,AISC}$ )
- · - Refined Estimate of Required Nodal Lateral Bracing Strength from AISC Commentary (not considering combined torsional and lateral bracing)

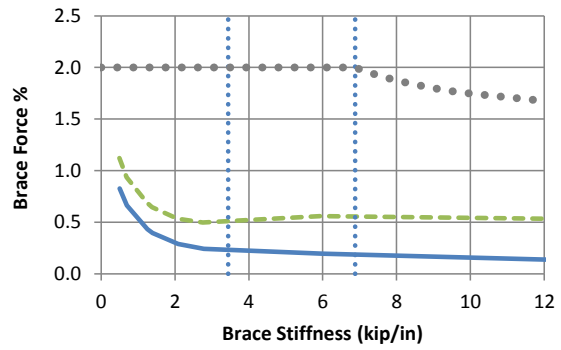
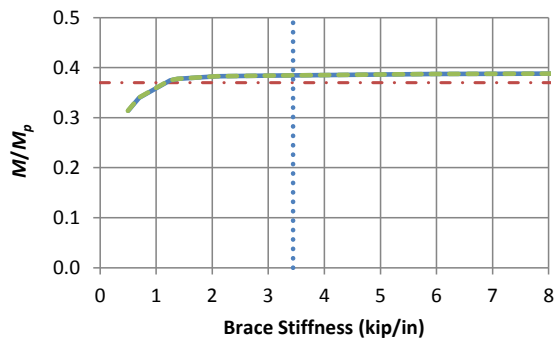
Fig. A.11. Case D310\*p knuckle and brace force vs. brace stiffness curves (Combined nodal lateral and nodal torsional bracing,  $L_b = 15$  ft,  $n = 1$ , positive bending)



(a) D3200p ( $\beta_T/\beta_n = 9.08$ )



(b) D3201p ( $\beta_T/\beta_n = 3.03$ )

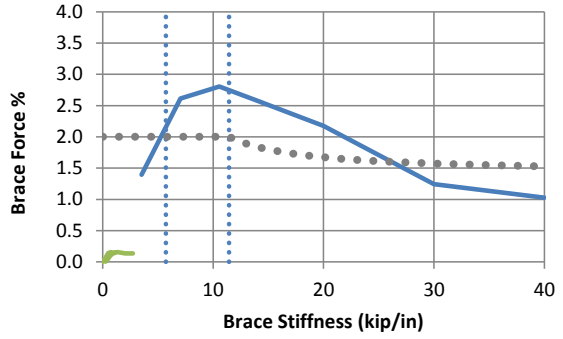
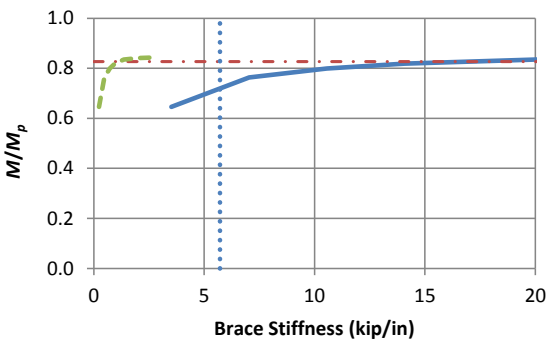


(c) D3202p ( $\beta_T/\beta_n = 1.01$ )

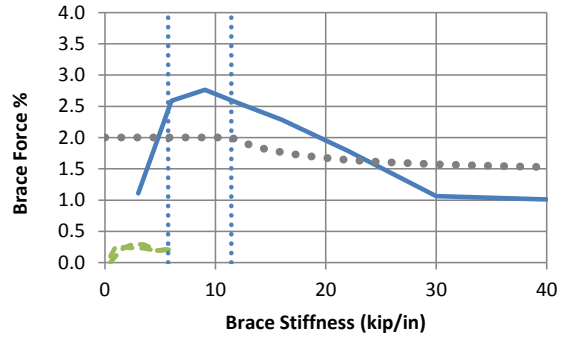
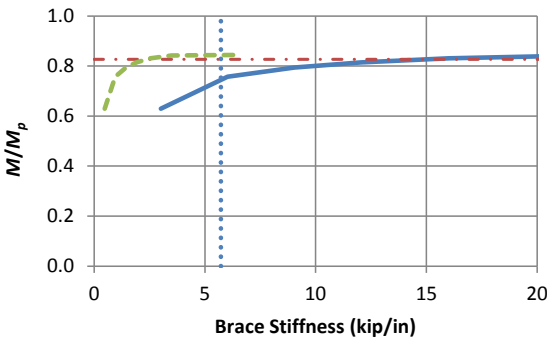
- Test Simulation Results, Torsional Bracing
- - - Test Simulation Results, Nodal Lateral Bracing
- . - . Rigid Bracing Strength
- · · · 1 and 2x AISC Ideal Torsional Bracing Stiffness ( $\beta_{IF,AISC}$  and  $2\beta_{IF,AISC}$ )
- · · · Refined Estimate of Required Torsional Bracing Strength (not considering combined torsional and lateral bracing)

Fig. A.12. Case D320\*p knuckle and brace force vs. brace stiffness curves (Combined nodal lateral and nodal torsional bracing,  $L_b = 15$  ft,  $n = 2$ , positive bending)

### A.3 Category En



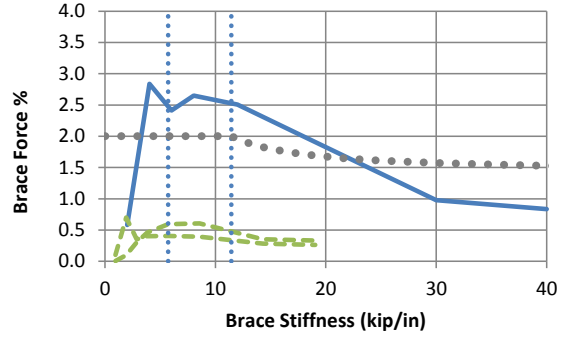
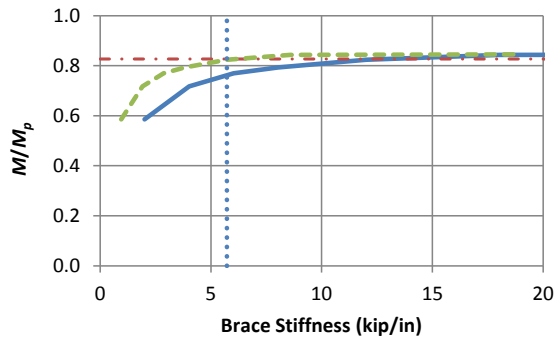
(a) E1200n ( $\beta_T/\beta_r = 14.7$ )



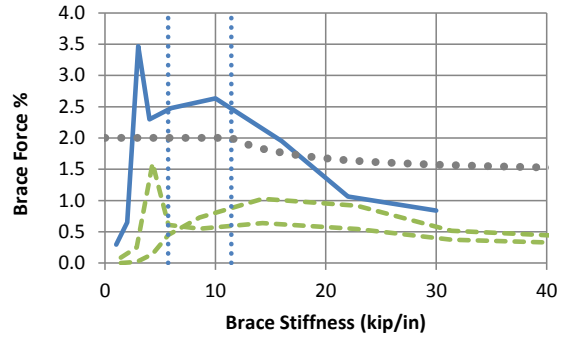
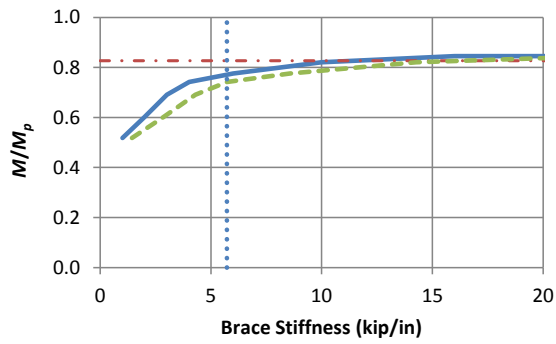
(b) E1201n ( $\beta_T/\beta_r = 6.31$ )

- Test Simulation Results, Torsional Bracing
- - - Test Simulation Results, Shear Panel Bracing
- · - Rigid Bracing Strength
- · · 1 and 2x AISC Ideal Torsional Bracing Stiffness ( $\beta_{IF,AISC}$  and  $2\beta_{IF,AISC}$ )
- · · Refined Estimate of Required Torsional Bracing Strength (not considering combined torsional and lateral bracing)

Fig. A.13. Case E120\*n knuckle and brace force vs. brace stiffness curves (Combined shear panel lateral lateral and nodal torsional bracing,  $L_b = 5$  ft,  $n = 2$ , negative bending)



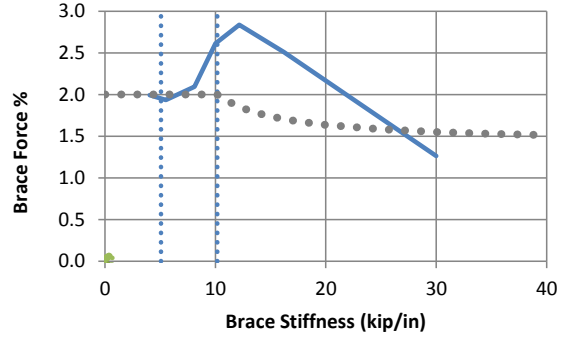
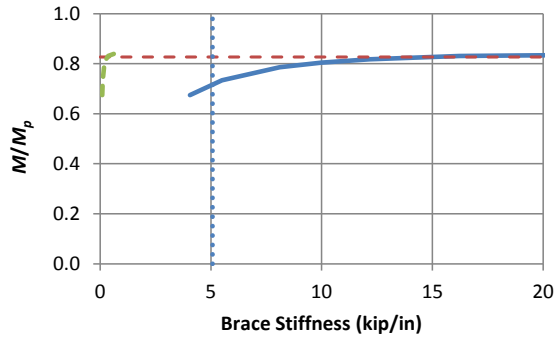
(c) E1202n ( $\beta_T/\beta_r = 2.10$ )



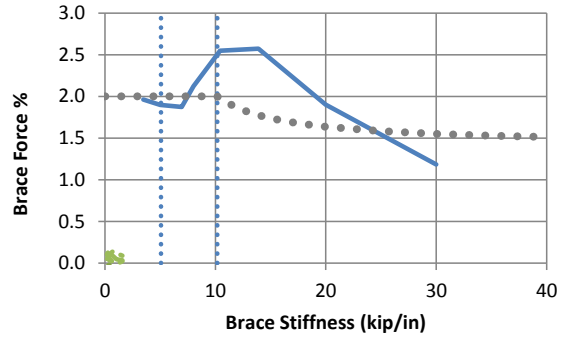
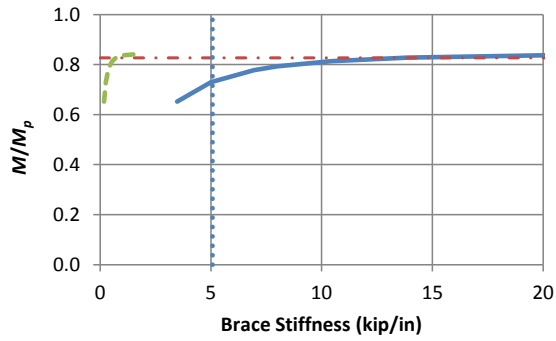
(d) E1203n ( $\beta_T/\beta_r = 0.70$ )

- Test Simulation Results, Torsional Bracing
- - - Test Simulation Results, Shear Panel Bracing
- . - Rigid Bracing Strength
- · · · 1 and 2x AISC Ideal Torsional Bracing Stiffness ( $\beta_{IF,AISC}$  and  $2\beta_{IF,AISC}$ )
- · · · Refined Estimate of Required Torsional Bracing Strength (not considering combined torsional and lateral bracing)

Fig. A.13 (continued). Case E120\*n knuckle and brace force vs. brace stiffness curves (Combined shear panel lateral and nodal torsional bracing,  $L_b = 5$  ft,  $n = 2$ , negative bending)



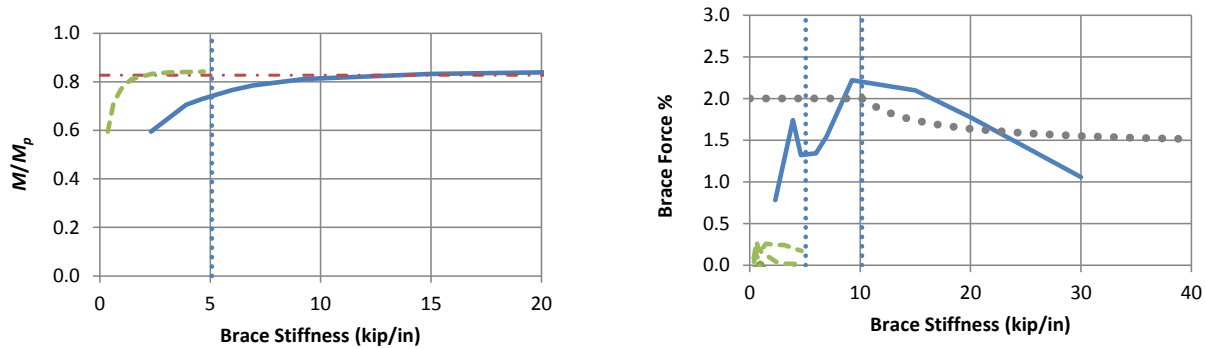
(a) E1300n ( $\beta_T/\beta_r = 44.7$ )



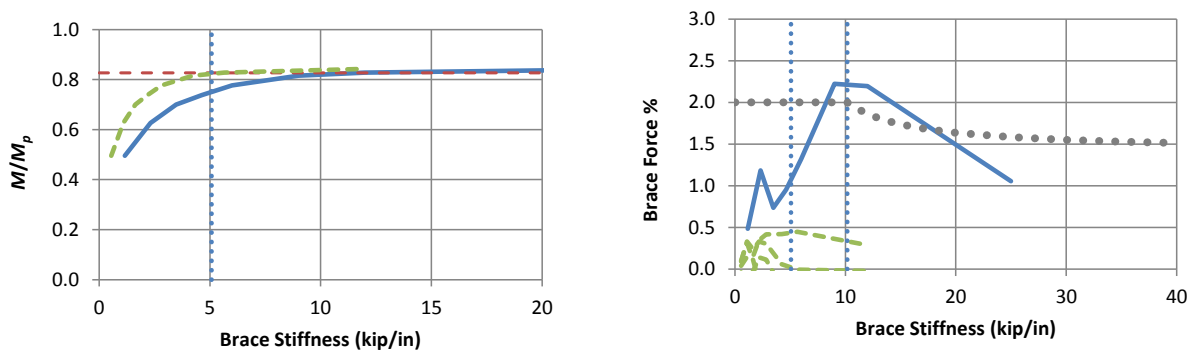
(b) E1301n ( $\beta_T/\beta_r = 19.2$ )

- Test Simulation Results, Torsional Bracing
- - - Test Simulation Results, Shear Panel Bracing
- . - . Rigid Bracing Strength
- 1 and 2x AISC Ideal Torsional Bracing Stiffness ( $\beta_{IF,AISC}$  and  $2\beta_{IF,AISC}$ )
- Refined Estimate of Required Torsional Bracing Strength (not considering combined torsional and lateral bracing)

Fig. A.14. Case E130\*n knuckle and brace force vs. brace stiffness curves (Combined shear panel lateral and nodal torsional bracing,  $L_b = 5$  ft,  $n = 3$ , negative bending)



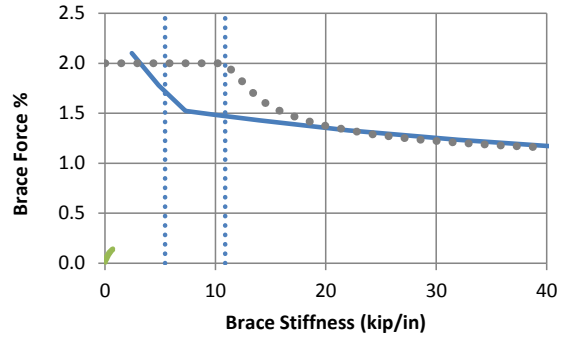
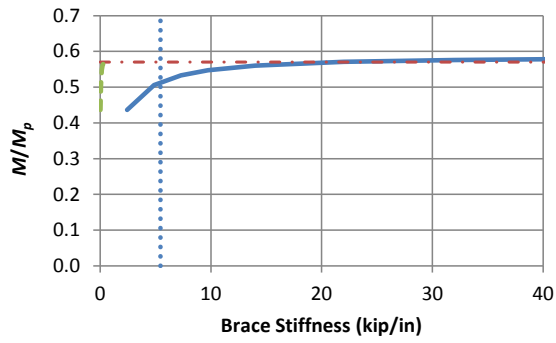
(c) E1302n ( $\beta_T/\beta_r = 6.38$ )



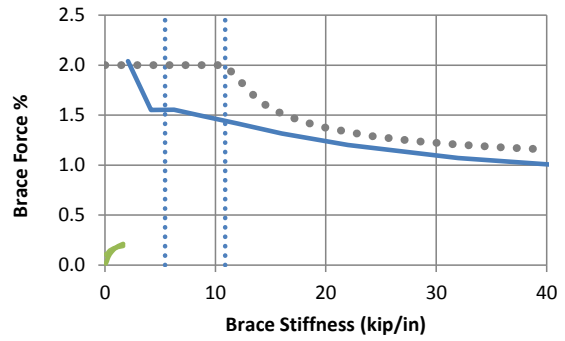
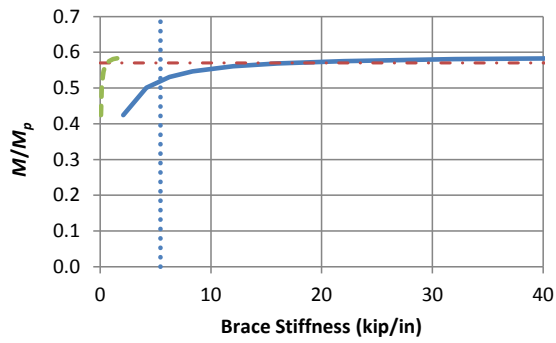
(d) E1303n ( $\beta_T/\beta_r = 2.13$ )

- Test Simulation Results, Torsional Bracing
- - - Test Simulation Results, Shear Panel Bracing
- · - Rigid Bracing Strength
- · · · 1 and 2x AISC Ideal Torsional Bracing Stiffness ( $\beta_{IF,AISC}$  and  $2\beta_{IF,AISC}$ )
- · · · Refined Estimate of Required Torsional Bracing Strength (not considering combined torsional and lateral bracing)

Fig. A.14 (continued). Case E130\*n knuckle and brace force vs. brace stiffness curves (Combined shear panel lateral and nodal torsional bracing,  $L_b = 5$  ft,  $n = 3$ , negative bending)



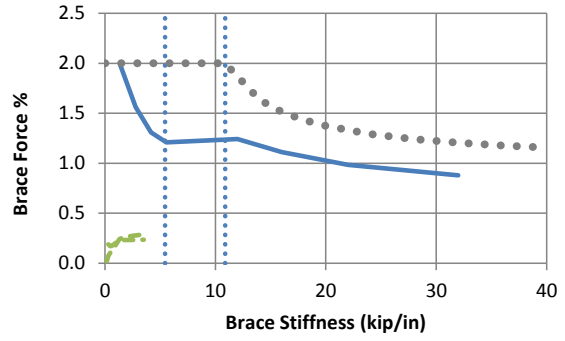
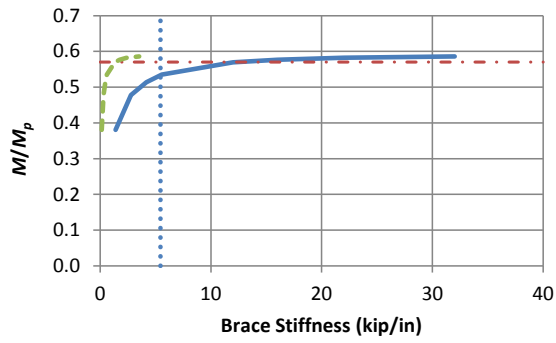
(a) E2200n ( $\beta_T/\beta_r = 63.6$ )



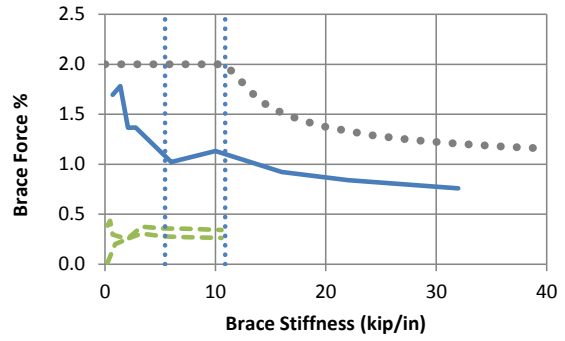
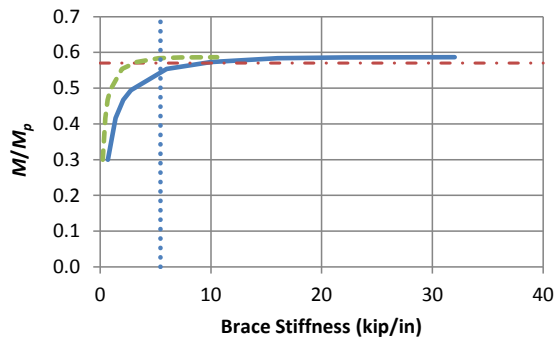
(b) E2201n ( $\beta_T/\beta_r = 27.2$ )

- Test Simulation Results, Torsional Bracing
- - - Test Simulation Results, Shear Panel Bracing
- . - . Rigid Bracing Strength
- · · · 1 and 2x AISC Ideal Torsional Bracing Stiffness ( $\beta_{IF,AISC}$  and  $2\beta_{IF,AISC}$ )
- · · · Refined Estimate of Required Torsional Bracing Strength (not considering combined torsional and lateral bracing)

Fig. A.15. Case E220\*n knuckle and brace force vs. brace stiffness curves (Combined shear panel lateral and nodal torsional bracing,  $L_b = 10$  ft,  $n = 2$ , negative bending)



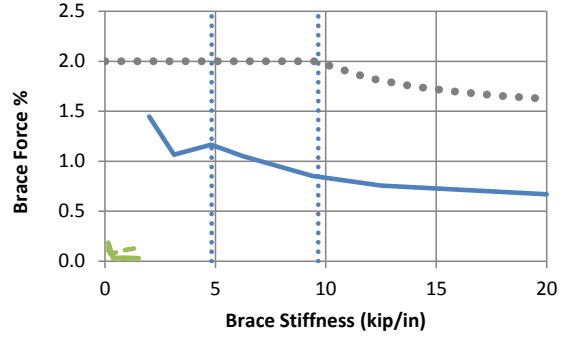
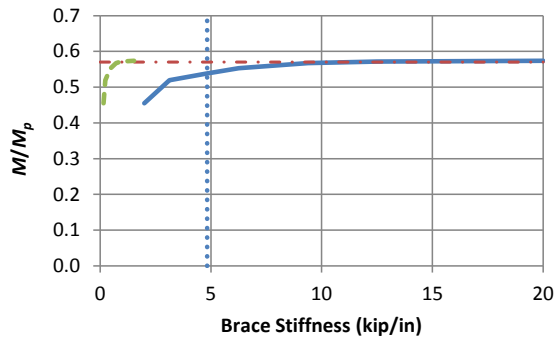
(c) E2202n ( $\beta_T/\beta_r = 9.08$ )



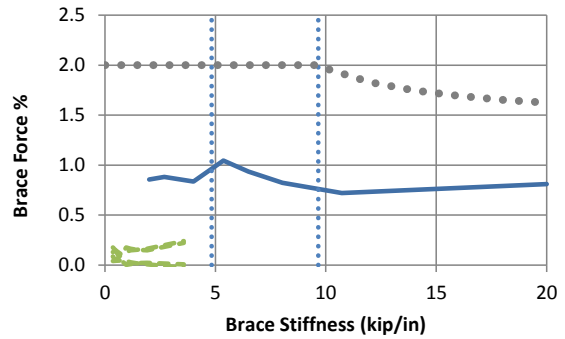
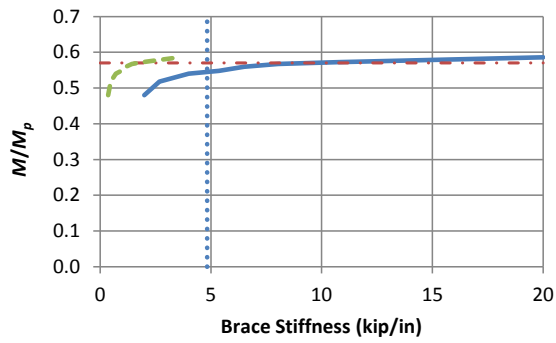
(d) E2203n ( $\beta_T/\beta_r = 3.03$ )

- Test Simulation Results, Torsional Bracing
- - - Test Simulation Results, Shear Panel Bracing
- · - Rigid Bracing Strength
- · · · 1 and 2x AISC Ideal Torsional Bracing Stiffness ( $\beta_{IF,AISC}$  and  $2\beta_{IF,AISC}$ )
- · · · Refined Estimate of Required Torsional Bracing Strength  
(not considering combined torsional and lateral bracing)

Fig. A.15 (continued). Case E220\*n knuckle and brace force vs. brace stiffness curves (Combined shear panel lateral and nodal torsional bracing,  $L_b = 10$  ft,  $n = 2$ , negative bending)



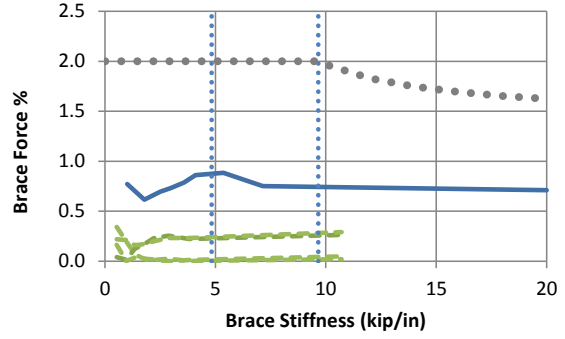
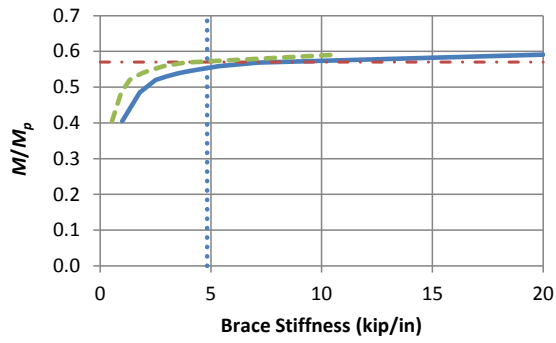
(a) E2300n ( $\beta_T/\beta_r = 13.1$ )



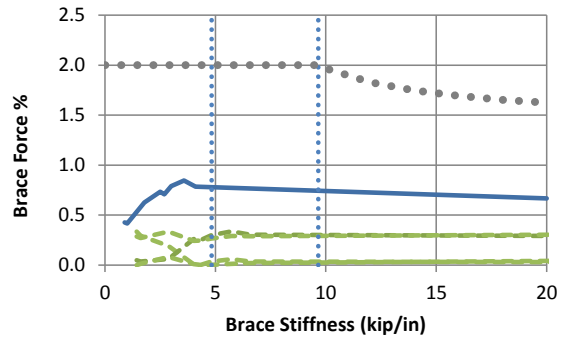
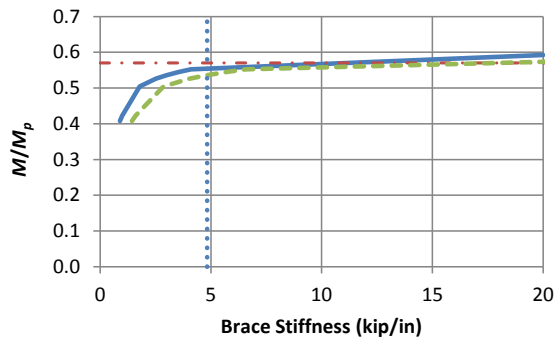
(b) E2301n ( $\beta_T/\beta_r = 5.61$ )

- Test Simulation Results, Torsional Bracing
- - - Test Simulation Results, Shear Panel Bracing
- . - . Rigid Bracing Strength
- · · · 1 and 2x AISC Ideal Torsional Bracing Stiffness ( $\beta_{IF,AISC}$  and  $2\beta_{IF,AISC}$ )
- · · · Refined Estimate of Required Torsional Bracing Strength  
(not considering combined torsional and lateral bracing)

Fig. A.16. Case E230\*n knuckle and brace force vs. brace stiffness curves  
(Combined shear panel lateral and nodal torsional bracing,  $L_b = 10$  ft,  $n = 3$ , negative bending)



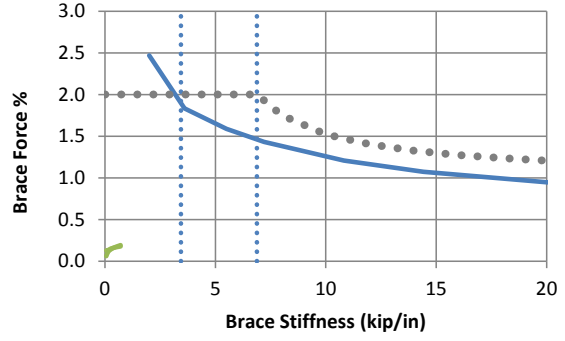
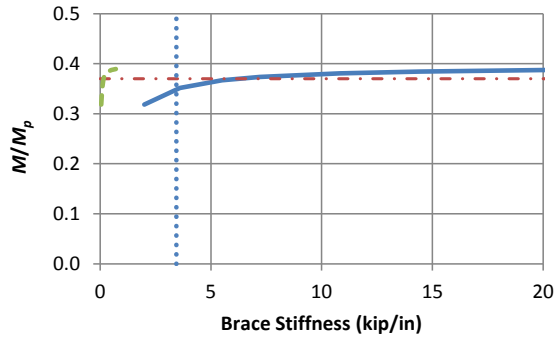
(c) E2302n ( $\beta_T/\beta_r = 1.87$ )



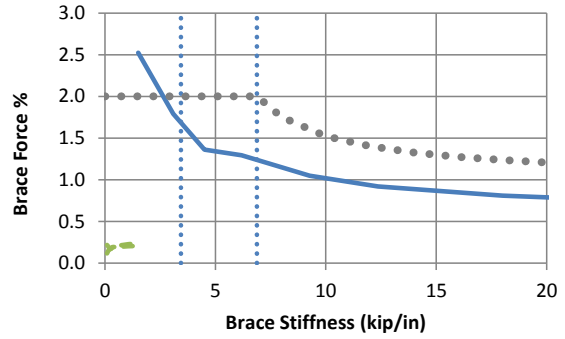
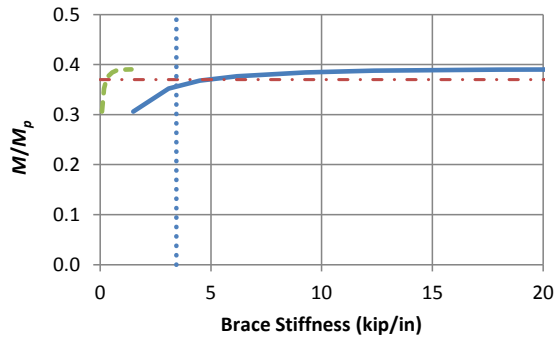
(d) E2303n ( $\beta_T/\beta_r = 0.62$ )

- Test Simulation Results, Torsional Bracing
- - - Test Simulation Results, Shear Panel Bracing
- · - Rigid Bracing Strength
- · · · 1 and 2x AISC Ideal Torsional Bracing Stiffness ( $\beta_{IF,AISC}$  and  $2\beta_{IF,AISC}$ )
- · · · Refined Estimate of Required Torsional Bracing Strength (not considering combined torsional and lateral bracing)

Fig. A.16 (continued). Case E230\*n knuckle and brace force vs. brace stiffness curves (Combined shear panel lateral and nodal torsional bracing,  $L_b = 10$  ft,  $n = 3$ , negative bending)



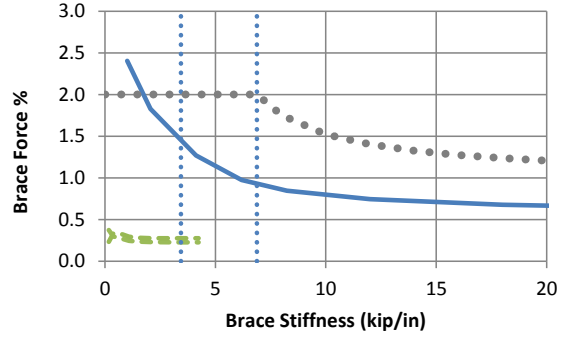
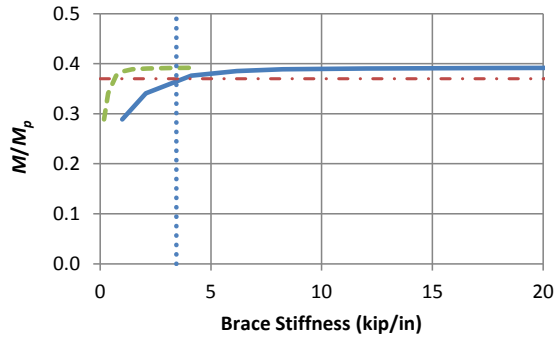
(a) E3200n ( $\beta_T/\beta_r = 39.7$ )



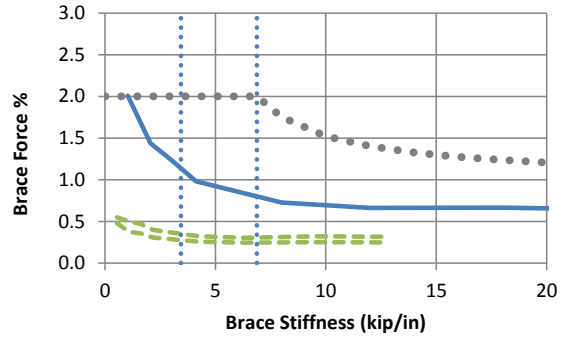
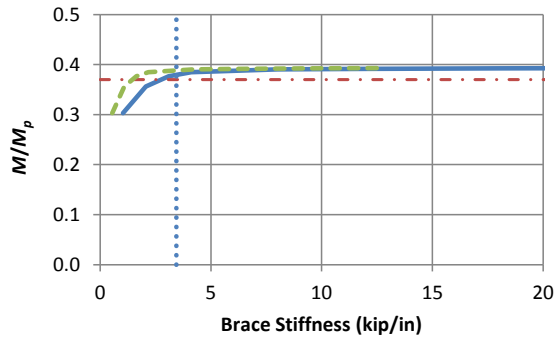
(b) E3201n ( $\beta_T/\beta_r = 17.0$ )

- Test Simulation Results, Torsional Bracing
- - - Test Simulation Results, Shear Panel Bracing
- . - Rigid Bracing Strength
- · · · 1 and 2x AISC Ideal Torsional Bracing Stiffness ( $\beta_{IF,AISC}$  and  $2\beta_{IF,AISC}$ )
- · · · Refined Estimate of Required Torsional Bracing Strength (not considering combined torsional and lateral bracing)

Fig. A.17. Case E320\*n knuckle and brace force vs. brace stiffness curves (Combined shear panel lateral and nodal torsional bracing,  $L_b = 15$  ft,  $n = 2$ , negative bending)



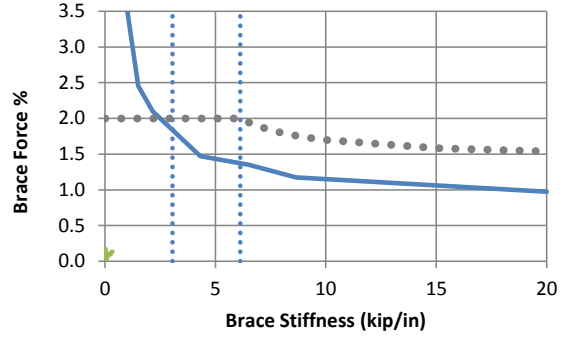
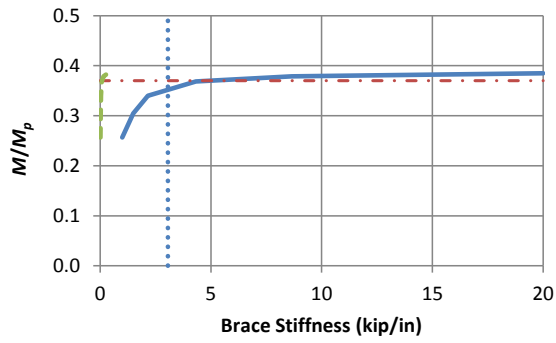
(c) E3202n ( $\beta_T/\beta_r = 5.67$ )



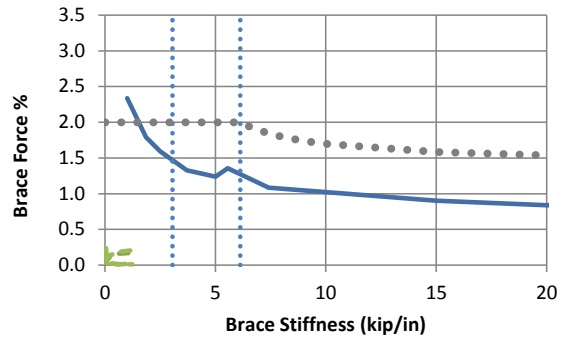
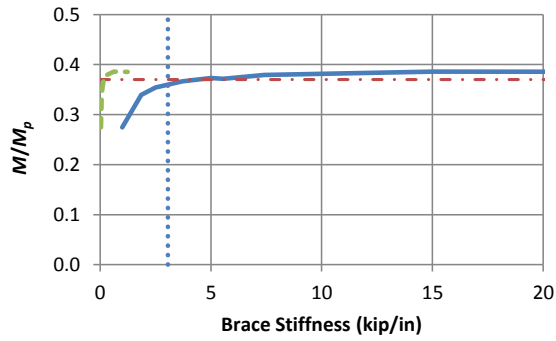
(d) E3203n ( $\beta_T/\beta_r = 1.89$ )

- Test Simulation Results, Torsional Bracing
- - - Test Simulation Results, Shear Panel Bracing
- · - Rigid Bracing Strength
- · · 1 and 2x AISC Ideal Torsional Bracing Stiffness ( $\beta_{IF,AISC}$  and  $2\beta_{IF,AISC}$ )
- · · Refined Estimate of Required Torsional Bracing Strength (not considering combined torsional and lateral bracing)

Fig. A.17 (continued). Case E320\*n knuckle and brace force vs. brace stiffness curves (Combined shear panel lateral and nodal torsional bracing,  $L_b = 15$  ft,  $n = 2$ , negative bending)



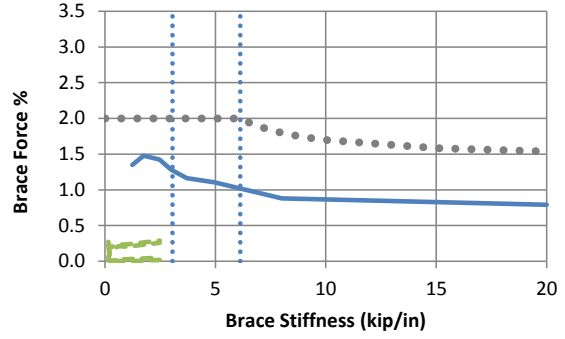
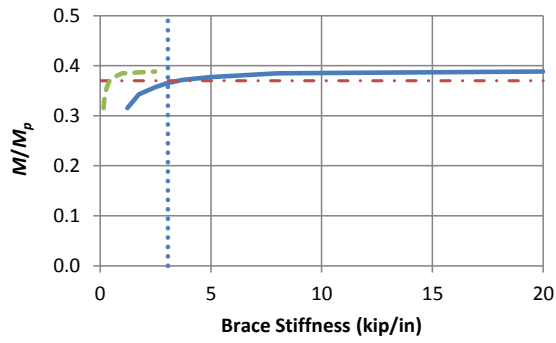
(a) E3300n ( $\beta_T/\beta_r = 56.5$ )



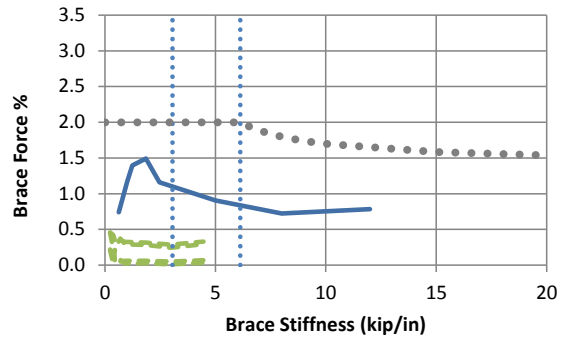
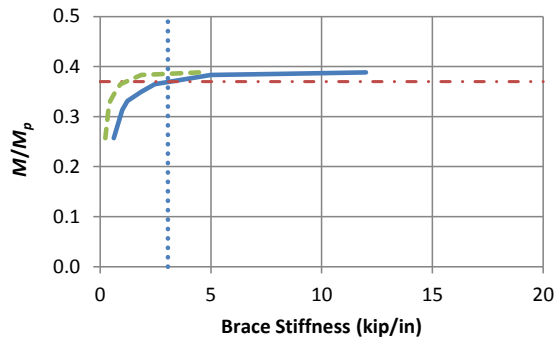
(b) E3301n ( $\beta_T/\beta_r = 24.2$ )

- Test Simulation Results, Torsional Bracing
- - - Test Simulation Results, Shear Panel Bracing
- . - Rigid Bracing Strength
- ..... 1 and 2x AISC Ideal Torsional Bracing Stiffness ( $\beta_{IF,AISC}$  and  $2\beta_{IF,AISC}$ )
- ..... Refined Estimate of Required Torsional Bracing Strength (not considering combined torsional and lateral bracing)

Fig. A.18. Case E330\*n knuckle and brace force vs. brace stiffness curves (Combined shear panel lateral and nodal torsional bracing,  $L_b = 15$  ft,  $n = 3$ , negative bending)



(c) E3302n ( $\beta_T/\beta_r = 8.07$ )

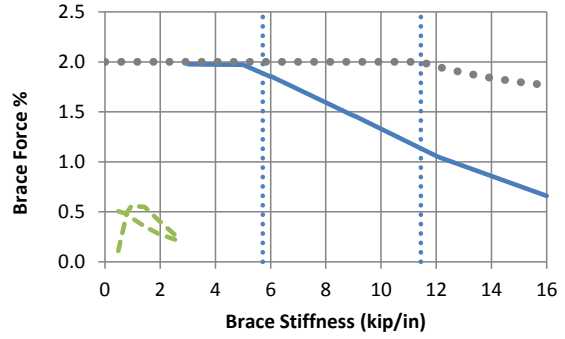
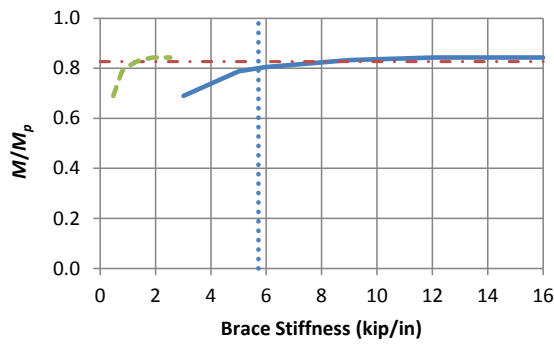


(d) E3303n ( $\beta_T/\beta_r = 2.69$ )

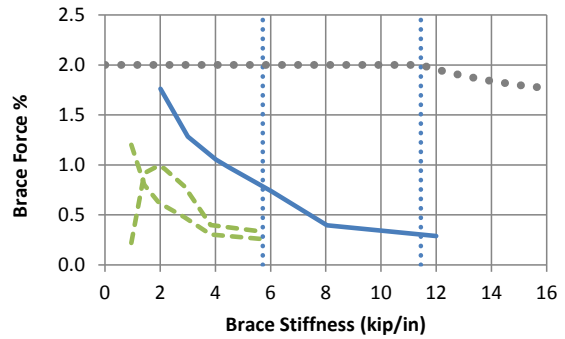
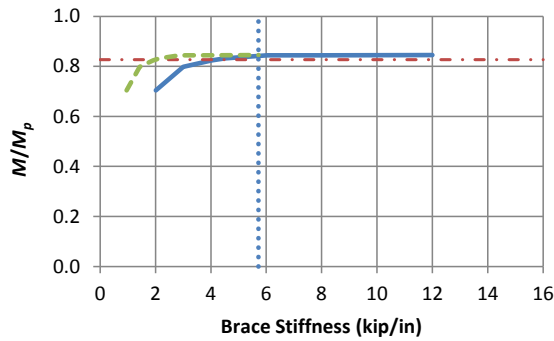
- Test Simulation Results, Torsional Bracing
- - - Test Simulation Results, Shear Panel Bracing
- · - Rigid Bracing Strength
- · · · 1 and 2x AISC Ideal Torsional Bracing Stiffness ( $\beta_{IF,AISC}$  and  $2\beta_{IF,AISC}$ )
- · · · Refined Estimate of Required Torsional Bracing Strength (not considering combined torsional and lateral bracing)

Fig. A.18 (continued). Case E330\*n knuckle and brace force vs. brace stiffness curves (Combined shear panel lateral and nodal torsional bracing,  $L_b = 15$  ft,  $n = 3$ , negative bending)

### A.4 Category Ep



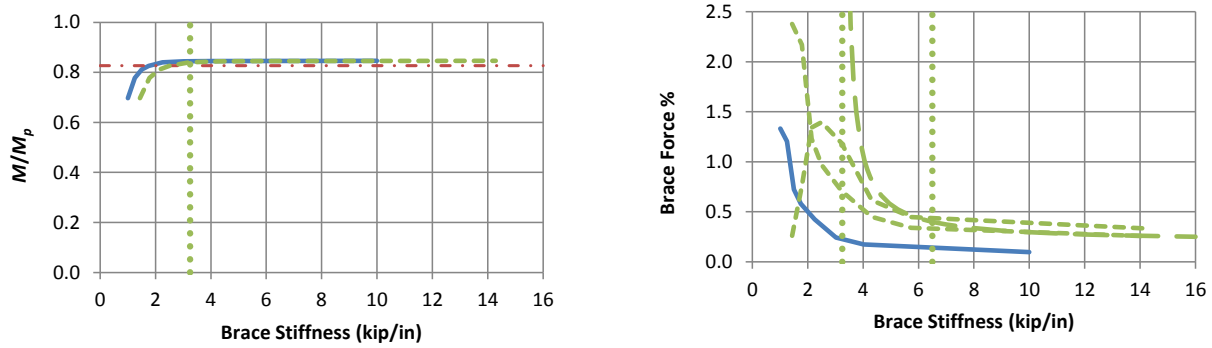
(a) E1200p ( $\beta_T/\beta_r = 6.31$ )



(b) E1201p ( $\beta_T/\beta_r = 2.10$ )

- Test Simulation Results, Torsional Bracing
- - - Test Simulation Results, Shear Panel Bracing
- · - Rigid Bracing Strength
- · · · 1 and 2x AISC Ideal Torsional Bracing Stiffness ( $\beta_{IF,AISC}$  and  $2\beta_{IF,AISC}$ )
- · · · Refined Estimate of Required Torsional Bracing Strength (not considering combined torsional and lateral bracing)
- · · · 1 and 2x AISC Ideal Shear Panel Bracing Stiffness ( $\beta_{IF,AISC}$  and  $2\beta_{IF,AISC}$ )
- · - Refined Estimate of Required Shear Panel Bracing Strength from AISC Commentary (not considering combined torsional and lateral bracing)

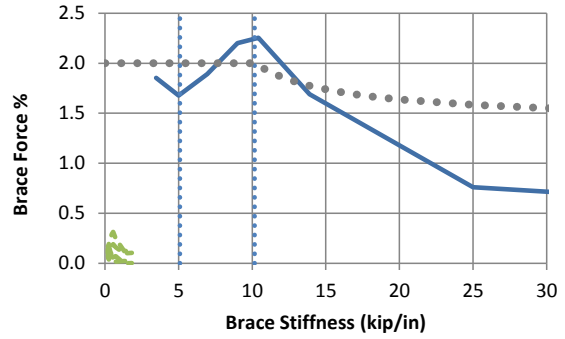
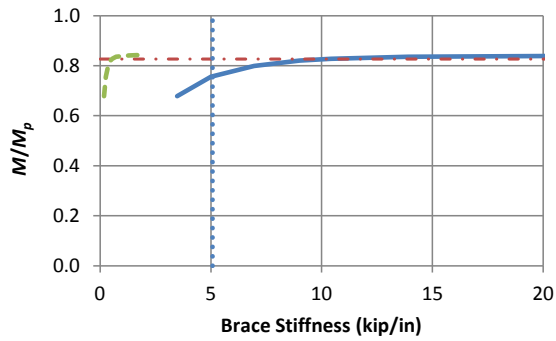
Fig. A.19. Case E120\*p knuckle and brace force vs. brace stiffness curves (Combined shear panel lateral and nodal torsional bracing,  $L_b = 5$  ft,  $n = 2$ , positive bending)



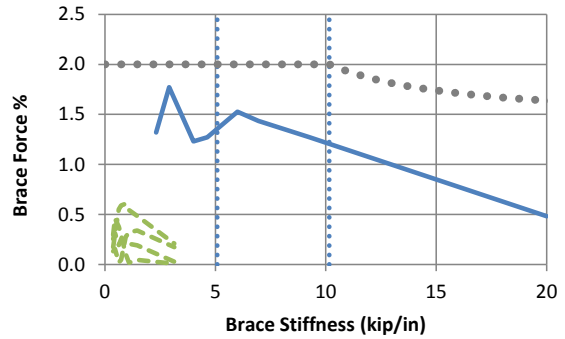
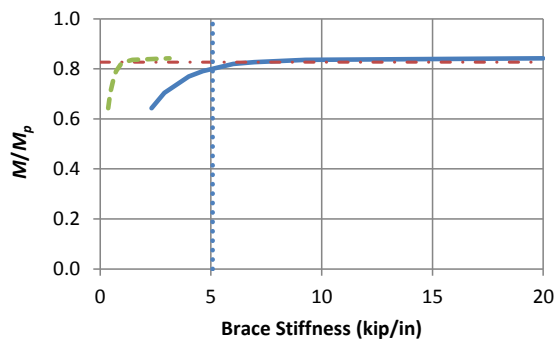
(c) E1202p ( $\beta_T/\beta_r = 0.70$ )

- Test Simulation Results, Torsional Bracing
- - - Test Simulation Results, Shear Panel Bracing
- · - Rigid Bracing Strength
- · · · 1 and 2x AISC Ideal Torsional Bracing Stiffness ( $\beta_{IF,AISC}$  and  $2\beta_{IF,AISC}$ )
- · · · Refined Estimate of Required Torsional Bracing Strength (not considering combined torsional and lateral bracing)
- · · · 1 and 2x AISC Ideal Shear Panel Bracing Stiffness ( $\beta_{IF,AISC}$  and  $2\beta_{IF,AISC}$ )
- · - Refined Estimate of Required Shear Panel Bracing Strength from AISC Commentary (not considering combined torsional and lateral bracing)

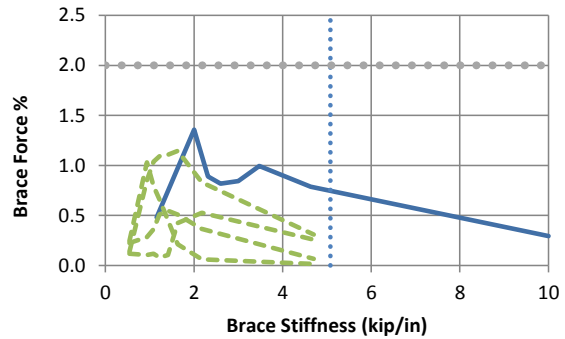
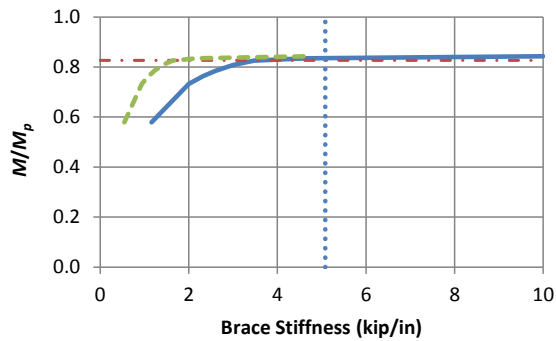
Fig. A.19(continued). Case E120\* p knuckle and brace force vs. brace stiffness curves (Combined shear panel lateral and nodal torsional bracing,  $L_b = 5$  ft,  $n = 2$ , positive bending)



(a) E1300p ( $\beta_T/\beta_r = 19.2$ )



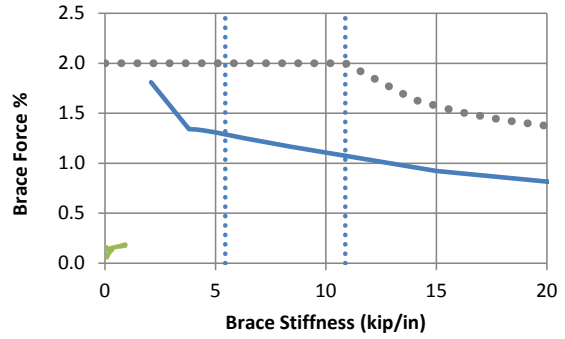
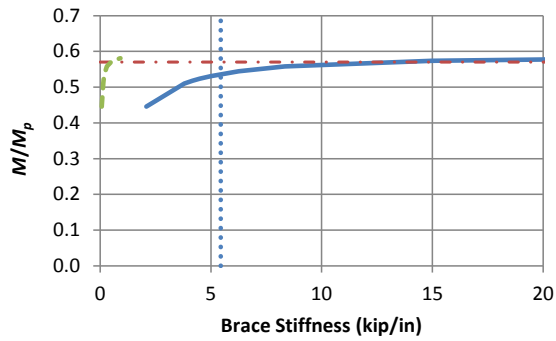
(b) E1301p ( $\beta_T/\beta_r = 6.38$ )



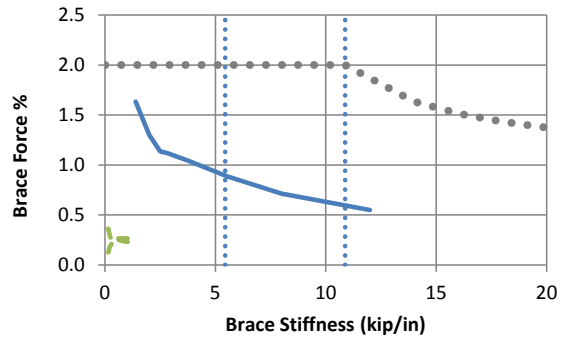
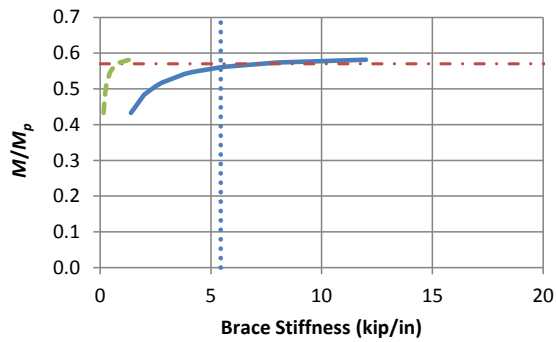
(c) E1302p ( $\beta_T/\beta_r = 2.13$ )

- Test Simulation Results, Torsional Bracing
- - - Test Simulation Results, Shear Panel Bracing
- - - Rigid Bracing Strength
- · · · 1 and 2x AISC Ideal Torsional Bracing Stiffness ( $\beta_{IF,AISC}$  and  $2\beta_{IF,AISC}$ )
- · · · Refined Estimate of Required Torsional Bracing Strength  
(not considering combined torsional and lateral bracing)

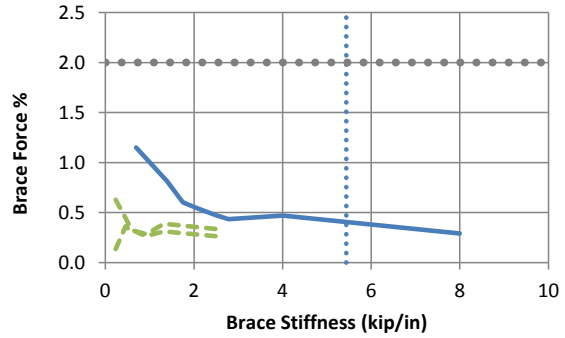
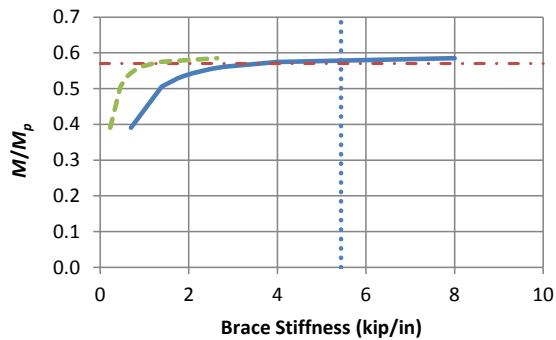
Fig. A.20. Case E130\*p knuckle and brace force vs. brace stiffness curves  
(Combined shear panel lateral and nodal torsional bracing,  $L_b = 5$  ft,  $n = 2$ , positive bending)



(a) E2200p ( $\beta_T/\beta_r = 27.2$ )



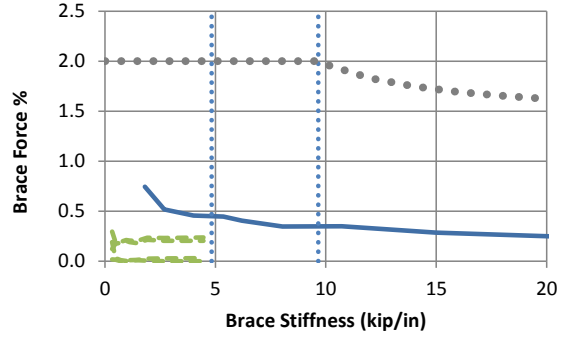
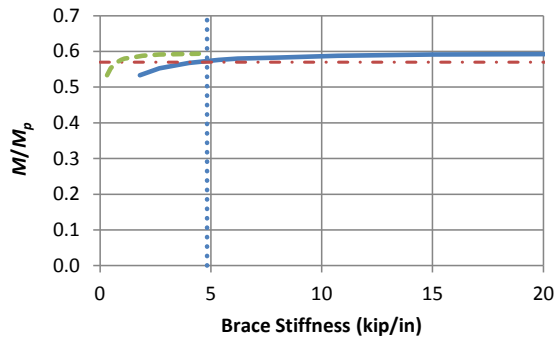
(b) E2201p ( $\beta_T/\beta_r = 9.08$ )



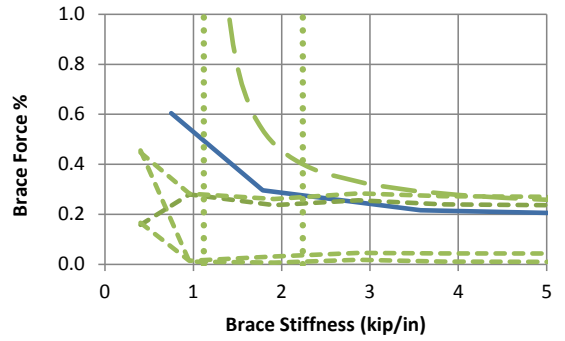
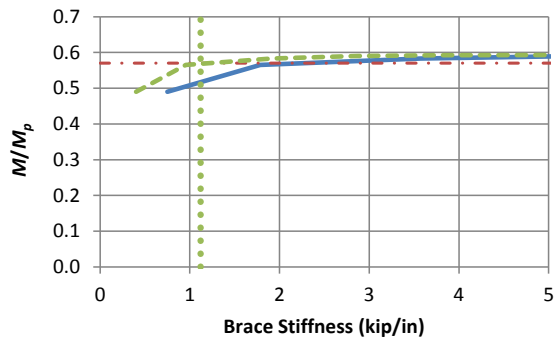
(c) E2202p ( $\beta_T/\beta_r = 2.13$ )

- Test Simulation Results, Torsional Brace
- - - Test Simulation Results, Nodal Lateral Brace
- . - . Rigid Bracing Strength
- · · · 1 and 2x AISC Ideal Torsional Bracing Stiffness ( $\beta_{iF,AISC}$  and  $2\beta_{iF,AISC}$ )
- · · · Refined Estimate of Required Torsional Bracing Strength (not considering combined torsional and lateral bracing)

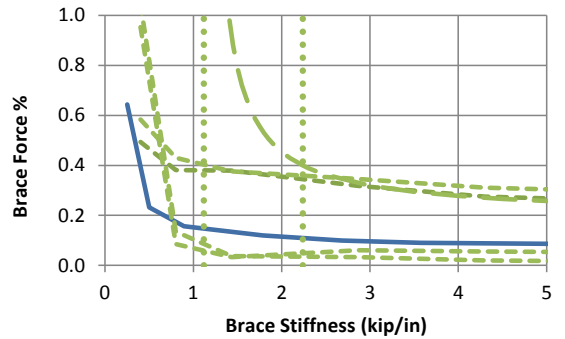
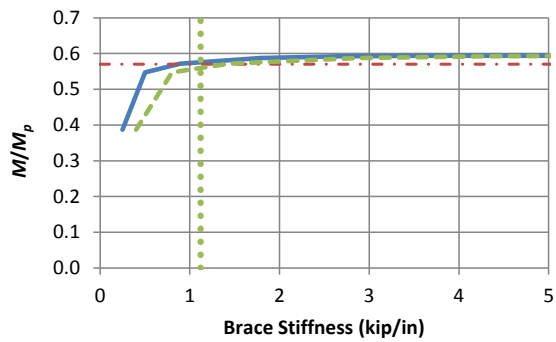
Fig. A.21. Case E220\*p knuckle and brace force vs. brace stiffness curves (Combined shear panel lateral and nodal torsional bracing,  $L_b = 10$  ft,  $n = 2$ , positive bending)



(a) E2300p ( $\beta_T/\beta_r = 5.61$ )



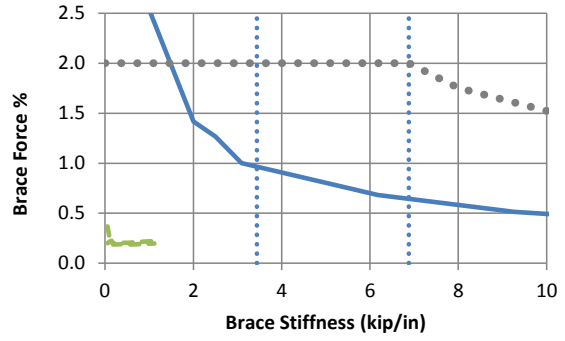
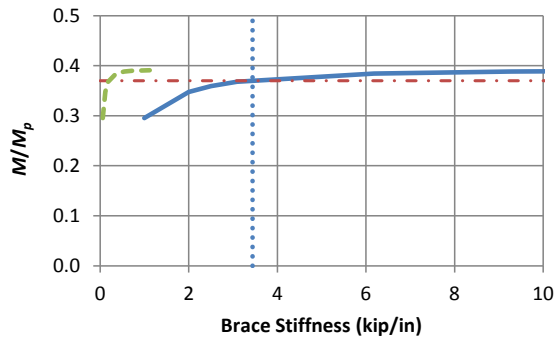
(b) E2301p ( $\beta_T/\beta_r = 1.87$ )



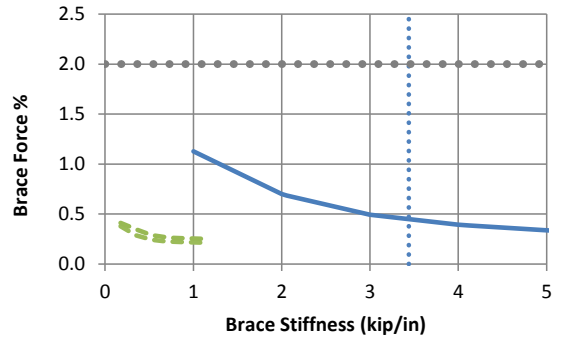
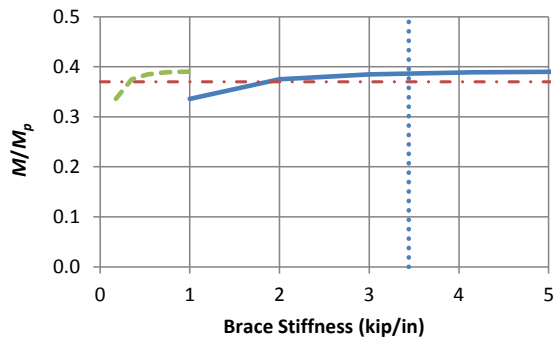
(c) E2302p ( $\beta_T/\beta_r = 0.62$ )

- Test Simulation Results, Torsional Bracing
- - - Test Simulation Results, Shear Panel Bracing
- · - Rigid Bracing Strength
- · · 1 and 2x AISC Ideal Torsional Bracing Stiffness ( $\beta_{IF,AISC}$  and  $2\beta_{IF,AISC}$ )
- · · Refined Estimate of Required Torsional Bracing Strength (not considering combined torsional and lateral bracing)
- · · 1 and 2x AISC Ideal Shear Panel Bracing Stiffness ( $\beta_{IF,AISC}$  and  $2\beta_{IF,AISC}$ )
- · - Refined Estimate of Required Shear Panel Bracing Strength from AISC Commentary (not considering combined torsional and lateral bracing)

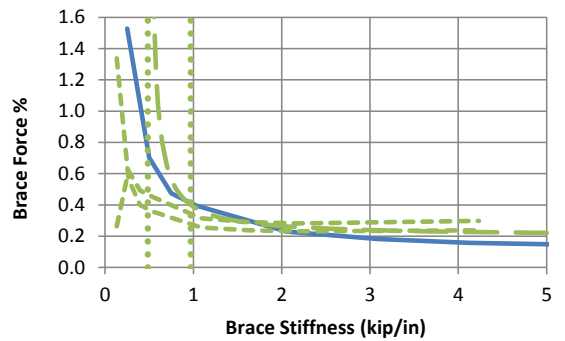
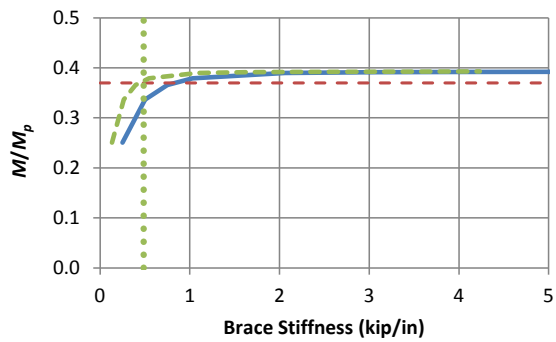
Fig. A.22. Case E230\*p knuckle and brace force vs. brace stiffness curves (Combined shear panel lateral and nodal torsional bracing,  $L_b = 10$  ft,  $n = 3$ , positive bending)



(a) E3200p ( $\beta_T/\beta_r = 17.0$ )



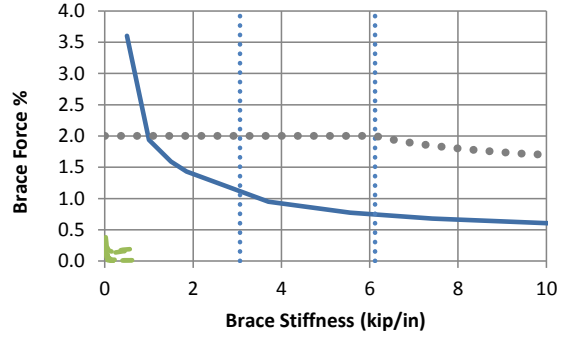
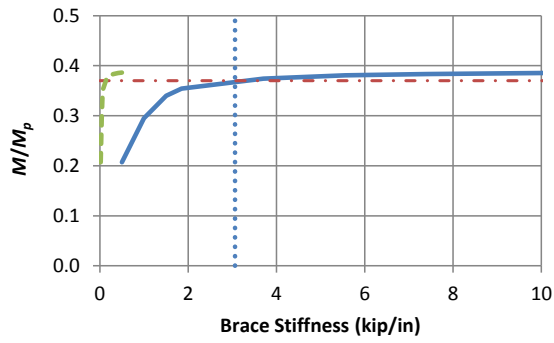
(b) E3201p ( $\beta_T/\beta_r = 5.67$ )



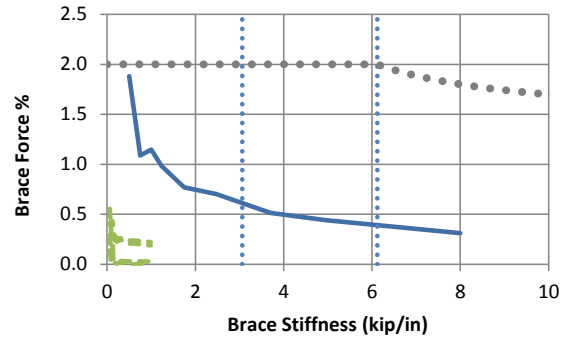
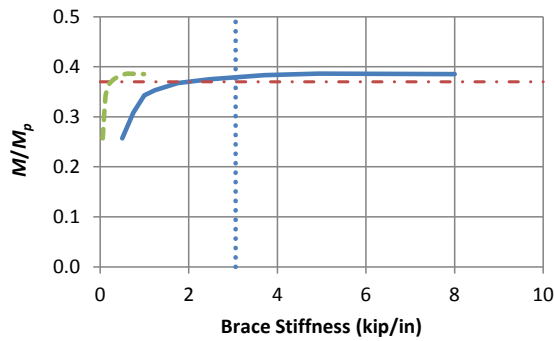
(c) E3202p ( $\beta_T/\beta_r = 1.89$ )

- Test Simulation Results, Torsional Bracing
- - - Test Simulation Results, Shear Panel Bracing
- · - Rigid Bracing Strength
- · · 1 and 2x AISC Ideal Torsional Bracing Stiffness ( $\beta_{IF,AISC}$  and  $2\beta_{IF,AISC}$ )
- · · Refined Estimate of Required Torsional Bracing Strength (not considering combined torsional and lateral bracing)
- · · 1 and 2x AISC Ideal Shear Panel Bracing Stiffness ( $\beta_{IF,AISC}$  and  $2\beta_{IF,AISC}$ )
- - - Refined Estimate of Required Shear Panel Bracing Strength from AISC Commentary (not considering combined torsional and lateral bracing)

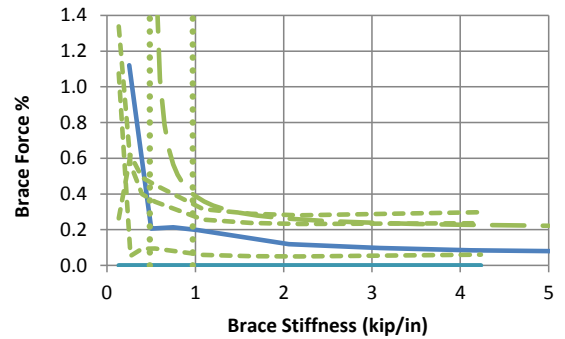
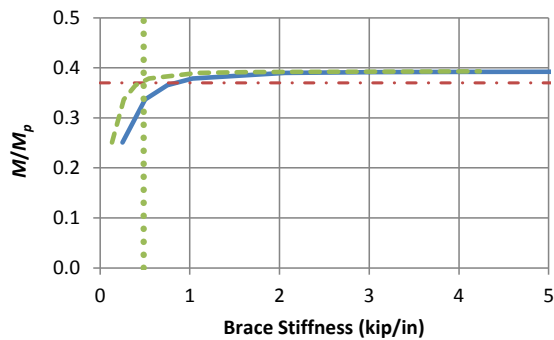
Fig. A.23. Case E320\*p knuckle and brace force vs. brace stiffness curves (Combined shear panel lateral and nodal torsional bracing,  $L_b = 15$  ft,  $n = 2$ , positive bending)



(a) E3300p ( $\beta_T/\beta_r = 24.2$ )



(b) E3301p ( $\beta_T/\beta_r = 8.07$ )

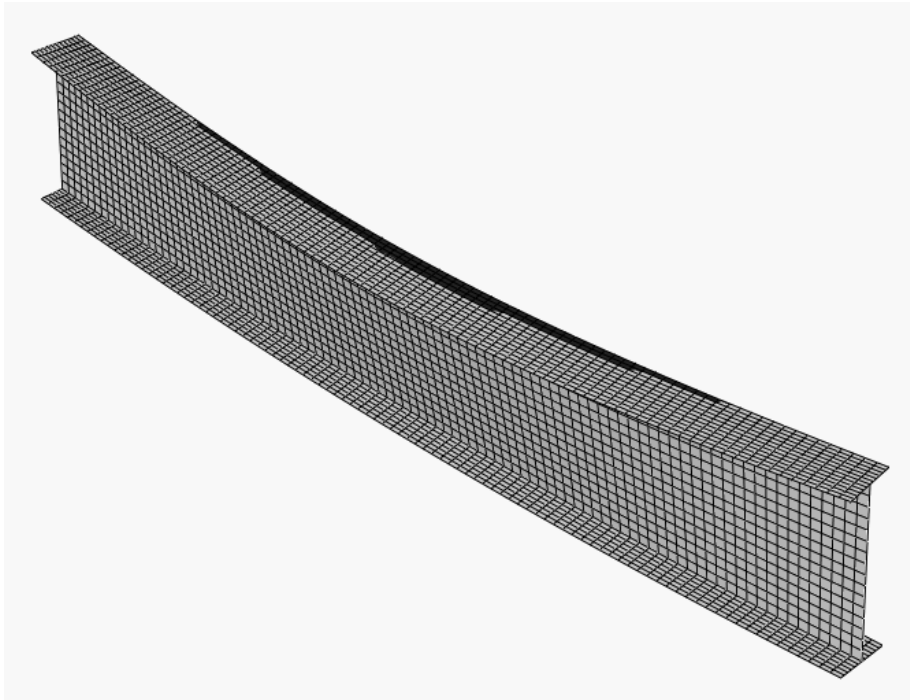


(c) E3302p ( $\beta_T/\beta_r = 1.89$ )

- Test Simulation Results, Torsional Bracing
- - - Test Simulation Results, Shear Panel Bracing
- · - Rigid Bracing Strength
- · · 1 and 2x AISC Ideal Torsional Bracing Stiffness ( $\beta_{IF,AISC}$  and  $2\beta_{IF,AISC}$ )
- · · Refined Estimate of Required Torsional Bracing Strength (not considering combined torsional and lateral bracing)
- · · 1 and 2x AISC Ideal Shear Panel Bracing Stiffness ( $\beta_{IF,AISC}$  and  $2\beta_{IF,AISC}$ )
- - - Refined Estimate of Required Shear Panel Bracing Strength from AISC Commentary (not considering combined torsional and lateral bracing)

Fig. A.24. Case E330\*p knuckle and brace force vs. brace stiffness curves (Combined shear panel lateral and nodal torsional bracing,  $L_b = 15$  ft,  $n = 3$ , positive bending)

### A.5 Category A Representative Deflected Geometry at Member Bending Limit Load



(a) A110 (1 kip/in) nodal lateral bracing scaled x10

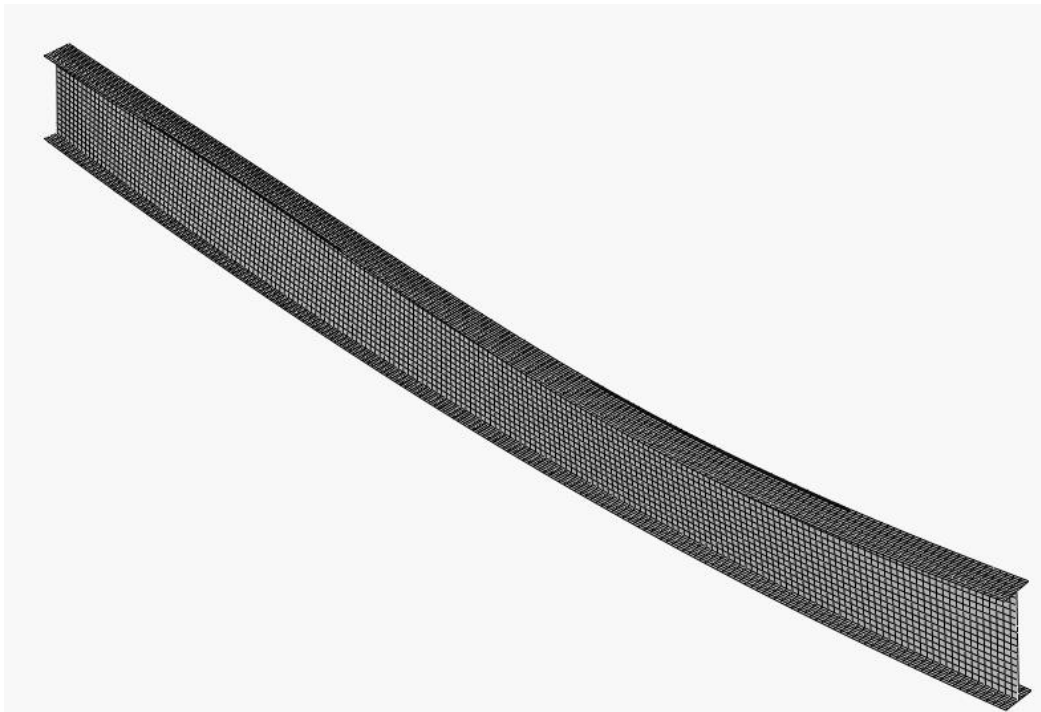


(b) A110 fully rigid nodal lateral bracing scaled x10

Fig. A.25. Case A110 deflected geometry at limit load

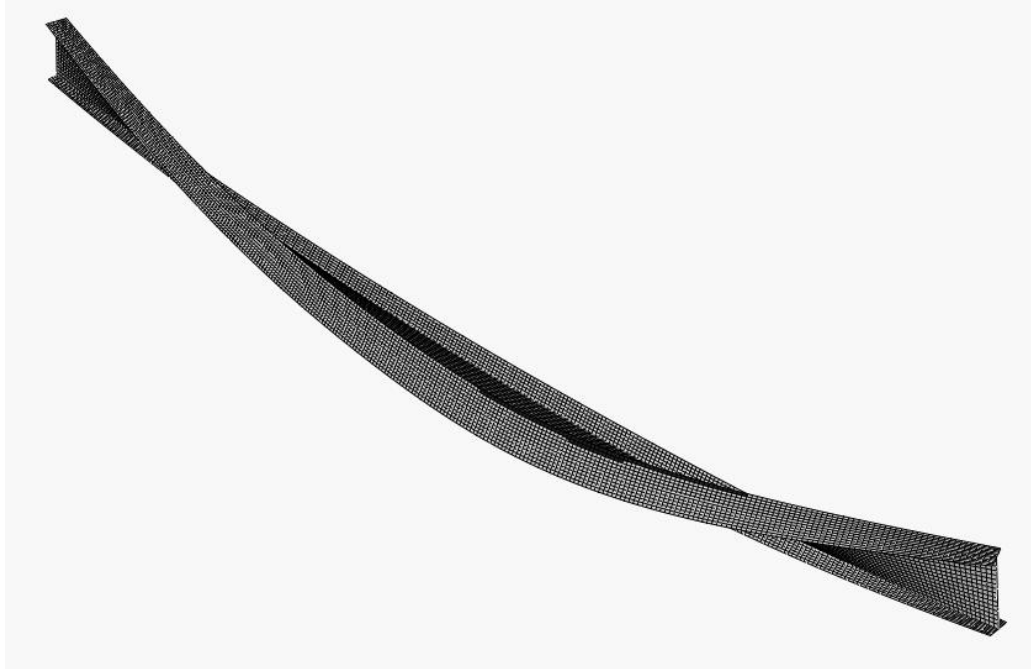


(a) A210 (3.2 kip/in) nodal lateral bracing scaled x10



(b) A210 fully rigid nodal lateral bracing scaled x10

Fig. A.26. Case A210 deflected geometry at limit load

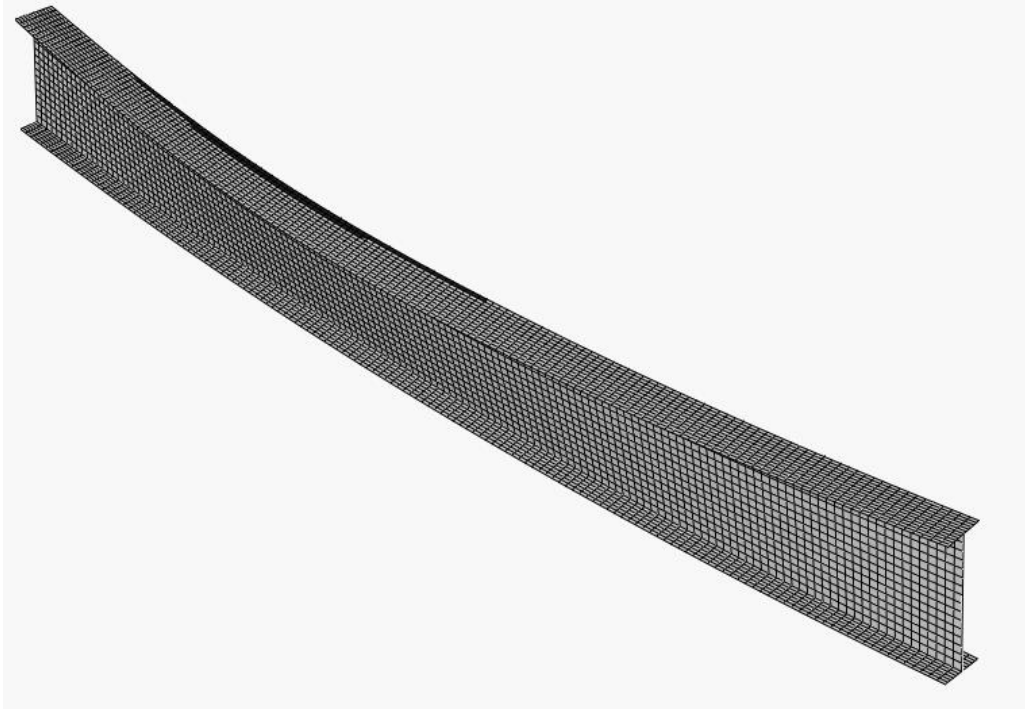


(a) A310 (0.75 kip/in) nodal lateral bracing scaled x10



(b) A310 fully rigid nodal lateral bracing scaled x10

Fig. A.27. Case A310 deflected geometry at limit load



(a) A120 (1.25 kip/in) nodal lateral bracing scaled x10



(b) A120 fully rigid nodal lateral bracing scaled x10

Fig. A.28. Case A120 deflected geometry at limit load

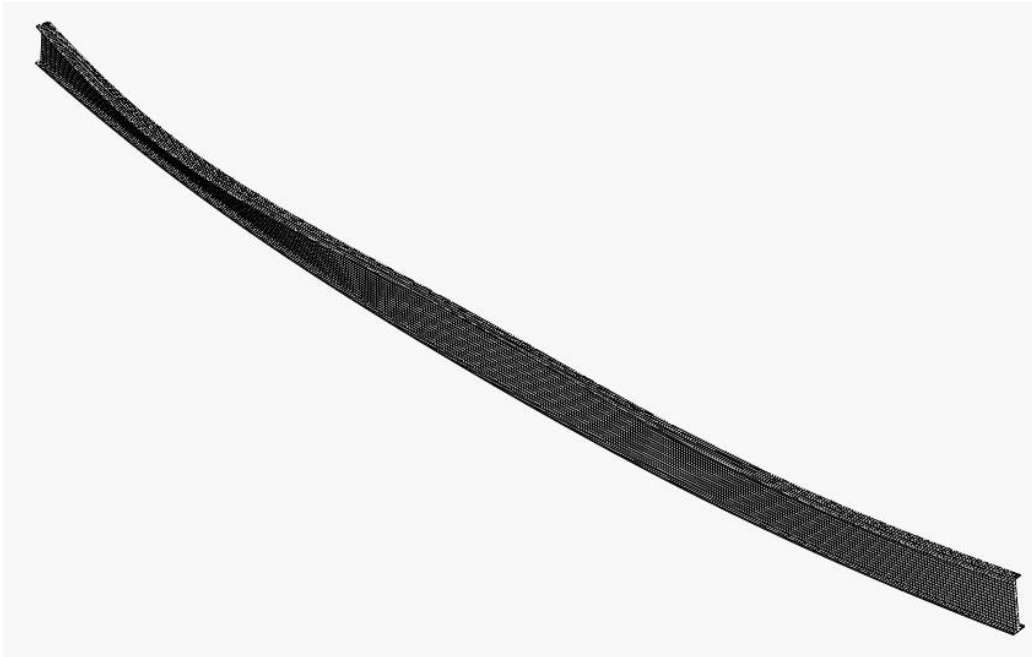


(a) A220 (2.2 kip/in) nodal lateral bracing scaled x10

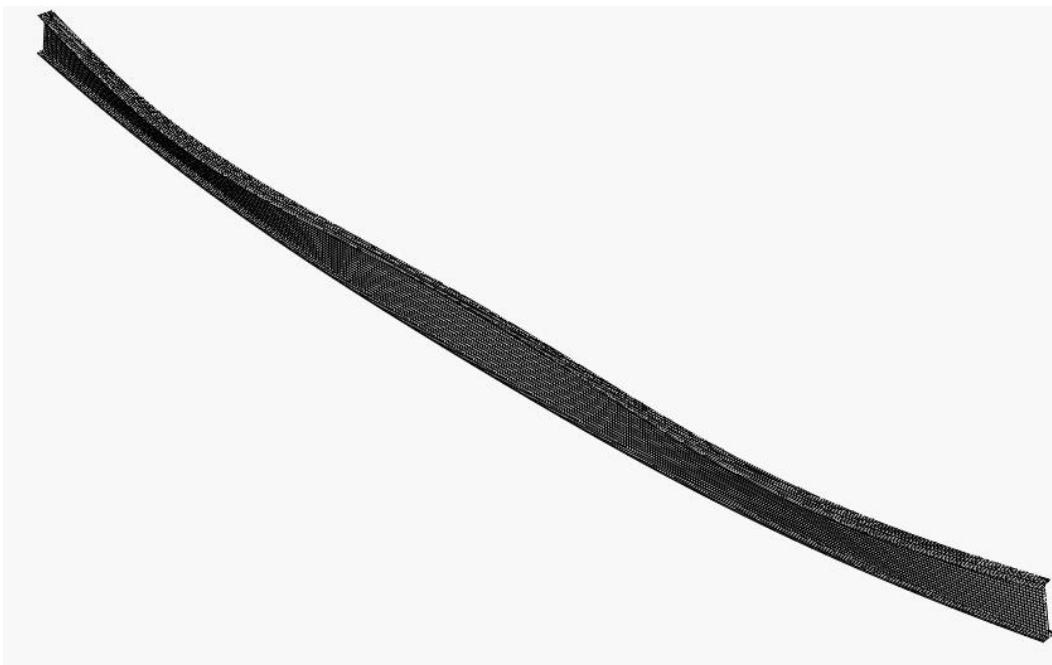


(b) A220 fully rigid nodal lateral bracing scaled x10

Fig. A.29. Case A220 deflected geometry at limit load



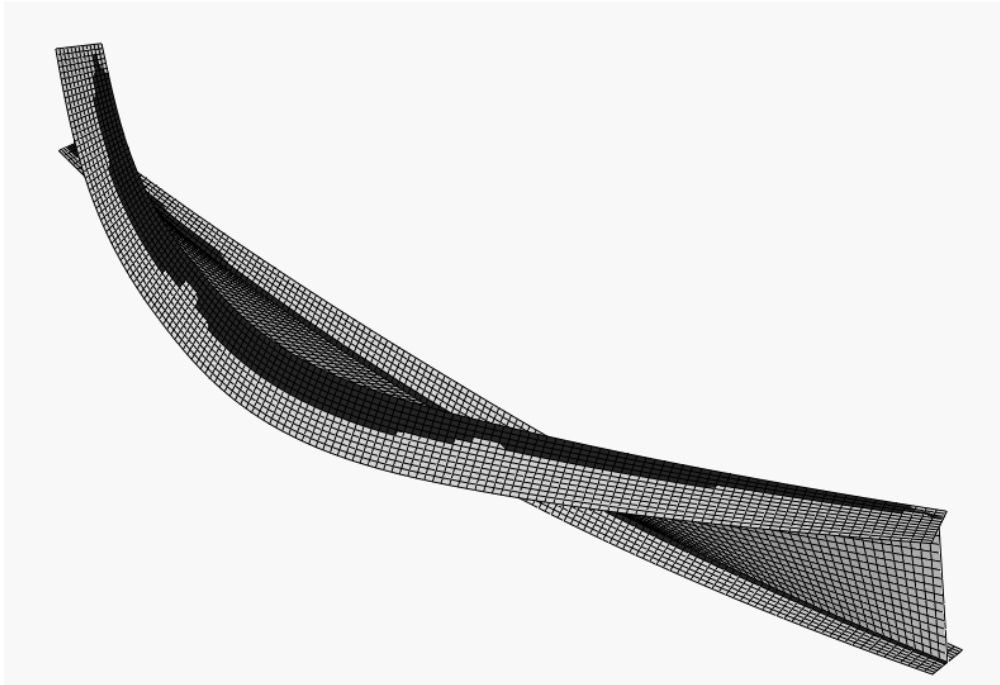
(a) A320 (2.76 kip/in) nodal lateral bracing scaled x10



(b) A320 fully rigid nodal lateral bracing scaled x10

Fig. A.30. Case A320 deflected geometry at limit load

## A.6 Category B Representative Deflected Geometry at Member Bending Limit Load



(a) B120 (2.75 kip/in) relative lateral bracing scaled x10



(b) B120 fully rigid relative lateral bracing scaled x10

Fig. A.31. Case B120 deflected geometry at limit load



(a) B220 (1.25 kip/in) relative lateral bracing scaled x10



(b) B220 fully rigid relative lateral bracing scaled x10

Fig. A.32. Case B220 deflected geometry at limit load



(a) B320 (0.9 kip/in) relative lateral bracing scaled x10



(b) B320 fully rigid relative lateral bracing scaled x10

Fig. A.33. Case B320 deflected geometry at limit load



(a) B130 (2.25 kip/in) relative lateral bracing scaled x10

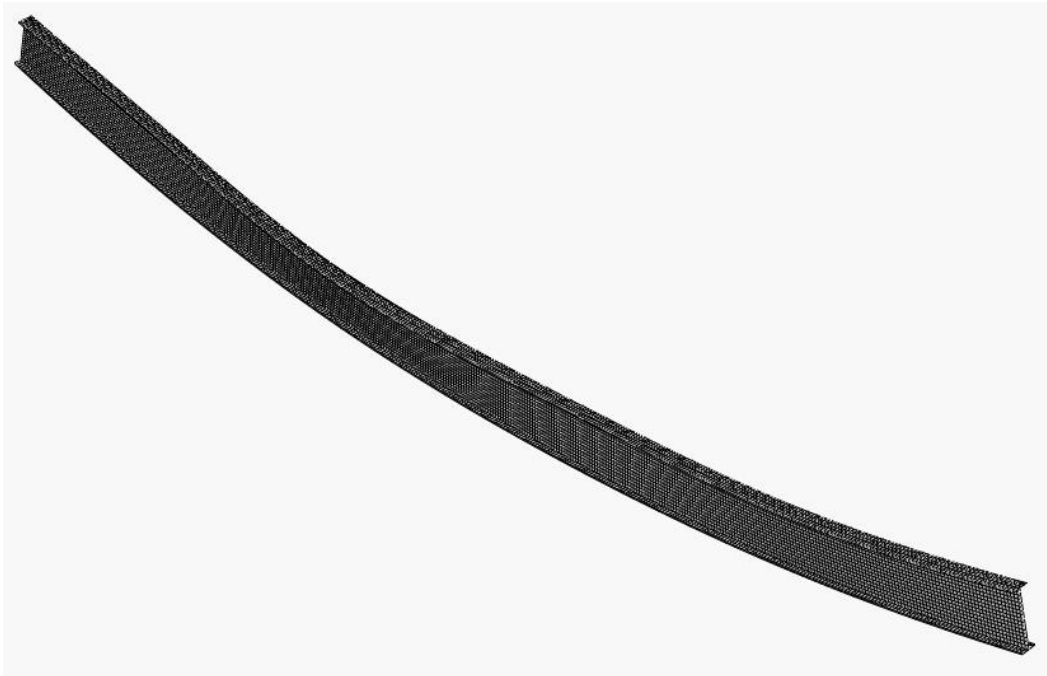


(b) B130 fully rigid relative lateral bracing scaled x10

Fig. A.34. Case B130 deflected geometry at limit load



(a) B230 (1.1 kip/in) relative lateral bracing scaled x10

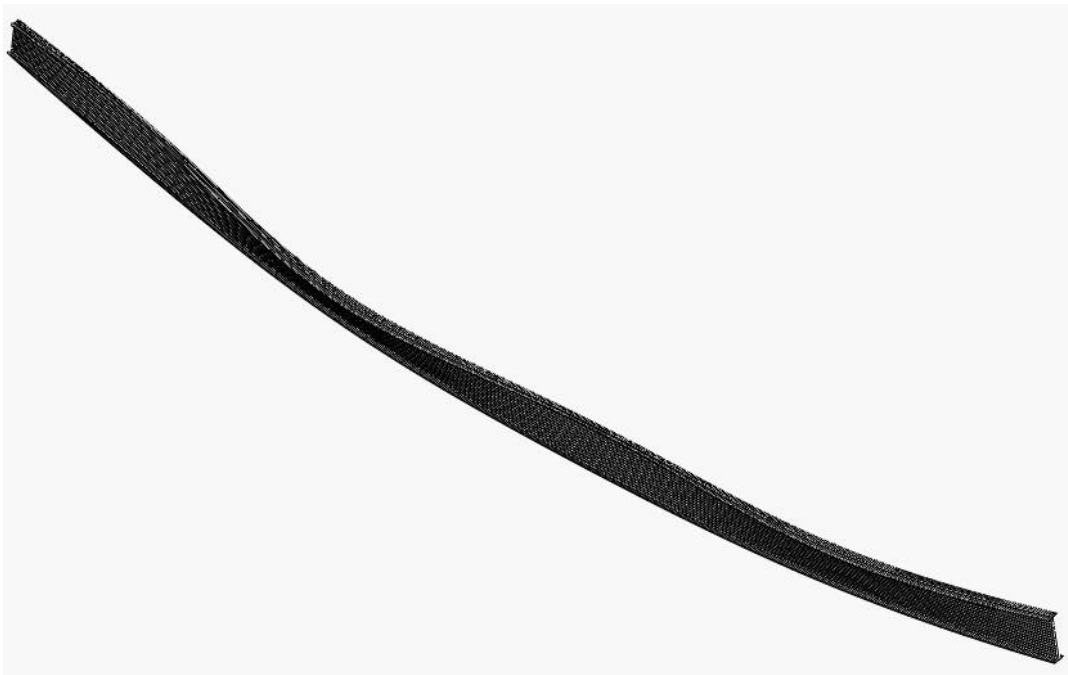


(b) B230 fully rigid relative lateral bracing scaled x10

Fig. A.35. Case B230 deflected geometry at limit load



(a) B330 (0.7 kip/in) relative lateral bracing scaled x10



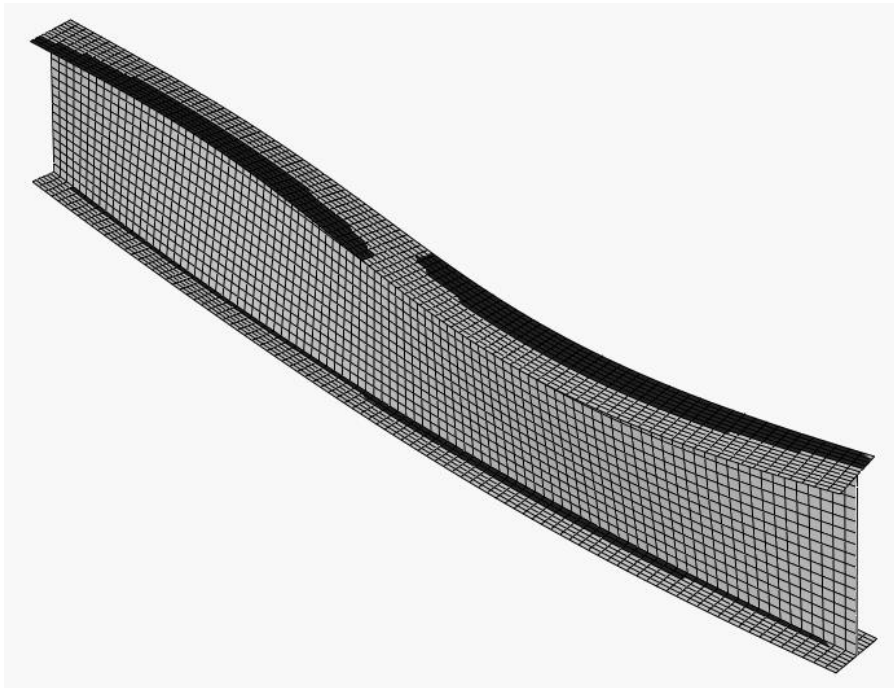
(b) B330 fully rigid relative lateral bracing scaled x10

Fig. A.36. Case B330 deflected geometry at limit load

**A.7 Category C Representative Deflected Geometry at Member Bending Limit Load**

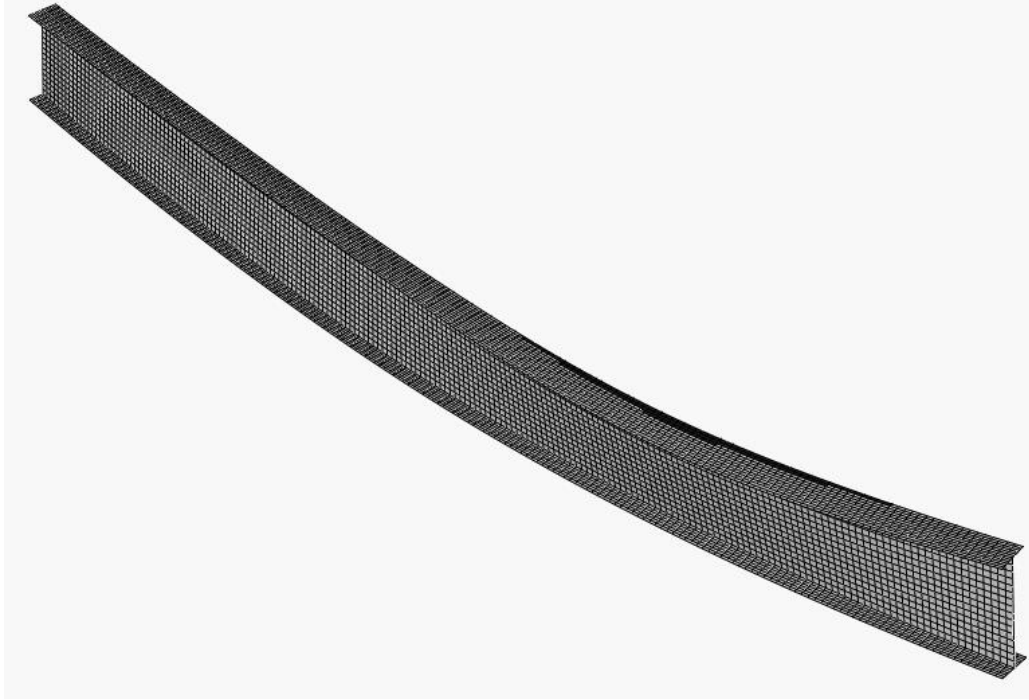


(a) C110 (25 kip/in) torsional bracing scaled x10



(b) C110 fully rigid torsional bracing scaled x10

Fig. A.37. Case C110 deflected geometry at limit load



(a) C210 (24.7 kip/in) torsional bracing scaled x10

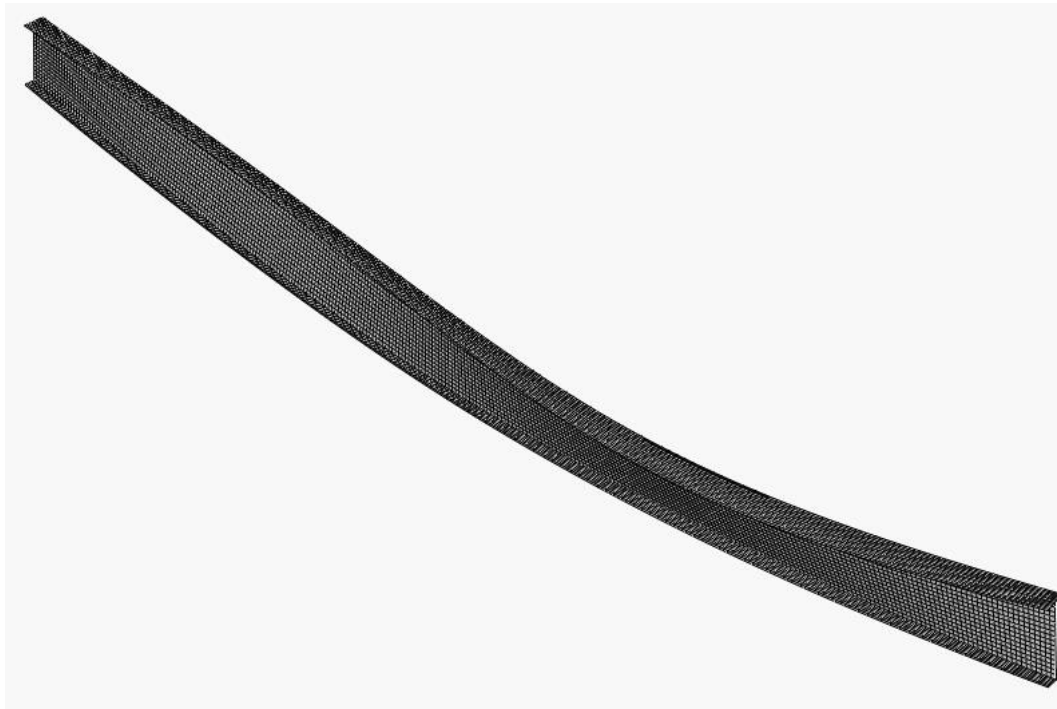


(b) C210 fully rigid torsional bracing scaled x10

Fig. A.38. Case C210 deflected geometry at limit load

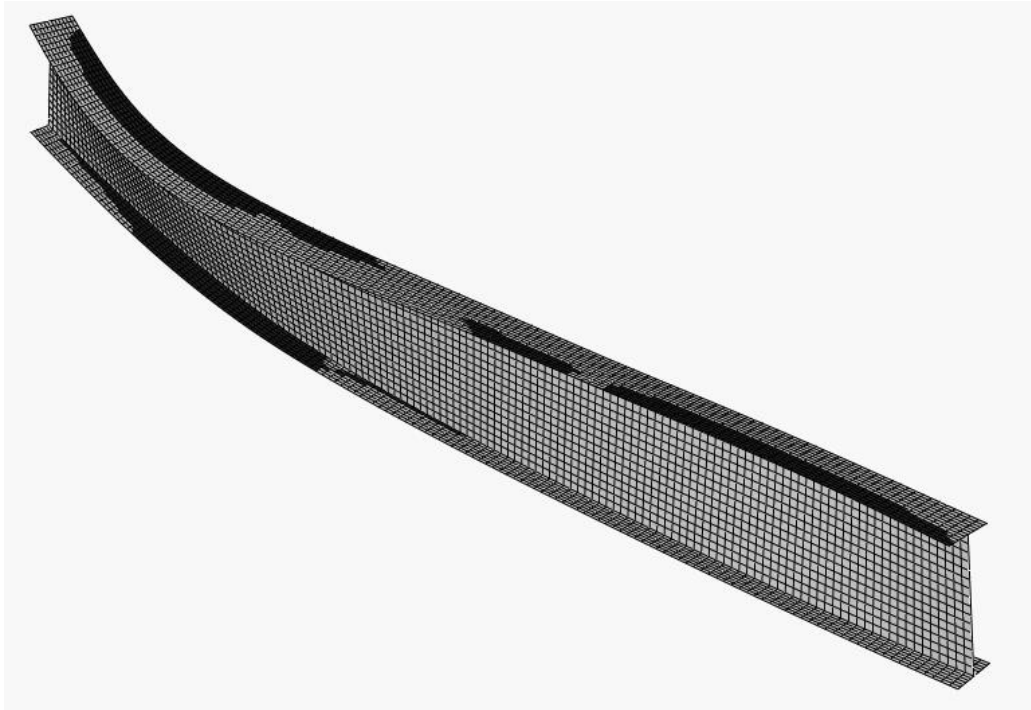


(a) C310 (14.8 kip/in) torsional bracing scaled x10



(b) C310 fully rigid torsional bracing scaled x10

Fig. A.39. Case C310 deflected geometry at limit load

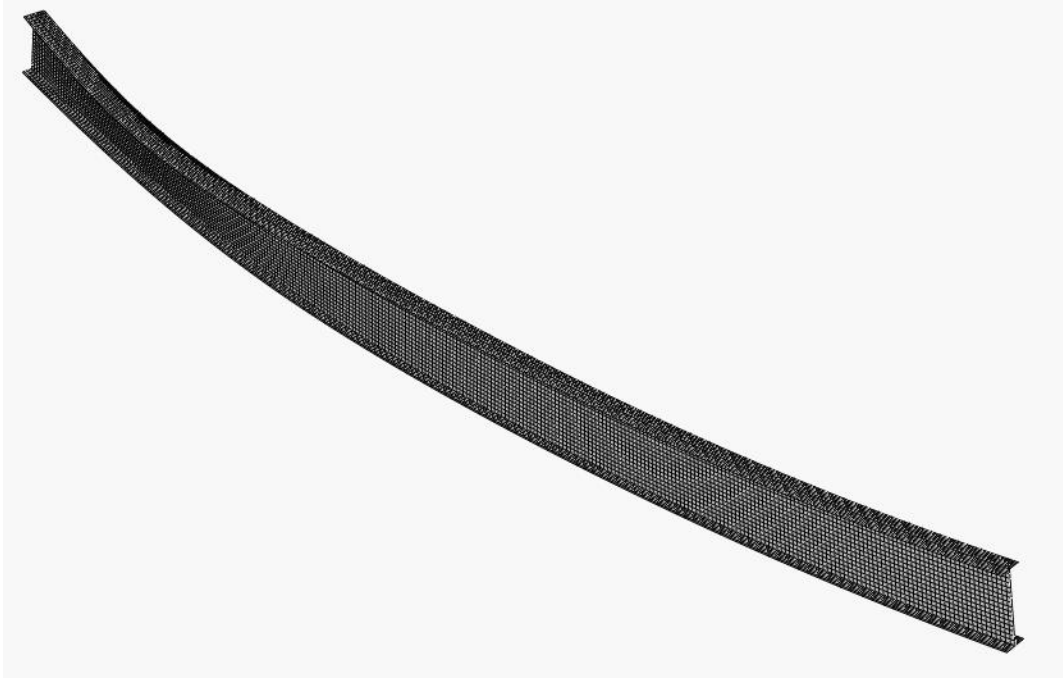


(a) C120 (16.1 kip/in) torsional bracing scaled x10

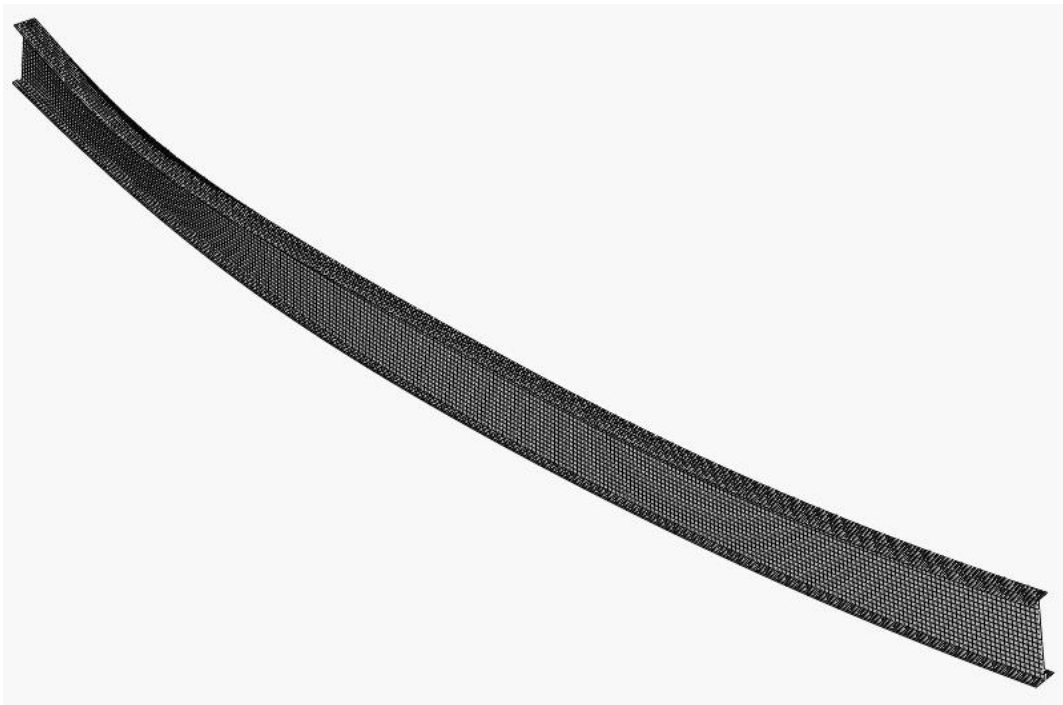


(b) C120 fully rigid torsional bracing scaled x10

Fig. A.40. Case C120 deflected geometry at limit load



(a) C220 (18.5 kip/in) torsional bracing scaled x10



(b) C220 fully rigid torsional bracing scaled x10

Fig. A.41. Case C220 deflected geometry at limit load



(a) C320 (11.1 kip/in) torsional bracing scaled x10



(b) C320 fully rigid torsional bracing scaled x10

Fig. A.42. Case C320 deflected geometry at limit load

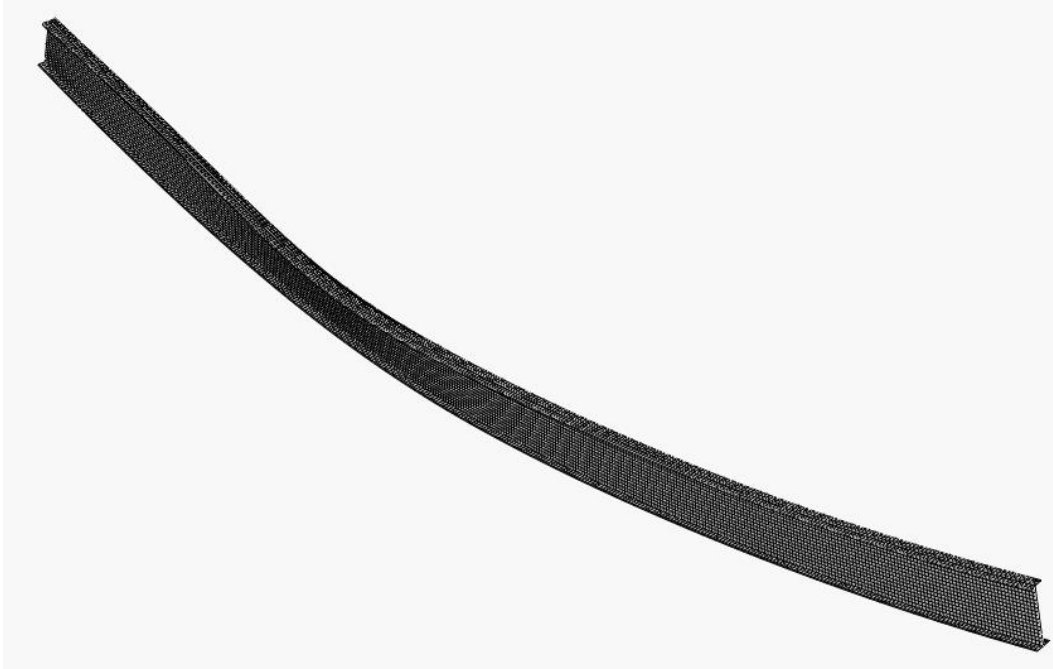


(a) C130 (14.3 kip/in) torsional bracing scaled x10

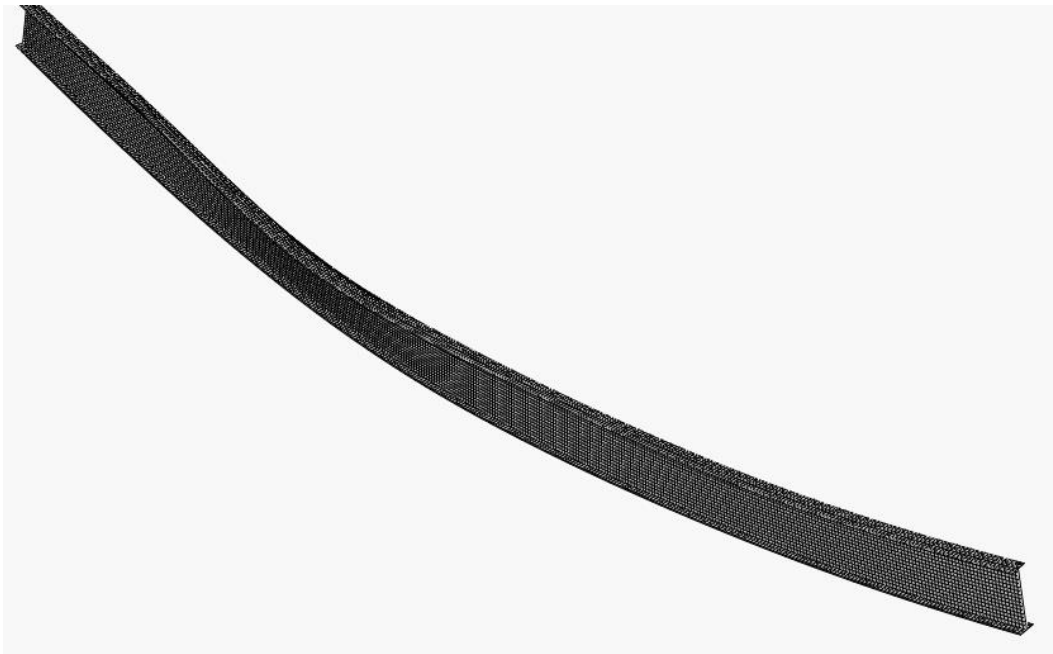


(b) C130 fully rigid torsional bracing scaled x10

Fig. A.43. Case C130 deflected geometry at limit load



(a) C230 (16.5 kip/in) torsional bracing scaled x10



(b) C230 fully rigid torsional bracing scaled x10

Fig. A.44. Case C230 deflected geometry at limit load



(a) C330 (9.9 kip/in) torsional bracing scaled x10



(b) C330 fully rigid torsional bracing scaled x10

Fig. A.45. Case C330 deflected geometry at limit load

## REFERENCES

- AISC (2010). "Code of Standard Practice for Steel Buildings and Bridges", AISC 303-05, *American Institute of Steel Construction*, Chicago, IL.
- AISC (2010). "Specification for Structural Steel Buildings", *American Institute of Steel Construction*, Inc. Chicago, IL. ANSI/AISC 360-10. (2010b).
- AISC (2010). "Specification for Structural Steel Building", ANSI/AISC 360-05, *American Institute of Steel Construction*, Chicago, IL. (2005).
- CEN (2005). Eurocode 3: Design of Steel Structures, Part 1-1: General Rules and rules for buildings, EN 1993-1-1:2005: E, Incorporating Corrigendum February 2006, European Committee for Standardization, Brussels, Belgium, 91 pp.
- Galambos, T.V. and Ketter, R. (1959). "Columns under Combined Bending and Thrust," *Journal of the Engineering Mechanics Division*, ASCE, 85(EM2), 135-152.
- Griffis, L., and White, D.W. "Stability Design of Steel Buildings", *AISC Design Guide 28*. (2014).
- Helwig, T.A. and Yura, J.A. (1999). "Torsional Bracing of Columns," *Journal of Structural Engineering*, American Society of Civil Engineers, 125(5), 547-555.
- Horne, M.R. and Grayson, W.R. (1983). "Parametric Finite Element Study of Transverse Stiffeners for Webs in Shear," Instability and Plastic Collapse of Steel Structures, Proceedings of the Michael R. Horne Conference, L.J. Morris (ed.), Granada Publishing, London, 329-341.
- Kim, Y.D. (2010). "Behavior and Design of Metal Building Frames using General Prismatic and Web-Tapered Steel I-Section Members," Doctoral dissertation, School of Civil and Environmental Engineering, Georgia Institute of Technology, Atlanta, GA, 528 pp.
- Kirby, P. A., and David A. Nethercot. (1979). "Design for structural stability". *Seoul, NY: Wiley*.
- LeMessurier, W.J. (1976). "A PRACTICAL METHOD OF SECOND ORDER ANALYSIS: PART I-PIN JOINTED SYSTEMS." *Engineering Journal* 13, no. 4
- Lutz, A.L., and Fisher, J. (1985). "A Unified Approach for Stability Bracing Requirements," *AISC Engineering Journal*, 22(4), 163-167.
- Plaut, R.H. (1993). "Requirements for Lateral Bracing of Columns with Two Spans," *ASCE Journal of Structural Division*, 119(10), 2913-2931.
- Plaut, R.H., and Yang, J.G. (1993). "Lateral Bracing Forces in Columns with Two Unequal Spans." *Journal of Structural Engineering*, ASCE, 119(10), 2896-2912.

- Simulia (2013). ABAQUS, *Software and Analysis Users Manual*, Version 6.13.
- Stanway, G. S., Chapman, J. C., and Dowling, P. J. (1992a). "A simply supported imperfect column with a transverse elastic restraint at any position. Part 1: behaviour." *Proc. Instn. Civ. Engrs., Strucs. and Bldgs.*, 94(2), 205-216.
- Stanway, G. S., Chapman, J. C., and Dowling, P. J. (1992b). "A simply supported imperfect column with a transverse elastic restraint at any position. Part 2: design models." *Proc. Instn. Civ. Engrs., Strucs. and Bldgs.*, 94(2), 217-218.
- Taylor, A. C. and Ojalvo, M. (1966). "Torsional Restraint of Lateral Buckling," *Journal of the Structural Division*, ASCE, ST2, 115-129.
- Timoshenko, S. and Gere, J. (1963). "Theory of Elastic Stability", *New York: McGraw- Hill*.
- Tran, D.Q. (2009). "Towards Improved Flange Bracing Requirements for Metal Building Frame Systems" Master's thesis, Georgia Institute of Technology, Atlanta, GA.
- Wang, L., and Helwig, T. A "Critical Imperfections for Beam Bracing Systems," *ASCE Journal of Structural Division*, 131(6), 933-940. (2005).
- White, D.W., Sharma, A., Kim, Y.D. and Bishop, C.D. (2011). "Flange Stability Bracing Behavior in Metal Building Frame Systems," Final Research Report to Metal Building Manufacturers Association, Structural Engineering, Mechanics and Materials Report No. 11-74, *School of Civil and Environmental Engineering*, Georgia Institute of Technology, Atlanta, GA, 361 pp.
- Winter G. "Lateral Bracing of Columns and Beams", *Trans. ASCE*, Part 1, 125,809-925. (1958).
- Yura, J. A. and Phillips, B. "Bracing Requirements for Elastic Steel Beams," *Report No. 1239-1*, Center for Transportation Research, University of Texas at Austin, May, 73. (1992).
- Yura, J. A., Phillips, B., Raju, S., and Webb, S.. "Bracing of Steel Beams in Bridges," *Report No. 1239-4F*, Center for Transportation Research, University of Texas at Austin, October, 80. (1992).
- Yura, J. A. "Bracing for Stability-State-of-the-Art", *Proceedings*, Structures Congress XIII, ASCE, Boston, MA, 1793-1797. (1995).
- Yura, J. A. "Winter's bracing approach revisited." *Engineering Structures* 8(10), 821-825. (1996).
- Yura, J.A. (2001). "Fundamentals of Beam Bracing," *Engineering Journal*, AISC, 38(1), 11-26.